NASA/TM–2016-219350

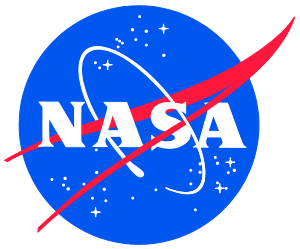

Space Shuttle Program (SSP) Dual Docked Operations (DDO)

Joel W. Sills, Jr.
Johnson Space Center, Houston, Texas

Erica E. Bruno
Analytical Mechanics Associates, Houston, Texas

November 2016

NASA STI Program . . . in Profile

Since its founding, NASA has been dedicated to the advancement of aeronautics and space science. The NASA scientific and technical information (STI) program plays a key part in helping NASA maintain this important role.

The NASA STI program operates under the auspices of the Agency Chief Information Officer. It collects, organizes, provides for archiving, and disseminates NASA's STI. The NASA STI program provides access to the NTRS Registered and its public interface, the NASA Technical Reports Server, thus providing one of the largest collections of aeronautical and space science STI in the world. Results are published in both non-NASA channels and by NASA in the NASA STI Report Series, which includes the following report types:

- TECHNICAL PUBLICATION. Reports of completed research or a major significant phase of research that present the results of NASA Programs and include extensive data or theoretical analysis. Includes compilations of significant scientific and technical data and information deemed to be of continuing reference value. NASA counter-part of peer-reviewed formal professional papers but has less stringent limitations on manuscript length and extent of graphic presentations.

- TECHNICAL MEMORANDUM. Scientific and technical findings that are preliminary or of specialized interest, e.g., quick release reports, working papers, and bibliographies that contain minimal annotation. Does not contain extensive analysis.

- CONTRACTOR REPORT. Scientific and technical findings by NASA-sponsored contractors and grantees.

- CONFERENCE PUBLICATION. Collected papers from scientific and technical conferences, symposia, seminars, or other meetings sponsored or co-sponsored by NASA.

- SPECIAL PUBLICATION. Scientific, technical, or historical information from NASA programs, projects, and missions, often concerned with subjects having substantial public interest.

- TECHNICAL TRANSLATION. English-language translations of foreign scientific and technical material pertinent to NASA's mission.

Specialized services also include organizing and publishing research results, distributing specialized research announcements and feeds, providing information desk and personal search support, and enabling data exchange services.

For more information about the NASA STI program, see the following:

- Access the NASA STI program home page at *http://www.sti.nasa.gov*

- E-mail your question to help@sti.nasa.gov

- Phone the NASA STI Information Desk at 757-864-9658

- Write to:

. . .. NASA STI Information Desk
. . .. Mail Stop 148
. . .. NASA Langley Research Center
. . .. Hampton, VA 23681-2199

NASA/TM–2016-219350

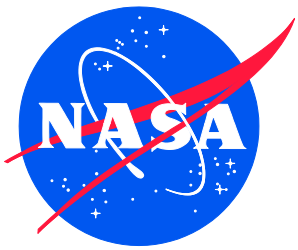

Space Shuttle Program (SSP) Dual Docked Operations (DDO)

Joel W. Sills, Jr.
Johnson Space Center, Houston, Texas

Erica E. Bruno
Analytical Mechanics Associates, Houston, Texas

National Aeronautics and
Space Administration

Langley Research Center
Hampton, Virginia 23681-2199

November 2016

Acknowledgments

This study and the results presented herein would not have been possible without the combined integrated efforts of multiple teams across many discipline and program teams. This effort reflects the hard work and dedication of individuals representing the SSP, ISSP, and their contractor community. The contributions of this diverse team have contributed to the Agency's understanding of DDO and are greatly appreciated.

The hypervelocity impact test program would not have been possible without the support and expertise of JSC's Hypervelocity Impact Technology Facility and the Boeing-Seattle Combined Effects Testing Facility.

Foreword

This document was completed January 2016, but was not published at that time due to other priorities. The NASA Engineering and Safety Center (NESC) is now releasing it as an informational document for future space flight missions with multiple docked vehicles. The content of the report is important to various disciplines, such as safety, environments, trajectory clearance, flight operations, thruster plume modeling, hypervelocity impacts and particle fluence. The document has been updated to use consistent nomenclature throughout as well as a general clean up; however, this document has not been standardized for consistent English Imperial and/or metric units. Care should be taken examining the tables and figures in each section. Statements regarding pending analyses were not updated as this document is capturing knowledge at the time of the original report. It is assumed that all analyses were completed and documented as required. Hyperlinks have been updated to the most current location of data, if still available.

Preface

This document describes the concept definition, studies, and analysis results generated by the Space Shuttle Program (SSP), International Space Station (ISS) Program (ISSP), and Mission Operations Directorate for implementing Dual Docked Operations (DDO) during mated Orbiter/ISS missions. This work was performed over a number of years. Due to the ever increasing visiting vehicle traffic to and from the ISS, it became apparent to both the ISSP and the SSP that there would arise occasions where conflicts between a visiting vehicle docking and/or undocking could overlap with a planned Space Shuttle launch and/or during docked operations. This potential conflict provided the genesis for evaluating risk mitigations to gain maximum flexibility for managing potential visiting vehicle traffic to and from the ISS and to maximize launch and landing opportunities for all visiting vehicles.

This document reflects the hard work and dedication of individuals representing the SSP, ISSP, and their contractor community. This team has contributed to the Agency's understanding of DDO and are greatly appreciated. The teams and their leads who contributed to this effort are as follows:

SSP Flight Operations and Integration Office - Joel Sills

SSP Orbiter Project Office (OPO) - Malise Fletcher

SSP Safety and Mission Assurance (S&MA) Office - Sally Davis

ISS Vehicle Integrated Performance, Environments, and Resources (VIPER) - W. Spetch and E. Menkin

ISS Environments - Courtney Steagall

ISS S&MA Office - Nathan Vassberg

ISS S&MA Risk Office - Mike Lutomski

Johnson Space Center (JSC) S&MA - Brian Rochon

JSC Proximity Operations Environments - Quyen Jones

The overarching goal of this effort was to assess the viability and readiness of the SSP to protect for DDO on any given mission. Discussion and results presented herein represent a generic assessment of the SSP and ISSP integrated safety and technical evaluations of DDO, realizing that mission-specific analysis and operational impacts are future work.

Table of Contents

List of Figures

List of Tables

Nomenclature

µm	Micron
AH	Attitude Hold
APU	Auxiliary Power Unit
AR&D	Automated Rendezvous and Docking
ASC	ascent
ATV	Automated Transfer Vehicle
C&T	Communications and Tracking
c.g.	Center of Gravity
CAMMP	Configuration Analysis Modeling and Mass Properties
CCTV	Closed Circuit Television
C_d	Coefficient of Drag
C_d	coefficient of drag
CETF	Combined Effects Test Facility
CIL	Critical Items List
cm	Centimeter
CMG	Control Moment Gyroscope
CoFR	Certificate of Flight Readiness
CREAM	Cognitive Reliability and Error Analysis Method
CSCS	Contingency Shuttle Crew Support
CW	Clohessy-Wiltshire (relative motion equations)
DAP	Digital Auto Pilot
DC-1	Docking Compartment One
DDO	Dual Docked Operations
Deg	Degree
DES	descent
DOF	Degree-of-Freedom
DSMC	Direct Simulation Monte Carlo
E3	Electromagnetic Environmental Effects
ECLSS	Environmental Control and Life Support System
EME	Electromagnetic Emission
EVA	Extravehicular Activity
FAWG	Flight Assessment Working Group
FD	Flight Day
FDD	Flight Design and Dynamics
FGB	Functional Cargo Block
FO&I	Flight Operations and Integration
FORP	Fuel/Oxidizer Reaction Products
FRS	Flight Readiness Statement
FRSI	Felt Reusable Surface Insulation
Ftu	Fatigue Strength
GFE	Government-Furnished Equipment
GN&C	Guidance, Navigation, and Control
HITF	Hypervelocity Impact Test Facility
HR	Hazard Report

HTV	H-II Transfer Vehicle
ICD	Interface Control Document
IGNC	Integrated Guidance, Navigation, and Control
IML	Inner Mold Line
in	Inches
ISS	International Space Station
ISSACS	International Space Station Analysis Coordinate System
ISSP	International Space Station Program
ITVC	Intensified (Black and White) Television Camera
JSC	Johnson Space Center
JTWG	Joint Technical Working Group
kg	Kilogram
km/s	Kilometer/Second
KOS	ISS Keep-Out Sphere
KSC	Kennedy Space Center
lb	Pound
lbm	Pound-Force
LCC	Launch Commit Criteria
LCH	Laser Camera Head
LCS	Laser Camera System
LDRI	Laser Dynamic Range Imager
LDT	Loads and Dynamics Team
LED	Light Emitting Diode
LESS	Leading Edge Structural System
LVLH	Local Vertical/Local Horizontal
m	Meter
MCS	Motion Control System
MIP	Mission Integration Plan
MLI	Multi-Layer Insulation
MLM	Multipurpose Laboratory Module
MM	Momentum Management
MMH	Monomethyl hydrazine
MMOD	Micrometeoroid and Orbital Debris
MOD	Mission Operations Directorate
MPLM	Multi-Purpose Logistics Module
MPM	Manipulator Pedestal Mounts
MRM1	Mini Research Module 1
MRM2	Mini Research Module 2
NASA	National Aeronautics and Space Administration
NCR	Nonconformance Report
NDMA	N-nitrosodimethylamine
NET	No Earlier Than
NIOSH	National Institute for Occupational Safety and Health
NSTS	National Space Transportation System
NTO	Nitrogen Tetroxide

NVR	Non-Volatile Residue
OBSS	Orbiter Boom Sensor System
ODS	Orbiter Docking System
OML	Outer Mold Line
OMRS	Operations and Maintenance Requirements and Specifications
OMS	Orbital Maneuvering System
OPF	Orbiter Processing Facility
OPO	Orbiter Project Office
PADME	Proximity Analysis for Dynamic Motion Effects
PIC	Plume Impingement Contamination
PIH	Payload Integration Hardware
PLB	Payload Bay
PLBD	Payload Bay Doors
PMA	Pressurized Mating Adapter
PPE	Personal Protective Equipment
PRA	Probability Risk Assessment
PRCB	Program Requirements Control Board
PRSD	Power Reactant Storage and Distribution
PRT	Problem Resolution Team
psf	Pounds per Square Foot
psi	Pounds Per Square Inch
PTU	Pan Tilt Unit
PVR	Program Verification Review
RCC	Reinforced Carbon-Carbon
RF	Radio Frequency
RMS	Remote Manipulator System
RPY	Roll-Pitch-Yaw (attitude sequence)
RS	Russian Segment
RSC	RMS Sideview Camera
RSC-E	Rocket Space Corporation-Energia
RSS	Root Sum Square
RV	Russian Vehicle (Soyuz or Progress)
S&MA	Safety and Mission Assurance
sec	seconds
SEM	Scanning Electron Microscopy
SiC	Silicon Carbide
SM	Service Module
SP	Sensor Package
SPHINX	Smooth Particle Hydrodynamics
SPIFEX	Shuttle Plume Impingement Flight Experiment
SRMS	Shuttle Remote Manipulator System
SRP	Safety Review Panel
SRP	Safety Review Panel
SSCS	Space to Space Communication System
SSO	Space Station Operations

SSP	Space Shuttle Program
TCS	Thermal Control System
TEA	Torque Equilibrium Attitude
TIM	Technical Interchange Meeting
TOPO	Trajectory Operations Officer
TPS	Thermal Protection System
UDMH	Unburned Unsymmetrical Dimethylhydrazine
UFORP	UDMH Fuel Oxidizer Reaction Products
ULF	Utilization Logistics Flight
USA	United Space Alliance
USOS	United States On-orbit Segment
VAC	Verification Analysis Cycle
VC	Vehicle Configuration
VIPER	Vehicle Integrated Performance and Environmental Resources
VLA	Verification Loads Analysis
VRCS	Vernier Reaction Control System
VVO	Visiting Vehicle Officer
WLE	Wing Leading Edge
WPRT	Window Problem Resolution Team
WSTF	White Sands Test Facility
WVS	Wireless Video System
XVV	X-axis in direction of Vertical Velocity
YPR	Yaw-Pitch-Roll (attitude sequence)
ZLV	Z-axis in direction of Local Vertical
σ	Sigma

1.0 Executive Summary

1.1 Introduction

Due to the ever increasing visiting vehicle traffic to and from the International Space Station (ISS), it became apparent to both the ISS Program (ISSP) and the Space Shuttle Program (SSP) that there would arise occasions where conflicts between a visiting vehicle docking and/or undocking could overlap with a planned SSP launch and/or during docked operations. This potential conflict provided the genesis for evaluating risk mitigations to gain maximum flexibility for managing potential visiting vehicle traffic to and from the ISS and to maximize launch and landing opportunities for all visiting vehicles. This document chronicles the concept definition studies and analysis results generated by both the SSP and the ISSP for Dual Docked Operations (DDO) involving the Orbiter and Russian vehicles (RVs) (i.e., Soyuz or Progress). The studies, analyses, and results presented summarize the work conducted over a 22-month timeframe from October 2008 through August 2010 by a cadre of SSP, ISSP, and, Mission Operations Directorate (MOD) teams.

To manage this wide-ranging issue, the program teams decided to approach this study in a piece-wise manner, focusing on the greatest portion of the visiting vehicle traffic and their potential overlap with Space Shuttle missions. For the purposes of this document, both the ISSP and the SSP defined DDO as the capability to perform a RV docking or undocking during a mated SSP mission to ISS. H-II Transfer Vehicle (HTV), Automated Transfer Vehicle (ATV), and commercial resupply vehicles were not considered.

The overarching goal of this effort was to assess the viability and readiness of the SSP to protect for DDO on any given mission. Discussion and results presented represent a generic assessment of the SSP and ISSP integrated safety and technical evaluations of DDO, realizing that mission-specific analysis and operational impacts are future work.

1.2 Requirements and Ground Rules

From the outset, a set of requirements and ground rules were established to set the framework for the study. The ISSP and SSP teams jointly agreed that DDO shall occur only at the following ISS Ports (see Figure 1-1):

1. Service Module (SM) Aft for docking and undocking
2. Docking Compartment One (DC-1) Nadir for docking and undocking
3. Functional Cargo Block (FGB) Nadir for undocking only
4. Multi-Purpose Research Module One (MRM1)
5. MRM2 Zenith for docking and undocking

RV docking or undocking is prohibited while a cargo element is on the Shuttle Remote Manipulator System (SRMS). RV docking or undocking during extravehicular activity (EVA), robotics, or during Orbiter dock/undock day is prohibited.

During RV dockings, the ISS shall be under Russian Segment (RS) control, and the Orbiter system shall remain passive. For undocking, two options shall be considered for mated stack control:

1. Undocking shall be performed with ISS mated stack under RS control only.
2. Undocking shall be performed with mated stack under Orbiter Vernier reaction control system (VRCS) jet control only. There shall be no consideration given to mixed RS and Orbiter control due to the complexity associated with the ISS solar array plan for either set of jets.

For docking of the Soyuz, DDO shall occur only during indirect Soyuz crew rotations. Therefore, there will be no more than 13 crew members onboard the ISS at a single time. RV undock/dock shall occur only over Russian ground track and during crew awake periods.

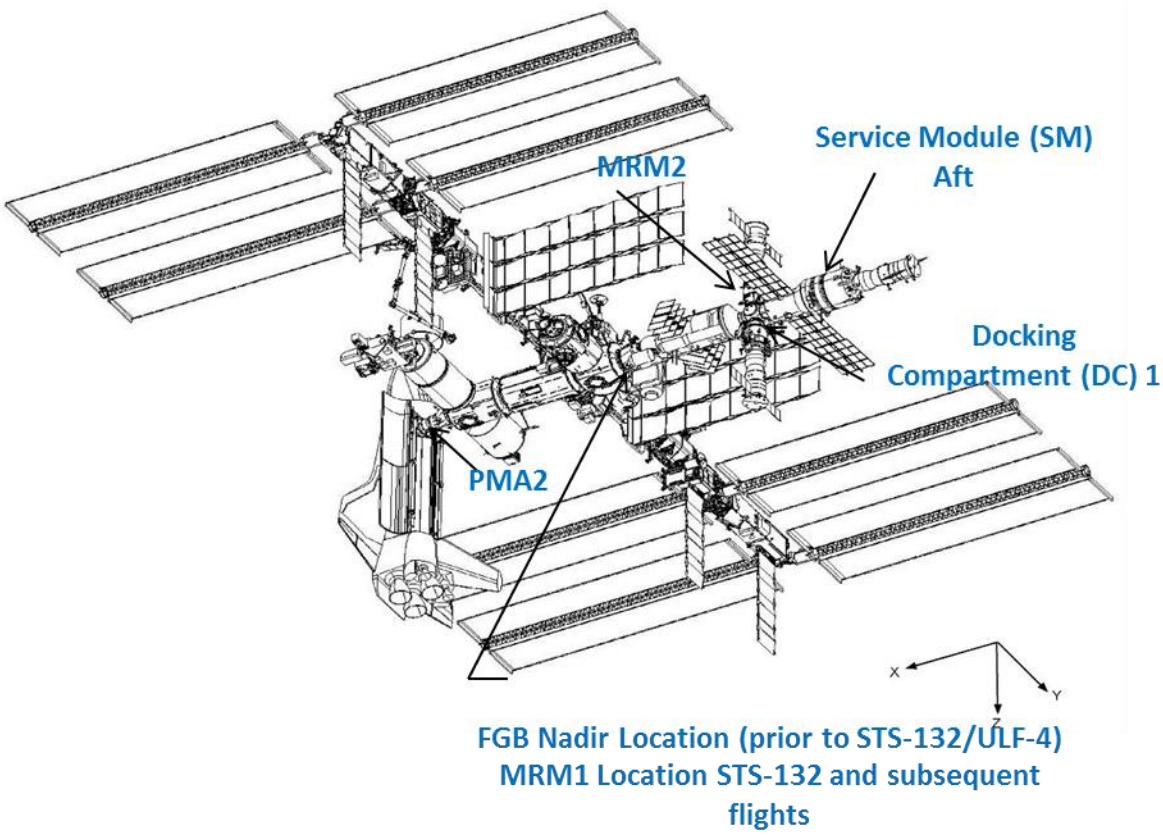

Figure 1-1. Representation of joint docked SSP/ISS mission configuration.

1.3 Thruster Contamination and Particle Fluence

To assess the viability of performing DDO, the ISSP delivered plume particle fluence and contamination deposition based on RV proximity operations to the SSP for evaluation. These environments will cause thruster plume contamination and erosion/pitting to Orbiter surfaces. The contamination is due to the deposition of unburned or partially burned propellant droplet material, while the erosion/pitting is mechanical damage due to high velocity impacts of

unburned propellant droplets. Initial contaminant deposit includes unburned unsymmetrical dimethylhydrazine (UDMH) and nitrogen tetroxide (NTO), monomethyl hydrazine (MMH)-nitrates, N-nitrosodimethylamine (NDMA), and non-volatile residue (NVR), which includes impurities in the propellant.

Particle fluence and contamination results were provided by ISSP for the following Orbiter surfaces: crew cabin windows, Orbiter boom sensor system (OBSS) sensors, cameras on payload bay (PLB) bulkheads, keel, and SRMS, payload bay door (PLBD) thermal control system (TCS) radiators, and general PLB surfaces.

Environments include particle fluence results for MRM2-based RV proximity operations to allow consideration of plume impingement on Orbiter wing reinforced carbon-carbon (RCC) due to an MRM2 event. For each RS docking port, the ISS Space Environments team simulated six approaches, one separation, and one Soyuz thruster test per the available data. These scenarios were developed using as-flown data. No translation or attitude dispersions were modeled. In all simulations, the RV centerline was coaxial throughout with the docking port centerline and with the vehicle maintaining a constant attitude. This technique was used because sufficient information for accurate modeling of translation or attitude dispersions is not available from RV flight simulations.

An additional analysis case involving a more conservative RV approach trajectory and attitude was provided by the ISS Space Environments team for assessment. RV approach proximity operations to the MRM2 docking port was selected for an alternative analysis case. The vehicle approach trajectory and attitude were selected to maximize particle fluence/contamination results for the front Orbiter windows (see Figure 1-2).

For this more conservative case, nominal RV lateral misalignment was limited to a 10° cone along the approach vector. The 10° cone is a specification value for the approaching vehicle. The 4° RV pitch results in higher particle fluence/contamination levels to the front Orbiter windows. The 4° pitch was selected to place the thrusters closest to the windows within the limits of the nominal approach. Results for this case indicate that particle fluence to front windows for the more conservative RV approach trajectory and attitude was higher than predictions in the original study by a factor of ~2.2, and contamination levels to front windows for the more conservative RV approach trajectory and attitude were higher than predictions in the original study by a factor of ~2.1.

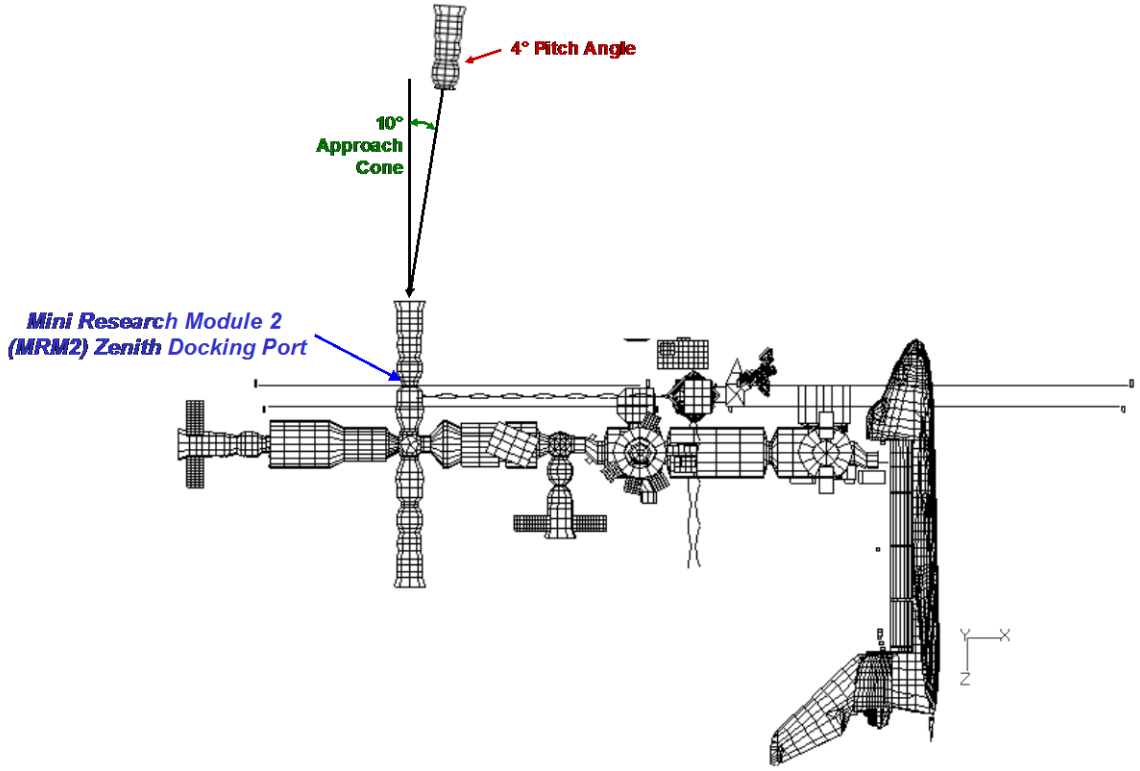

Figure 1-2. Approach trajectory and attitude for alternative approach analysis case.

A RV abort scenario for vehicle proximity operations to the MRM2 docking port was assessed and environments were provided to SSP personnel. The abort scenario was synthesized from nominal approach jet firing data. The RV proximity operations to the MRM2 docking port was selected for the abort scenario. The scenario involves an approach and backout, both of which were modeled using available jet firing data for nominal RV approach proximity operations. The range offset was applied such that the last lateral engine thruster firing occurs at the minimum range for Orbiter window exposure (see Figure 1-3).

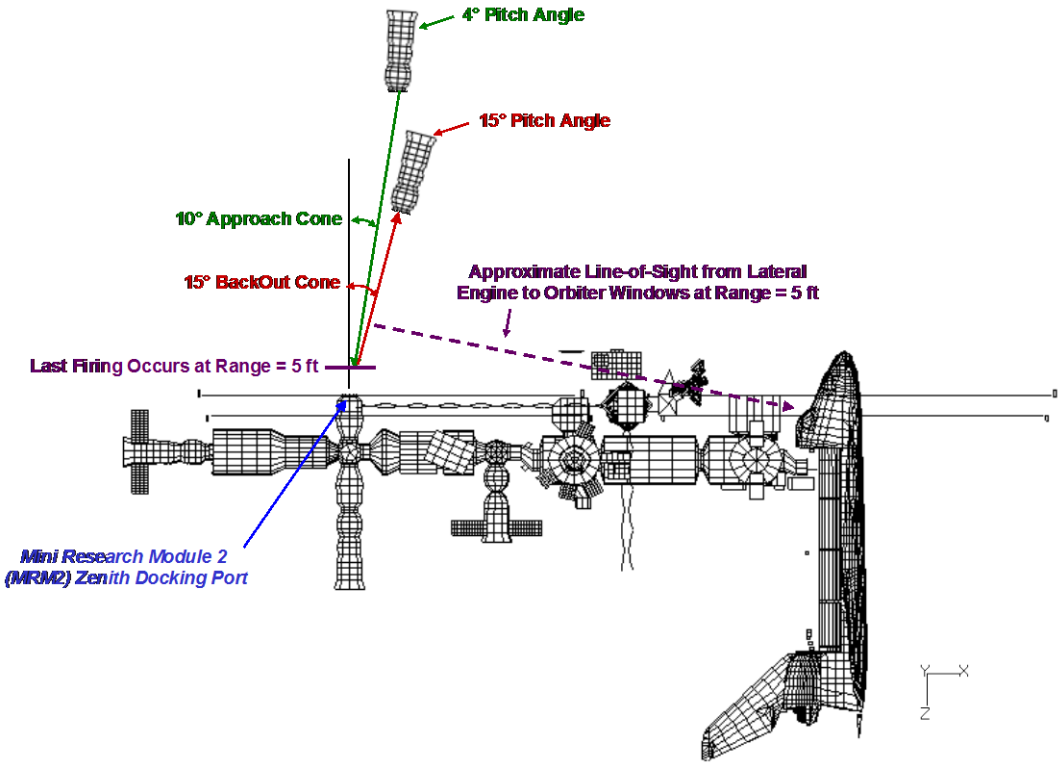

Figure 1-3. RV trajectory and attitude assumptions for the abort scenario.

Table 1-1 summarizes the particle fluence for the Orbiter windows, considered the most sensitive vehicle surface when exposed to the particle fluence. In addition, separate particle fluence results were generated from the abort scenario case for 1 to 5 microns (μm), 6 to 10 μm, and 11 to 12 μm diameter particle groups to support planned SSP ground hypervelocity impact tests as shown in Figure 1-4.

Table 1-1. Analysis case summary for orbiter windows.

	Nominal Approach	Alternative/Bounded Nominal Approach	Abort Scenario - Approach	Abort Scenario - Back-out	Abort Total
Approach Cone Half-Angle *degrees*	**0**	**10**	**10**	**15**	**-**
Russian Vehicle Pitch Angle *degrees*	**0**	**4***	**4***	**15****	**-**
Offset Applied (to fix last firing at range = 5 ft)	**N**	**N**	**Y**	**Y**	**-**
Particle Fluence to Fwd-Stbd Fuselage Window (Front) *particles/cm^2*	**2279**	**5006**	**6580**	**30754**	**37335**
Particle Fluence to Fwd-Port Fuselage Window (Front) *particles/cm^2*	**2274**	**5047**	**6501**	**30678**	**37179**
Reference Section	**5.2.1**	**5.2.2**	**5.2.3**	**5.2.3**	**5.2.3**

*Pitch angle held at 4 degrees to maximize particle fluence to Orbiter front windows.

**Pitch angle of up to 15 degrees. Pitch angles less than 15° selected as needed to maximize particle fluence to Orbiter front windows.

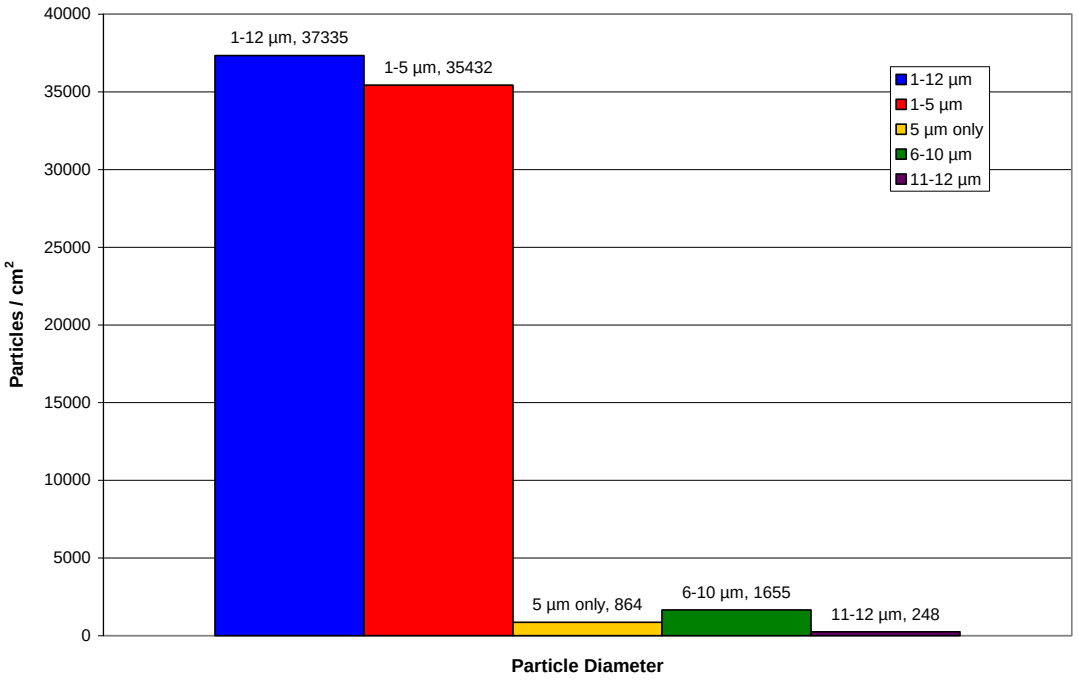

Figure 1-4. Particle fluence by diameter to the Orbiter forward-starboard front window for the RV abort scenario.

1.4 Proximity Operations Environments

The ISS Loads and Dynamics Team (LDT) provided RV proximity operation loads when approaching the SM aft port, DC-1 nadir port, FGB nadir port, and MRM2 zenith port. These loads are based on post-flight reconstructions of RV approach trajectories to the ISS. A Monte Carlo analysis of the data was used to develop the models. For the analysis, the plume flowfield uncertainty factor was set to its maximum value for all jet firings to ensure conservatism in the model. For off-nominal plume pressure cases, a dual jet plume amplification factor of 1.634 was implemented. The 1.634 amplification factor addresses superposition of two-jets and provides additional conservatism.

RV undocking force time histories were generated for the RVs using dynamic analyses that are based on the stiffness characteristics of the Probe and Cone mechanism's plunger system. The undocking forces are calculated from a simple mass-spring system that consists of four plungers, located symmetrically about the interface, activated after the hooks and latches are released. It was assumed that the mass of the ISS was sufficiently larger than the undocking vehicle to justify using only a one mass system with a grounded spring. No other external forces are included in the model.

1.5 Approach and Separation Trajectory Assessments

Approach and separation clearances to ISS, as well as abort trajectories, were assessed during this study. Separation and docking analyses are required to confirm compliance with on-orbit Interface Control Document (ICD) requirements defined in Appendix S of NSTS-21000-IDD-ISS paragraph S.4.2.3.5.3. From over 500 cases that were run, only 12 of the worst cases were

selected for detailed vehicle clearance analysis. Cases include both RV failed motion control system and nominal separation scenarios. The FGB-nadir port was ruled out for DDO due to Orbiter tail impingement within the 45° half-angle Kurs antenna signal cone. For the same reason, the MRM1 at the FGB-nadir point was ruled out for DDO. This signal interference keeps the approaching vehicle from communicating with the ISS. The FGB-nadir port separation for DDO provides a close clearance between a RV on the DC1 port.

The NASA safety community and the Russians conducted extensive reviews of these trajectories. The two-fault tolerant guidelines were applied to RVs, with the implicit understanding that NASA would never receive complete documentation.

However, over the course of detailed technical discussions concerning the architecture and docking operations, to include flight histories, agreement was achieved. In cases where the vehicles were not two-fault tolerant, nonconformance reports (NCRs) were written by the Russians, and the risks were accepted by the SSP and ISSP using the rationale of flight history to explain these situations.

1.5.1 Orbiter Assessment Results

The Orbiter Project Office (OPO) reviewed all ISSP-provided induced environments and performed assessments of all their subsystems. Regarding particle impingement, the threat posed to the RCC hardware is taken seriously, and inspections for surface damage will be included as appropriate to ensure the "Late Mission" micrometeoroid and orbital debris (MMOD) inspection is performed in accordance with operational flight rules. However, no damage to RCC is predicted, even if the late inspection constraint cannot be met.

For the thermal protection system (TPS), post-flight MMOD inspections demonstrate that damage to tiles/blankets/felt reusable surface insulation (FRSI) from light fast particles is generally less severe than the damage of light fast particles to the RCC. Since the detailed Soyuz docking evaluation has determined there is no issue for RCC, no issue would be expected for tiles/blankets/FRSI. Therefore, there are no constraints for TPS.

The closed circuit television (CCTV) system's greatest vulnerability is in the camera lenses. The forward and aft bulkhead cameras and the SRMS Elbow camera must be pointed away from the plume flow to avoid direct contact by the plume particles. The SRMS wrist camera and the Orbiter RMS Sideview camera (RSC) should be protected from direct contact by the plume particles. If these constraints are not met, damage would result in degraded video pictures both by unwanted glints from pits on the wrist camera lens and/or blurring from the residue.

Regarding SRMS/OBSS positioning, the OBSS receives particle impacts to some degree for all port locations. To mitigate this, the intensified television camera (ITVC)/laser dynamic range imager (LDRI) optics are not to be in the line of sight of the source of particle fluence. The OBSS constraint is to place it out of the line of sight of the plume. These positions have already been developed.

Particle impingement on the Orbiter windows was analyzed, and the Windows Problem Resolution Team (PRT) assessment is that the pane strength test of laboratory-created specimens shows no adverse degradation to thermal pane strength as a result of the nominal and bounded nominal environments for DDO. A 3-sigma (σ) strength value of 6,212 pounds per square inch

(psi) stress is used, which exceeds the minimum entry/descent certification strength minimum value of 5,010 psi stress for thermal pane fused silica glass.

The testing performed does not encompass the abort scenario environment, and the Windows PRT was not comfortable extrapolating their results to this environment. The testing performed was at the edge of the bounded nominal environment. The PRT used 5 μm particles of a certain fluence, and 10 μm particles of certain fluence. The strength of the glass was not sensitive to the two particle sizes nor the fluence prescribed for the nominal and bounded nominal cases. For the nominal and bounded cases, the strength of the glass was adequate for launch and landing; however, a determination on whether or not the strength of the glass was adequate for aborts cannot be made based on the data set in hand. During testing, the Windows PRT tried to insert as much potential scatter as possible with the available 17 specimens from 8 windows.

Toxicity concerns for ground processing primarily center on the NDMA residue from the UDMH fuel oxidizer reaction products (UFORP). A secondary consideration is the nonvolatile salts that may accumulate in the PLB since these do no liberate in a vacuum environment. The UFORP components evaporate within 45 minutes from a surface at 25 °C. The nonvolatile particulate salts are eye and skin irritants per the Material Safety Data Sheet (MSDS), but use of personal protective equipment (PPE) will mitigate these concerns. Therefore, there are no constraints pertaining to toxicity. Forward work will involve sampling after the first DDO to include destructive testing of the TCS blanket cover to determine worst-case contamination quantity and composition. The Kennedy Space Center (KSC) industrial hygiene group has been engaged in this study, and no issues are foreseen. As an additional precaution, EVA is not allowed as per ground rules during a DDO, and the only exposure risk to the UFORP is in the area immediately around the engine bells of the SM.

1.5.2 SSP Flight Operations and Integration (FO&I) Assessment Results

All FO&I areas of responsibility assessed the viability for DDO. The Space Transportation System (STS)-130/20A mission was used as the pathfinder for this study. Existing certifications were applied generically where possible. All Joint Technical Working Groups (JTWGs) assessed the ISSP-provided environments for viability to perform DDO. Power/Avionics, Environmental Control and Life Support System (ECLSS), Power/Avionics, and Communication and Tracking (C&T), and electromagnetic effects panels completed generic assessments with no issues identified. The Thermal Control System (TCS), Vehicle Configuration (VC), Loads and Dynamics, and Flight Control and Structures panels require mission-specific analyses and documentation updates.

Peak docking/undocking loads for both STS-130/20A and STS-131/19A demonstrated no limit load exceedances, with the peak load at 37 percent and 35 percent of the ICD limit loads, respectively. There were no constraints to DDO identified.

Flight Control DDO results showed that Orbiter maintains control within attitude deadbands, and propellant usage was as expected, with all Shuttle Operations Data Book (SODB) constraints satisfied. The constraint was that DDO is certified using VRCS only, and only for undocking.

The C&T Panel used the Soyuz/Progress System Data Book, the Space Shuttle Circuit Margin Data Book, and the EV7 radio frequency (RF) Data Base to ensure compatibility between RV and Orbiter communication systems. All ports were evaluated. Results indicated that the Orbiter

Ku-band requires restriction, either by mask or by placing the system in standby mode. There were no other constraints on either the Orbiter communication system or the Russian communication system, pending Russian concurrence. However, reflections from the RV could cause damage to Space Station Operations (SSO), the ISS Ku-band system, and the RV.

The ISSP-provided Orbiter/ISS interface acceleration time histories for STS-131/19A were used to verify that RV docking/undocking loads and frequencies do not adversely affect the Orbiter/ISS interface and payloads. This configuration was selected to generate worst-case responses for STS-132/Unpressurized Logistics Flight (ULF) 4 and subs. The STS-134/ULF6 manifest was selected based on payload frequency content. Resulting payload maximum (max)/minimum (min) load factors were compared to verification loads analysis (VLA) max/min load factors, and each DDO payload max/min was enveloped over all docking cases. All Orbiter/ISS interface loads were within ICD allowables. For the docking ports that were examined, there were no constraints for DDO for STS-132/ULF4 and subs.

FO&I completed all required assessments to determine viability for performing DDO for all technical areas of responsibility. These assessments were based on formally delivered ISS environments documented in the ISS on-orbit ICDs. Work on STS-132/ ULF4 and subsequent missions are in progress. Assessments and evaluations for each flight where the possibility of DDO could occur are being incorporated into the Certificate of Flight Readiness (CoFR) process. The new environments will be vetted after the additional data are received.

1.5.3 S&MA Assessments

The integrated S&MA team members (ISSP, JSC, and SSP) met many times over the course of the DDO analysis period. Joint S&MA discussions and efforts included: reviewing the affected integrated hazard and risk baseline for docked operations; many hours of detailed background of the content development and rationale for the hazard reports; exchange of corporate knowledge; and identification of potential areas where engineering analysis might be needed to obtain a thorough review of the risk baseline.

Recommendations from the SSP S&MA office include the following:

1. Concurrence with the hazard analyses and risk characterization contained in the JSC S&MA analysis.
2. No show stoppers were identified that preclude DDO, although there is a high level of uncertainty concerning the hazard analyses.
3. If the ISSP requirements mandate DDO, then these risks should be carefully considered against the requirements mandating DDO and, if possible, the ISSP and SSP should reconsider scheduling and other constraints to avoid DDO.
4. Any risk mitigation such as development of operational responses, however extensive, or further engineering analysis (including Russian-generated engineering analysis), should be pursued to reduce the potential risk that the current limited and high-level assessment presents.

The ISS S&MA Office working in collaboration with the SSP Office agrees that no show stoppers have been identified that preclude DDO and if the ISSP requirements mandate DDO, that these risks be carefully considered against the requirements mandating DDO.

ISS S&MA evaluated hazards associated with visiting vehicles and incorporated their findings into their hazard reports and controls. For any risk mitigation on a specific mission where DDO is required, mission-specific development of operational responses however extensive, or further engineering analysis, including Russian-generated engineering analysis, should be pursued to further reduce the potential risks.

JSC S&MA stated that the DDO assessment shows that this operational condition represents an increase in risk to the Orbiter. Docking/undocking aborts present a higher risk than normal, but quantifying the risk is difficult because of a lack of data, open causes, and undeveloped operational impacts. The primary hazards are collision, ISS structural overload, and Orbiter structural overload.

The probability of an off-nominal scenario involving a RV dynamic operation remains high (about 1 in 20), although there is not a consensus in the S&MA community or an agreed-to methodology for computing the probability. However, because the joint ISS/Orbiter/Russian operational response to an off-nominal scenario is undeveloped, an off-nominal scenario may increase risk to the Orbiter.

SSP Safety Panel chairs reviewed the approach to DDO safety assessment and have no additional concerns.

1.6 Recommendations

The SSP S&MA position is that no safety show stoppers have been identified that preclude DDO, although there is a high level of uncertainty concerning the hazard analyses. If ISSP requirements mandated performing DDO, the risks should be carefully considered against those requirements.

The ISS S&MA position is to avoid DDO unless it must be performed. ISSP would look at mission-specific cases.

It is important to note that the primary operational impacts are loss of activities for one docked day, sleep shift required, and complexity of operations with communications and docked Orbiter activities. These impacts would need assessing on an individual mission basis.

The overriding consensus from these reviews is that DDO can be performed, but it should not be done unless required because of Agency priorities. For any scenario involving MRM1 docking and undocking, rigorous analysis and evaluation would be required by both the SSP and ISS communities, as this port was ground ruled out in all assessments performed to date due to limited clearance with the Orbiter vertical tail. Additionally, mission-specific risks and operational complexities will need to be assessed as part of the risk trade if a decision is made to protect DDO for a particular flight.

2.0 DDO Operations

The ISS is frequented by visiting vehicles, which ferry crew members and deliver ISS elements and supplies. These visiting vehicles include the Orbiter and RVs. Current ISS visiting vehicle launch constraints present a concern of the RV flights to ISS overlapping with Orbiter flights, an activity referred to as DDO. DDO is the capability to perform one RV docking or undocking during a mated Orbiter to the ISS mission, as shown in Figure 2-1.

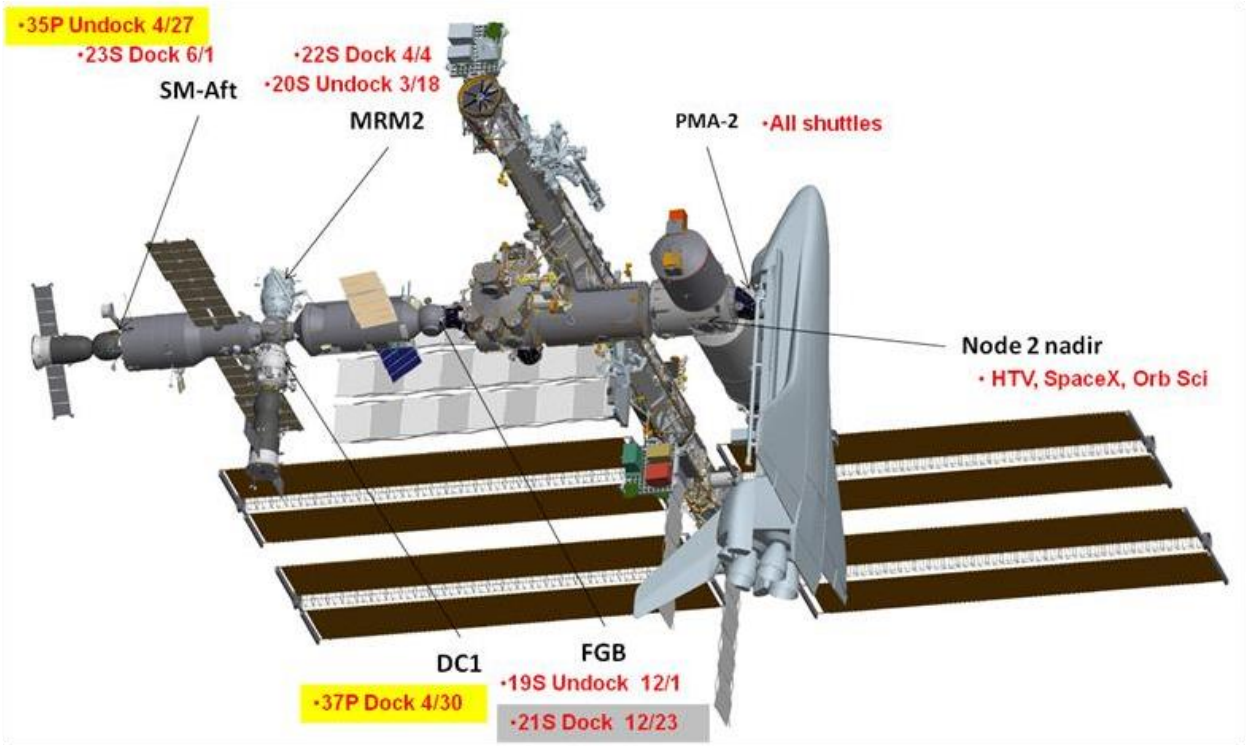

Figure 2-1. Representation of joint docked RV/Orbiter/ISS mission configuration.

2.1 Identified Impacts Evaluated in DDO Assessments

The potential impacts resulting from DDO on Orbiter hardware, Orbiter government-furnished equipment (GFE), and ISS are identified below. This list is representative of the impacts assessed in the results presented herein, but is not limited to:

a. ISS/RV Induced Environments:
   1. Docking and structural loads
   2. Thermal (mission specific)
   3. Thruster plume impingement loads, contamination, and erosion
   4. RF threats
b. ISS docking port clearance (including Trajectory Analysis and Physical Clearance)
c. RV Nominal and Abort Trajectories and/or corridors
d. Orbiter Hardware, Software, and Operations
e. Orbiter Guidance, Navigation, and Control (GN&C) while mated to ISS stack
f. Orbiter Hardware, GFE
g. Failure Modes and Effects Analysis/Critical Items List (CIL) of the Orbiter/ISS mated stack configuration
h. Robotics Operations of OBSS and SRMS
i. Flight-Specific Mission Operations Timeline, procedures, and training

3.0 Ground Rules and Assumptions

For this joint assessment, a common set of ground rules and assumptions were established and refined as results were made available. These ground rules and assumptions were categorized into technical and schedule.

3.1 Technical Ground Rules and Assumptions

a. DDO shall occur at the following ISS Ports only
   1. SM Aft - docking and undocking
   2. DC-1 Nadir - docking and undocking
   3. FGB Nadir - undocking only
   4. MRM2 Zenith - docking and undocking
   5. MRM1 - This docking port is not specifically addressed in this study, but will be addressed post STS-132/ULF4, if necessary.

b. RV docking or undocking is prohibited while a cargo element is on the SRMS.

c. RV docking or undocking during EVA and/or docked robotics activities or during Orbiter dock/undock day is prohibited.

d. During RV dockings, the ISS shall be under RS control, and the Orbiter system shall remain passive.

e. For undocking, only two options shall be considered for mated stack control.
   1. Undocking shall be performed with ISS mated stack under RS control only.
   2. Undocking shall be performed with mated stack under Orbiter VRCS jet control only.

f. There shall be no analysis or consideration for looking at VRCS jet fail case that leads to Alt-Primary Reaction Control System (PRCS) jet control for this case.

g. There shall be no consideration given to mix Russian segment and Orbiter control due to the complexity associated with the ISS solar array plan for either set of jets.

3.2 Schedule Ground Rules and Assumptions

a. For Soyuz dockings, DDO shall only occur during indirect Soyuz crew rotations with no more than 13 total crew on board ISS during mated operations.

b. RV undock/dock shall occur over Russian Ground track only.

c. RV undock/dock shall occur during crew awake periods.

d. RV relocation during Orbiter/ISS mated operations is not considered.

e. Propellant shall be prioritized for planned Orbiter mated stack maneuvers to/from the dock/undocked attitude and budgeted as required.

4.0 Environments

RV proximity operations (i.e., docking and undocking) to ISS have never been performed with Orbiter present and raise a number of technical issues. In particular, the possibility of RV proximity operations to ISS with a docked Orbiter has raised concerns regarding thruster plume induced contamination and particle impacts/erosion to external Orbiter surfaces. Thruster plume

induced contamination and particle fluence/erosion are characterized by the ISS Space Environments team.

4.1 Thruster Plume Effects and Modeling

ISS surfaces as well as potential hazards to EVA as the Fuel/Oxidizer Reaction Products (FORP) contain toxic byproducts. Initial contaminant deposit includes unburned UDMH and NTO, MMH nitrates, NDMA, and NVR, which includes impurities in propellant. Initial contamination deposits are of interest in evaluations of potential toxicity levels. Permanent contaminant deposit that remains after evaporation of volatile material includes MMH-nitrates and NVR. Permanent contamination deposits are of interest in evaluations of surface optical property degradation. Data obtained during the plume impingement contamination (PIC) experiment on STS-74 showed most volatile components evaporated within 45 minutes from a surface at 25° C [1].

External surfaces on the ISS can be mechanically damaged (eroded/pitted) when impacted by high velocity unburned liquid propellant drops present in bipropellant thruster plumes. Optical surfaces and surfaces with thin coatings, such as windows and camera lenses, are of primary concern. Thruster plume induced contamination and erosion/pitting have been observed on SSP flight experiments. The Shuttle Plume Impingement Flight Experiment (SPIFEX) on STS-64 and the PIC experiment both demonstrated pitting from plume particles, Figure 4-1. Surface pits from 1 to 24 μm in diameter were observed with scanning electron microscopy (SEM) [1, 2].

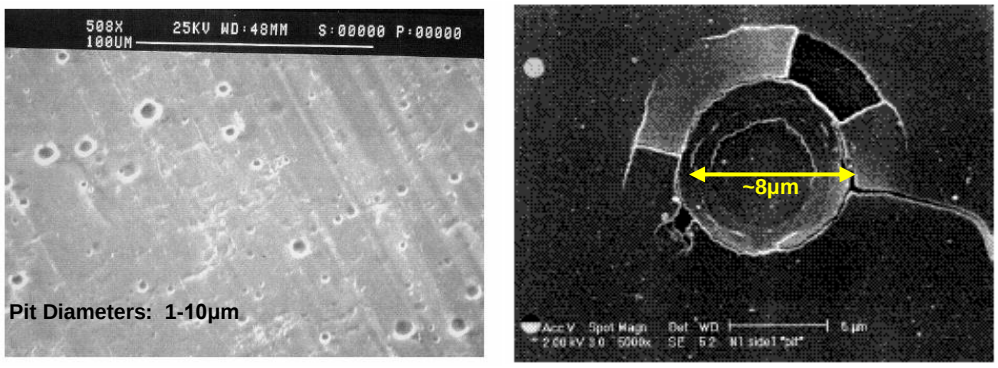

Figure 4-1. Thruster induced pits on SPIFEX aluminum witness coupon (left) and PIC glass camera lens (right).

The ISS Space Environments team bipropellant thruster plume model is a semi-empirical model that uses flight experiment and chamber test data for contamination characterization [3]. The model describes the number density and velocity distribution of unburned fuel droplets (particles) in a thruster plume with respect to particle size and angle from plume centerline. The thruster plume particle sizes and respective velocities are based on a model chronicled in reference [4]; however, the droplet flux model was revised in 2008 by the ISS Space Environments team to reduce excess conservatism and improve correlation with flight experiment and ground test data [5]. The revised plume model specifies unburned propellant droplets with diameters between 1 and 12 μm and limiting velocities ranging from 2.5 to 3 km/s, as summarized in Table 4-1. The normalized plume particle/droplet distribution by angle off of the plume centerline is shown in Figure 4-2.

Table 4-1. Particle sizes and velocities in ISS bipropellant thruster plumes based on the 2008 droplet flux model.

Particle Size **(μm)**	Limiting Particle Velocity **(km/s)**	Kinetic Energy* **(J)**
1	3.05	3.53E-09
5	2.9	3.99E-07
10	2.65	2.67E-06

*Kinetic energy calculated for a NTO particle; density = 1.45g/cc

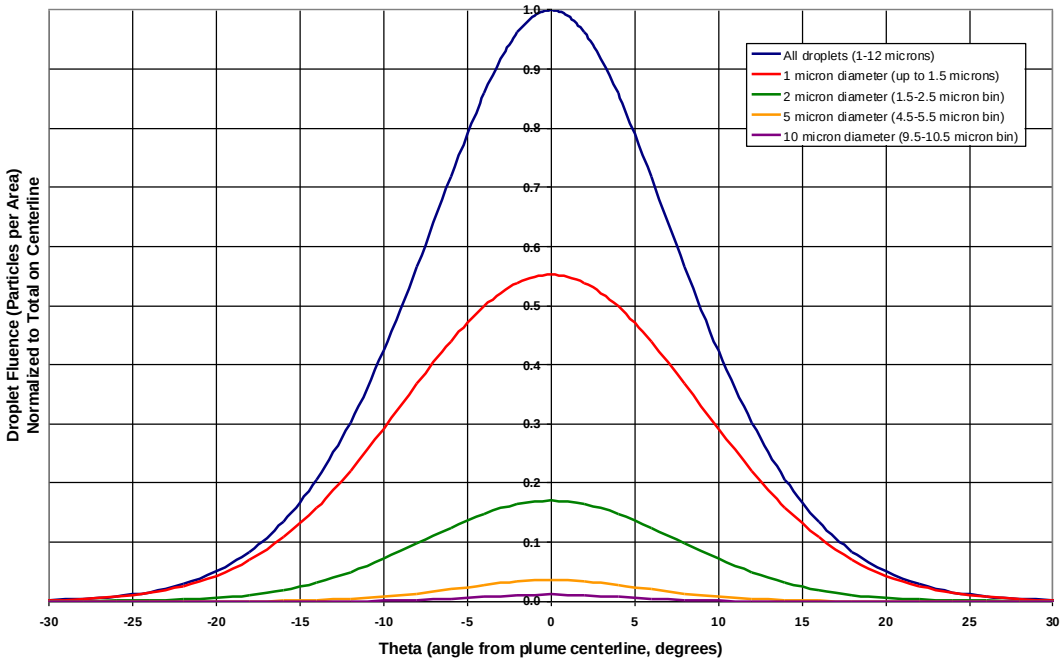

Figure 4-2. Normalized droplet fluence versus angle off-centerline for various droplet sizes.

The particle distribution is coded inside the NASAN-3 contamination computer model. NASAN-3 is an integrated computer model, utilizing NASTRAN™ geometric models, view factor calculations, and transport routines to analyze induced contamination on an ISS configuration, with results available in tabular or graphical formats. The thruster plume particle distribution was adapted for each ISS engine type depending on thrust, propellant mass flow rate, and nozzle length [4, 6]. Using NASAN-3, RV thruster firings can be simulated to calculate contamination and particle fluence to Orbiter surfaces.

4.2 RV Proximity Operations

The RV traffic to ISS involves multiple ISS docking ports, as shown in Figure 4-3. The FGB nadir, DC-1 nadir, SM aft, and the MRM2 zenith docking ports were all considered for DDO studies. RV thruster firing activities that could result in plume impingement to docked Orbiter surfaces include approach/docking proximity operations and undocking/separation proximity operations. Soyuz thruster tests, which typically occur a few days prior to vehicle undocking, could result in plume impingement to the Orbiter. Thruster plume induced contamination and particle fluence to Orbiter external surfaces due to ISS reboost/attitude control thruster firings (from the SM or mated Progress vehicles) is negligible. Figure 4-4 shows some example

hemispherical views from RV thrusters that may plume Orbiter surfaces during ISS proximity operations.

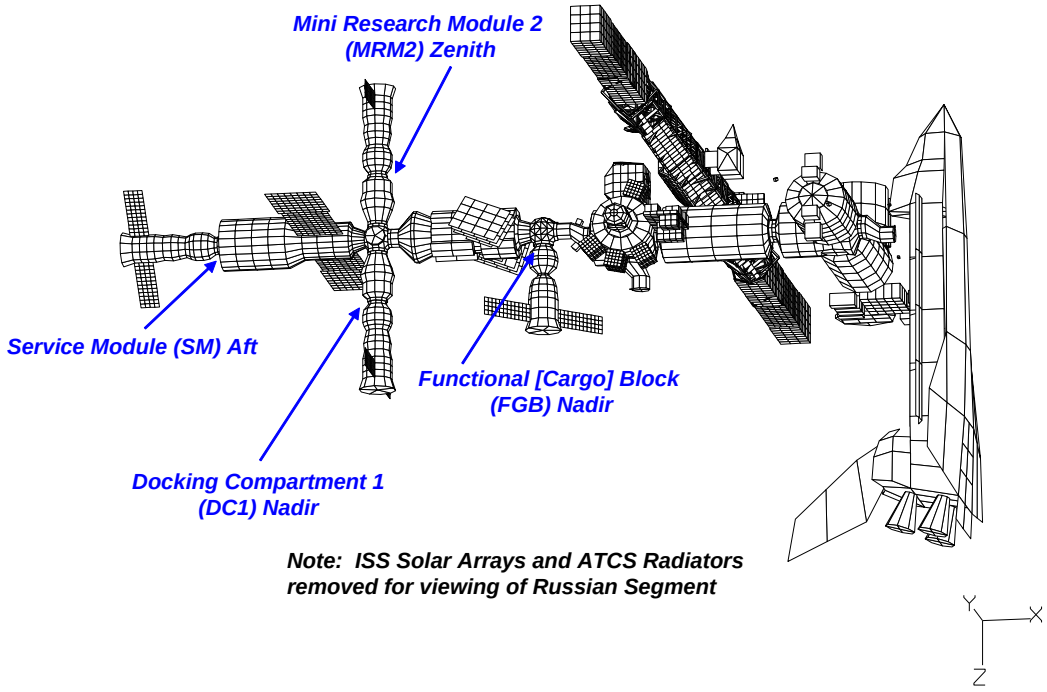

Figure 4-3. RV docking ports (Stage 5R Configuration, November 2009).

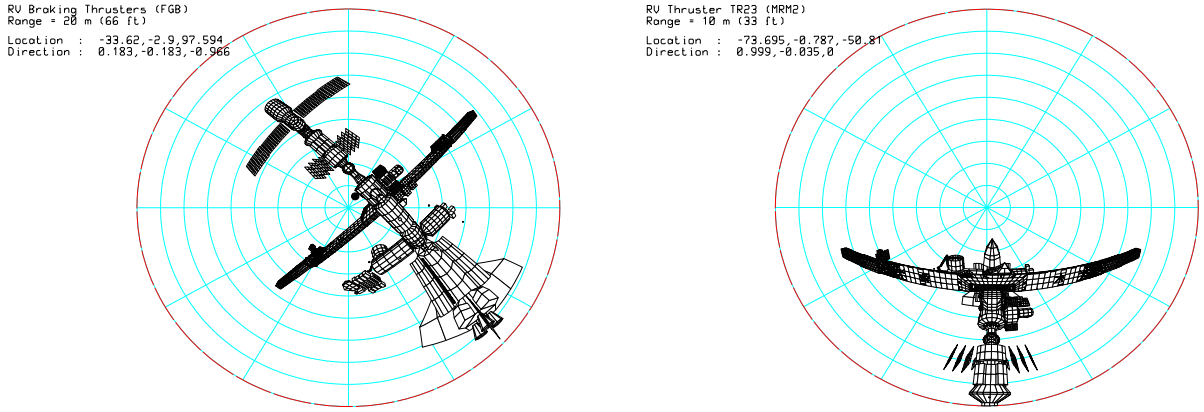

a) RV braking thruster at range of 20 meters (m) from FGB nadir docking port.

b) RV side-firing thruster at range of 10 m from MRM2 zenith docking port.

Figure 4-4. Example hemispherical views from Russian vehicle thrusters during ISS proximity operations.

Available jet firing data for RV proximity operations is limited. The ISS Space Environments team utilizes post-flight jet firing histories provided by Rocket and Space Corporation-Energia (RSC-E) for analyses involving RV approaches to ISS. The relevant post-flight data set includes six nominal approach cases with vehicle range and thruster firing records (2S, 3S, 8S Soyuz missions and 14P, 15P, 16P Progress missions). For RV separations, RSC-E provided a generic timeline of RV braking thruster firings (side-firing/lateral thrusters not characterized). The range

and thruster firing timelines for the six approach cases and generic separation case are mapped to each of the four RS docking ports (accounting for docking port orientation as defined in SSP 30129 [7]) for analysis purposes.

Sufficient information for accurate modeling of translation or attitude dispersions during approach and separation proximity operations is not available. With the exception of MRM2 separations, for which RSC-E supplied specific trajectory information, the ISS Space Environments team typically assumes the RVs remain straight, level, and aligned with the docking port during simulations. RSC-E has concurred with this practice. No jet firing data are available for off-nominal or contingency scenarios (e.g., abort, thruster failure).

Soyuz thruster tests are performed manually by the crew inside the vehicle. The crew utilizes the hand controllers to fire the thrusters and monitors the command response on the Soyuz displays. The crew procedure is to deflect the hand controllers for 1 second in each direction. If the crew does not see the appropriate response on their display in a given axis, they will then repeat the test in that axis [8]. To simulate a Soyuz thruster test, the ISS Space Environments team assumes each Soyuz thruster is fired for 2 seconds total (1 second for the baseline test and 1 second for the potential repeat test).

4.3 Orbiter Sensitive Surfaces

The SSP identified the Orbiter sensitive surfaces of concern for thruster plume contamination and particle impact damage. These surfaces, shown in Figure 4-5, include:

1. Crew cabin windows
2. OBSS sensors
3. Cameras on PLB bulkheads, keel, and SRMS
4. PLBD TCS radiators
5. General PLB surfaces (bottom, sides, and bulkheads)
6. RCC located on the Orbiter wing leading edge (WLE)

The ISS Space Environments team conducted an analysis program to characterize plume contamination deposition and particle fluences to these Orbiter surfaces due to RV proximity operations and thruster tests. Plume contamination and particle fluence analysis results for listed items 1 to 5 are reported in Table 4-2 through Table 4-6. The ISS Space Environments team conducted an in-depth test and analysis program to assess integrated thruster plume particle impact damage to the Orbiter RCC. The details of this activity are reported in Section 4.7.

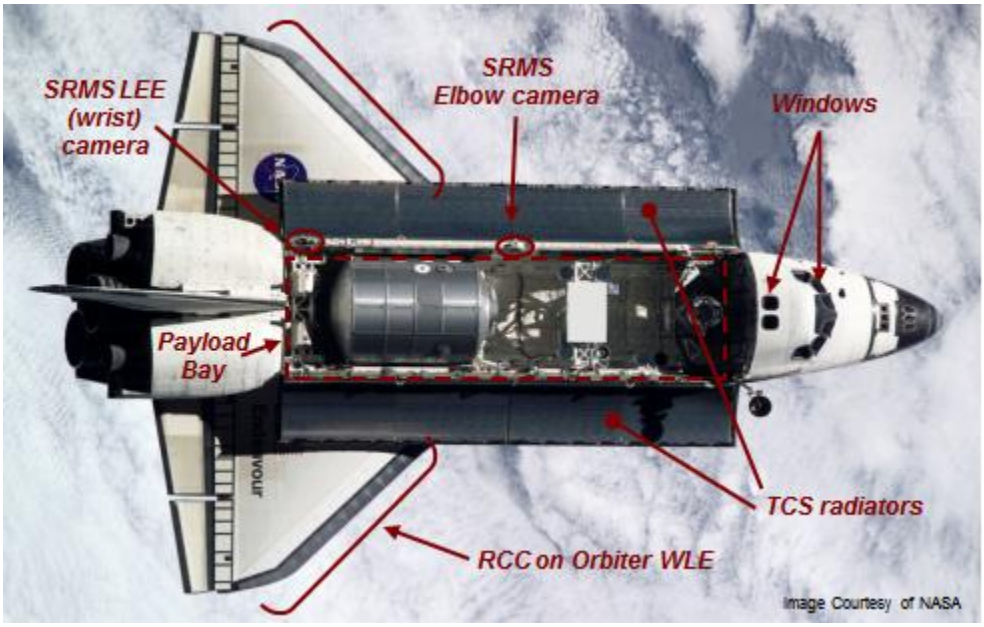

a) Space Shuttle Orbiter on-orbit.

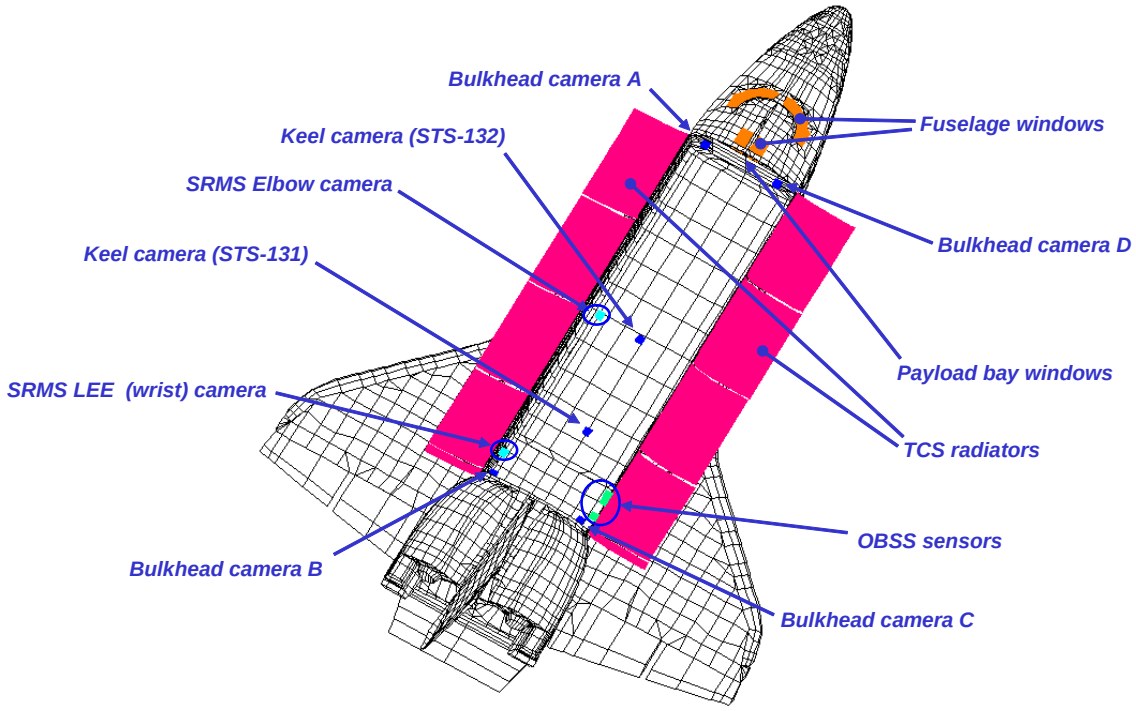

b) Space Shuttle Orbiter NASTRAN™ model.

Figure 4-5. Orbiter surfaces of concern for thruster plume induced contamination and particle impact damage.

4.4 Thruster Plume Particle Fluence and Contamination to Orbiter Sensitive Surfaces

ISS Space Environments team conducted analyses to characterize RV thruster pluming of Orbiter windows, cameras, OBSS, TCS radiators, and PLB surfaces during DDO. Analysis products included

1. Particle fluence results for evaluating potential erosion;
2. Initial contaminant deposit results for toxicity evaluations;
3. Final contaminant deposit results for surface optical property degradation evaluations.

Thruster plume induced erosion calculations are specific to the impacted material. The Space Environments team lacks sufficient data on Orbiter surfaces/materials to support this type of analysis. Therefore, particle fluence results (i.e., total number of particles per square centimeter per event) were provided instead so that Orbiter could evaluate impact damage to their materials. The particle fluences were calculated for particle diameter bins of 1-5, 6-10, and 11-12 μm. These sizes were selected to support planned SSP ground hypervelocity impact testing (i.e., 5 and 10 μm diameters are common projectile sizes for hypervelocity impact testing).

Calculations of thruster induced contamination addressed both initial and final contaminant deposit. The initial deposit, including unburned UDMH and NTO, MMH-nitrates, NDMA, and NVR, was provided to support Orbiter evaluation of toxicology issues. The final or permanent contaminant deposit, including MMH-nitrates, NDMA, and NVR, was provided to support Orbiter evaluation of surface optical property degradation.

Particle fluence and contamination analysis results for nominal RV proximity operations are reported in Tables 4-2 through 4-6. An alternative analysis case for nominal RV approach proximity operations is presented in Section 4.5. This alternative case was selected to produce more conservative results for the Orbiter windows specifically. Thruster induced particle fluence results for a synthetic abort scenario, which was tailored to maximize pluming to the Orbiter windows, are reported in Section 4.6. The ISS and Orbiter direction conventions used to report the analysis results are shown in Figure 4-6.

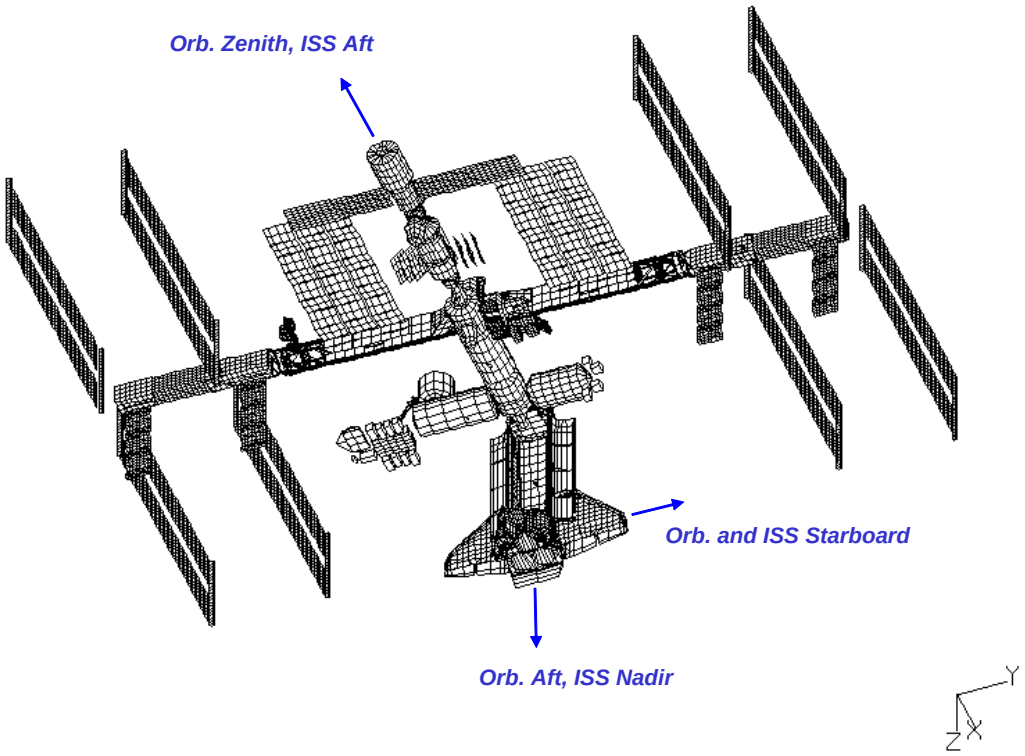

Figure 4-6. ISS and Orbiter direction conventions.

The OPO must determine acceptability of RV thruster pluming of Orbiter external surfaces. The thruster plume particle fluence and contamination analysis results reported herein were delivered to the OPO for evaluation of potential impacts to Orbiter hardware. [9, 10, 11]

4.4.1 Nominal RV Proximity Operations

Thruster induced particle fluence and contamination deposition for nominal RV proximity operations were analyzed using available RV jet firing data as described in Section 4.2. For nominal proximity operations, the ISS Space Environments team assumed the RVs remain straight, level, and aligned with the docking port for all simulations except for RV separations from the MRM2 docking port. RSC-E supplied specific trajectory information for this case. For the purposes of this analysis, RV proximity operations consist of three events: approach, thruster test (Soyuz only), and separation.

Example results for approach are shown in the color contours in Figure 4-7 and Figure 4-8. Figure 4-7 shows the predicted fluence of particles with 1 to 5 µm diameters for the 8S approach jet firing history applied to each docking port. Figure 4-8 shows the predicted initial and final contamination deposition for the same jet firing history applied to the FGB nadir docking port.

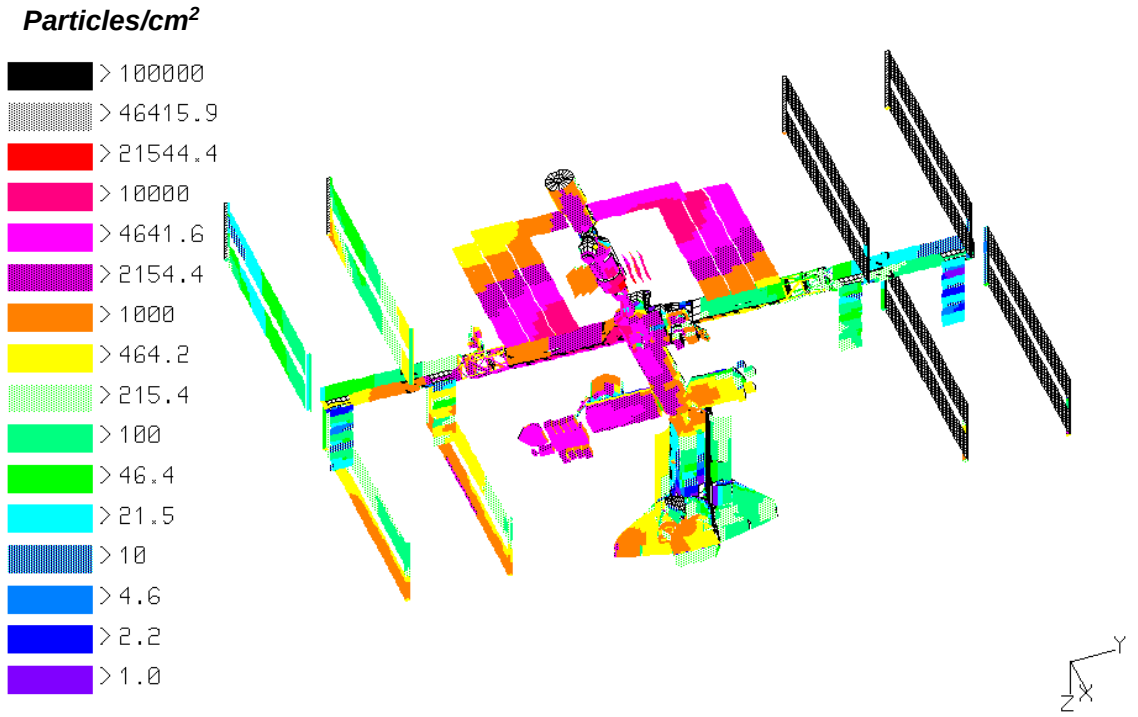

a) Results for approach to FGB nadir (view of ISS with Orbiter mated).

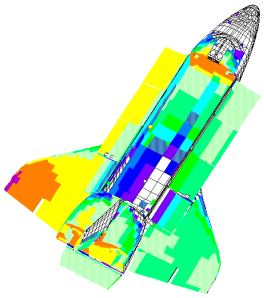

b) Results for approach to FGB nadir (view of Orbiter only).

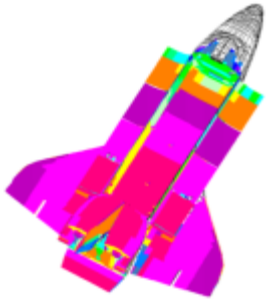

c) Results for approach to DC-1 nadir.

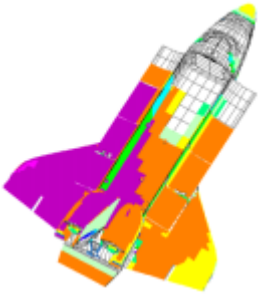

d) Results for approach to SM aft.

e) Results for approach to MRM2 zenith.

Figure 4-7. Example particle fluence results for RV approach (1 to 5 μm particles; 8S-based jet firing history).

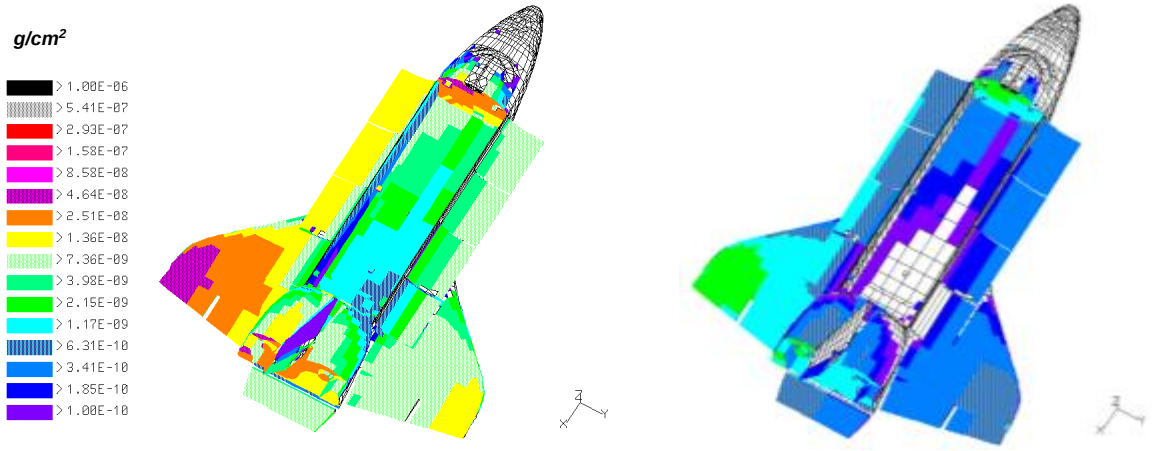

a) Initial plume contamination results.

b) Final/permanent plume contamination results.

Figure 4-8. Example plume contamination results for Russian vehicle approach to FGB nadir (8S-based jet firing history).

Tabular results for each of the Orbiter sensitive surfaces (i.e., windows, OBSS sensors, cameras, TCS radiators, and PLB) are provided in Table 4-2 through Table 4-6. The tabular results include particle fluence, initial contamination, and final (i.e., permanent) contamination to the applicable surface for RV proximity operations to each of the four docking ports (i.e., FGB Nadir, DC-1 Nadir, SM Aft, and MRM2 Zenith). The particle fluence results are further broken out by particle diameter bins (i.e., 1 to 5 µm, 6 to 10 µm, and 11to 12 µm).

For RV approach proximity operations, all six nominal approach cases were analyzed (i.e., post-flight cases 2S, 3S, 8S Soyuz missions, and 14P, 15P, 16P Progress missions). For conservatism, the maximum plume particle fluence/contamination result from all six approach cases is reported in the tabular results. It should be noted that the maximum result was determined uniquely for each sensitive surface and docking port combination. For example, the 8S Soyuz jet firing history produced the maximum particle fluence to Orbiter front windows for RV approach to the MRM2 docking port. This is demonstrated by Figure 4-9, which shows the cumulative particle fluence to the Orbiter front windows versus range for all six jet firing histories.

It should be noted that the smallest particles constitute the vast majority in the fluence results. For example, for the 8S approach jet firing history applied to the MRM2 docking port, the 1 to 2 µm diameter particles constitute over 92 percent of the particle fluence to the Orbiter front windows. Additional information is provided in Figure 4-10, which shows the cumulative particle fluence versus range for various particle sizes. This could be an important consideration when interpreting hypervelocity impact test results, since 5 µm is the smallest projectile diameter typically used for this kind of testing.

The tabular results in Table 4-2 through Table 4-6 include a single event max corresponding to the maximum fluence/contamination value out of all individual proximity operations events (i.e., RV approach, Soyuz thruster test, and RV separation). The tabular results include the total for all three events (i.e., results for approach, Soyuz thruster test, and separation combined). In checks of results, the separation and Soyuz thruster test results were usually minor compared to the

approach results. However, given the limited available data, applying the single event max values for evaluating any individual proximity operations event (i.e., RV approach, Soyuz thruster test, or RV separation) is recommended for conservatism.

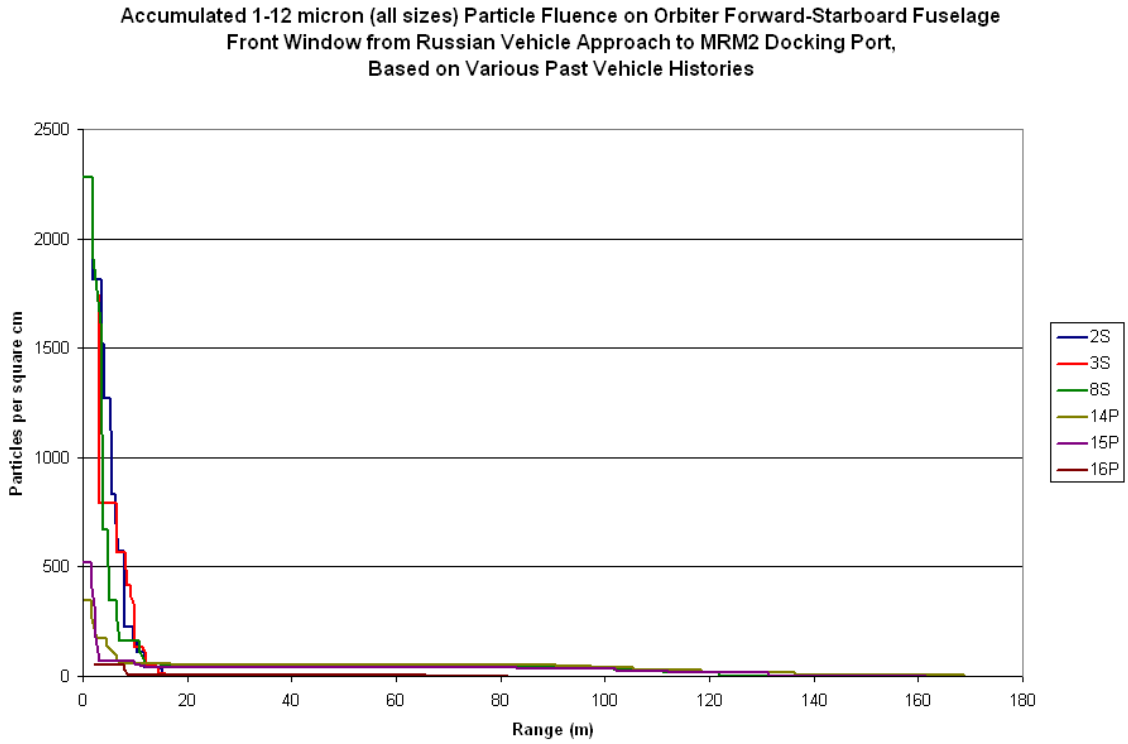

Figure 4-9. Cumulative particle fluence vs. range for RV approach to the MRM2 docking port.

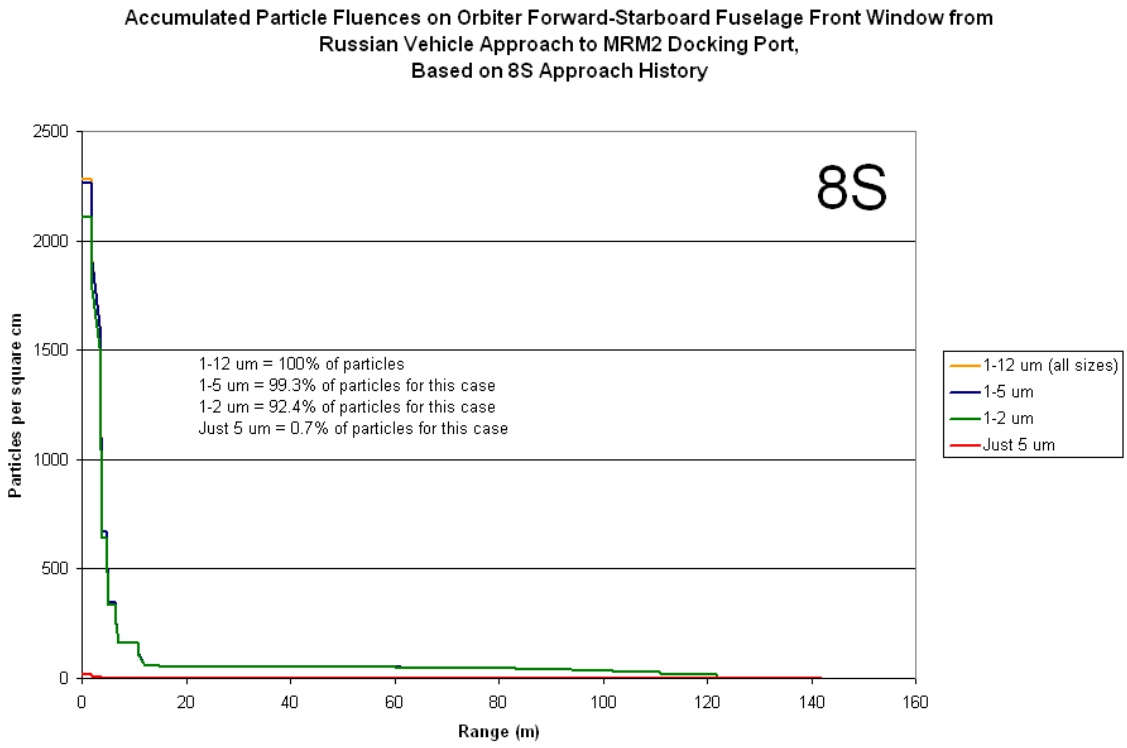

Figure 4-10. Cumulative particle fluence vs. range by particle size for RV approach to the MRM2 docking port.

Table 4-2. Tabular Results for Orbiter Windows.

FGB Nadir Proximity Operations Particle Fluence Results (in particles/cm^2) for Orbiter Windows

		1-5 µm Particles		6-10 µm Particles		11-12 µm Particles		All Particles (1-12 µm)	
Window	Surface Normal Direction	Single Event Max	Total*	Single Event Max	Total*	Single Event Max	Total*	Single Event Max	Total*
Fwd-Stbd fuselage window (side)	Orb starboard/ISS starboard	2	2	0	0	0	0	2	2
Fwd-Stbd fuselage window (middle)	Orb stbd-fwd/ISS stbd-zenith	0	0	0	0	0	0	0	0
Fwd-Stbd fuselage window (front)	Orb forward/ISS zenith	0	0	0	0	0	0	0	0
Fwd-Stbd fuselage window (overhead)	Orb zenith/ISS aft	0	0	0	0	0	0	0	0
Fwd-Port fuselage window (side)	Orb port/ISS port	9	9	0	0	0	0	9	9
Fwd-Port fuselage window (middle)	Orb port-fwd/ISS port-zenith	0	0	0	0	0	0	0	0
Fwd-Port fuselage window (front)	Orb forward/ISS zenith	0	0	0	0	0	0	0	0
Fwd-Port fuselage window (overhead)	Orb zenith/ISS aft	9	9	0	0	0	0	9	9
Payload bay window (starboard)	Orb aft/ISS nadir	0	0	0	0	0	0	0	0
Payload bay window (port)	Orb aft/ISS nadir	0	0	0	0	0	0	0	0

DC1 Nadir Proximity Operations Particle Fluence Results (in particles/cm^2) for Orbiter Windows

		1-5 µm Particles		6-10 µm Particles		11-12 µm Particles		All Particles (1-12 µm)	
Window	Surface Normal Direction	Single Event Max	Total*	Single Event Max	Total*	Single Event Max	Total*	Single Event Max	Total*
Fwd-Stbd fuselage window (side)	Orb starboard/ISS starboard	0	0	0	0	0	0	0	0
Fwd-Stbd fuselage window (middle)	Orb stbd-fwd/ISS stbd-zenith	0	0	0	0	0	0	0	0
Fwd-Stbd fuselage window (front)	Orb forward/ISS zenith	0	0	0	0	0	0	0	0
Fwd-Stbd fuselage window (overhead)	Orb zenith/ISS aft	10	10	0	0	0	0	10	10
Fwd-Port fuselage window (side)	Orb port/ISS port	1	1	0	0	0	0	1	1
Fwd-Port fuselage window (middle)	Orb port-fwd/ISS port-zenith	0	0	0	0	0	0	0	0
Fwd-Port fuselage window (front)	Orb forward/ISS zenith	0	0	0	0	0	0	0	0
Fwd-Port fuselage window (overhead)	Orb zenith/ISS aft	0	0	0	0	0	0	0	0
Payload bay window (starboard)	Orb aft/ISS nadir	0	0	0	0	0	0	0	0
Payload bay window (port)	Orb aft/ISS nadir	0	0	0	0	0	0	0	0

SM Aft Proximity Operations Particle Fluence Results (in particles/cm^2) for Orbiter Windows

		1-5 µm Particles		6-10 µm Particles		11-12 µm Particles		All Particles (1-12 µm)	
Window	Surface Normal Direction	Single Event Max	Total*	Single Event Max	Total*	Single Event Max	Total*	Single Event Max	Total*
Fwd-Stbd fuselage window (side)	Orb starboard/ISS starboard	0	0	0	0	0	0	0	0
Fwd-Stbd fuselage window (middle)	Orb stbd-fwd/ISS stbd-zenith	0	0	0	0	0	0	0	0
Fwd-Stbd fuselage window (front)	Orb forward/ISS zenith	0	0	0	0	0	0	0	0
Fwd-Stbd fuselage window (overhead)	Orb zenith/ISS aft	0	0	0	0	0	0	0	0
Fwd-Port fuselage window (side)	Orb port/ISS port	20	20	0	0	0	0	20	20
Fwd-Port fuselage window (middle)	Orb port-fwd/ISS port-zenith	0	0	0	0	0	0	0	0
Fwd-Port fuselage window (front)	Orb forward/ISS zenith	0	0	0	0	0	0	0	0
Fwd-Port fuselage window (overhead)	Orb zenith/ISS aft	0	0	0	0	0	0	0	0
Payload bay window (starboard)	Orb aft/ISS nadir	0	0	0	0	0	0	0	0
Payload bay window (port)	Orb aft/ISS nadir	0	0	0	0	0	0	0	0

MRM2 Zenith Proximity Operations Particle Fluence Results (in particles/cm^2) for Orbiter Windows

		1-5 µm Particles		6-10 µm Particles		11-12 µm Particles		All Particles (1-12 µm)	
Window	Surface Normal Direction	Single Event Max	Total*	Single Event Max	Total*	Single Event Max	Total*	Single Event Max	Total*
Fwd-Stbd fuselage window (side)	Orb starboard/ISS starboard	1238	1238	5	5	0	0	1243	1243
Fwd-Stbd fuselage window (middle)	Orb stbd-fwd/ISS stbd-zenith	1703	1703	8	8	0	0	1712	1712
Fwd-Stbd fuselage window (front)	Orb forward/ISS zenith	2264	2264	14	14	0	0	2279	2279
Fwd-Stbd fuselage window (overhead)	Orb zenith/ISS aft	485	485	0	0	0	0	485	485
Fwd-Port fuselage window (side)	Orb port/ISS port	1240	1240	5	5	0	0	1245	1245
Fwd-Port fuselage window (middle)	Orb port-fwd/ISS port-zenith	1735	1735	9	9	0	0	1743	1743
Fwd-Port fuselage window (front)	Orb forward/ISS zenith	2259	2259	14	14	0	0	2274	2274
Fwd-Port fuselage window (overhead)	Orb zenith/ISS aft	487	487	0	0	0	0	487	487
Payload bay window (starboard)	Orb aft/ISS nadir	0	0	0	0	0	0	0	0
Payload bay window (port)	Orb aft/ISS nadir	0	0	0	0	0	0	0	0

Initial Deposition Results (in g/cm^2) for Orbiter Windows

		FGB Nadir		DC1 Nadir		SM Aft		MRM2 Zenith	
Window	Surface Normal Direction	Single Event Max	Total*	Single Event Max	Total*	Single Event Max	Total*	Single Event Max	Total*
Fwd-Stbd fuselage window (side)	Orb starboard/ISS starboard	1.1E-10	1.1E-10	4.5E-11	4.5E-11	2.6E-16	2.6E-16	3.5E-08	3.5E-08
Fwd-Stbd fuselage window (middle)	Orb stbd-fwd/ISS stbd-zenith	0.0E+00	0.0E+00	8.4E-16	8.4E-16	4.6E-15	4.6E-15	4.8E-08	4.8E-08
Fwd-Stbd fuselage window (front)	Orb forward/ISS zenith	0.0E+00	0.0E+00	0.0E+00	0.0E+00	0.0E+00	0.0E+00	6.3E-08	6.3E-08
Fwd-Stbd fuselage window (overhead)	Orb zenith/ISS aft	0.0E+00	0.0E+00	6.6E-10	6.6E-10	0.0E+00	0.0E+00	2.2E-08	2.2E-08
Fwd-Port fuselage window (side)	Orb port/ISS port	3.9E-10	3.9E-10	7.9E-11	7.9E-11	5.0E-10	5.0E-10	3.6E-08	3.6E-08
Fwd-Port fuselage window (middle)	Orb port-fwd/ISS port-zenith	0.0E+00	0.0E+00	2.3E-13	2.3E-13	0.0E+00	0.0E+00	4.9E-08	4.9E-08
Fwd-Port fuselage window (front)	Orb forward/ISS zenith	0.0E+00	0.0E+00	0.0E+00	0.0E+00	0.0E+00	0.0E+00	6.4E-08	6.4E-08
Fwd-Port fuselage window (overhead)	Orb zenith/ISS aft	4.8E-10	4.8E-10	3.7E-13	3.7E-13	0.0E+00	0.0E+00	2.2E-08	2.2E-08
Payload bay window (starboard)	Orb aft/ISS nadir	0.0E+00	0.0E+00	0.0E+00	0.0E+00	0.0E+00	0.0E+00	0.0E+00	0.0E+00
Payload bay window (port)	Orb aft/ISS nadir	1.4E-11	1.4E-11	9.3E-11	9.3E-11	0.0E+00	0.0E+00	0.0E+00	0.0E+00

Permanent Deposition Results (in g/cm^2) for Orbiter Windows

		FGB Nadir		DC1 Nadir		SM Aft		MRM2 Zenith	
Window	Surface Normal Direction	Single Event Max	Total*	Single Event Max	Total*	Single Event Max	Total*	Single Event Max	Total*
Fwd-Stbd fuselage window (side)	Orb starboard/ISS starboard	6.1E-12	6.1E-12	2.5E-12	2.5E-12	1.4E-17	1.4E-17	1.9E-09	1.9E-09
Fwd-Stbd fuselage window (middle)	Orb stbd-fwd/ISS stbd-zenith	0.0E+00	0.0E+00	4.7E-17	4.7E-17	2.5E-16	2.5E-16	2.6E-09	2.6E-09
Fwd-Stbd fuselage window (front)	Orb forward/ISS zenith	0.0E+00	0.0E+00	0.0E+00	0.0E+00	0.0E+00	0.0E+00	3.5E-09	3.5E-09
Fwd-Stbd fuselage window (overhead)	Orb zenith/ISS aft	0.0E+00	0.0E+00	3.6E-11	3.6E-11	0.0E+00	0.0E+00	1.2E-09	1.2E-09
Fwd-Port fuselage window (side)	Orb port/ISS port	2.1E-11	2.1E-11	4.4E-12	4.4E-12	2.8E-11	2.8E-11	2.0E-09	2.0E-09
Fwd-Port fuselage window (middle)	Orb port-fwd/ISS port-zenith	0.0E+00	0.0E+00	1.3E-14	1.3E-14	0.0E+00	0.0E+00	2.7E-09	2.7E-09
Fwd-Port fuselage window (front)	Orb forward/ISS zenith	0.0E+00	0.0E+00	0.0E+00	0.0E+00	0.0E+00	0.0E+00	3.5E-09	3.5E-09
Fwd-Port fuselage window (overhead)	Orb zenith/ISS aft	2.6E-11	2.6E-11	2.0E-14	2.0E-14	0.0E+00	0.0E+00	1.2E-09	1.2E-09
Payload bay window (starboard)	Orb aft/ISS nadir	0.0E+00	0.0E+00	0.0E+00	0.0E+00	0.0E+00	0.0E+00	0.0E+00	0.0E+00
Payload bay window (port)	Orb aft/ISS nadir	8.0E-13	8.0E-13	5.2E-12	5.2E-12	0.0E+00	0.0E+00	0.0E+00	0.0E+00

*Approach, Soyuz Thruster Test, and Separation results combined

Table 4-3. Tabular Results for Orbiter Boom Sensor System.

FGB Nadir Proximity Operations Particle Fluence Results (in particles/cm^2) for OBSS

		1-5 µm Particles		6-10 µm Particles		11-12 µm Particles		All Particles (1-12 µm)	
Sensor	Receiver Surface	Single Event Max	Total*	Single Event Max	Total*	Single Event Max	Total*	Single Event Max	Total*
IDC	Orb port/ISS port	11	11	0	0	0	0	11	11
IDC	Orb aft/ISS nadir	0	0	0	0	0	0	0	0
IDC	Orb starboard/ISS starboard	0	0	0	0	0	0	0	0
IDC	Orb forward/ISS zenith	0	0	0	0	0	0	0	0
IDC	Orb zenith/ISS aft	99	99	0	0	0	0	100	100
IDC	Orb nadir/ISS forward	0	0	0	0	0	0	0	0
LCS	Orb port/ISS port	5	5	0	0	0	0	6	6
LCS	Orb aft/ISS nadir	31	31	0	0	0	0	31	31
LCS	Orb starboard/ISS starboard	0	0	0	0	0	0	0	0
LCS	Orb forward/ISS zenith	0	0	0	0	0	0	0	0
LCS	Orb zenith/ISS aft	70	70	0	0	0	0	70	70
LCS	Orb nadir/ISS forward	0	0	0	0	0	0	0	0
LDRI-ITVC	Orb port/ISS port	4	4	0	0	0	0	4	4
LDRI-ITVC	Orb aft/ISS nadir	96	96	0	0	0	0	96	96
LDRI-ITVC	Orb starboard/ISS starboard	0	0	0	0	0	0	0	0
LDRI-ITVC	Orb forward/ISS zenith	0	0	0	0	0	0	0	0
LDRI-ITVC	Orb zenith/ISS aft	56	56	1	1	0	0	56	56
LDRI-ITVC	Orb nadir/ISS forward	0	0	0	0	0	0	0	0

DC1 Nadir Proximity Operations Particle Fluence Results (in particles/cm^2) for OBSS

		1-5 µm Particles		6-10 µm Particles		11-12 µm Particles		All Particles (1-12 µm)	
Sensor	Receiver Surface	Single Event Max	Total*	Single Event Max	Total*	Single Event Max	Total*	Single Event Max	Total*
IDC	Orb port/ISS port	2120	2205	116	118	18	18	2255	2342
IDC	Orb aft/ISS nadir	324	324	23	23	4	4	351	351
IDC	Orb starboard/ISS starboard	0	0	0	0	0	0	0	0
IDC	Orb forward/ISS zenith	1980	2200	38	43	4	5	2022	2248
IDC	Orb zenith/ISS aft	32775	34060	1820	1845	288	289	34882	36193
IDC	Orb nadir/ISS forward	0	0	0	0	0	0	0	0
LCS	Orb port/ISS port	2177	2257	119	121	19	19	2315	2396
LCS	Orb aft/ISS nadir	3160	3160	94	94	12	12	3266	3266
LCS	Orb starboard/ISS starboard	0	0	0	0	0	0	0	0
LCS	Orb forward/ISS zenith	259	259	20	20	3	3	282	282
LCS	Orb zenith/ISS aft	33633	34828	1867	1887	294	295	35793	37010
LCS	Orb nadir/ISS forward	0	0	0	0	0	0	0	0
LDRI-ITVC	Orb port/ISS port	2257	2321	123	124	19	19	2400	2464
LDRI-ITVC	Orb aft/ISS nadir	3089	3089	93	93	12	12	3194	3194
LDRI-ITVC	Orb starboard/ISS starboard	0	0	0	0	0	0	0	0
LDRI-ITVC	Orb forward/ISS zenith	1776	1976	39	42	6	6	1822	2024
LDRI-ITVC	Orb zenith/ISS aft	35627	36614	1971	1983	307	308	37904	38904
LDRI-ITVC	Orb nadir/ISS forward	0	0	0	0	0	0	0	0

SM Aft Proximity Operations Particle Fluence Results (in particles/cm^2) for OBSS

		1-5 µm Particles		6-10 µm Particles		11-12 µm Particles		All Particles (1-12 µm)	
Sensor	Receiver Surface	Single Event Max	Total*	Single Event Max	Total*	Single Event Max	Total*	Single Event Max	Total*
IDC	Orb port/ISS port	69	121	1	1	0	0	70	122
IDC	Orb aft/ISS nadir	0	0	0	0	0	0	0	0
IDC	Orb starboard/ISS starboard	0	0	0	0	0	0	0	0
IDC	Orb forward/ISS zenith	317	481	2	4	0	0	320	484
IDC	Orb zenith/ISS aft	2008	3046	16	23	0	1	2024	3069
IDC	Orb nadir/ISS forward	0	0	0	0	0	0	0	0
LCS	Orb port/ISS port	69	121	1	1	0	0	69	122
LCS	Orb aft/ISS nadir	0	0	0	0	0	0	0	0
LCS	Orb starboard/ISS starboard	0	0	0	0	0	0	0	0
LCS	Orb forward/ISS zenith	0	0	0	0	0	0	0	0
LCS	Orb zenith/ISS aft	2002	3033	16	23	0	1	2018	3056
LCS	Orb nadir/ISS forward	0	0	0	0	0	0	0	0
LDRI-ITVC	Orb port/ISS port	67	117	1	1	0	0	68	118
LDRI-ITVC	Orb aft/ISS nadir	0	0	0	0	0	0	0	0
LDRI-ITVC	Orb starboard/ISS starboard	0	0	0	0	0	0	0	0
LDRI-ITVC	Orb forward/ISS zenith	335	575	3	4	0	0	338	579
LDRI-ITVC	Orb zenith/ISS aft	1991	2992	16	23	0	1	2008	3016
LDRI-ITVC	Orb nadir/ISS forward	0	0	0	0	0	0	0	0

MRM2 Zenith Proximity Operations Particle Fluence Results (in particles/cm^2) for OBSS

		1-5 µm Particles		6-10 µm Particles		11-12 µm Particles		All Particles (1-12 µm)	
Sensor	Receiver Surface	Single Event Max	Total*	Single Event Max	Total*	Single Event Max	Total*	Single Event Max	Total*
IDC	Orb port/ISS port	0	0	0	0	0	0	0	0
IDC	Orb aft/ISS nadir	0	0	0	0	0	0	0	0
IDC	Orb starboard/ISS starboard	0	0	0	0	0	0	0	0
IDC	Orb forward/ISS zenith	13	13	0	0	0	0	13	13
IDC	Orb zenith/ISS aft	5	5	0	0	0	0	5	5
IDC	Orb nadir/ISS forward	0	0	0	0	0	0	0	0
LCS	Orb port/ISS port	0	0	0	0	0	0	0	0
LCS	Orb aft/ISS nadir	0	0	0	0	0	0	0	0
LCS	Orb starboard/ISS starboard	0	0	0	0	0	0	0	0
LCS	Orb forward/ISS zenith	0	0	0	0	0	0	0	0
LCS	Orb zenith/ISS aft	5	5	0	0	0	0	5	5
LCS	Orb nadir/ISS forward	0	0	0	0	0	0	0	0
LDRI-ITVC	Orb port/ISS port	0	0	0	0	0	0	0	0
LDRI-ITVC	Orb aft/ISS nadir	0	0	0	0	0	0	0	0
LDRI-ITVC	Orb starboard/ISS starboard	0	0	0	0	0	0	0	0
LDRI-ITVC	Orb forward/ISS zenith	2	2	0	0	0	0	2	2
LDRI-ITVC	Orb zenith/ISS aft	7	7	0	0	0	0	7	7
LDRI-ITVC	Orb nadir/ISS forward	0	0	0	0	0	0	0	0

Initial Deposition Results (in g/cm^2) for OBSS

		FGB Nadir		DC1 Nadir		SM Aft		MRM2 Zenith	
Sensor	Receiver Surface	Single Event Max	Total*	Single Event Max	Total*	Single Event Max	Total*	Single Event Max	Total*
IDC	Orb port/ISS port	4.8E-10	4.9E-10	7.1E-08	7.3E-08	1.7E-09	3.0E-09	1.1E-11	1.1E-11
IDC	Orb aft/ISS nadir	4.0E-11	4.0E-11	1.1E-08	1.1E-08	0.0E+00	0.0E+00	0.0E+00	0.0E+00
IDC	Orb starboard/ISS starboard	0.0E+00	0.0E+00	0.0E+00	0.0E+00	0.0E+00	0.0E+00	0.0E+00	0.0E+00
IDC	Orb forward/ISS zenith	2.3E-10	2.6E-10	5.0E-08	5.6E-08	8.0E-09	1.2E-08	5.9E-10	6.7E-10
IDC	Orb zenith/ISS aft	5.8E-09	5.9E-09	1.1E-06	1.1E-06	5.1E-08	7.7E-08	3.3E-10	3.5E-10
IDC	Orb nadir/ISS forward	0.0E+00	0.0E+00	0.0E+00	0.0E+00	0.0E+00	0.0E+00	0.0E+00	0.0E+00
LCS	Orb port/ISS port	3.3E-10	3.3E-10	7.3E-08	7.5E-08	1.7E-09	3.0E-09	1.1E-11	1.1E-11
LCS	Orb aft/ISS nadir	2.2E-09	2.2E-09	9.1E-08	9.1E-08	0.0E+00	0.0E+00	0.0E+00	0.0E+00
LCS	Orb starboard/ISS starboard	0.0E+00	0.0E+00	0.0E+00	0.0E+00	0.0E+00	0.0E+00	0.0E+00	0.0E+00
LCS	Orb forward/ISS zenith	2.5E-11	2.5E-11	9.8E-09	9.8E-09	8.8E-12	1.1E-11	0.0E+00	0.0E+00
LCS	Orb zenith/ISS aft	5.0E-09	5.0E-09	1.1E-06	1.2E-06	5.0E-08	7.6E-08	3.3E-10	3.3E-10
LCS	Orb nadir/ISS forward	0.0E+00	0.0E+00	0.0E+00	0.0E+00	0.0E+00	0.0E+00	0.0E+00	0.0E+00
LDRI-ITVC	Orb port/ISS port	2.5E-10	2.5E-10	7.5E-08	7.7E-08	1.7E-09	2.9E-09	4.6E-11	4.6E-11
LDRI-ITVC	Orb aft/ISS nadir	3.1E-09	3.1E-09	8.9E-08	8.9E-08	0.0E+00	0.0E+00	0.0E+00	0.0E+00
LDRI-ITVC	Orb starboard/ISS starboard	0.0E+00	0.0E+00	0.0E+00	0.0E+00	0.0E+00	0.0E+00	0.0E+00	0.0E+00
LDRI-ITVC	Orb forward/ISS zenith	2.0E-10	2.3E-10	4.3E-08	4.8E-08	8.5E-09	1.4E-08	4.8E-10	4.8E-10
LDRI-ITVC	Orb zenith/ISS aft	3.9E-09	4.0E-09	1.2E-06	1.2E-06	5.0E-08	7.5E-08	8.5E-10	9.2E-10
LDRI-ITVC	Orb nadir/ISS forward	0.0E+00	0.0E+00	0.0E+00	0.0E+00	0.0E+00	0.0E+00	0.0E+00	0.0E+00

Permanent Deposition Results (in g/cm^2) for OBSS

		FGB Nadir		DC1 Nadir		SM Aft		MRM2 Zenith	
Sensor	Receiver Surface	Single Event Max	Total*	Single Event Max	Total*	Single Event Max	Total*	Single Event Max	Total*
IDC	Orb port/ISS port	2.6E-11	2.7E-11	3.9E-09	4.0E-09	9.4E-11	1.6E-10	5.8E-13	5.8E-13
IDC	Orb aft/ISS nadir	2.2E-12	2.2E-12	6.2E-10	6.2E-10	0.0E+00	0.0E+00	0.0E+00	0.0E+00
IDC	Orb starboard/ISS starboard	0.0E+00	0.0E+00	0.0E+00	0.0E+00	0.0E+00	0.0E+00	0.0E+00	0.0E+00
IDC	Orb forward/ISS zenith	1.3E-11	1.4E-11	2.8E-09	3.1E-09	4.4E-10	6.7E-10	3.2E-11	3.7E-11
IDC	Orb zenith/ISS aft	3.2E-10	3.3E-10	6.1E-08	6.3E-08	2.8E-09	4.2E-09	1.8E-11	1.9E-11
IDC	Orb nadir/ISS forward	0.0E+00	0.0E+00	0.0E+00	0.0E+00	0.0E+00	0.0E+00	0.0E+00	0.0E+00
LCS	Orb port/ISS port	1.8E-11	1.8E-11	4.0E-09	4.1E-09	9.3E-11	1.6E-10	5.8E-13	5.8E-13
LCS	Orb aft/ISS nadir	1.2E-10	1.2E-10	5.0E-09	5.0E-09	0.0E+00	0.0E+00	0.0E+00	0.0E+00
LCS	Orb starboard/ISS starboard	0.0E+00	0.0E+00	0.0E+00	0.0E+00	0.0E+00	0.0E+00	0.0E+00	0.0E+00
LCS	Orb forward/ISS zenith	1.4E-12	1.4E-12	5.4E-10	5.4E-10	4.8E-13	6.0E-13	0.0E+00	0.0E+00
LCS	Orb zenith/ISS aft	2.7E-10	2.8E-10	6.2E-08	6.4E-08	2.8E-09	4.2E-09	1.8E-11	1.8E-11
LCS	Orb nadir/ISS forward	0.0E+00	0.0E+00	0.0E+00	0.0E+00	0.0E+00	0.0E+00	0.0E+00	0.0E+00
LDRI-ITVC	Orb port/ISS port	1.4E-11	1.4E-11	4.2E-09	4.2E-09	9.2E-11	1.6E-10	2.5E-12	2.5E-12
LDRI-ITVC	Orb aft/ISS nadir	1.7E-10	1.7E-10	4.9E-09	4.9E-09	0.0E+00	0.0E+00	0.0E+00	0.0E+00
LDRI-ITVC	Orb starboard/ISS starboard	0.0E+00	0.0E+00	0.0E+00	0.0E+00	0.0E+00	0.0E+00	0.0E+00	0.0E+00
LDRI-ITVC	Orb forward/ISS zenith	1.1E-11	1.3E-11	2.4E-09	2.7E-09	4.7E-10	8.0E-10	2.6E-11	2.6E-11
LDRI-ITVC	Orb zenith/ISS aft	2.2E-10	2.2E-10	6.6E-08	6.7E-08	2.8E-09	4.2E-09	4.7E-11	5.1E-11
LDRI-ITVC	Orb nadir/ISS forward	0.0E+00	0.0E+00	0.0E+00	0.0E+00	0.0E+00	0.0E+00	0.0E+00	0.0E+00

*Approach, Soyuz Thruster Test, and Separation results combined

Table 4-4. Tabular Results for Orbiter Payload Bay and SRMS Cameras.

FGB Nadir Proximity Operations Particle Fluence Results (in particles/cm^2) for Payload Bay Bulkhead Cameras (A - D)

		1-5 µm Particles		6-10 µm Particles		11-12 µm Particles		All Particles (1-12 µm)	
Camera	Receiver Surface	Single Event Max	Total*	Single Event Max	Total*	Single Event Max	Total*	Single Event Max	Total*
A	Orb port/ISS port	0	0	0	0	0	0	0	0
A	Orb aft/ISS nadir	1929	1929	38	38	3	3	1970	1970
A	Orb starboard/ISS starboard	19	19	0	0	0	0	20	20
A	Orb forward/ISS zenith	0	0	0	0	0	0	0	0
A	Orb zenith/ISS aft	662	663	10	10	1	1	673	674
A	Orb nadir/ISS forward	0	0	0	0	0	0	0	0
B	Orb port/ISS port	0	0	0	0	0	0	0	0
B	Orb aft/ISS nadir	112	112	0	0	0	0	113	113
B	Orb starboard/ISS starboard	0	0	0	0	0	0	0	0
B	Orb forward/ISS zenith	1	1	0	0	0	0	1	1
B	Orb zenith/ISS aft	7	7	0	0	0	0	7	7
B	Orb nadir/ISS forward	0	0	0	0	0	0	0	0
C	Orb port/ISS port	0	0	0	0	0	0	0	0
C	Orb aft/ISS nadir	147	147	2	2	0	0	150	150
C	Orb starboard/ISS starboard	0	0	0	0	0	0	0	0
C	Orb forward/ISS zenith	0	0	0	0	0	0	0	0
C	Orb zenith/ISS aft	16	16	0	0	0	0	16	16
C	Orb nadir/ISS forward	0	0	0	0	0	0	0	0
D	Orb port/ISS port	42	42	0	0	0	0	43	43
D	Orb aft/ISS nadir	1301	1301	17	17	1	1	1319	1319
D	Orb starboard/ISS starboard	0	0	0	0	0	0	0	0
D	Orb forward/ISS zenith	0	0	0	0	0	0	0	0
D	Orb zenith/ISS aft	431	431	4	4	0	0	435	436

FGB Nadir Proximity Operations Particle Fluence Results (in particles/cm^2) for Payload Bay Keel Cameras

		1-5 µm Particles		6-10 µm Particles		11-12 µm Particles		All Particles (1-12 µm)	
Camera	Receiver Surface	Single Event Max	Total*	Single Event Max	Total*	Single Event Max	Total*	Single Event Max	Total*
STS-131	Orb port/ISS port	0	0	0	0	0	0	0	0
STS-131	Orb aft/ISS nadir	0	0	0	0	0	0	0	0
STS-131	Orb starboard/ISS starboard	0	0	0	0	0	0	0	0
STS-131	Orb forward/ISS zenith	0	0	0	0	0	0	0	0
STS-131	Orb zenith/ISS aft	1	1	0	0	0	0	1	1
STS-131	Orb nadir/ISS forward	0	0	0	0	0	0	0	0
STS-132	Orb port/ISS port	1	1	0	0	0	0	1	1
STS-132	Orb aft/ISS nadir	60	60	0	0	0	0	60	60
STS-132	Orb starboard/ISS starboard	0	0	0	0	0	0	0	0
STS-132	Orb forward/ISS zenith	0	0	0	0	0	0	0	0
STS-132	Orb zenith/ISS aft	68	68	0	0	0	0	68	68
STS-132	Orb nadir/ISS forward	0	0	0	0	0	0	0	0

FGB Nadir Proximity Operations Particle Fluence Results (in particles/cm^2) for SRMS Cameras

		1-5 µm Particles		6-10 µm Particles		11-12 µm Particles		All Particles (1-12 µm)	
Camera	Receiver Surface	Single Event Max	Total*	Single Event Max	Total*	Single Event Max	Total*	Single Event Max	Total*
SRMS LEE (wrist)	Orb port/ISS port	0	0	0	0	0	0	0	0
SRMS LEE (wrist)	Orb aft/ISS nadir	33	33	0	0	0	0	33	33
SRMS LEE (wrist)	Orb starboard/ISS starboard	1	1	0	0	0	0	1	1
SRMS LEE (wrist)	Orb forward/ISS zenith	1	1	0	0	0	0	1	1
SRMS LEE (wrist)	Orb zenith/ISS aft	85	85	0	0	0	0	86	86
SRMS LEE (wrist)	Orb nadir/ISS forward	0	0	0	0	0	0	0	0
SRMS Elbow	Orb port/ISS port	0	0	0	0	0	0	0	0
SRMS Elbow	Orb aft/ISS nadir	1757	1757	36	36	3	3	1796	1796
SRMS Elbow	Orb starboard/ISS starboard	18	18	0	0	0	0	18	18
SRMS Elbow	Orb forward/ISS zenith	0	0	0	0	0	0	0	0
SRMS Elbow	Orb zenith/ISS aft	618	619	10	10	1	1	629	630
SRMS Elbow	Orb nadir/ISS forward	0	0	0	0	0	0	0	0

DC1 Nadir Proximity Operations Particle Fluence Results (in particles/cm^2) for Payload Bay Bulkhead Cameras (A - D)

		1-5 µm Particles		6-10 µm Particles		11-12 µm Particles		All Particles (1-12 µm)	
Camera	Receiver Surface	Single Event Max	Total*	Single Event Max	Total*	Single Event Max	Total*	Single Event Max	Total*
A	Orb port/ISS port	0	0	0	0	0	0	0	0
A	Orb aft/ISS nadir	85	85	0	0	0	0	85	85
A	Orb starboard/ISS starboard	2	2	0	0	0	0	2	2
A	Orb forward/ISS zenith	0	0	0	0	0	0	0	0
A	Orb zenith/ISS aft	99	99	0	0	0	0	99	99
A	Orb nadir/ISS forward	0	0	0	0	0	0	0	0
B	Orb port/ISS port	0	0	0	0	0	0	0	0
B	Orb aft/ISS nadir	446	446	24	24	3	3	473	473
B	Orb starboard/ISS starboard	1889	1937	97	97	14	14	2000	2048
B	Orb forward/ISS zenith	1719	1913	39	41	5	5	1762	1959
B	Orb zenith/ISS aft	36739	37640	1777	1787	252	252	38768	39679
B	Orb nadir/ISS forward	0	0	0	0	0	0	0	0
C	Orb port/ISS port	1907	1956	110	110	17	17	2034	2083
C	Orb aft/ISS nadir	757	757	44	44	8	8	808	808
C	Orb starboard/ISS starboard	0	0	0	0	0	0	0	0
C	Orb forward/ISS zenith	1717	1910	44	47	7	7	1767	1964
C	Orb zenith/ISS aft	37682	38582	2139	2149	337	337	40158	41068
C	Orb nadir/ISS forward	0	0	0	0	0	0	0	0
D	Orb port/ISS port	2	2	0	0	0	0	2	2
D	Orb aft/ISS nadir	73	73	0	0	0	0	73	73
D	Orb starboard/ISS starboard	0	0	0	0	0	0	0	0
D	Orb forward/ISS zenith	0	0	0	0	0	0	0	0
D	Orb zenith/ISS aft	64	64	0	0	0	0	64	64
D	Orb nadir/ISS forward	0	0	0	0	0	0	0	0

DC1 Nadir Proximity Operations Particle Fluence Results (in particles/cm^2) for Payload Bay Keel Cameras

		1-5 µm Particles		6-10 µm Particles		11-12 µm Particles		All Particles (1-12 µm)	
Camera	Receiver Surface	Single Event Max	Total*	Single Event Max	Total*	Single Event Max	Total*	Single Event Max	Total*
STS-131	Orb port/ISS port	42	46	2	2	0	0	44	49
STS-131	Orb aft/ISS nadir	2912	2912	78	78	10	10	2999	2999
STS-131	Orb starboard/ISS starboard	3	3	0	0	0	0	3	3
STS-131	Orb forward/ISS zenith	1701	1882	99	110	14	15	1814	2007
STS-131	Orb zenith/ISS aft	23952	26001	1279	1402	199	216	25430	27619
STS-131	Orb nadir/ISS forward	0	0	0	0	0	0	0	0
STS-132	Orb port/ISS port	18	20	2	2	0	0	20	22
STS-132	Orb aft/ISS nadir	2010	2065	38	43	6	7	2054	2115
STS-132	Orb starboard/ISS starboard	33	36	3	3	1	1	36	40
STS-132	Orb forward/ISS zenith	0	0	0	0	0	0	0	0
STS-132	Orb zenith/ISS aft	23620	26160	2042	2262	380	420	26042	28842
STS-132	Orb nadir/ISS forward	0	0	0	0	0	0	0	0

DC1 Nadir Proximity Operations Particle Fluence Results (in particles/cm^2) for SRMS Cameras

		1-5 µm Particles		6-10 µm Particles		11-12 µm Particles		All Particles (1-12 µm)	
Camera	Receiver Surface	Single Event Max	Total*	Single Event Max	Total*	Single Event Max	Total*	Single Event Max	Total*
SRMS LEE (wrist)	Orb port/ISS port	0	0	0	0	0	0	0	0
SRMS LEE (wrist)	Orb aft/ISS nadir	3235	3235	91	91	10	10	3336	3336
SRMS LEE (wrist)	Orb starboard/ISS starboard	1897	1961	93	94	13	13	2003	2069
SRMS LEE (wrist)	Orb forward/ISS zenith	1950	2168	37	41	5	5	1992	2215
SRMS LEE (wrist)	Orb zenith/ISS aft	33482	34643	1624	1642	233	234	35339	36520
SRMS LEE (wrist)	Orb nadir/ISS forward	0	0	0	0	0	0	0	0
SRMS Elbow	Orb port/ISS port	0	0	0	0	0	0	0	0
SRMS Elbow	Orb aft/ISS nadir	2062	2096	40	43	5	5	2106	2144
SRMS Elbow	Orb starboard/ISS starboard	1163	1289	93	104	17	19	1273	1411
SRMS Elbow	Orb forward/ISS zenith	0	0	0	0	0	0	0	0
SRMS Elbow	Orb zenith/ISS aft	27250	30194	2219	2460	402	446	29871	33099
SRMS Elbow	Orb nadir/ISS forward	0	0	0	0	0	0	0	0

SM Aft Proximity Operations Particle Fluence Results (in particles/cm^2) for Payload Bay Bulkhead Cameras (A - D)

		1-5 µm Particles		6-10 µm Particles		11-12 µm Particles		All Particles (1-12 µm)	
Camera	Receiver Surface	Single Event Max	Total*	Single Event Max	Total*	Single Event Max	Total*	Single Event Max	Total*
A	Orb port/ISS port	0	0	0	0	0	0	0	0
A	Orb aft/ISS nadir	0	0	0	0	0	0	0	0
A	Orb starboard/ISS starboard	0	0	0	0	0	0	0	0
A	Orb forward/ISS zenith	0	0	0	0	0	0	0	0
A	Orb zenith/ISS aft	0	0	0	0	0	0	0	0
A	Orb nadir/ISS forward	0	0	0	0	0	0	0	0
B	Orb port/ISS port	0	0	0	0	0	0	0	0
B	Orb aft/ISS nadir	0	0	0	0	0	0	0	0
B	Orb starboard/ISS starboard	39	70	1	1	0	0	40	72
B	Orb forward/ISS zenith	547	1009	12	22	1	1	559	1032
B	Orb zenith/ISS aft	3043	4908	64	104	4	6	3111	5018
B	Orb nadir/ISS forward	0	0	0	0	0	0	0	0
C	Orb port/ISS port	61	106	1	1	0	0	62	107
C	Orb aft/ISS nadir	0	0	0	0	0	0	0	0
C	Orb starboard/ISS starboard	0	0	0	0	0	0	0	0
C	Orb forward/ISS zenith	356	612	3	5	0	0	359	617
C	Orb zenith/ISS aft	2054	3095	19	26	1	1	2073	3122
C	Orb nadir/ISS forward	0	0	0	0	0	0	0	0
D	Orb port/ISS port	0	0	0	0	0	0	0	0
D	Orb aft/ISS nadir	0	0	0	0	0	0	0	0
D	Orb starboard/ISS starboard	0	0	0	0	0	0	0	0
D	Orb forward/ISS zenith	0	0	0	0	0	0	0	0
D	Orb zenith/ISS aft	0	0	0	0	0	0	0	0
D	Orb nadir/ISS forward	0	0	0	0	0	0	0	0

SM Aft Proximity Operations Particle Fluence Results (in particles/cm^2) for Payload Bay Keel Cameras

		1-5 µm Particles		6-10 µm Particles		11-12 µm Particles		All Particles (1-12 µm)	
Camera	Receiver Surface	Single Event Max	Total*	Single Event Max	Total*	Single Event Max	Total*	Single Event Max	Total*
STS-131	Orb port/ISS port	15	26	0	0	0	0	16	26
STS-131	Orb aft/ISS nadir	0	0	0	0	0	0	0	0
STS-131	Orb starboard/ISS starboard	1	2	0	0	0	0	1	2
STS-131	Orb forward/ISS zenith	259	428	3	6	0	0	263	434
STS-131	Orb zenith/ISS aft	2140	3187	25	40	1	2	2166	3229
STS-131	Orb nadir/ISS forward	0	0	0	0	0	0	0	0
STS-132	Orb port/ISS port	5	5	0	0	0	0	5	5
STS-132	Orb aft/ISS nadir	0	0	0	0	0	0	0	0
STS-132	Orb starboard/ISS starboard	1	1	0	0	0	0	1	1
STS-132	Orb forward/ISS zenith	59	59	0	0	0	0	59	59
STS-132	Orb zenith/ISS aft	1082	1082	8	8	0	0	1090	1090
STS-132	Orb nadir/ISS forward	0	0	0	0	0	0	0	0

SM Aft Proximity Operations Particle Fluence Results (in particles/cm^2) for SRMS Cameras

		1-5 µm Particles		6-10 µm Particles		11-12 µm Particles		All Particles (1-12 µm)	
Camera	Receiver Surface	Single Event Max	Total*	Single Event Max	Total*	Single Event Max	Total*	Single Event Max	Total*
SRMS LEE (wrist)	Orb port/ISS port	0	0	0	0	0	0	0	0
SRMS LEE (wrist)	Orb aft/ISS nadir	0	0	0	0	0	0	0	0
SRMS LEE (wrist)	Orb starboard/ISS starboard	42	78	1	2	0	0	43	80
SRMS LEE (wrist)	Orb forward/ISS zenith	531	995	12	22	1	1	543	1019
SRMS LEE (wrist)	Orb zenith/ISS aft	3112	5096	66	112	4	7	3182	5215
SRMS LEE (wrist)	Orb nadir/ISS forward	0	0	0	0	0	0	0	0
SRMS Elbow	Orb port/ISS port	0	0	0	0	0	0	0	0
SRMS Elbow	Orb aft/ISS nadir	0	0	0	0	0	0	0	0
SRMS Elbow	Orb starboard/ISS starboard	25	38	0	1	0	0	26	38
SRMS Elbow	Orb forward/ISS zenith	242	379	4	6	0	0	246	385
SRMS Elbow	Orb zenith/ISS aft	2719	3972	38	61	2	3	2759	4035
SRMS Elbow	Orb nadir/ISS forward	0	0	0	0	0	0	0	0

MRM2 Zenith Proximity Operations Particle Fluence Results (in particles/cm^2) for Payload Bay Bulkhead Cameras (A - D)

		1-5 µm Particles		6-10 µm Particles		11-12 µm Particles		All Particles (1-12 µm)	
Camera	Receiver Surface	Single Event Max	Total*	Single Event Max	Total*	Single Event Max	Total*	Single Event Max	Total*
A	Orb port/ISS port	0	0	0	0	0	0	0	0
A	Orb aft/ISS nadir	0	0	0	0	0	0	0	0
A	Orb starboard/ISS starboard	1	1	0	0	0	0	1	1
A	Orb forward/ISS zenith	5	5	0	0	0	0	5	5
A	Orb zenith/ISS aft	88	88	0	0	0	0	88	88
A	Orb nadir/ISS forward	0	0	0	0	0	0	0	0
B	Orb port/ISS port	0	0	0	0	0	0	0	0
B	Orb aft/ISS nadir	0	0	0	0	0	0	0	0
B	Orb starboard/ISS starboard	0	0	0	0	0	0	0	0
B	Orb forward/ISS zenith	0	0	0	0	0	0	0	0
B	Orb zenith/ISS aft	0	0	0	0	0	0	0	0
B	Orb nadir/ISS forward	0	0	0	0	0	0	0	0
C	Orb port/ISS port	0	0	0	0	0	0	0	0
C	Orb aft/ISS nadir	0	0	0	0	0	0	0	0
C	Orb starboard/ISS starboard	0	0	0	0	0	0	0	0
C	Orb forward/ISS zenith	0	0	0	0	0	0	0	0
C	Orb zenith/ISS aft	0	0	0	0	0	0	0	0
C	Orb nadir/ISS forward	0	0	0	0	0	0	0	0
D	Orb port/ISS port	0	0	0	0	0	0	0	0
D	Orb aft/ISS nadir	0	0	0	0	0	0	0	0
D	Orb starboard/ISS starboard	0	0	0	0	0	0	0	0
D	Orb forward/ISS zenith	0	0	0	0	0	0	0	0
D	Orb zenith/ISS aft	0	0	0	0	0	0	0	0
D	Orb nadir/ISS forward	0	0	0	0	0	0	0	0

MRM2 Zenith Proximity Operations Particle Fluence Results (in particles/cm^2) for Payload Bay Keel Cameras

		1-5 µm Particles		6-10 µm Particles		11-12 µm Particles		All Particles (1-12 µm)	
Camera	Receiver Surface	Single Event Max	Total*	Single Event Max	Total*	Single Event Max	Total*	Single Event Max	Total*
STS-131	Orb port/ISS port	0	0	0	0	0	0	0	0
STS-131	Orb aft/ISS nadir	0	0	0	0	0	0	0	0
STS-131	Orb starboard/ISS starboard	0	0	0	0	0	0	0	0
STS-131	Orb forward/ISS zenith	0	0	0	0	0	0	0	0
STS-131	Orb zenith/ISS aft	0	0	0	0	0	0	0	0
STS-131	Orb nadir/ISS forward	0	0	0	0	0	0	0	0
STS-132	Orb port/ISS port	0	0	0	0	0	0	0	0
STS-132	Orb aft/ISS nadir	0	0	0	0	0	0	0	0
STS-132	Orb starboard/ISS starboard	0	0	0	0	0	0	0	0
STS-132	Orb forward/ISS zenith	0	0	0	0	0	0	0	0
STS-132	Orb zenith/ISS aft	1	1	0	0	0	0	1	1
STS-132	Orb nadir/ISS forward	0	0	0	0	0	0	0	0

MRM2 Zenith Proximity Operations Particle Fluence Results (in particles/cm^2) for SRMS Cameras

		1-5 µm Particles		6-10 µm Particles		11-12 µm Particles		All Particles (1-12 µm)	
Camera	Receiver Surface	Single Event Max	Total*	Single Event Max	Total*	Single Event Max	Total*	Single Event Max	Total*
SRMS LEE (wrist)	Orb port/ISS port	0	0	0	0	0	0	0	0
SRMS LEE (wrist)	Orb aft/ISS nadir	0	0	0	0	0	0	0	0
SRMS LEE (wrist)	Orb starboard/ISS starboard	0	0	0	0	0	0	0	0
SRMS LEE (wrist)	Orb forward/ISS zenith	4	4	0	0	0	0	4	4
SRMS LEE (wrist)	Orb zenith/ISS aft	0	0	0	0	0	0	0	0
SRMS LEE (wrist)	Orb nadir/ISS forward	0	0	0	0	0	0	0	0
SRMS Elbow	Orb port/ISS port	0	0	0	0	0	0	0	0
SRMS Elbow	Orb aft/ISS nadir	0	0	0	0	0	0	0	0
SRMS Elbow	Orb starboard/ISS starboard	0	0	0	0	0	0	0	0
SRMS Elbow	Orb forward/ISS zenith	38	38	0	0	0	0	38	38
SRMS Elbow	Orb zenith/ISS aft	9	9	0	0	0	0	9	9
SRMS Elbow	Orb nadir/ISS forward	0	0	0	0	0	0	0	0

Initial Deposition Results (in g/cm^2) for Payload Bay Bulkhead Cameras (A - D)

		FGB Nadir		DC1 Nadir		SM Aft		MRM2 Zenith	
Camera	Receiver Surface	Single Event Max	Total*	Single Event Max	Total*	Single Event Max	Total*	Single Event Max	Total*
A	Orb port/ISS port	0.0E+00	0.0E+00	0.0E+00	0.0E+00	0.0E+00	0.0E+00	0.0E+00	0.0E+00
A	Orb aft/ISS nadir	5.1E-08	5.1E-08	4.6E-09	4.6E-09	0.0E+00	0.0E+00	0.0E+00	0.0E+00
A	Orb starboard/ISS starboard	5.4E-10	5.6E-10	1.4E-10	1.4E-10	3.1E-17	3.1E-17	5.3E-11	5.3E-11
A	Orb forward/ISS zenith	0.0E+00	0.0E+00	0.0E+00	0.0E+00	0.0E+00	0.0E+00	1.9E-10	1.9E-10
A	Orb zenith/ISS aft	1.8E-08	1.9E-08	5.8E-09	5.8E-09	0.0E+00	0.0E+00	3.7E-09	3.7E-09
A	Orb nadir/ISS forward	0.0E+00	0.0E+00	0.0E+00	0.0E+00	0.0E+00	0.0E+00	0.0E+00	0.0E+00
B	Orb port/ISS port	0.0E+00	0.0E+00	0.0E+00	0.0E+00	0.0E+00	0.0E+00	0.0E+00	0.0E+00
B	Orb aft/ISS nadir	2.8E-09	2.8E-09	1.4E-08	1.4E-08	0.0E+00	0.0E+00	0.0E+00	0.0E+00
B	Orb starboard/ISS starboard	1.2E-10	1.3E-10	6.0E-08	6.1E-08	1.0E-09	1.9E-09	6.6E-18	6.6E-18
B	Orb forward/ISS zenith	2.9E-10	3.3E-10	4.2E-08	4.6E-08	1.4E-08	2.6E-08	0.0E+00	0.0E+00
B	Orb zenith/ISS aft	2.8E-09	2.9E-09	1.1E-06	1.2E-06	7.9E-08	1.3E-07	7.3E-11	7.3E-11
B	Orb nadir/ISS forward	0.0E+00	0.0E+00	0.0E+00	0.0E+00	0.0E+00	0.0E+00	0.0E+00	0.0E+00
C	Orb port/ISS port	1.3E-10	1.4E-10	6.4E-08	6.6E-08	1.5E-09	2.6E-09	8.1E-12	8.1E-12
C	Orb aft/ISS nadir	3.7E-09	3.7E-09	2.6E-08	2.6E-08	0.0E+00	0.0E+00	0.0E+00	0.0E+00
C	Orb starboard/ISS starboard	0.0E+00	0.0E+00	0.0E+00	0.0E+00	0.0E+00	0.0E+00	0.0E+00	0.0E+00
C	Orb forward/ISS zenith	1.7E-10	2.0E-10	4.2E-08	4.6E-08	9.0E-09	1.5E-08	1.7E-14	1.7E-14
C	Orb zenith/ISS aft	3.2E-09	3.3E-09	1.3E-06	1.3E-06	5.2E-08	7.8E-08	3.6E-11	3.6E-11
C	Orb nadir/ISS forward	0.0E+00	0.0E+00	0.0E+00	0.0E+00	0.0E+00	0.0E+00	0.0E+00	0.0E+00
D	Orb port/ISS port	1.2E-09	1.2E-09	1.3E-10	1.3E-10	7.4E-18	7.4E-18	1.1E-12	1.1E-12
D	Orb aft/ISS nadir	3.5E-08	3.6E-08	4.1E-09	4.1E-09	0.0E+00	0.0E+00	0.0E+00	0.0E+00
D	Orb starboard/ISS starboard	0.0E+00	0.0E+00	0.0E+00	0.0E+00	0.0E+00	0.0E+00	0.0E+00	0.0E+00
D	Orb forward/ISS zenith	0.0E+00	0.0E+00	0.0E+00	0.0E+00	4.2E-17	4.2E-17	0.0E+00	0.0E+00
D	Orb zenith/ISS aft	1.2E-08	1.3E-08	3.5E-09	3.5E-09	3.5E-15	3.5E-15	0.0E+00	0.0E+00
D	Orb nadir/ISS forward	0.0E+00	0.0E+00	0.0E+00	0.0E+00	0.0E+00	0.0E+00	0.0E+00	0.0E+00

Initial Deposition Results (in g/cm^2) for Payload Bay Keel Cameras

		FGB Nadir		DC1 Nadir		SM Aft		MRM2 Zenith	
Camera	Receiver Surface	Single Event Max	Total*	Single Event Max	Total*	Single Event Max	Total*	Single Event Max	Total*
STS-131	Orb port/ISS port	2.6E-11	2.8E-11	1.4E-09	1.5E-09	3.8E-10	6.4E-10	0.0E+00	0.0E+00
STS-131	Orb aft/ISS nadir	2.3E-10	2.3E-10	8.1E-08	8.1E-08	0.0E+00	0.0E+00	0.0E+00	0.0E+00
STS-131	Orb starboard/ISS starboard	1.8E-11	1.8E-11	1.0E-10	1.1E-10	4.0E-11	5.7E-11	0.0E+00	0.0E+00
STS-131	Orb forward/ISS zenith	7.8E-11	1.0E-10	5.5E-08	6.1E-08	6.6E-09	1.1E-08	0.0E+00	0.0E+00
STS-131	Orb zenith/ISS aft	1.4E-09	1.5E-09	7.9E-07	8.6E-07	5.4E-08	8.1E-08	1.9E-12	1.9E-12
STS-131	Orb nadir/ISS forward	0.0E+00	0.0E+00	0.0E+00	0.0E+00	0.0E+00	0.0E+00	0.0E+00	0.0E+00
STS-132	Orb port/ISS port	7.9E-11	8.2E-11	7.6E-10	8.4E-10	1.3E-10	1.3E-10	0.0E+00	0.0E+00
STS-132	Orb aft/ISS nadir	3.1E-09	3.1E-09	5.6E-08	5.9E-08	0.0E+00	0.0E+00	0.0E+00	0.0E+00
STS-132	Orb starboard/ISS starboard	1.4E-11	1.5E-11	1.4E-09	1.5E-09	2.4E-11	2.4E-11	0.0E+00	0.0E+00
STS-132	Orb forward/ISS zenith	4.4E-11	5.8E-11	0.0E+00	0.0E+00	1.4E-09	1.4E-09	0.0E+00	0.0E+00
STS-132	Orb zenith/ISS aft	3.9E-09	4.1E-09	9.7E-07	1.1E-06	2.7E-08	2.7E-08	5.9E-11	5.9E-11
STS-132	Orb nadir/ISS forward	0.0E+00	0.0E+00	0.0E+00	0.0E+00	0.0E+00	0.0E+00	0.0E+00	0.0E+00

Initial Deposition Results (in g/cm^2) for SRMS Cameras

		FGB Nadir		DC1 Nadir		SM Aft		MRM2 Zenith	
Camera	Receiver Surface	Single Event Max	Total*	Single Event Max	Total*	Single Event Max	Total*	Single Event Max	Total*
SRMS LEE (wrist)	Orb port/ISS port	0.0E+00	0.0E+00	0.0E+00	0.0E+00	0.0E+00	0.0E+00	0.0E+00	0.0E+00
SRMS LEE (wrist)	Orb aft/ISS nadir	2.6E-09	2.6E-09	9.1E-08	9.1E-08	0.0E+00	0.0E+00	0.0E+00	0.0E+00
SRMS LEE (wrist)	Orb starboard/ISS starboard	2.4E-10	2.4E-10	6.0E-08	6.2E-08	1.1E-09	2.1E-09	5.4E-12	5.4E-12
SRMS LEE (wrist)	Orb forward/ISS zenith	2.8E-10	3.2E-10	4.8E-08	5.4E-08	1.4E-08	2.6E-08	2.1E-10	2.1E-10
SRMS LEE (wrist)	Orb zenith/ISS aft	6.5E-09	6.6E-09	1.1E-06	1.1E-06	8.1E-08	1.3E-07	2.6E-11	2.6E-11
SRMS LEE (wrist)	Orb nadir/ISS forward	0.0E+00	0.0E+00	0.0E+00	0.0E+00	0.0E+00	0.0E+00	0.0E+00	0.0E+00
SRMS Elbow	Orb port/ISS port	0.0E+00	0.0E+00	0.0E+00	0.0E+00	0.0E+00	0.0E+00	0.0E+00	0.0E+00
SRMS Elbow	Orb aft/ISS nadir	4.7E-08	4.7E-08	5.8E-08	5.9E-08	0.0E+00	0.0E+00	0.0E+00	0.0E+00
SRMS Elbow	Orb starboard/ISS starboard	5.8E-10	5.9E-10	4.6E-08	5.2E-08	6.4E-10	9.5E-10	1.5E-11	1.5E-11
SRMS Elbow	Orb forward/ISS zenith	3.7E-11	7.2E-11	0.0E+00	0.0E+00	6.1E-09	9.5E-09	1.3E-09	1.3E-09
SRMS Elbow	Orb zenith/ISS aft	1.9E-08	2.0E-08	1.1E-06	1.2E-06	6.8E-08	9.9E-08	3.1E-10	3.1E-10
SRMS Elbow	Orb nadir/ISS forward	0.0E+00	0.0E+00	0.0E+00	0.0E+00	0.0E+00	0.0E+00	0.0E+00	0.0E+00

*Approach, Soyuz Thruster Test, and Separation results combined

Permanent Deposition Results (in g/cm^2) for Payload Bay Bulkhead Cameras (A - D)

		FGB Nadir		DC1 Nadir		SM Aft		MRM2 Zenith	
Camera	Receiver Surface	Single Event Max	Total*	Single Event Max	Total*	Single Event Max	Total*	Single Event Max	Total*
A	Orb port/ISS port	0.0E+00	0.0E+00	0.0E+00	0.0E+00	0.0E+00	0.0E+00	0.0E+00	0.0E+00
A	Orb aft/ISS nadir	2.8E-09	2.8E-09	2.5E-10	2.5E-10	0.0E+00	0.0E+00	0.0E+00	0.0E+00
A	Orb starboard/ISS starboard	3.0E-11	3.1E-11	7.9E-12	7.9E-12	1.7E-18	1.7E-18	2.9E-12	2.9E-12
A	Orb forward/ISS zenith	0.0E+00	0.0E+00	0.0E+00	0.0E+00	0.0E+00	0.0E+00	1.0E-11	1.0E-11
A	Orb zenith/ISS aft	1.0E-09	1.0E-09	3.2E-10	3.2E-10	0.0E+00	0.0E+00	2.0E-10	2.0E-10
A	Orb nadir/ISS forward	0.0E+00	0.0E+00	0.0E+00	0.0E+00	0.0E+00	0.0E+00	0.0E+00	0.0E+00
B	Orb port/ISS port	0.0E+00	0.0E+00	0.0E+00	0.0E+00	0.0E+00	0.0E+00	0.0E+00	0.0E+00
B	Orb aft/ISS nadir	1.6E-10	1.6E-10	7.9E-10	7.9E-10	0.0E+00	0.0E+00	0.0E+00	0.0E+00
B	Orb starboard/ISS starboard	6.8E-12	7.1E-12	3.3E-09	3.4E-09	5.7E-11	1.0E-10	3.6E-19	3.6E-19
B	Orb forward/ISS zenith	1.6E-11	1.8E-11	2.3E-09	2.6E-09	7.9E-10	1.4E-09	0.0E+00	0.0E+00
B	Orb zenith/ISS aft	1.5E-10	1.6E-10	6.3E-08	6.4E-08	4.4E-09	7.0E-09	4.0E-12	4.0E-12
B	Orb nadir/ISS forward	0.0E+00	0.0E+00	0.0E+00	0.0E+00	0.0E+00	0.0E+00	0.0E+00	0.0E+00
C	Orb port/ISS port	7.3E-12	7.5E-12	3.5E-09	3.6E-09	8.3E-11	1.4E-10	4.4E-13	4.4E-13
C	Orb aft/ISS nadir	2.0E-10	2.0E-10	1.4E-09	1.4E-09	0.0E+00	0.0E+00	0.0E+00	0.0E+00
C	Orb starboard/ISS starboard	0.0E+00	0.0E+00	0.0E+00	0.0E+00	0.0E+00	0.0E+00	0.0E+00	0.0E+00
C	Orb forward/ISS zenith	9.6E-12	1.1E-11	2.3E-09	2.6E-09	5.0E-10	8.5E-10	9.4E-16	9.4E-16
C	Orb zenith/ISS aft	1.8E-10	1.8E-10	7.0E-08	7.1E-08	2.9E-09	4.3E-09	2.0E-12	2.0E-12
C	Orb nadir/ISS forward	0.0E+00	0.0E+00	0.0E+00	0.0E+00	0.0E+00	0.0E+00	0.0E+00	0.0E+00
D	Orb port/ISS port	6.6E-11	6.8E-11	7.3E-12	7.3E-12	4.1E-19	4.1E-19	6.2E-14	6.2E-14
D	Orb aft/ISS nadir	1.9E-09	2.0E-09	2.3E-10	2.3E-10	0.0E+00	0.0E+00	0.0E+00	0.0E+00
D	Orb starboard/ISS starboard	0.0E+00	0.0E+00	0.0E+00	0.0E+00	0.0E+00	0.0E+00	0.0E+00	0.0E+00
D	Orb forward/ISS zenith	0.0E+00	0.0E+00	0.0E+00	0.0E+00	2.3E-18	2.3E-18	0.0E+00	0.0E+00
D	Orb zenith/ISS aft	6.8E-10	7.0E-10	1.9E-10	1.9E-10	1.9E-16	1.9E-16	0.0E+00	0.0E+00
D	Orb nadir/ISS forward	0.0E+00	0.0E+00	0.0E+00	0.0E+00	0.0E+00	0.0E+00	0.0E+00	0.0E+00

Permanent Deposition Results (in g/cm^2) for Payload Bay Keel Cameras

		FGB Nadir		DC1 Nadir		SM Aft		MRM2 Zenith	
Camera	Receiver Surface	Single Event Max	Total*	Single Event Max	Total*	Single Event Max	Total*	Single Event Max	Total*
STS-131	Orb port/ISS port	1.4E-12	1.5E-12	7.5E-11	8.3E-11	2.1E-11	3.5E-11	0.0E+00	0.0E+00
STS-131	Orb aft/ISS nadir	1.3E-11	1.3E-11	4.5E-09	4.5E-09	0.0E+00	0.0E+00	0.0E+00	0.0E+00
STS-131	Orb starboard/ISS starboard	9.7E-13	1.0E-12	5.7E-12	6.1E-12	2.2E-12	3.2E-12	0.0E+00	0.0E+00
STS-131	Orb forward/ISS zenith	4.3E-12	5.7E-12	3.0E-09	3.4E-09	3.6E-10	6.0E-10	0.0E+00	0.0E+00
STS-131	Orb zenith/ISS aft	7.5E-11	8.0E-11	4.4E-08	4.7E-08	3.0E-09	4.5E-09	1.1E-13	1.1E-13
STS-131	Orb nadir/ISS forward	0.0E+00	0.0E+00	0.0E+00	0.0E+00	0.0E+00	0.0E+00	0.0E+00	0.0E+00
STS-132	Orb port/ISS port	4.3E-12	4.5E-12	4.2E-11	4.6E-11	7.0E-12	7.0E-12	0.0E+00	0.0E+00
STS-132	Orb aft/ISS nadir	1.7E-10	1.7E-10	3.1E-09	3.2E-09	0.0E+00	0.0E+00	0.0E+00	0.0E+00
STS-132	Orb starboard/ISS starboard	7.7E-13	8.3E-13	7.5E-11	8.3E-11	1.3E-12	1.3E-12	0.0E+00	0.0E+00
STS-132	Orb forward/ISS zenith	2.4E-12	3.2E-12	0.0E+00	0.0E+00	8.0E-11	8.0E-11	0.0E+00	0.0E+00
STS-132	Orb zenith/ISS aft	2.2E-10	2.3E-10	5.4E-08	5.9E-08	1.5E-09	1.5E-09	3.3E-12	3.3E-12
STS-132	Orb nadir/ISS forward	0.0E+00	0.0E+00	0.0E+00	0.0E+00	0.0E+00	0.0E+00	0.0E+00	0.0E+00

Permanent Deposition Results (in g/cm^2) for SRMS Cameras

		FGB Nadir		DC1 Nadir		SM Aft		MRM2 Zenith	
Camera	Receiver Surface	Single Event Max	Total*	Single Event Max	Total*	Single Event Max	Total*	Single Event Max	Total*
SRMS LEE (wrist)	Orb port/ISS port	0.0E+00	0.0E+00	0.0E+00	0.0E+00	0.0E+00	0.0E+00	0.0E+00	0.0E+00
SRMS LEE (wrist)	Orb aft/ISS nadir	1.4E-10	1.4E-10	5.0E-09	5.0E-09	0.0E+00	0.0E+00	0.0E+00	0.0E+00
SRMS LEE (wrist)	Orb starboard/ISS starboard	1.3E-11	1.3E-11	3.3E-09	3.4E-09	6.3E-11	1.1E-10	3.0E-13	3.0E-13
SRMS LEE (wrist)	Orb forward/ISS zenith	1.5E-11	1.8E-11	2.7E-09	3.0E-09	7.7E-10	1.4E-09	1.1E-11	1.1E-11
SRMS LEE (wrist)	Orb zenith/ISS aft	3.6E-10	3.6E-10	5.8E-08	6.0E-08	4.5E-09	7.3E-09	1.4E-12	1.4E-12
SRMS LEE (wrist)	Orb nadir/ISS forward	0.0E+00	0.0E+00	0.0E+00	0.0E+00	0.0E+00	0.0E+00	0.0E+00	0.0E+00
SRMS Elbow	Orb port/ISS port	0.0E+00	0.0E+00	0.0E+00	0.0E+00	0.0E+00	0.0E+00	0.0E+00	0.0E+00
SRMS Elbow	Orb aft/ISS nadir	2.6E-09	2.6E-09	3.2E-09	3.3E-09	0.0E+00	0.0E+00	0.0E+00	0.0E+00
SRMS Elbow	Orb starboard/ISS starboard	3.2E-11	3.3E-11	2.6E-09	2.8E-09	3.5E-11	5.3E-11	8.5E-13	8.5E-13
SRMS Elbow	Orb forward/ISS zenith	2.1E-12	4.0E-12	0.0E+00	0.0E+00	3.4E-10	5.2E-10	7.2E-11	7.2E-11
SRMS Elbow	Orb zenith/ISS aft	1.1E-09	1.1E-09	6.1E-08	6.7E-08	3.8E-09	5.5E-09	1.7E-11	1.7E-11
SRMS Elbow	Orb nadir/ISS forward	0.0E+00	0.0E+00	0.0E+00	0.0E+00	0.0E+00	0.0E+00	0.0E+00	0.0E+00

*Approach, Soyuz Thruster Test, and Separation results combined

Table 4-5. Tabular Results for TCS Radiators.

FGB Nadir Proximity Operations Particle Fluence Results (in particles/cm^2) for Orbiter TCS Radiators

		1-5 µm Particles		6-10 µm Particles		11-12 µm Particles		All Particles (1-12 µm)	
Radiator	Surface Normal Direction	Single Event Max	Total*	Single Event Max	Total*	Single Event Max	Total*	Single Event Max	Total*
TCS Starboard [Max on Surface]	Orb zenith/ISS aft	307	309	3	3	0	0	311	312
TCS Port [Max on Surface]	Orb zenith/ISS aft	736	750	16	16	2	2	754	767
TCS Starboard [Surface Average]	Orb zenith/ISS aft	128	128	1	1	0	0	129	129
TCS Port [Surface Average]	Orb zenith/ISS aft	380	382	7	7	1	1	388	390

DC1 Nadir Proximity Operations Particle Fluence Results (in particles/cm^2) for Orbiter TCS Radiators

		1-5 µm Particles		6-10 µm Particles		11-12 µm Particles		All Particles (1-12 µm)	
Radiator	Surface Normal Direction	Single Event Max	Total*	Single Event Max	Total*	Single Event Max	Total*	Single Event Max	Total*
TCS Starboard [Max on Surface]	Orb zenith/ISS aft	27809	29692	1381	1502	201	220	29391	31414
TCS Port [Max on Surface]	Orb zenith/ISS aft	26790	28679	1083	1204	165	185	28039	30067
TCS Starboard [Surface Average]	Orb zenith/ISS aft	9031	9995	392	434	50	55	9472	10485
TCS Port [Surface Average]	Orb zenith/ISS aft	8989	9947	393	435	50	56	9433	10439

SM Aft Proximity Operations Particle Fluence Results (in particles/cm^2) for Orbiter TCS Radiators

		1-5 µm Particles		6-10 µm Particles		11-12 µm Particles		All Particles (1-12 µm)	
Radiator	Surface Normal Direction	Single Event Max	Total*	Single Event Max	Total*	Single Event Max	Total*	Single Event Max	Total*
TCS Starboard [Max on Surface]	Orb zenith/ISS aft	1608	2401	11	15	0	0	1619	2416
TCS Port [Max on Surface]	Orb zenith/ISS aft	3713	6464	130	263	13	28	3856	6755
TCS Starboard [Surface Average]	Orb zenith/ISS aft	874	1163	4	5	0	0	878	1168
TCS Port [Surface Average]	Orb zenith/ISS aft	1839	2948	41	76	3	6	1883	3031

MRM2 Zenith Proximity Operations Particle Fluence Results (in particles/cm^2) for Orbiter TCS Radiators

		1-5 µm Particles		6-10 µm Particles		11-12 µm Particles		All Particles (1-12 µm)	
Radiator	Surface Normal Direction	Single Event Max	Total*	Single Event Max	Total*	Single Event Max	Total*	Single Event Max	Total*
TCS Starboard [Max on Surface]	Orb zenith/ISS aft	601	659	0	0	0	0	601	659
TCS Port [Max on Surface]	Orb zenith/ISS aft	596	654	0	0	0	0	596	654
TCS Starboard [Surface Average]	Orb zenith/ISS aft	80	87	0	0	0	0	80	87
TCS Port [Surface Average]	Orb zenith/ISS aft	96	104	0	0	0	0	96	104

Initial Deposition Results (in g/cm^2) for Orbiter TCS Radiators

		FGB Nadir		DC1 Nadir		SM Aft		MRM2 Zenith	
Radiator	Surface Normal Direction	Single Event Max	Total*	Single Event Max	Total*	Single Event Max	Total*	Single Event Max	Total*
TCS Starboard [Max on Surface]	Orb zenith/ISS aft	9.4E-09	1.0E-08	8.8E-07	9.4E-07	4.1E-08	6.1E-08	2.2E-08	2.4E-08
TCS Port [Max on Surface]	Orb zenith/ISS aft	2.5E-08	2.6E-08	7.9E-07	8.5E-07	1.0E-07	1.9E-07	2.2E-08	2.4E-08
TCS Starboard [Surface Average]	Orb zenith/ISS aft	5.3E-09	5.4E-09	2.7E-07	3.0E-07	2.2E-08	3.0E-08	3.1E-09	3.3E-09
TCS Port [Surface Average]	Orb zenith/ISS aft	1.3E-08	1.3E-08	2.7E-07	3.0E-07	4.8E-08	7.9E-08	3.9E-09	4.3E-09

Permanent Deposition Results (in g/cm^2) for Orbiter TCS Radiators

		FGB Nadir		DC1 Nadir		SM Aft		MRM2 Zenith	
Radiator	Surface Normal Direction	Single Event Max	Total*	Single Event Max	Total*	Single Event Max	Total*	Single Event Max	Total*
TCS Starboard [Max on Surface]	Orb zenith/ISS aft	5.2E-10	5.5E-10	4.8E-08	5.2E-08	2.2E-09	3.4E-09	1.2E-09	1.3E-09
TCS Port [Max on Surface]	Orb zenith/ISS aft	1.4E-09	1.4E-09	4.3E-08	4.7E-08	5.8E-09	1.0E-08	1.2E-09	1.3E-09
TCS Starboard [Surface Average]	Orb zenith/ISS aft	2.9E-10	3.0E-10	1.5E-08	1.6E-08	1.2E-09	1.6E-09	1.7E-10	1.8E-10
TCS Port [Surface Average]	Orb zenith/ISS aft	6.9E-10	7.1E-10	1.5E-08	1.6E-08	2.7E-09	4.4E-09	2.2E-10	2.4E-10

*Approach, Soyuz Thruster Test, and Separation results combined

Table 4-6. Tabular Results for Payload Bay Surfaces.

FGB Nadir Proximity Operations Particle Fluence Results (in particles/cm^2) for Orbiter Payload Bay Surfaces

		1-5 µm Particles		6-10 µm Particles		11-12 µm Particles		All Particles (1-12 µm)	
Item	Surface Normal Direction	Single Event Max	Total*	Single Event Max	Total*	Single Event Max	Total*	Single Event Max	Total*
Bottom [Max on Surface]	Orb zenith/ISS aft	431	432	5	5	0	0	436	437
Starboard side [Max on Surface]	Orb port/ISS port	48	48	0	0	0	0	48	48
Port side [Max on Surface]	Orb starboard/ISS starboard	44	44	1	1	0	0	45	45
Forward bulkhead [Max on Surface]	Orb aft/ISS nadir	2005	2006	40	40	3	3	2048	2049
Aft bulkhead [Max on Surface]	Orb forward/ISS zenith	1	1	0	0	0	0	1	1
Bottom [Surface Average]	Orb zenith/ISS aft	64	64	0	0	0	0	64	65
Starboard side [Surface Average]	Orb port/ISS port	15	15	0	0	0	0	15	15
Port side [Surface Average]	Orb starboard/ISS starboard	16	16	0	0	0	0	16	16
Forward bulkhead [Surface Average]	Orb aft/ISS nadir	1202	1202	19	19	1	1	1222	1222
Aft bulkhead [Surface Average]	Orb forward/ISS zenith	0	0	0	0	0	0	0	0

DC1 Nadir Proximity Operations Particle Fluence Results (in particles/cm^2) for Orbiter Payload Bay Surfaces

		1-5 µm Particles		6-10 µm Particles		11-12 µm Particles		All Particles (1-12 µm)	
Item	Surface Normal Direction	Single Event Max	Total*	Single Event Max	Total*	Single Event Max	Total*	Single Event Max	Total*
Bottom [Max on Surface]	Orb zenith/ISS aft	29712	32128	1957	2169	367	407	32036	34704
Starboard side [Max on Surface]	Orb port/ISS port	2285	2460	126	139	20	22	2432	2621
Port side [Max on Surface]	Orb starboard/ISS starboard	2241	2414	118	131	20	22	2379	2568
Forward bulkhead [Max on Surface]	Orb aft/ISS nadir	442	442	0	0	0	0	442	442
Aft bulkhead [Max on Surface]	Orb forward/ISS zenith	1713	1907	44	46	6	6	1763	1960
Bottom [Surface Average]	Orb zenith/ISS aft	15042	16648	877	971	134	148	16053	17768
Starboard side [Surface Average]	Orb port/ISS port	998	1104	51	56	7	8	1056	1168
Port side [Surface Average]	Orb starboard/ISS starboard	993	1099	51	56	7	8	1051	1163
Forward bulkhead [Surface Average]	Orb aft/ISS nadir	73	73	0	0	0	0	73	73
Aft bulkhead [Surface Average]	Orb forward/ISS zenith	1453	1618	28	30	4	4	1485	1651

SM Aft Proximity Operations Particle Fluence Results (in particles/cm^2) for Orbiter Payload Bay Surfaces

		1-5 µm Particles		6-10 µm Particles		11-12 µm Particles		All Particles (1-12 µm)	
Item	Surface Normal Direction	Single Event Max	Total*	Single Event Max	Total*	Single Event Max	Total*	Single Event Max	Total*
Bottom [Max on Surface]	Orb zenith/ISS aft	2862	4815	63	116	4	8	2928	4939
Starboard side [Max on Surface]	Orb port/ISS port	70	121	1	1	0	0	70	122
Port side [Max on Surface]	Orb starboard/ISS starboard	63	122	1	3	0	0	65	126
Forward bulkhead [Max on Surface]	Orb aft/ISS nadir	0	0	0	0	0	0	0	0
Aft bulkhead [Max on Surface]	Orb forward/ISS zenith	546	1021	12	23	1	1	559	1046
Bottom [Surface Average]	Orb zenith/ISS aft	1300	1823	15	24	1	1	1316	1848
Starboard side [Surface Average]	Orb port/ISS port	37	52	0	0	0	0	37	52
Port side [Surface Average]	Orb starboard/ISS starboard	44	76	1	2	0	0	45	77
Forward bulkhead [Surface Average]	Orb aft/ISS nadir	0	0	0	0	0	0	0	0
Aft bulkhead [Surface Average]	Orb forward/ISS zenith	376	678	6	10	0	0	382	688

MRM2 Zenith Proximity Operations Particle Fluence Results (in particles/cm^2) for Orbiter Payload Bay Surfaces

		1-5 µm Particles		6-10 µm Particles		11-12 µm Particles		All Particles (1-12 µm)	
Item	Surface Normal Direction	Single Event Max	Total*	Single Event Max	Total*	Single Event Max	Total*	Single Event Max	Total*
Bottom [Max on Surface]	Orb zenith/ISS aft	123	123	0	0	0	0	123	123
Starboard side [Max on Surface]	Orb port/ISS port	6	6	0	0	0	0	6	6
Port side [Max on Surface]	Orb starboard/ISS starboard	18	18	0	0	0	0	18	18
Forward bulkhead [Max on Surface]	Orb aft/ISS nadir	0	0	0	0	0	0	0	0
Aft bulkhead [Max on Surface]	Orb forward/ISS zenith	59	59	0	0	0	0	59	59
Bottom [Surface Average]	Orb zenith/ISS aft	3	3	0	0	0	0	3	3
Starboard side [Surface Average]	Orb port/ISS port	1	1	0	0	0	0	1	1
Port side [Surface Average]	Orb starboard/ISS starboard	1	1	0	0	0	0	1	1
Forward bulkhead [Surface Average]	Orb aft/ISS nadir	0	0	0	0	0	0	0	0
Aft bulkhead [Surface Average]	Orb forward/ISS zenith	14	14	0	0	0	0	14	14

Initial Deposition Results (in g/cm^2) for Orbiter Payload Bay Surfaces

		FGB Nadir		DC1 Nadir		SM Aft		MRM2 Zenith	
Item	Surface Normal Direction	Single Event Max	Total*	Single Event Max	Total*	Single Event Max	Total*	Single Event Max	Total*
Bottom [Max on Surface]	Orb zenith/ISS aft	1.3E-08	1.3E-08	1.0E-06	1.1E-06	7.5E-08	1.3E-07	7.3E-09	7.5E-09
Starboard side [Max on Surface]	Orb port/ISS port	1.4E-09	1.5E-09	7.5E-08	8.2E-08	1.7E-09	3.0E-09	5.1E-10	5.2E-10
Port side [Max on Surface]	Orb starboard/ISS starboard	1.3E-09	1.3E-09	6.9E-08	7.5E-08	1.7E-09	3.3E-09	9.4E-10	9.4E-10
Forward bulkhead [Max on Surface]	Orb aft/ISS nadir	5.3E-08	5.3E-08	1.8E-08	1.8E-08	1.7E-12	1.7E-12	6.2E-16	6.2E-16
Aft bulkhead [Max on Surface]	Orb forward/ISS zenith	3.0E-10	3.4E-10	4.1E-08	4.6E-08	1.4E-08	2.7E-08	2.3E-09	2.3E-09
Bottom [Surface Average]	Orb zenith/ISS aft	3.3E-09	3.5E-09	5.0E-07	5.6E-07	3.3E-08	4.6E-08	2.7E-10	2.8E-10
Starboard side [Surface Average]	Orb port/ISS port	5.8E-10	6.0E-10	3.2E-08	3.5E-08	9.0E-10	1.3E-09	4.9E-11	4.9E-11
Port side [Surface Average]	Orb starboard/ISS starboard	5.9E-10	6.1E-10	3.2E-08	3.5E-08	1.1E-09	2.0E-09	6.2E-11	6.2E-11
Forward bulkhead [Surface Average]	Orb aft/ISS nadir	3.2E-08	3.3E-08	4.1E-09	4.1E-09	1.0E-14	1.0E-14	6.6E-18	6.6E-18
Aft bulkhead [Surface Average]	Orb forward/ISS zenith	1.4E-10	1.7E-10	3.5E-08	3.9E-08	9.6E-09	1.7E-08	5.1E-10	5.1E-10

Permanent Deposition Results (in g/cm^2) for Orbiter Payload Bay Surfaces

		FGB Nadir		DC1 Nadir		SM Aft		MRM2 Zenith	
Item	Surface Normal Direction	Single Event Max	Total*	Single Event Max	Total*	Single Event Max	Total*	Single Event Max	Total*
Bottom [Max on Surface]	Orb zenith/ISS aft	6.9E-10	7.2E-10	5.7E-08	6.3E-08	4.1E-09	7.0E-09	4.0E-10	4.1E-10
Starboard side [Max on Surface]	Orb port/ISS port	7.8E-11	8.1E-11	4.1E-09	4.5E-09	9.4E-11	1.6E-10	2.8E-11	2.9E-11
Port side [Max on Surface]	Orb starboard/ISS starboard	7.1E-11	7.4E-11	3.8E-09	4.1E-09	9.3E-11	1.8E-10	5.2E-11	5.2E-11
Forward bulkhead [Max on Surface]	Orb aft/ISS nadir	2.9E-09	2.9E-09	1.0E-09	1.0E-09	9.6E-14	9.6E-14	3.4E-17	3.4E-17
Aft bulkhead [Max on Surface]	Orb forward/ISS zenith	1.6E-11	1.8E-11	2.3E-09	2.5E-09	7.9E-10	1.5E-09	1.3E-10	1.3E-10
Bottom [Surface Average]	Orb zenith/ISS aft	1.8E-10	1.9E-10	2.8E-08	3.1E-08	1.8E-09	2.5E-09	1.5E-11	1.5E-11
Starboard side [Surface Average]	Orb port/ISS port	3.2E-11	3.3E-11	1.7E-09	1.9E-09	5.0E-11	7.1E-11	2.7E-12	2.7E-12
Port side [Surface Average]	Orb starboard/ISS starboard	3.2E-11	3.4E-11	1.7E-09	1.9E-09	6.3E-11	1.1E-10	3.4E-12	3.4E-12
Forward bulkhead [Surface Average]	Orb aft/ISS nadir	1.8E-09	1.8E-09	2.2E-10	2.2E-10	5.5E-16	5.5E-16	3.7E-19	3.7E-19
Aft bulkhead [Surface Average]	Orb forward/ISS zenith	8.0E-12	9.3E-12	1.9E-09	2.2E-09	5.3E-10	9.5E-10	2.8E-11	2.8E-11

*Approach, Soyuz Thruster Test, and Separation results combined

4.5 Alternative Analysis Case for Nominal RV Approach Proximity Operations

The analysis results presented in Section 4.4 are considered to be representative (not bounding) given the limited RV proximity operations jet firing data. The OPO requested an alternative analysis case involving a more conservative RV approach trajectory and attitude. Due to reentry requirements, the Orbiter windows represent the limiting vehicle sensitive hardware for thruster plume particle impact damage. Therefore, the alternative analysis case focused on the Orbiter windows. RV approach to the MRM2 zenith docking port produced the highest particle fluence and contamination results to the Orbiter windows in the original study, so the MRM2 docking port was selected for the alternative analysis case.

Per the RS Specification [12], the nominal RV lateral misalignment is limited to a 10° cone along the approach vector. The angular misalignment in pitch, yaw, and roll is limited to ±4° for nominal approach. The ISS Space Environments team performed a parametric study to determine the RV approach trajectory and attitude within these limits that would maximize or bound particle fluence/contamination results to the front Orbiter windows for the available data set. The selected approach trajectory and attitude is demonstrated in Figure 4-11. As shown, assuming the RV approaches along the forward edge of the 10° cone positions the vehicle as close as possible to front Orbiter windows, thus maximizing plume impingement. Additionally, assuming a 4° RV pitch brings the centerlines of the RV side-firing thrusters closer to the Orbiter windows for maximum particle fluence/contamination levels. It should be noted that the original space environments analysis (presented in Section 4.4) assumed no lateral or angular misalignment for RV approach.

The alternative analysis case with the bounding RV trajectory and attitude assumption was applied to all six nominal approach cases (i.e., post-flight cases 2S, 3S, 8S Soyuz missions, and 14P, 15P, 16P Progress missions). For conservatism, the maximum plume particle

fluence/contamination result to the Orbiter windows from all six approach cases was taken. No changes were made to the Soyuz thruster test or RV separation for the alternative analysis case.

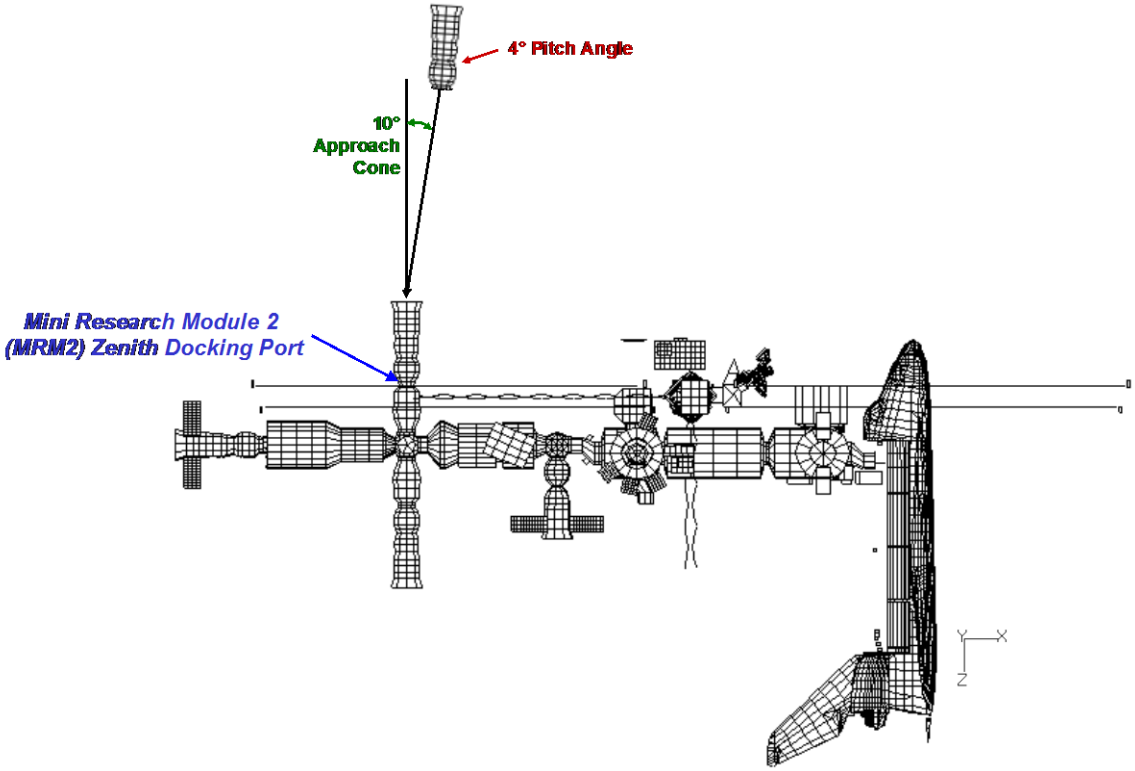

Figure 4-11. Approach trajectory and attitude for alternative approach analysis case.

Tabular results including particle fluence, initial contamination, and final (i.e., permanent) contamination to the Orbiter windows for RV proximity operations to the MRM2 zenith docking port are provided in Table 4-7. The particle fluence results are broken out by particle diameter bins (i.e., 1-5 µm, 6-10 µm, and 11-12 µm). The tabular results include a single event max, which corresponds to the maximum fluence/contamination value out of all individual proximity operations events (i.e., approach, Soyuz thruster test, and separation). The tabular results include the total for all three events (i.e., results for approach, Soyuz thruster test, and separation combined).

The particle fluence to the Orbiter front windows for the alternative analysis case is higher than the predictions in the original study by a factor of about 2.2. Likewise, the contamination levels to front windows for the bounding RV approach trajectory and attitude were higher than predictions in the original study by a factor of approximately 2.1. Refer to Table 4-2 for the original particle fluence and contamination results to the Orbiter windows (i.e., assuming no lateral or angular misalignment for RV approach).

Table 4-7. Tabular Results for the Alternative Analysis Case.

MRM2 Zenith Proximity Operations Particle Fluence Results (in particles/cm^2) for Orbiter Windows
(Alternative Analysis Case with Bounding Russian Vehicle Approach Trajectory and Attitude)

		1-5 µm Particles		6-10 µm Particles		11-12 µm Particles		All Particles (1-12 µm)	
Window	Surface Normal Direction	Single Event Max	Total*	Single Event Max	Total*	Single Event Max	Total*	Single Event Max	Total*
Fwd-Stbd fuselage window (side)	Orb starboard/ISS starboard	2715	2715	37	37	2	2	2754	2754
Fwd-Stbd fuselage window (middle)	Orb stbd-fwd/ISS stbd-zenith	3693	3693	60	60	4	4	3756	3756
Fwd-Stbd fuselage window (front)	Orb forward/ISS zenith	4905	4905	94	94	7	7	5006	5006
Fwd-Stbd fuselage window (overhead)	Orb zenith/ISS aft	1333	1333	1	1	0	0	1334	1334
Fwd-Port fuselage window (side)	Orb port/ISS port	2743	2743	37	37	2	2	2781	2781
Fwd-Port fuselage window (middle)	Orb port-fwd/ISS port-zenith	3817	3817	61	61	4	4	3881	3881
Fwd-Port fuselage window (front)	Orb forward/ISS zenith	4946	4946	94	94	7	7	5047	5047
Fwd-Port fuselage window (overhead)	Orb zenith/ISS aft	1341	1341	1	1	0	0	1342	1342
Payload bay window (starboard)	Orb aft/ISS nadir	0	0	0	0	0	0	0	0
Payload bay window (port)	Orb aft/ISS nadir	0	0	0	0	0	0	0	0

Initial deposition results (in g/cm^2) for Orbiter Windows
(Alternative Analysis Case with Bounding Russian Vehicle Approach Trajectory and Attitude)

		MRM2 Zenith	
Window	Surface Normal Direction	Single Event Max	Total*
Fwd-Stbd fuselage window (side)	Orb starboard/ISS starboard	7.2E-08	7.2E-08
Fwd-Stbd fuselage window (middle)	Orb stbd-fwd/ISS stbd-zenith	1.0E-07	1.0E-07
Fwd-Stbd fuselage window (front)	Orb forward/ISS zenith	1.3E-07	1.3E-07
Fwd-Stbd fuselage window (overhead)	Orb zenith/ISS aft	4.4E-08	4.4E-08
Fwd-Port fuselage window (side)	Orb port/ISS port	7.5E-08	7.5E-08
Fwd-Port fuselage window (middle)	Orb port-fwd/ISS port-zenith	1.0E-07	1.0E-07
Fwd-Port fuselage window (front)	Orb forward/ISS zenith	1.3E-07	1.3E-07
Fwd-Port fuselage window (overhead)	Orb zenith/ISS aft	4.4E-08	4.4E-08
Payload bay window (starboard)	Orb aft/ISS nadir	0.0E+00	0.0E+00
Payload bay window (port)	Orb aft/ISS nadir	0.0E+00	0.0E+00

Permanent deposition results (in g/cm^2) for Orbiter Windows
(Alternative Analysis Case with Bounding Russian Vehicle Approach Trajectory and Attitude)

		MRM2 Zenith	
Window	Surface Normal Direction	Single Event Max	Total*
Fwd-Stbd fuselage window (side)	Orb starboard/ISS starboard	4.0E-09	4.0E-09
Fwd-Stbd fuselage window (middle)	Orb stbd-fwd/ISS stbd-zenith	5.5E-09	5.5E-09
Fwd-Stbd fuselage window (front)	Orb forward/ISS zenith	7.4E-09	7.4E-09
Fwd-Stbd fuselage window (overhead)	Orb zenith/ISS aft	2.4E-09	2.4E-09
Fwd-Port fuselage window (side)	Orb port/ISS port	4.1E-09	4.1E-09
Fwd-Port fuselage window (middle)	Orb port-fwd/ISS port-zenith	5.7E-09	5.7E-09
Fwd-Port fuselage window (front)	Orb forward/ISS zenith	7.4E-09	7.4E-09
Fwd-Port fuselage window (overhead)	Orb zenith/ISS aft	2.4E-09	2.4E-09
Payload bay window (starboard)	Orb aft/ISS nadir	0.0E+00	0.0E+00
Payload bay window (port)	Orb aft/ISS nadir	0.0E+00	0.0E+00

*Approach, Soyuz Thruster Test, and Separation results combined

4.6 Synthetic RV Abort Scenario

The analysis results presented in Sections 4.4 and 4.5 apply for nominal RV proximity operations. The OPO requested an analysis of a RV abort scenario. No jet firing data are available for RV aborts, so an abort scenario was synthesized from nominal approach jet firing data with OPO concurrence. As with the alternative analysis case for approach (Section 4.5), the synthetic abort analysis focused on the Orbiter windows which represent the limiting Orbiter sensitive hardware for thruster plume particle impact damage. The MRM2 docking port was selected for the abort scenario as the worst case docking port for the Orbiter windows.

Ground rules for the abort scenario were established by the ISSP Integration Office/VIPER with OPO concurrence. An approach and backout portion was defined for the abort scenario. For the approach portion, the RV was assumed to operate within nominal limits for lateral and angular misalignment. For the backout portion, RV lateral misalignment was assumed to be limited to a 15° cone along the approach vector. The angular misalignment in pitch, yaw, and roll was assumed to be limited to ±15° for off-nominal performance. The ISS Space Environments team performed a parametric study to determine the RV trajectory and attitude within these limits that

would maximize particle fluence to the front Orbiter windows for the available dataset. Example findings from the parametric study are shown in Figure 4-12, which gives particle fluence versus range for various trajectory and pitch angle assumptions. As the figure shows, the pitch angle assumption had a far more dramatic effect on the total particle fluence than the trajectory assumption. For both example cases, there is a negligible difference in results for a vehicle approaching along the centerline of the docking port axis versus a vehicle approaching along the forward edge of a 10° half angle cone. However, there is a dramatic difference in results between vehicle pitch angles of 0°, 4°, and 15°.

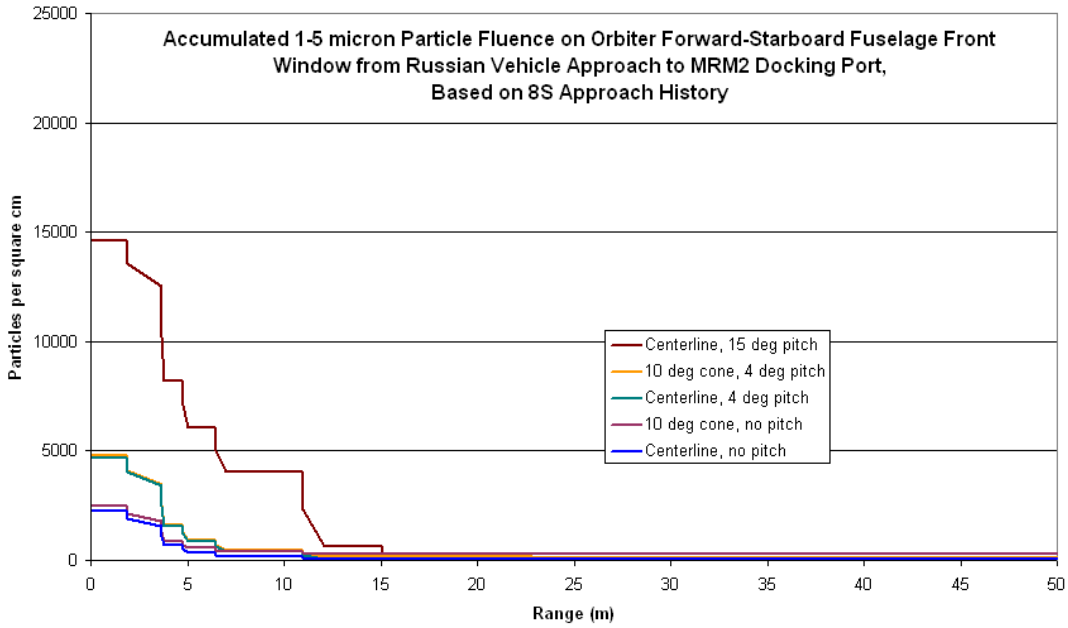

a) Example results for the 8S jet firing history.

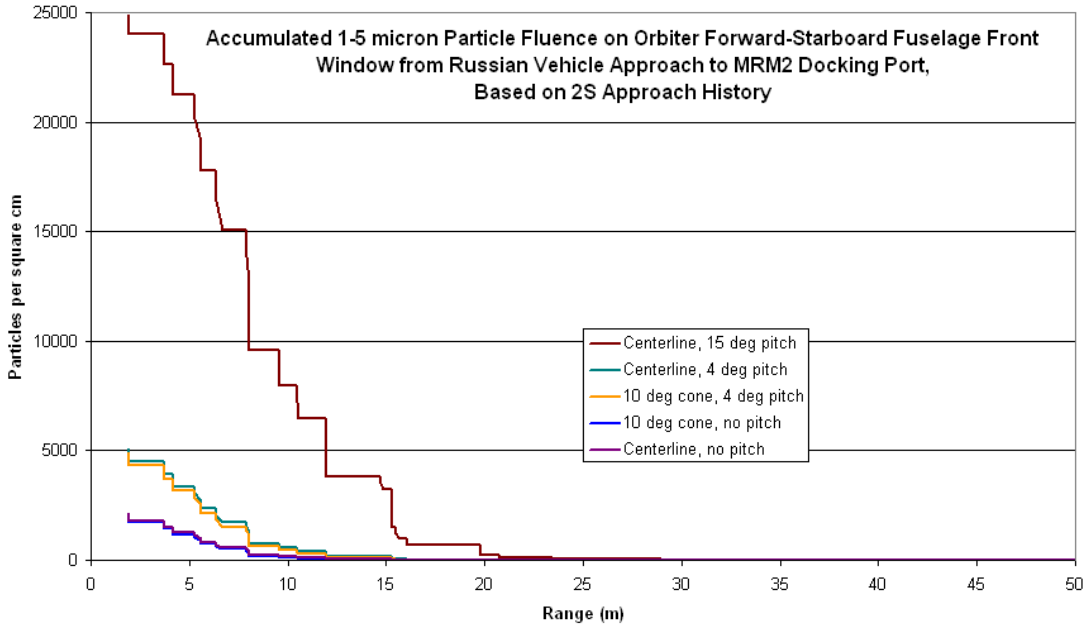

b) Example results for the 2S jet firing history.

Figure 4-12. RV approach cone and attitude variation effects on particle fluence.

The selected trajectory and attitude for the abort scenario approach and backout are demonstrated in Figure 4-13. As shown, the RV approach along the forward edge of the 10° cone is assumed to position the vehicle as close as possible to front Orbiter window. Additionally, assuming a 4° RV pitch brings the centerlines of the RV side-firing thrusters closer to the Orbiter windows for maximum particle fluence/contamination levels during the approach portion. For the backout portion of the abort, the RV was assumed to follow a trajectory along the forward edge of the 15° cone. The RV pitch angle was adjusted for each backout firing up to the limit of 15° to hold the RV thruster plume centerlines as close as possible to the Orbiter windows. Finally, a range offset was applied such that the last lateral engine thruster firing would occur at the minimum range (i.e., worst case range) for Orbiter window exposure. The minimum range for Orbiter window exposure to a lateral engine thruster firing occurs when the RV docking interface is 5 ft (1.5 m) from the docking port, as demonstrated by Figure 4-14.

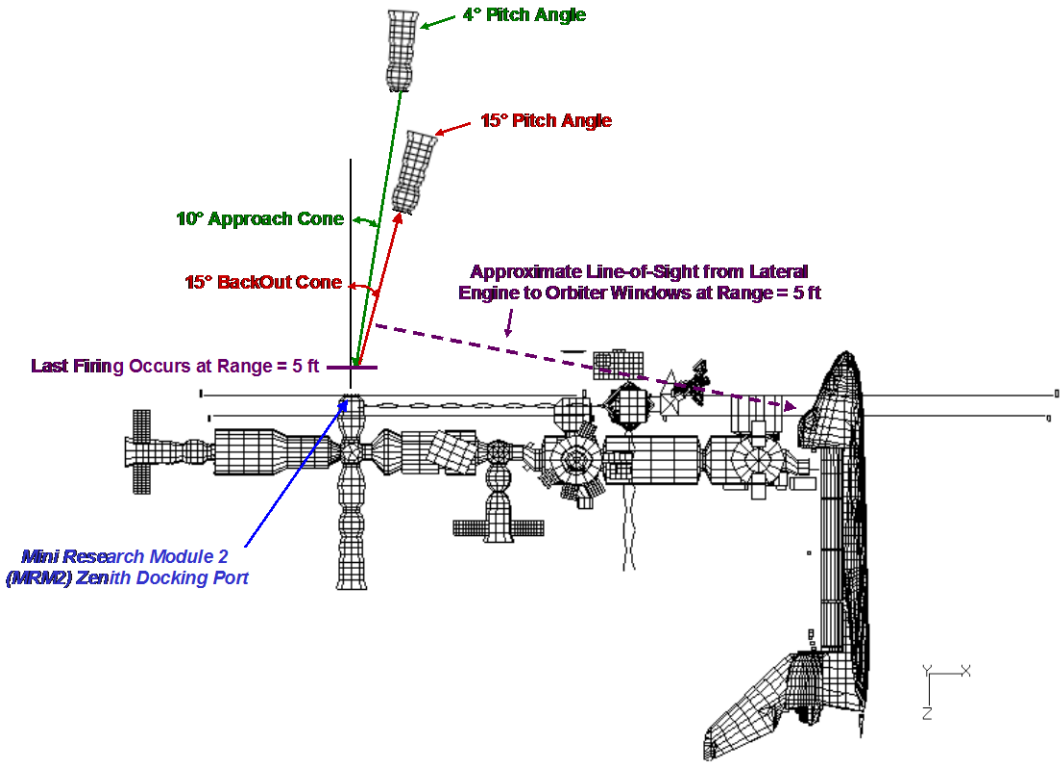

Figure 4-13. RV trajectory and attitude assumptions for the abort scenario.

Both approach and backout portions of the abort scenario were modeled using available jet firing data for nominal RV approach proximity operations. The RV trajectory and attitude assumptions were applied to all six nominal approach cases (i.e., post-flight cases 2S, 3S, 8S Soyuz missions and 14P, 15P, 16P Progress missions), and the maximum plume particle fluence results to the Orbiter windows from all six cases were taken. Please note that the approach jet firing data were applied to the backout portion rather than the separation jet firing data. This is because the generic timeline for RV separation only characterizes the RV braking thruster firings. The lateral thruster firings, which are of primary interest for pluming of the Orbiter windows during proximity operations to the MRM2 docking port, are not characterized in the generic separation timeline. Application of the approach jet firing data (for which the lateral thruster firings are characterized) to the backout portion is conservative in comparison for this particular scenario.

Tabular results including particle fluence to the Orbiter windows for the synthetic abort scenario are provided in Table 4-8. Plume contamination analysis was not conducted since thruster plume particle impact damage is the primary concern due to Orbiter window reentry requirements. The particle fluence results are broken out by particle diameter bins (i.e., 1 to 5 µm, 6 to 10 µm, and 11 to 12 µm). Additionally, the individual results for the approach and backout portions, and combined total are provided.

Table 4-8. Tabular Results for the Synthetic Abort Scenario.

MRM2 Zenith Proximity Operations Particle Fluence Results (in particles per square cm) for Orbiter Windows
Abort Scenario (Approach within 10 deg cone & 4 deg pitch to 5ft; back-out within 15 deg cone & 15 deg pitch)

		1-5 µm Particles			5 µm Particles Only
Window	Surface Normal Direction	Approach Max	BackOut Max	Abort Total*	Abort Total*
Fwd-Stbd fuselage window (side)	Orb starboard/ISS starboard	2614	15086	17699	385
Fwd-Stbd fuselage window (middle)	Orb stbd-fwd/ISS stbd-zenith	4943	23189	28132	658
Fwd-Stbd fuselage window (front)	Orb forward/ISS zenith	6437	28995	35432	864
Fwd-Stbd fuselage window (overhead)	Orb zenith/ISS aft	1712	16633	18346	314
Fwd-Port fuselage window (side)	Orb port/ISS port	2862	16035	18897	446
Fwd-Port fuselage window (middle)	Orb port-fwd/ISS port-zenith	4915	23784	28699	677
Fwd-Port fuselage window (front)	Orb forward/ISS zenith	6367	28898	35265	865
Fwd-Port fuselage window (overhead)	Orb zenith/ISS aft	1728	16752	18480	321
Payload bay window (starboard)	Orb aft/ISS nadir	0	0	0	0
Payload bay window (port)	Orb aft/ISS nadir	0	0	0	0

		6-10 µm Particles		
Window	Surface Normal Direction	Approach Max	BackOut Max	Abort Total*
Fwd-Stbd fuselage window (side)	Orb starboard/ISS starboard	23	668	691
Fwd-Stbd fuselage window (middle)	Orb stbd-fwd/ISS stbd-zenith	92	1141	1233
Fwd-Stbd fuselage window (front)	Orb forward/ISS zenith	128	1526	1655
Fwd-Stbd fuselage window (overhead)	Orb zenith/ISS aft	2	511	513
Fwd-Port fuselage window (side)	Orb port/ISS port	23	843	866
Fwd-Port fuselage window (middle)	Orb port-fwd/ISS port-zenith	79	1208	1286
Fwd-Port fuselage window (front)	Orb forward/ISS zenith	119	1538	1657
Fwd-Port fuselage window (overhead)	Orb zenith/ISS aft	2	520	523
Payload bay window (starboard)	Orb aft/ISS nadir	0	0	0
Payload bay window (port)	Orb aft/ISS nadir	0	0	0

		11-12 µm Particles		
Window	Surface Normal Direction	Approach Max	BackOut Max	Abort Total*
Fwd-Stbd fuselage window (side)	Orb starboard/ISS starboard	1	91	92
Fwd-Stbd fuselage window (middle)	Orb stbd-fwd/ISS stbd-zenith	8	170	178
Fwd-Stbd fuselage window (front)	Orb forward/ISS zenith	15	233	248
Fwd-Stbd fuselage window (overhead)	Orb zenith/ISS aft	0	58	58
Fwd-Port fuselage window (side)	Orb port/ISS port	1	132	133
Fwd-Port fuselage window (middle)	Orb port-fwd/ISS port-zenith	5	194	200
Fwd-Port fuselage window (front)	Orb forward/ISS zenith	15	242	257
Fwd-Port fuselage window (overhead)	Orb zenith/ISS aft	0	60	60
Payload bay window (starboard)	Orb aft/ISS nadir	0	0	0
Payload bay window (port)	Orb aft/ISS nadir	0	0	0

		All Particles (1-12 µm)		
Window	Surface Normal Direction	Approach Max	BackOut Max	Abort Total*
Fwd-Stbd fuselage window (side)	Orb starboard/ISS starboard	2637	15845	18482
Fwd-Stbd fuselage window (middle)	Orb stbd-fwd/ISS stbd-zenith	5044	24499	29543
Fwd-Stbd fuselage window (front)	Orb forward/ISS zenith	6580	30754	37335
Fwd-Stbd fuselage window (overhead)	Orb zenith/ISS aft	1715	17202	18917
Fwd-Port fuselage window (side)	Orb port/ISS port	2886	17011	19896
Fwd-Port fuselage window (middle)	Orb port-fwd/ISS port-zenith	4999	25186	30185
Fwd-Port fuselage window (front)	Orb forward/ISS zenith	6501	30678	37179
Fwd-Port fuselage window (overhead)	Orb zenith/ISS aft	1730	17332	19062
Payload bay window (starboard)	Orb aft/ISS nadir	0	0	0
Payload bay window (port)	Orb aft/ISS nadir	0	0	0

*Approach and Back-out results combined

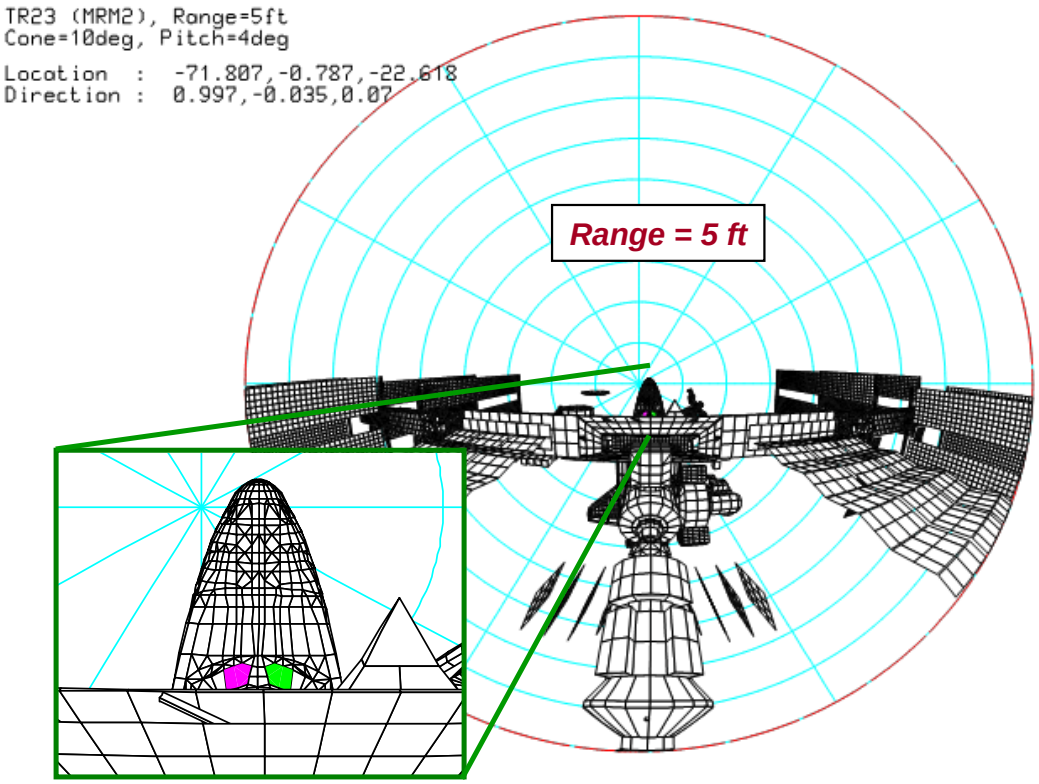

Figure 4-14. Hemispherical view to Orbiter front windows from RV lateral engine at range-to-dock of 5 ft.

The particle fluence to the Orbiter front windows for the synthetic abort scenario is higher than the predictions in the original study by a factor of about 16. Table 4-9 provides a summary of the analysis assumptions and particle fluence results to the Orbiter front windows for the original nominal approach analysis (Tables 4-2 through 4-6), the alternative analysis case for nominal approach (Table 4-7), and the abort scenario (Table 4-8). As the table indicates, the backout portion of the abort scenario accounts for the majority of the particle fluence results. This is because the pitch angle was adjusted for each firing (up to 15°) to induce worst-case plume impingement.

Table 4-9. Analysis Case Summary for Orbiter Windows.

	Nominal Approach	Alternative/Bounded Nominal Approach	Abort Scenario - Approach	Abort Scenario - Back-out	Abort Total
Approach Cone Half-Angle *degrees*	**0**	**10**	**10**	**15**	**-**
Russian Vehicle Pitch Angle *degrees*	**0**	**4***	**4***	**15****	**-**
Offset Applied (to fix last firing at range = 5 ft)	**N**	**N**	**Y**	**Y**	**-**
Particle Fluence to Fwd-Stbd Fuselage Window (Front) *particles/cm^2*	**2279**	**5006**	**6580**	**30754**	**37335**
Particle Fluence to Fwd-Port Fuselage Window (Front) *particles/cm^2*	**2274**	**5047**	**6501**	**30678**	**37179**
Reference Section	**5.2.1**	**5.2.2**	**5.2.3**	**5.2.3**	**5.2.3**

*Pitch angle held at 4 degrees to maximize particle fluence to Orbiter front windows.

**Pitch angle of up to 15 degrees. Pitch angles less than 15° selected as needed to maximize particle fluence to Orbiter front windows.

It should be noted the smallest particles constitute the vast majority in the fluence results. For the abort scenario specifically, the 1 to 5 µm diameter particles constitute approximately 95 percent of the particle fluence to the Orbiter front windows. There are 5 µm particles that represent only about 2.3 percent of the total fluence. This could be an important consideration when interpreting hypervelocity impact test results since 5 µm is the smallest projectile diameter typically used. See Figure 4-15 for additional details on particle size distribution for the synthetic abort scenario.

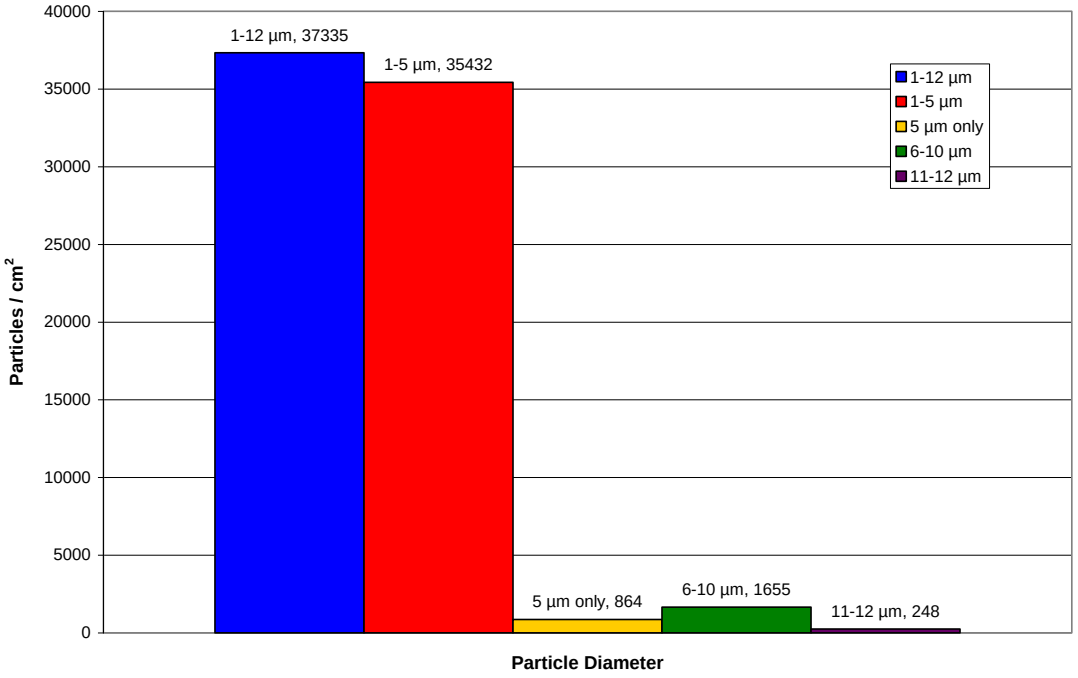

Figure 4-15. Particle fluence by diameter to the Orbiter forward-starboard front window for the RV abort scenario.

4.7 Integrated Thruster Plume Particle Impact Damage Assessment for Orbiter RCC

The ISS Space Environments team was first alerted to the possibility of DDO in 2006. The ISSP Integration Office/VIPER tasked the ISS Space Environments team to identify any potential issues that may require long lead times to demonstrate the feasibility of simultaneous Orbiter and RV operations [13]. The team identified thruster plume particle impact damage of the Orbiter WLE RCC (see Figure 4-16) as one such issue. The RCC protects the WLEs for maximum temperatures reached during atmospheric reentry. RCC uses a thin coating of silicon carbide (SiC) (30 ± 10 mils or approximately 500 to 1000 μm). This coating prevents oxidation and subsequent degradation of the carbon-carbon substrate during reentry and is of great concern for thruster particle impacts [14, 15]. No previous analytical or test data were available for thruster plume particle impact damage to RCC.

Figure 4-16. Orbiter on-orbit; view of RCC on WLEs.

The SiC coating is applied with a dry pack material made up of alumina, silicon, and silicon carbide, and then placed in a furnace. A diffusion reaction takes place between the dry pack and carbon-carbon in which the outer layers of the carbon-carbon are converted to silicon carbide with no increase in thickness. Surface cracks can develop in the silicon carbide coating due to differences in thermal expansion, so the RCC is impregnated with tetraethyl orthosilicate for further resistance to oxidation. The RCC is then sealed with a glossy overcoat of sodium silicate glass, which is referred to as Type-A glass [14,15]. Figure 4-17 shows an illustration of RCC layers as well as a polished cross-section. The largest acceptable RCC damage from a single particle impact was identified by the Orbiter Leading Edge Structural System (LESS) Problem Resolution Team (PRT) to be 0.082 in x 0.091 in x 0.041 in (~2100 by 2300 by 1000 μm) in depth [16]. RCC surface erosion/coating removal due to multiple impacts must be addressed considering the high particle fluences present in thruster plumes.

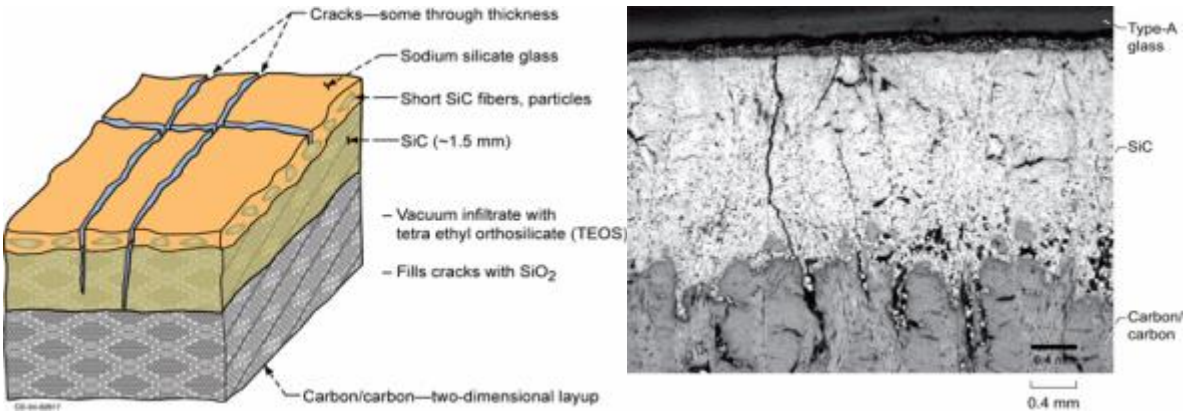

Figure 4-17. Illustration of RCC material layers (left) and polished RCC cross-section (right) [15].

The ISS Space Environments team initiated a test and analysis program to characterize thruster plume particle damage to Orbiter RCC. Hypervelocity impact testing was performed to determine if a single thruster plume particle could penetrate the SiC coating (Section 4.7.1). The test data were then used to calibrate analysis tools to extrapolate ground test data to thruster plume particle conditions (Section 4.7.2). The test and analysis results were finally coupled with particle fluence calculations (Section 4.7.3) to characterize surface erosion due to multiple particle impacts (Section 4.7.4). The details of this test/analysis program will be presented herein.

It should be noted that the test/analysis program to characterize thruster plume particle damage to Orbiter RCC was conducted prior to the 2008 revision to the thruster plume droplet flux model described in Section 4.1. The original model specified unburned propellant droplets with diameters between 1 and 100 μm [4] (see Table 4-10) and is conservative in comparison. The particle size and velocity distribution for the original model was used to select RCC impact testing conditions and to calculate thruster plume particle fluences for the RCC integrated damage assessment.

Table 4-10. Particle sizes and velocities in ISS bipropellant thruster plumes based on the original droplet flux model.

Particle Size **(μm)**	Limiting Particle Velocity **(km/s)**	Kinetic Energy* **(kJ)**
100	1.0	3.8E-01
50	1.4	9.3E-02
20	2.2	1.5E-02
10	2.65	2.7E-03
5	2.9	4.0E-04
1	3.05	3.5E-06

*Kinetic energy calculated for a NTO particle; density = 1.45g/cc.

4.7.1 Hypervelocity Impact Testing of RCC

The RCC sample used for impact testing was provided by Don Curry, an Orbiter RCC specialist in the thermal design branch of JSC Structural Engineering Division and a member of the LESS

PRT. The sample was the scrap remnant of an approximately 6 x 6 in piece. The scrap was cut to obtain two pieces (approximately 1.5 x 3 in each) for testing. Each piece was partitioned lengthwise into thirds for a total of six witness coupons with dimensions of approximately 1.5 x 1 in each. Figure 4-18 shows a diagram of the original sample with markings to denote cuts.

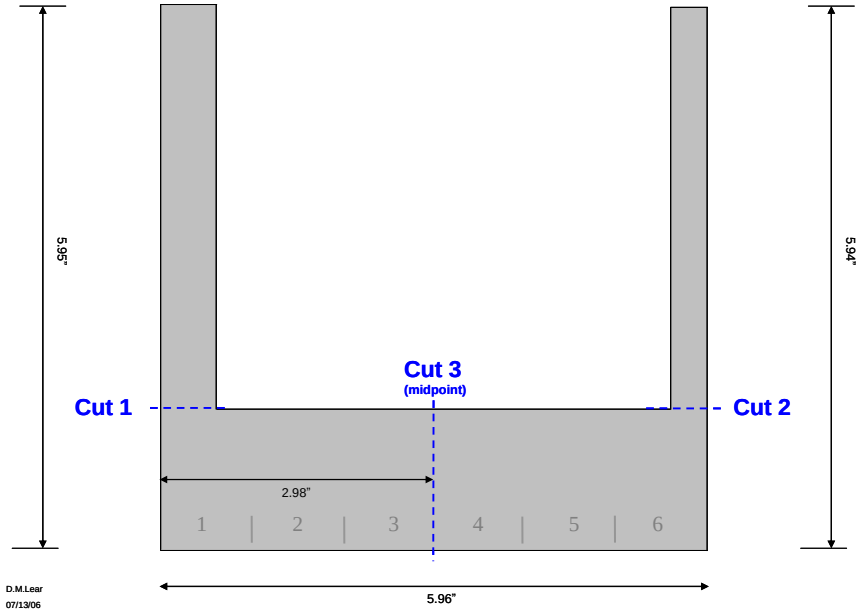

Figure 4-18. Diagram of RCC sample.

Thruster-induced damage/erosion of RCC could be evaluated by exposing an RCC sample to thruster firings. Unfortunately, test facilities with this capability were not accessible for this study. Instead, RCC samples were impacted with simulated thruster plume particles. This was accomplished using a light gas gun and projectiles with comparable sizes, densities, and velocities expected in thruster plumes. The light gas gun testing was conducted by the JSC Hypervelocity Impact Test Facility (HITF) at Rice University.

The impact testing was performed at normal impingement angles to maximize impact damage. Soda-lime glass beads with density 2.44g/cc were selected as the best available projectile to match density of thruster plume particles. (Note: MMH density = 0.88g/cc; NTO density = 1.45g/cc). Three tests were planned with glass beads at appropriate sizes and velocities for thruster plumes. One additional test was planned as an extreme case using 100 μm particles accelerated to 3 km/s (limiting velocity for a 100 μm particle is 1 km/s; see Table 4-10). It should be noted that the smallest thruster particle size of 1 μm has the highest flux and would be of great interest for ground testing. However, projectiles of this size are difficult to obtain and reliably impact at the intended specimen location. Therefore, this option was not considered.

Table 4-11 provides a summary of the test conditions. Each test used multiple glass bead projectiles for good characterization of surface damage. However, the quantity of projectiles per shot was limited to minimize crater overlapping. All test velocities were greater than or equal to the respective limiting velocities in thruster plumes. Test 1-C experienced a large error band in velocity, so the projectile size and target velocity was duplicated in Test 1-E for more accurate results. No impact testing was performed on the sixth witness coupon.

Table 4-11. RCC impact test summary.

Test ID	Projectile Material	Projectile Density (g/cm^3)	Projectile Diameter (μm)	Velocity (km/s)	Kinetic Energy (J)	Comment
1-A	Soda-Lime Glass	2.44	4.5 - 5.5 μm	2.92	6.8E-07	
1-B	Soda-Lime Glass	2.44	20 - 25 μm	2.37	4.1E-05	
1-C	Soda-Lime Glass	2.44	95 - 105 μm	1.0 - 1.5	-	
1-D	Soda-Lime Glass	2.44	95 - 105 μm	3.04	5.9E-03	
1-E	Soda-Lime Glass	2.44	95 - 105 μm	1.03	6.8E-04	*Test 1-C Repeat*

From visual inspection, it was difficult to determine that the RCC had been impacted. Only the witness coupon for Test 1-D showed visible signs of surface alteration. HITF provided several microscopic images of the RCC test samples. Figure 4-19 gives an example of these images taken by SEM. The smooth area on the left of the images is a strip of copper tape that was placed on the border between coupons. HITF used this smooth surface for inspection after each test shot to ensure projectiles impacted the witness coupon as intended.

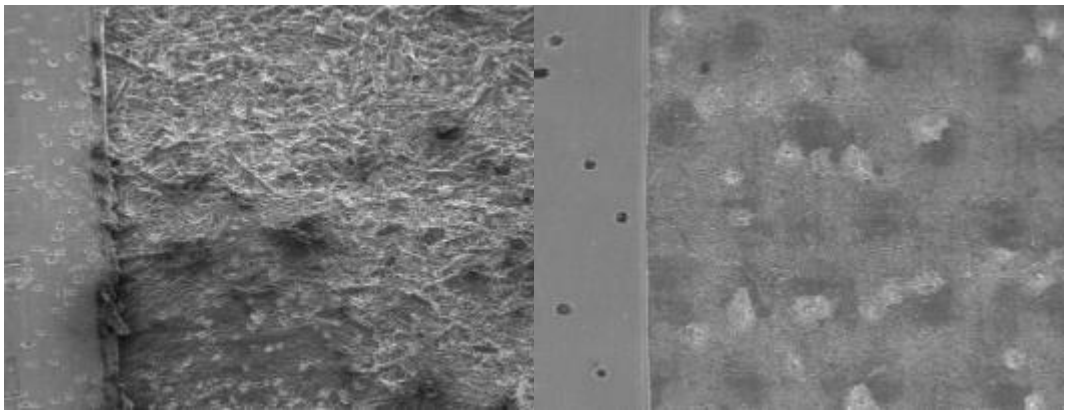

Figure 4-19. SEM images of RCC samples from Test 1-A (left) and Test 1-D (right).

Optical imagery to characterize RCC impact test samples was performed at the Combined Effects Test Facility (CETF) located at Boeing-Seattle. The first objective for the optical imaging was to estimate thickness of SiC coating on RCC. To accomplish this, several images were taken viewing the edge of the RCC sample. An example image is shown in Figure 4-20. This image was taken at 50x magnification with an optical microscope. From the image, the top surface is seen to be rough and uneven. The lighter color material extending downward from the top surface is the SiC coating. The coating thickness varied across the samples, but was generally greater than 0.5 mm (~20 mils) and less than 1.0 mm (~40 mils). This agrees with the SiC coating thickness specification of 30 ± 10 mils. It should be noted that the optical microscope can experience false colors at some magnifications.

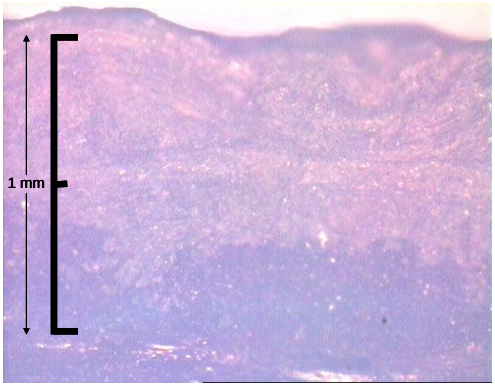

Figure 4-20. View of silicon carbide coating from edge of RCC sample.

In addition, optical imaging was used to characterize the surface of unshot RCC for comparison with impacted test articles. From visual inspection, the RCC surface was rough and textured. Qualitative comparison between clean and impacted samples may be important in determining surface degradation. To characterize the surface of the unshot sample (witness coupon #6), 14 optical images were taken with varying magnifications from 50x to 1000x. These images suggested a very textured and rough surface, as shown in Figure 4-21. In this figure, long and short carbon fibers are clearly present. The shiny portions of the surface (especially visible at 400x) may be an indication of the glossy top coating that seals the silicon carbide (i.e., Type-A glass). Several out-of-focus areas are present in the images due to the surface unevenness. CETF made a qualitative estimate of the size of the surface defects. In general, the surface defects had a minimum lateral dimension of approximately 40 μm and a vertical variance of approximately ±20 μm. Impact craters must be larger than these surface defects to be distinguished with optical microscope.

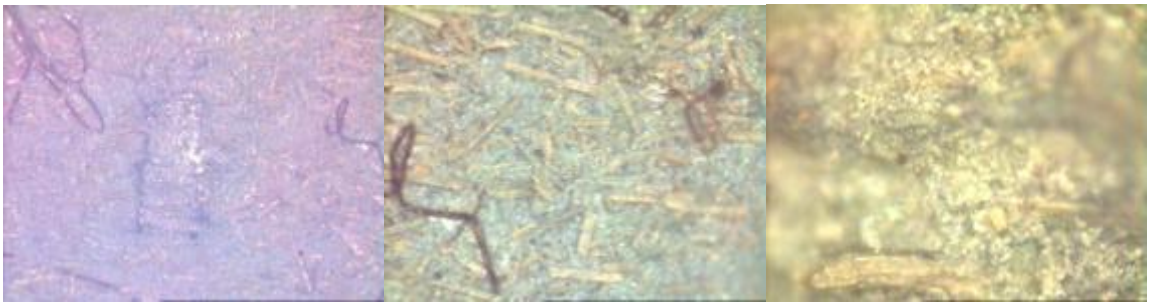

Figure 4-21. Unshot RCC sample at 50x (left), 100x (center), and 400x (right).

The final objective for optical imaging was to measure crater diameters and depths for a representative set from each impact test sample. Characterization of crater damage as a function of particle size and velocity can be used to determine if thruster particle impacts may penetrate the SiC coating. Furthermore, this data may be used in combination with particle fluence calculations to determine an effective amount of surface erosion that may occur due to thruster firings.

Unfortunately, the impact features on the Test 1-A sample were too small to be identified on the rough surface, and no measurement was made. For Tests 1-B, 1-C, and 1-E, CETF found the craters extremely difficult to distinguish from natural surface defects, though several

measurements exceeded the minimum defect dimension. Some measurements were taken for these samples; however, CETF advised that the results cannot be considered valid due to uncertainty in crater identification. Therefore, measurements for these test samples are not reported herein.

Only Test 1-D resulted in craters large enough to be easily distinguished as impact features instead of surface imperfections. CETF measured a total of 24 craters from this sample. It was observed that the craters generally had two damage zones: an area of irregular shape where surface material has been removed to expose underlying fibers, and a smaller nearly-circular dark area near the center of the exposed fibers. CETF provided approximate diameters for both zones along with the measured crater depths. A summary of the Test 1-D sample measurements is provided in Table 4-12.

Table 4-12. Summary of Test 1-D impact crater measurements.

	Center Diameter* (μm)	Flake Diameter* (μm)	Crater Depth* (μm)
Average:	**129.6**	**251.3**	**43.1**
Min:	**90.0**	**180.0**	**4.0**
Max:	**180.0**	**330.0**	**100.0**
Std Dev:	**24.8**	**44.2**	**22.2**

* Measurement error of +/-10μm applies.

To determine the crater depth, CETF focused on the surface of the sample, and then on the bottom of the crater, with the distance between focal planes giving an estimate of the crater depth. Some judgment is associated with this technique, especially in identifying the top of the uneven surface. Figure 4-22 shows an example of this technique for the deepest crater measured. The image on the left shows the impact feature with focus on the top surface, and the image on the right shows the same feature with focus on the bottom of the crater.

Results from Test 1-D crater measurements show a minimum crater depth of 4 μm and maximum of 100 μm (average 43 μm). Crater diameters were typically 3 to 5 times the depth, with the largest crater diameter of 330 μm for the flake zone. It is hypothesized that the flake zone is due to shattering of the glass coating applied to the top surface, but additional testing would be required to investigate this.

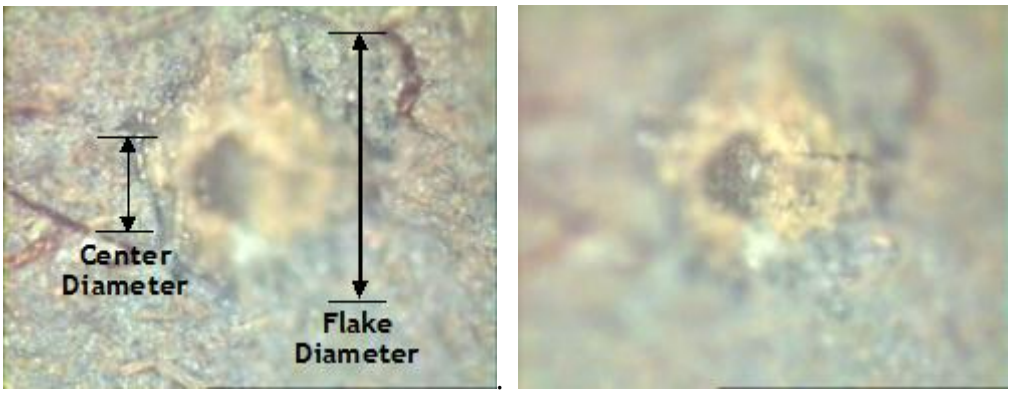

Figure 4-22. Deepest crater observed from Test 1-D with focus on RCC surface (left) and bottom of crater (right) to determine depth.

No impact testing measurements showed craters that penetrated the SiC coating (minimum depth of 20 mils or approximately 500 μm), with margin to spare. Test 1-D produced the largest impact features, but the velocity for this test exceeded the limiting velocity for thruster particles of the same size by a factor of three. In addition, the density of the glass bead projectile used for testing was higher than the density of particles in thruster plumes. Combining these factors, the Test 1-D sample experienced approximately 15 times the maximum kinetic energy expected in the most energetic thruster plume particles. In conclusion, test results show no concern for exposure of carbon-carbon material due to a single thruster plume particle impact.

4.7.2 Analytical Damage Characterization

Although RCC impact test results show no issue for SiC coating penetration due to individual thruster particle impacts, excessive material removal/surface erosion resulting from multiple impacts must be addressed. Crater damage due to smaller particles (≤5 μm in diameter) was not characterized by the impact testing, and particles of this size are the highest flux in thruster plumes. The ISS Space Environments team took an analytical approach to characterizing surface erosion due to multiple particle impacts by extrapolating impact test data for larger particles (i.e., diameters ~100 μm) to the highest flux thruster plume particles (i.e., smaller particle diameters ~1 to 5 μm). This analytical approach involved simulation of thruster plume particle impacts using the Los Alamos National Laboratory SPHINX (Smooth Particle Hydrodynamics) code. See Figure 4-23 for an example particle impact simulation from SPHINX.

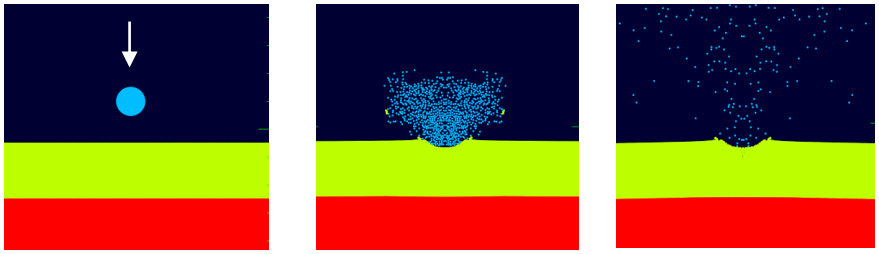

Figure 4-23. Example SPHINX particle impact simulation.

The general approaches for analytical damage characterization were to:

1. Use SPHINX to duplicate measurements from Test 1-D. 100 μm diameter particle, normal impact of glass bead to SiC at 3.04 km/s.
2. Perform SPHINX analyses to characterize damage for thruster plume particle impacts.
    a. 5 μm diameter particle, normal impact of NTO to SiC at 2.9 km/s.
    b. 20 μm diameter particle, normal impact of NTO to SiC at 2.2 km/s.
    c. 100 μm diameter particle, normal impact of NTO to SiC at 1.0 km/s.
3. Calculate particle fluence to Orbiter RCC due to RV thruster firings during proximity operations.
4. Linearly scale damage for a single particle impact by predicted particle fluence for an integrated damage assessment.

The first step in the approach is critical for calibrating the RCC material properties in SPHINX so that it accurately models impact damage. SPHINX is particularly sensitive to the material yield strength. Material properties for the SiC layer (specifically, the yield strength) were of chief

concern since most of the thruster plume particle impact damage would affect this layer. RCC specialists in the LESS PRT provided an estimated yield strength range for the SiC coating of 3,000 to 50,000 psi. For comparison, the yield strength for bulk SiC is approximately 300,000 psi (single crystal) [17]. The SiC coating yield strength is especially difficult to estimate due to the nonuniformity of the conversion coating as well as strain rate effects for hypervelocity impacts. The velocities that the thruster plume particles are traveling at will produce shock waves upon impact. As a result, material properties such as yield strength will vary significantly from readily available material properties. For example, the rate of deformation or the strain rate in a hypervelocity impact will be orders of magnitude ($>10^4$ s^{-1}) greater than the strain rates applied in typical engineering stress-strain measurements ($\sim10^{-3}$ s^{-1}) that are used to determine yield strength.

The ISS Space Environments team performed a parametric study with SPHINX to simulate ground Test 1-D (i.e., 100 μm glass bead projectile impacting SiC at 3.04 km/s) using increasing yield strengths for Type A and SiC. Results from the parametric study were compared against crater measurements from the hypervelocity impact testing to gauge appropriate yield strengths. Figure 4-24 through Figure 4-26 show SPHINX analysis results for various SiC yield strengths compared to the minimum, average, and maximum crater diameter, depth, and volume from Test 1-D. The parametric study showed that assuming a SiC yield strength of 90,000 psi gave the best correlation of SPHINX analysis results with ground test measurement. These values were applied for subsequent analyses of thruster plume particle impacts to RCC.

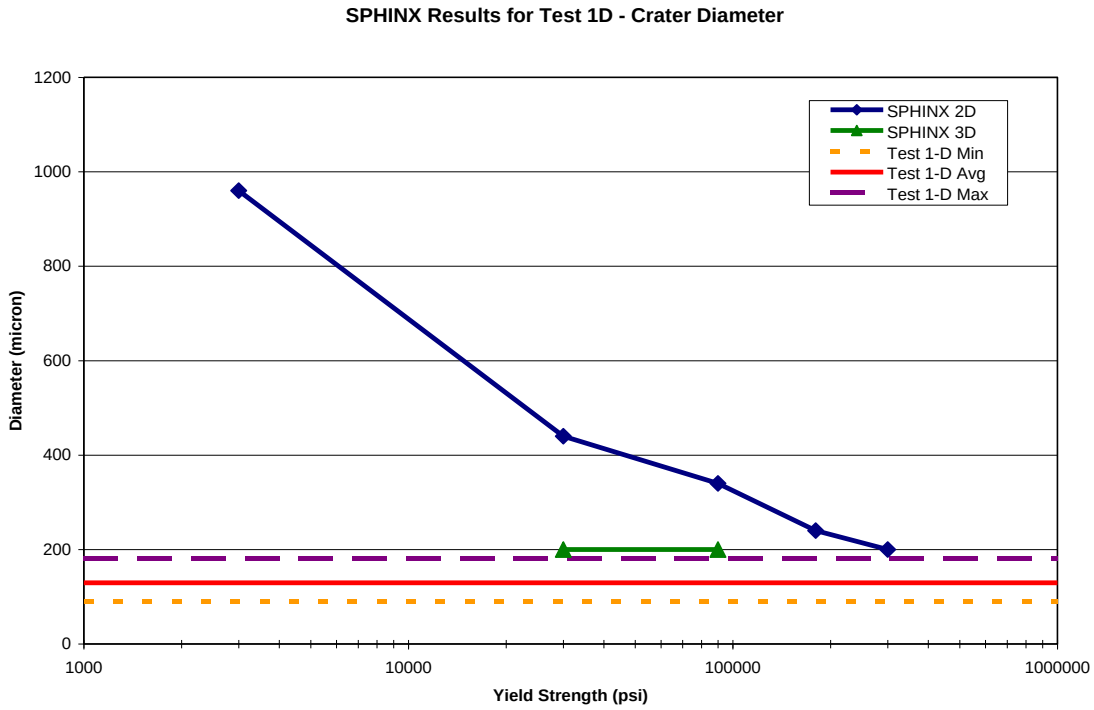

Note: SPHINX Plot measurements have an error band of +/- 20μm and Test 1-D crater measurements have error band of +/-

Figure 4-24. Crater diameters predicted by SPHINX analysis for various SiC yield strengths compared to measured crater diameters from Test 1-D.

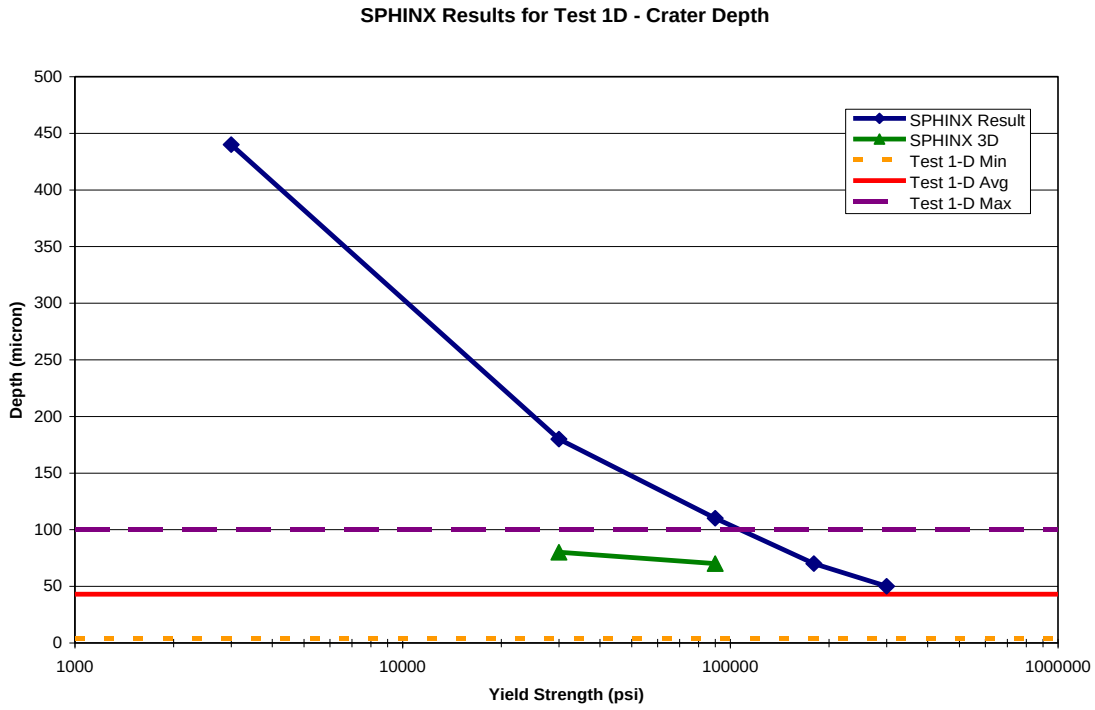

Note: SPHINX Plot measurements have an error band of +/- 20µm and Test 1-D crater measurements have error band of +/-

Figure 4-25. Crater depths predicted by SPHINX analysis for various SiC yield strengths compared to measured crater depths from Test 1-D.

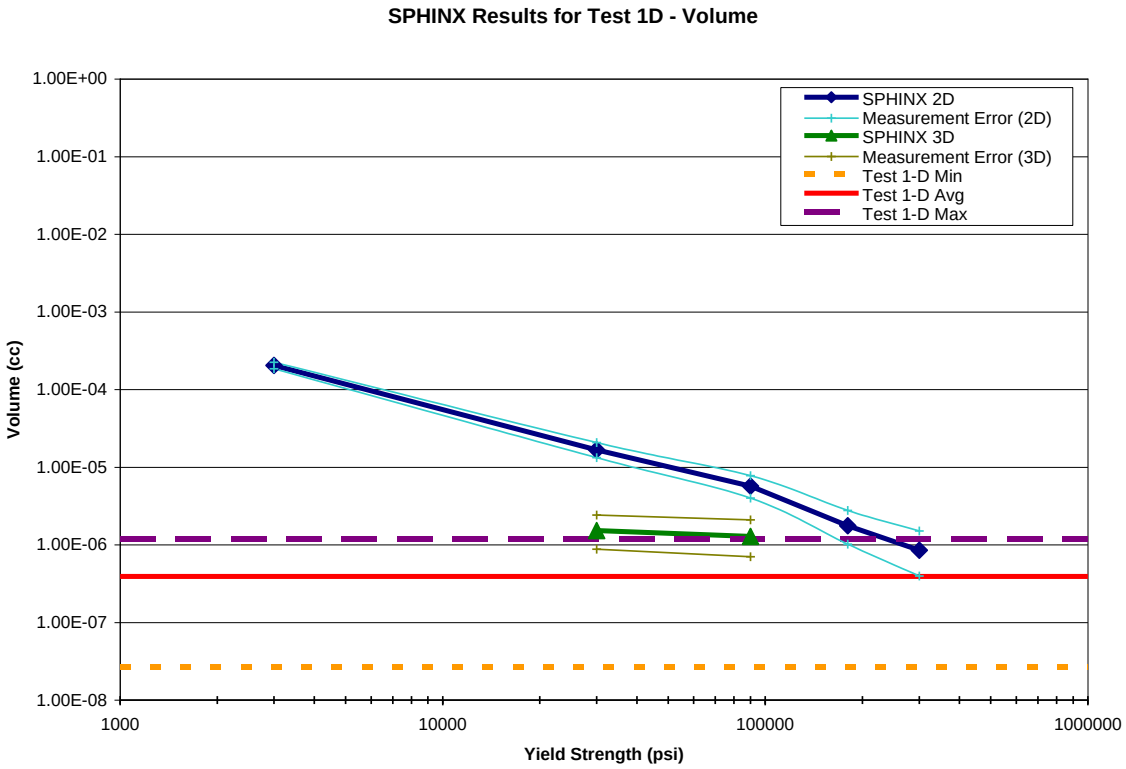

Figure 4-26. Crater volumes based on SPHINX analysis for various SiC yield strengths compared to crater volumes determined from Test 1-D measurements.

A summary of Type A, SiC, and RCC substrate material properties are shown in Table 4-13. Most of these material properties were provided by the LESS PRT; however, the SiC yield strength of 90,000 psi for SPHINX analyses was based on the parametric study findings. The LESS PRT concurred to the use of the SiC yield strength of 90,000 psi for SPHINX analyses of thruster plume particle impacts to RCC. However, the LESS PRT requested that some analysis cases be performed with a SiC yield strength of 30,000 psi as a comparison point for sensitivity.

Table 4-14 shows the SPHINX analysis case summary for thruster plume particle impacts to RCC. The first three cases corresponded to three plume particle sizes and velocities of interest. Cases 4 and 5 were comparison cases assuming a lower SiC yield strength (of 30,000 psi). A comparison case for the 100 μm plume particle was not included considering the low flux expected for particles this size. As the table indicates, the Type A coating was neglected for SPHINX simulations of thruster plume particle impacts. The Type A was difficult to model since there is no thickness specification and assuming there is no Type A present is conservative (i.e., results is more damage to the SiC layer). The LESS PRT concurred to this assumption. Additionally, modeling of the RCC substrate was not required. The SiC layer thickness was sufficient to prevent boundary effects for simulations, and omitting the unnecessary RCC substrate from the model greatly improved computational efficiency. Finally, all SPHINX analyses were performed with normal impingement angles to maximize crater depths. (Crater depth is maximum for normal incidence angles vs. oblique.)

Table 4-13. RCC material properties.

	Type A [1]	SiC	RCC Substrate
Shear Modulus (psi)	4.06×10^6	4.07×10^6 [2]	1.09×10^6
Yield Strength (psi)	4,500	90,000 [3]	800 - 12,000 [4]
Density (g/cc)	2.44	2.3	1.67
Thickness (mils)	1.5	20 - 40	n/a

[1] Modeled in SPHINX as Soda Lime Glass

[2] Based on Young's Modulus of 1×10^7 psi (from Fig. 8.10 of JSC-63036) and Poisson's Ratio of 0.23

[3] From parametric study comparing Test1-D measurements with SPHINX analysis results

[4] 800 psi in tension and 12,000 psi in compression

Table 4-14. SPHINX analysis case matrix (numbered by priority)

SiC Yield Strenth (psi)	30000	90000
Type A Yield Strength	n/a	n/a
Particle Diameter / Velocity (Expected Particle Fluence)		
5 µm / 2.9 km/s (high particle fluence)	4	1
20 µm / 2.2 km/s (moderate particle fluence)	5	2
100 µm / 1.0 km/s (low particle fluence)		3

The SPHINX simulations consisted of single particle impacts (i.e., 1 projectile) to a SiC target. The 3-D SPHINX simulations used for the plume particle analysis had high computational demands, so the minimum SiC surface area necessary to prevent boundary effects was selected. Figure 4-27 shows example SPHINX output for Analysis Case 1 at the moment of the projectile impact and the subsequent crater formed.

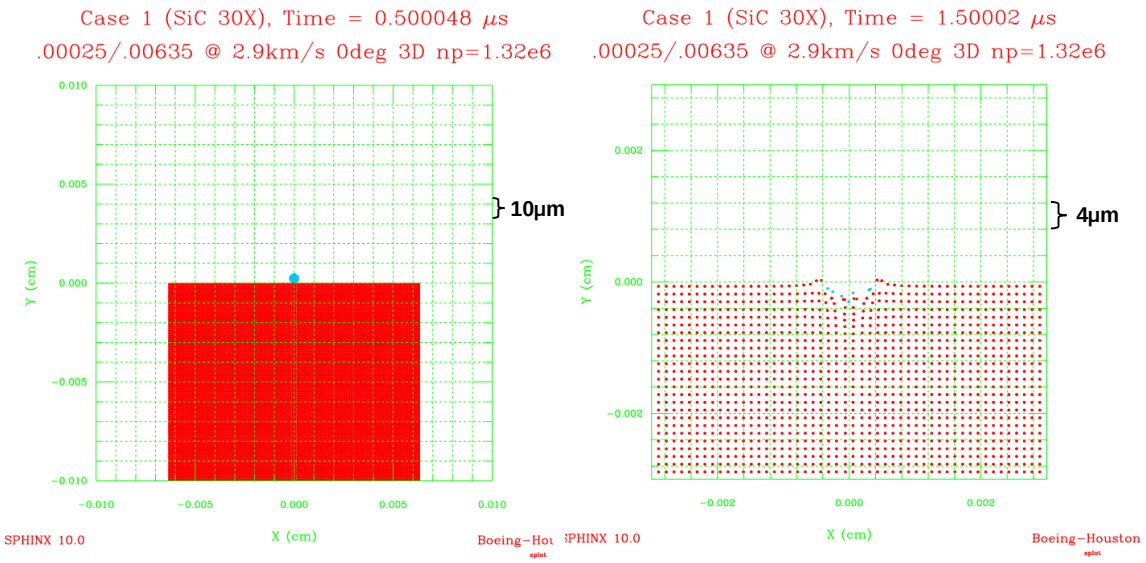

Figure 4-27. Example SPHINX analysis result: Case 1 (5 μm particle at 2.92 km/s), SiC yield strength = 90,000 psi

SPHINX analysis results for crater diameter, depth, and volume are shown in Figure 4-28 through Figure 4-30. These SPHINX results represent impact damage due to a single thruster plume particle impact. This damage must be scaled by the predicted RV thruster plume particle fluence to the Orbiter RCC due to DDO for an integrated damage assessment.

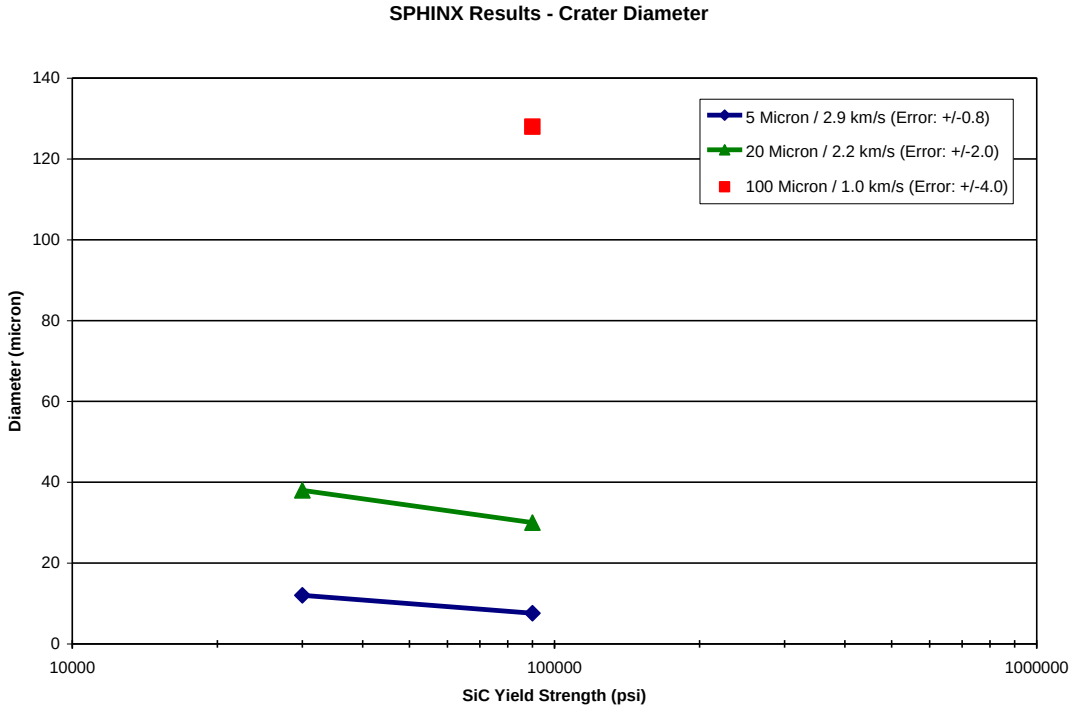

Figure 4-28. Crater diameters predicted by SPHINX analysis for thruster plume particle impacts to SiC.

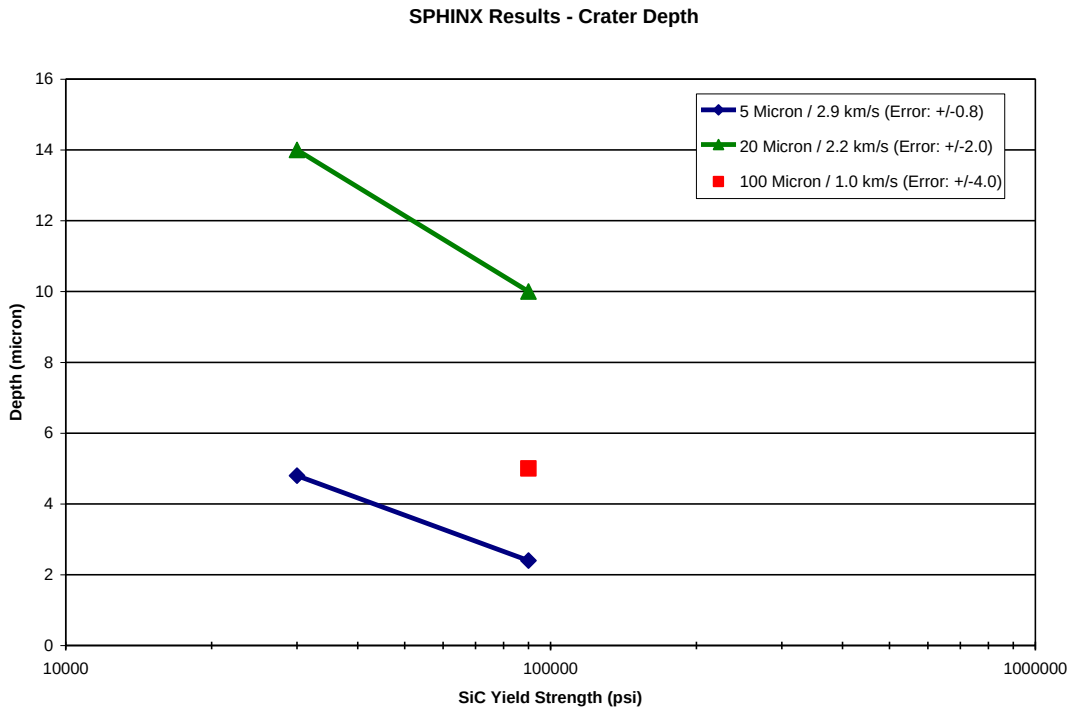

Figure 4-29. Crater depths predicted by SPHINX analysis for thruster plume particle impacts to SiC.

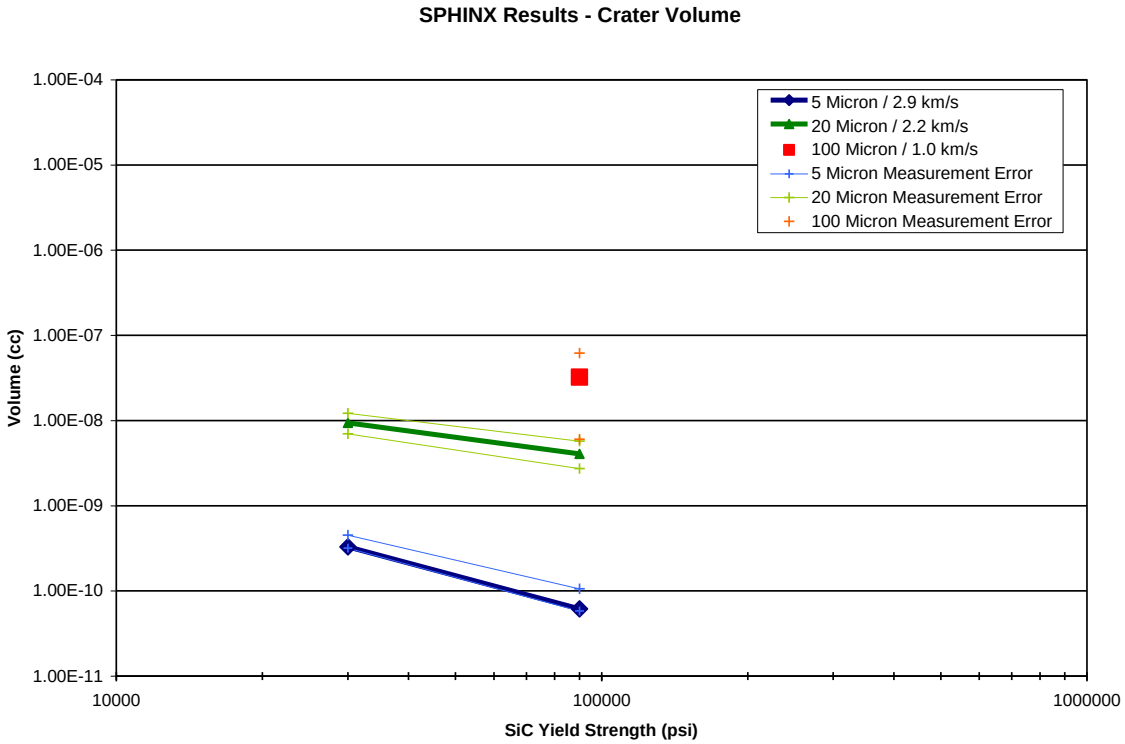

Figure 4-30. Crater volumes based on SPHINX analysis for thruster plume particle impacts to SiC.

4.7.3 Particle Fluence Calculation

Particle fluence to the Orbiter RCC was calculated for nominal RV approach and separation proximity operations using input data and methodology described in Section 4.1 with three exceptions. First, at the time the RCC test/analysis program was conducted, the ISS configuration did not include the MRM2 zenith docking port, which was incorporated in subsequent DDO studies (refer to Figure 4-3). Secondly, the RCC particle fluence was calculated prior to the 2008 revision to the thruster plume droplet flux model described in Section 4.1. The original model, which specified unburned propellant droplets with diameters between 1 and 100 μm, produced more conservative particle fluence results for the RCC. Finally, rather than calculating particle fluence on Orbiter NASTRAN™ model surfaces, particle fluence contour plots were generated in the approximate plane of the wings. A to-scale Orbiter outline (traced from Figure 4-31) was overlaid on the contour plots to allow quick estimation of the particle fluence at different points on the wings.

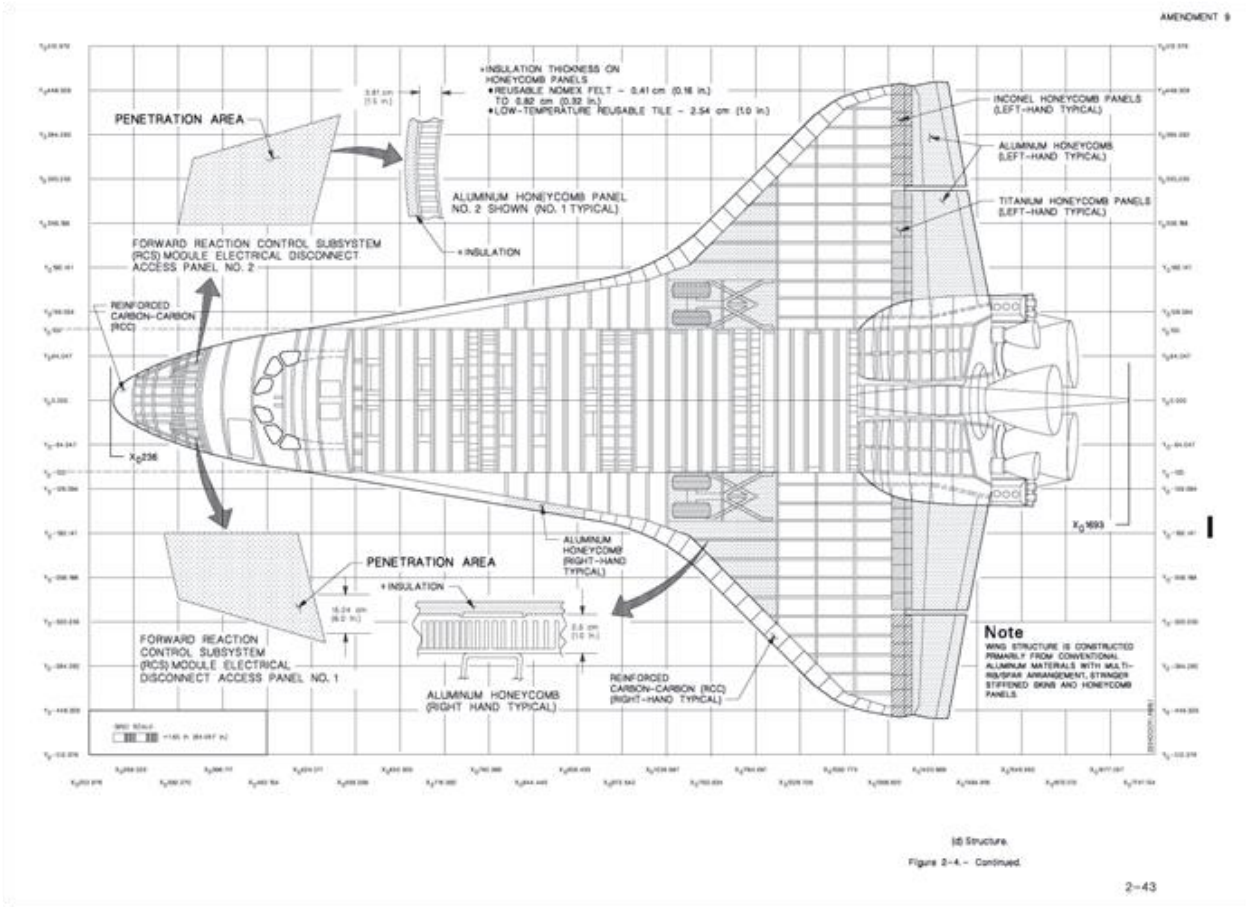

Figure 4-31. To-scale Orbiter schematic used to generate outline superimposed on contour plots [18].

RV proximity operations were analyzed for each of the three RS docking ports. Contour plots were generated to show the maximum particle fluence results per event. In checks of results, the separation results were usually minor compared to the approach results. However, given the limited available data, applying the max values for evaluating RV approach or separation is

recommended for conservatism. Soyuz thruster tests were not included in the RCC analyses, but this is expected to be enveloped by the results reported for RV approach and separation.

For each docking port, three separate contour plots were generated to show maximum particle fluence per event (i.e., approach or separation) for three particle size groups: 1-5, 6-20, and 21-100 µm. These size bins were selected to correspond with particle sizes used in the RCC impact testing and subsequent SPHINX analyses. All plots were generated at the X = 65 ft plane in the ISS Structural Reference Frame because the X = 65 ft plane is approximately coplanar with the dorsal surface of the Orbiter wings (i.e., the surface facing ISS) when Orbiter is docked to Pressurized Mating Adapter 2 (PMA2) located on Node 2 forward. A resolution of 1.0 ft by 1.0 ft was used for the contour plots. Result plots apply to the plane of the Orbiter wings and are not valid for other surfaces (e.g., radiators, TPS, windows, etc.).

Figure 4-32 shows the particle fluences due to a nominal RV approach or separation with the DC-1 nadir docking port. The Orbiter WLE RCC panels are enveloped within the "bands" outlined on the wings. As shown in Figure 4-32a, the predicted fluence of 1 to 5 µm particles is as high as 2.15 to 4.64 million particles per square centimeter on some parts of the RCC. Figure 4-32b shows the 6 to 20 µm diameter particle fluence for the same RV proximity operations event. The highest particle fluence level on the RCC for this particle size range is between 464 and 1000 particles per square centimeter. The 21 to 100 µm diameter particle fluence for the DC-1 nadir docking port is provided in Figure 4-32c. Less than one particle of this size per square centimeter is estimated on the RCC.

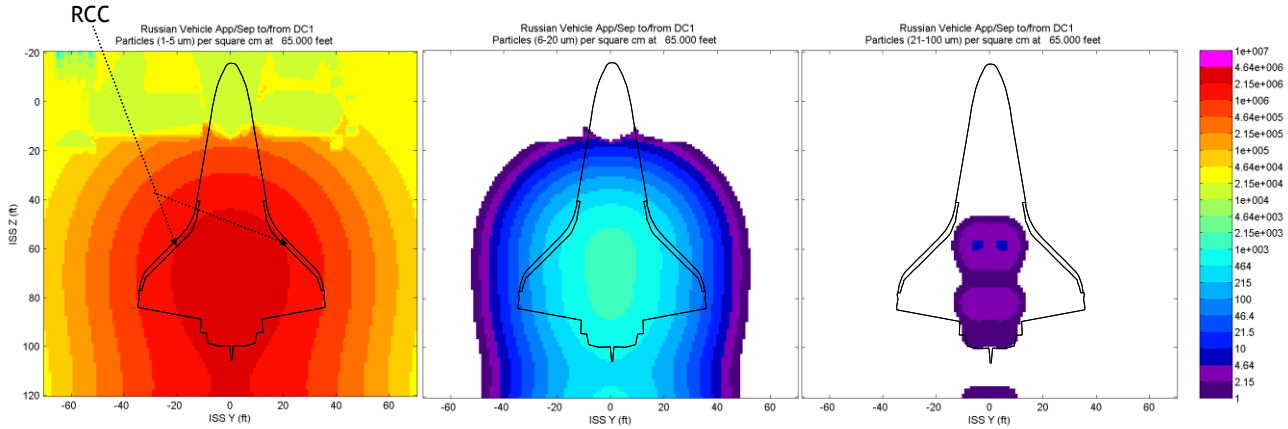

Particle Diameters: 1-5 µm
(Velocity ~ 3 km/s)
Max Particle Fluence ≤ 4.64E+6/cm²

Particle Diameters: 6-20 µm
(Velocity ~ 2.5 km/s)
Max Particle Fluence ≤ 1000/cm²

Particle Diameters: 21-100 µm
(Velocity ~ 1 to 2 km/s)
Max Particle Fluence < 1/cm²

Figure 4-32. Particle fluences due to nominal RV approach to or separation from the DC-1 nadir docking port for (a) 1-5 µm diameter particles, (b) 6-20 µm diameter particles, and (c) 21-100 µm diameter particles.

Figure 4-33 provides the particle fluence results for a RV approach to or separation from the SM aft port. Figure 4-34 provides the particle fluence results for a RV approach or separation with the FGB nadir docking port. The peak particle fluence from all three docking ports resulted from proximity operation to DC-1 Nadir, with up to 4.64 million particles per square centimeter possible. Since these results were produced with the original plume droplet flux model (rather

than the revised 2008 droplet flux model), they are expected to be conservative by roughly 1 to 2 orders of magnitude.

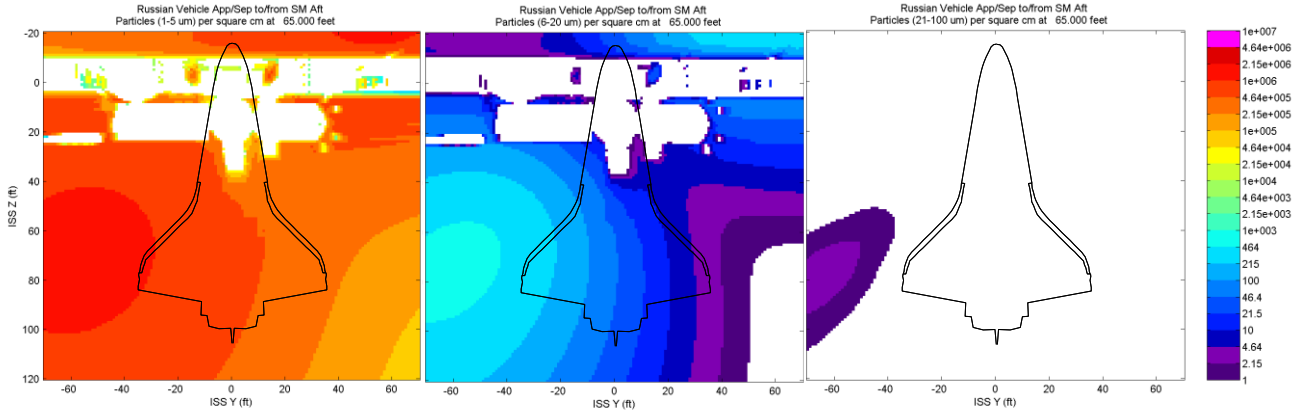

Particle Diameters: 1-5 µm
(Velocity ~ 3 km/s)
Max Particle Fluence ≤ 2.15E+6/cm²

Particle Diameters: 6-20 µm
(Velocity ~ 2.5 km/s)
Max Particle Fluence ≤ 464/cm²

Particle Diameters: 21-100 µm
(Velocity ~ 1 to 2 km/s)
Max Particle Fluence < 1/cm²

Figure 4-33. Particle fluences due to nominal RV approach to or separation from the SM aft docking port for (a) 1-5 µm diameter particles, (b) 6-20 µm diameter particles, and (c) 21-100 µm diameter particles.

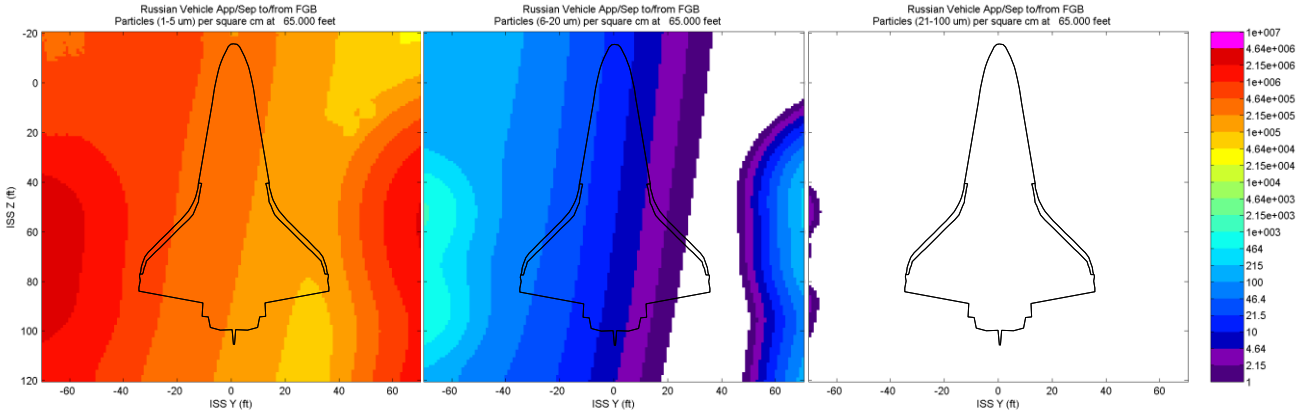

Particle Diameters: 1-5 µm
(Velocity ~ 3 km/s)
Max Particle Fluence ≤ 1E+6/cm²

Particle Diameters: 6-20 µm
(Velocity ~ 2.5 km/s)
Max Particle Fluence ≤ 215/cm²

Particle Diameters: 21-100 µm
(Velocity ~ 1 to 2 km/s)
Max Particle Fluence < 1/cm²

Figure 4-34. Particle fluences due to nominal RV approach to or separation from the FBG nadir docking port for (a) 1-5 µm diameter particles, (b) 6-20 µm diameter particles, and (c) 21-100 µm diameter particles.

It should be noted that the ISS elements provide limited shielding for Orbiter against thruster firings, though little, if any, shielding is afforded for the WLE RCC. The particle fluence in white areas is off-scale low, in some instances due to this shielding effect. It should be noted that the Orbiter payload doors, which are open when the Orbiter is mated to the ISS, will provide additional shielding to some RCC panels, though this is not accounted for in the analysis. It should be noted that accounting for lateral translation or attitude variation on the part of the RV may result in higher or lower particle fluence to the RCC (i.e., effectively shifting the contours).

Sufficient information for accurate modeling of translation or attitude dispersions during approach and separation proximity operations is not available.

Subsequent analyses were performed (contemporary with analysis reported in Section 5.2) to address particle fluence to Orbiter WLE RCC associated with RV proximity operations to the MRM2 zenith port. In contrast to the other docking ports, particle fluences to RCC for MRM2 proximity operations were calculated with the 2008 revised droplet flux model to surfaces on an Orbiter NASTRAN™ model. RCC analysis results for the 1 to 5 µm diameter particles were dramatically lower than the results for the other docking ports – less than 100 particles per square centimeter per event. This result may be used as a bounding value for the 6 to 10 µm and 11 to 12 µm particle size groups. Figure 4-35 shows example particle fluence results for RV approach to the MRM2 zenith docking port.

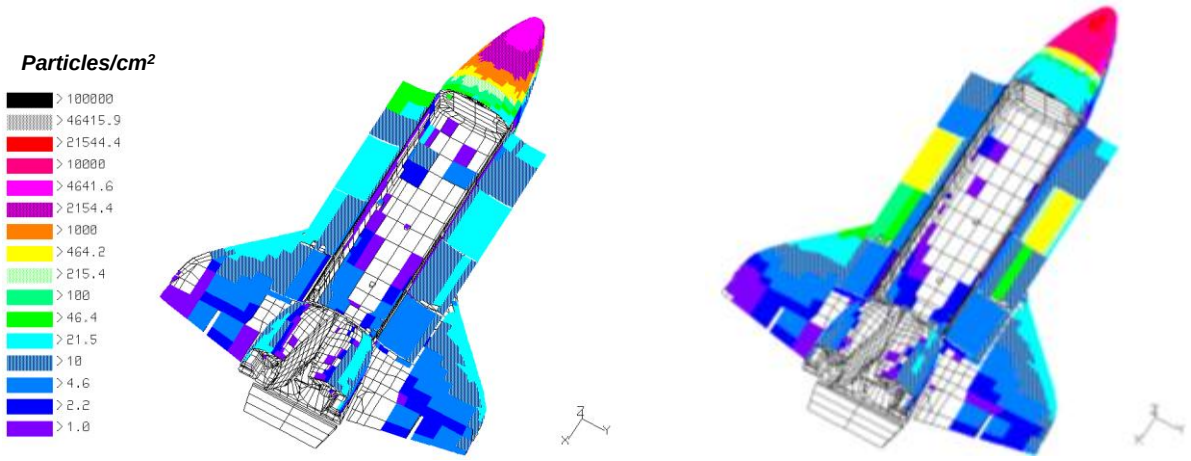

a) Results for the 8S-based jet firing history. b) Results for the 15P-based jet firing history.

Figure 4-35. Example particle fluence results for RV approach to MRM2 zenith (1 to 5 µm particles).

4.7.4 RCC Integrated Damage Assessment

The RCC integrated damage assessment was performed by linearly scaling impact damage for a single particle by the predicted thruster plume particle fluence. The impact damage for a single particle was determined analytically using the SPHINX code with correlations to ground test data (as described in Section 4.1). Thruster induced particle fluence was calculated for RV approach and separation to each RS docking port to determine the maximum particle fluence per event (as described in Section 4.1). The integration of these results into an RCC damage estimate will be presented herein.

Thruster plume induced damage to WLE RCC during DDO was calculated as a SiC coating erosion depth. Recall that the RCC uses a thin coating of silicon carbide (30±10 mils) to prevent oxidation of the substrate during reentry. Therefore, depth of coating removal is of primary interest. Two methods were utilized to evaluate damage.

a. Method 1: Average erosion depth estimate based on crater damage volume for single particles scaled linearly by particle fluence for a single event.

b. Method 2: Maximum erosion depth estimate based on total damage surface area and individual crater depths.

Additionally, recall that the baseline SPHINX analyses were performed assuming a SiC yield strength of 90,000 psi, which had the best agreement with ground test data. However, the LESS PRT requested that SPHINX analyses be performed assuming a reduced SiC yield strength of 30,000 psi as a comparison point. Naturally, the reduced SiC yield strength assumption resulted in increased thruster plume particle impact damage compared to the baseline assumption. To support LESS PRT review of the comparison data for analysis sensitivity to yield strength, the RCC integrated damage was calculated for two cases:

a. Case 1 (Baseline Case): Crater damage for all particle sizes based on SPHINX results for SiC yield strength of 90,000 psi.
b. Case 2 (Comparison Case): Crater damage for 1 to 5 µm and 6 to 20 µm particles based on SPHINX results for SiC yield strength of 30,000 psi. Crater damage for 21-100 µm particles based on SPHINX results for SiC yield strength of 90,000 psi.

Both methods for estimating damage were applied to each case to give a range of thruster induced erosion depths. For conservatism, impact damage was taken for the largest particle in each size bin (i.e., particles in 1 to 5 µm size range all modeled as 5 µm diameter particles), although the smallest particles have the greatest contribution to particle fluence. In addition, the damage estimates were taken for the highest fluence point of the RCC for the worst docking port (DC-1 Nadir).

A summary of the estimated erosion depths for each case and method is provided in Table 4-15. As shown in this table, the estimated depth of SiC erosion ranges from 0.11 to 0.87 mils based on baseline SPHINX results for SiC yield strength of 90,000 psi. For the comparison case (using SPHINX results for the reduced SiC yield strength of 30,000 psi), the estimated depth of erosion ranges from 0.61 to 1.88 mils. Both cases show little SiC erosion compared to the SiC thickness of 30±10 mils. Figure 4-36 and Figure 4-37 demonstrate the different methods for estimating damage in more detail using Case 1 as an example.

Table 4-15. Integrated Damage Assessment Results: Estimated Depth of SiC Coating Erosion.

Particle Diameter (µm)	Particle Fluence (#/cm^2)	**Case 1** Estimated Erosion Depth (mils)		**Case 2** Estimated Erosion Depth (mils)	
		Average (Method 1)	Max (Method 2)	Average (Method 1)	Max (Method 2)
5	4.64E+06	1.13E-01	0.28	6.02E-01	1.13
20	1000	1.60E-03	0.39	3.69E-03	0.55
100	1	1.27E-05	0.20	1.27E-05	0.20
	Total:	***0.11***	***0.87***	***0.61***	***1.88***

Particle fluence taken from max results for DC1 docking port.

Note: SiC thickness is 30±10 mils

Particle Diameter (μm)	Particle Fluence (#/cm^2)	Crater Vol. per particle (cm^3)	Total Vol. (cm^3/cm^2)	Avg. Depth (cm)	Avg. Depth (mils)
5	4.64E+06	6.17E-11	2.86E-04	2.86E-04	1.127E-01
20	1000	4.06E-09	4.06E-06	4.06E-06	1.598E-03
100	1	3.22E-08	3.22E-08	3.22E-08	1.269E-05
		TOTAL:	2.90E-04	2.90E-04	**0.114**

Particle fluence taken from max results for DC1 docking port.

Represent crater volume as an equivalent rectangular volume to estimate average depth.

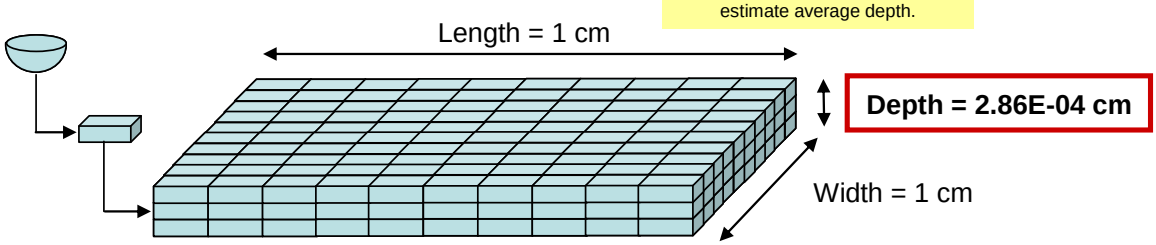

Figure 4-36. Demonstration of Method 1 average erosion depth estimate for Case 1 integrated damage calculation.

Particle Diameter (μm)	Particle Fluence (#/cm^2)	Crater Diameter (μm)	Total SA (cm^2/cm^2)	Maximum Depth (μm and mils)
5	4.64E+06	7.6	2.10E+00	2.1 Layers of 2.4μm deep pits. Maximum depth is 3 layers: **2.4μm * 3 = 7.2μm (or 0.28 mils)**
20	1000	30.0	7.07E-03	Less than 1 layer of 10μm deep pits. Maximum depth is 1 layer: **10μm * 1 = 10μm (or 0.39 mils)**
100	1	128.0	1.29E-04	Less than 1 layer of 5μm deep pits. Maximum depth is 1 layer: **5μm * 1 = 5μm (or 0.20 mils)**
			TOTAL:	**Maximum Depth: 0.87 mils**

Particle fluence taken from max results for DC1 docking port.

To calculate maximum depth, assume depth of each layer is the same as the depth of a single crater. Then add crater depths linearly (as if craters are stacked).

Depth = 2.4 + 2.4 + 2.4 = 7.2 μm

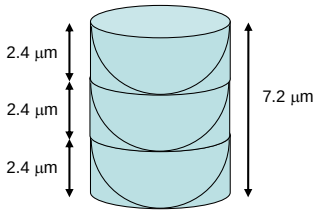

Figure 4-37. Demonstration of Method 2 maximum erosion depth estimate for Case 1 integrated damage calculation.

There were several conservative aspects to the analysis approach that should be considered when evaluating the results. To maximize crater depth, the ISS Space Environments team assumed normal impacts of all thruster plume particles to the RCC, although many of the particles are expected to impact at oblique angles. (Crater depth is maximum for normal incidence angles vs. oblique.) Additionally, the team assumed that all thruster plume particles were traveling at the limiting velocity, though the majority of particles are expected to travel at less than the limiting velocity. Crater damage was then taken for the largest particle in each size bin (i.e., particles in 1 to 5 μm size range all modeled as 5 μm diameter particles), though the smaller particles are the

highest flux. The integrated damage assessment was performed for the highest fluence point on the RCC for the worst-case docking port (DC-1 Nadir). Additionally, the particle fluence for the DC-1 nadir docking port was calculated with the original plume droplet flux model, which is conservative in comparison to the current model (2008 droplet flux model). It should be noted, however, that linearly scaling damage for a single particle impact by the predicted particle fluence may not be conservative. Furthermore, the available RV jet firing data used for the analysis is limited and is not believed to envelope all thruster plume conditions.

The OPO must determine acceptability of RV thruster induced damage to Orbiter WLE RCC. Therefore, this integrated damage assessment was delivered to the LESS PRT for review and evaluation [19]. The RCC test and analysis program was conducted in coordination with the Orbiter Structures Loads and Dynamics Panel and the LESS PRT. No technical issues were identified with the ground test or analysis approach.

4.8 Plume Pressure Force

4.8.1 Nominal Approach/Separation Plume Pressures

The ISS LDT analyzed the effects of plume impingement on the Orbiter-mated ISS configuration due to Soyuz vehicle approach to the different RV docking ports. This analysis identified the peak normal and shear plume pressures on the Orbiter components.

These data are applicable to all future Space Shuttle flights to ISS given no expected changes in the ISS configuration that will change the plume pressure results.

4.8.1.1 Plume Pressure Calculation

The plume impingement trajectory database for RV proximity operations contains 270 approach jet firing history cases, which were derived from 8 Russian as-flown trajectories and 1 generic trajectory. These trajectories do not cover failed capture or aborts.

The 270 trajectories were evaluated for induced loads on ISS for all preflight ISS verifications analysis cycles. Recently, the 270 cases were filtered to the 126 approach cases that consistently produced the maximum loading on the ISS. The two generic separation cases were included for completeness for a total of 128 cases. For the STS-132/ULF4 flight, this set of 128 cases was assessed for plume impingement pressures on the mated Orbiter/ISS configuration and identified peak normal and shear plume pressures on Orbiter components.

The ISS system, surface geometry models used were per the Verification Analysis Cycle (VAC)-ULF4 analysis, based on the Rev AC assembly sequence. The models reflected the ULF4 final mated configuration with the MRM1 module attached to the FGB nadir docking port. RV approach/separation to/from the SM aft, DC-1 nadir, and MRM2 zenith ports was assessed. For the case of the FGB/MRM1 nadir port, DDO was ruled out “due to Kurs antenna cone impingement” with the Orbiter. Only separation was analyzed.

All approach and separation plume impingement cases were applied to the mated Orbiter/ISS model. The overall peak normal and shear plume pressures with their corresponding plume duration for the Orbiter components are given in Table 4-16 for each docking port (units of lbs/sq. ft (psf) and seconds) and includes data for all Orbiter surfaces that were analyzed.

Plume pressure contour plots of the Orbiter PLBDs were created for selected cases to illustrate the pressure distribution over the doors. Representative plume pressure contours on the Orbiter PLBD are shown in Figure 4-38 and Figure 4-39.

Table 4-16. Peak Normal and Shear Plume Pressures

	Approach/Separation for DC-1 Nadir	
	Normal	Shear
Orbiter	Pressure	Pressure
Component/Hardware	psf	psf
AIRBRAKE	0.0123	0.0023
PAYLOAD BAY	0.0019	0.0016
PAYLOAD BAY DOOR PORT	0.0111	0.0038
PAYLOAD BAY DOOR STBD	0.0112	0.0034
COCKPIT	0.0080	0.0015
AFT ENGINES	0.0156	0.0056
ODS	0.0106	0.0032
OMS	0.0148	0.0023
PORT_SIDE	0.0028	0.0040
STBD_SIDE	0.0027	0.0039
TAIL	0.0278	0.0077
TAILTIP	0.0287	0.0092
WINGS	0.0115	0.0016

	Approach/Separation for SM Aft	
	Normal	Shear
Orbiter	Pressure	Pressure
Component/Hardware	psf	psf
AIRBRAKE	0.0015	0.0003
PAYLOAD BAY	0.0000	0.0000
PAYLOAD BAY DOOR PORT	0.0025	0.0008
PAYLOAD BAY DOOR STBD	0.0025	0.0008
COCKPIT	0.0027	0.0005
AFT ENGINES	0.0020	0.0007
ODS	0.0029	0.0009
OMS	0.0020	0.0005
PORT_SIDE	0.0002	0.0004
STBD_SIDE	0.0002	0.0004
TAIL	0.0019	0.0008
TAILTIP	0.0020	0.0007
WINGS	0.0020	0.0005

	Approach/Separation for MRM2 Zenith	
	Normal	Shear
Orbiter	Pressure	Pressure
Component/Hardware	psf	psf
AIRBRAKE	0.0008	0.0004
PAYLOAD BAY	0.0000	0.0000
PAYLOAD BAY DOOR PORT	0.0069	0.0023
PAYLOAD BAY DOOR STBD	0.0077	0.0024
COCKPIT	0.0098	0.0017
AFT ENGINES	0.0013	0.0005
ODS	0.0087	0.0028
OMS	0.0017	0.0004
PORT_SIDE	0.0001	0.0008
STBD_SIDE	0.0001	0.0008
TAIL	0.0016	0.0007
TAILTIP	0.0012	0.0005
WINGS	0.0047	0.0014

	Separation from MRM1 Nadir	
	Normal	Shear
Orbiter	Pressure	Pressure
Component/Hardware	psf	psf
AIRBRAKE	0.0005	0.0001
PAYLOAD BAY	0.0001	0.0001
PAYLOAD BAY DOOR PORT	0.0018	0.0004
PAYLOAD BAY DOOR STBD	0.0013	0.0003
COCKPIT	0.0007	0.0002
AFT ENGINES	0.0010	0.0004
ODS	0.0008	0.0003
OMS	0.0013	0.0003
PORT_SIDE	0.0002	0.0004
STBD_SIDE	0.0002	0.0003
TAIL	0.0008	0.0004
TAILTIP	0.0007	0.0003
WINGS	0.0025	0.0005

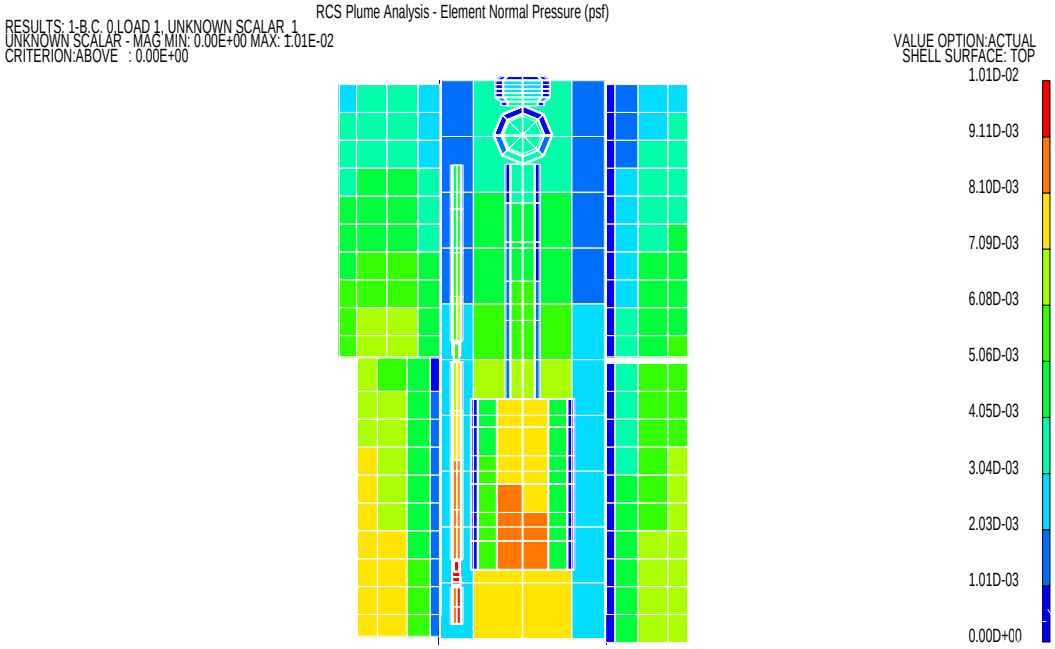

Figure 4-38. Peak normal pressure on port PLBDs - DC-1-Nadir.

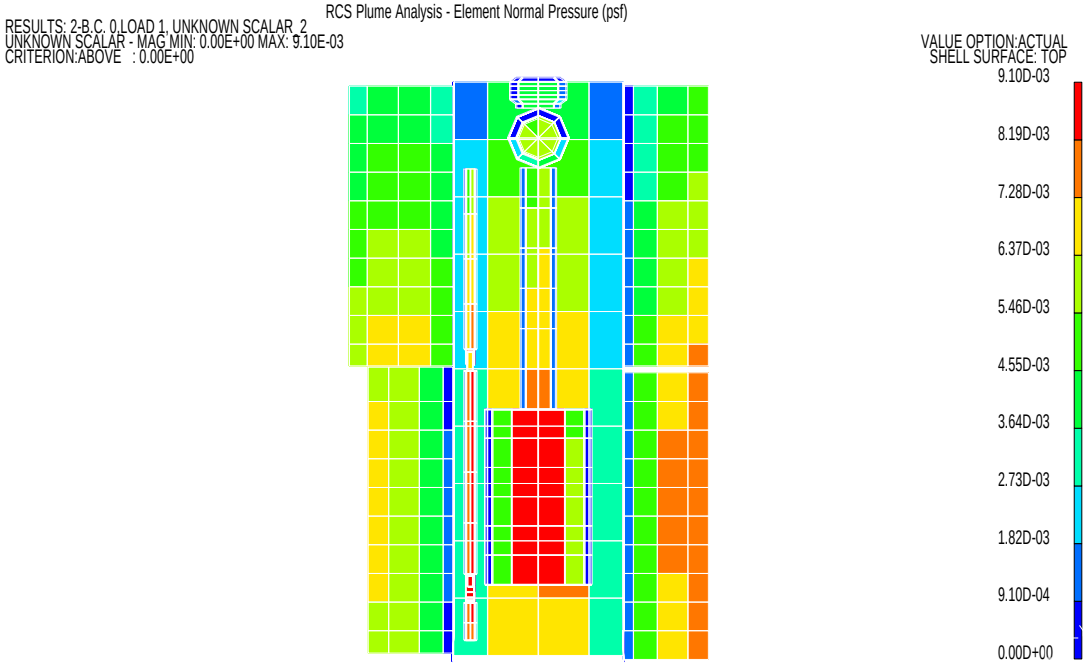

Figure 4-39. Peak normal pressure on starboard PLBDs - DC-1-Nadir.

4.8.1.2 Recommendations for Orbiter Team Dynamic Analyses

The nominal pressure values in **Error! Reference source not found.** were delivered to the OPO for the Orbiter specific analyses. For the PLBD dynamic loads analyses, the LDT provided Orbiter with the recommendation to assume 10 consecutive pulses in the dynamic analysis. This

number was based on a survey of the trajectory database, which showed a maximum of six firings that could be considered consecutive firings. These firings were not of the same duration nor were they in the same direction. Since this number came from a limited set of as-flown histories, the LDT recommended that the Orbiter team assume a maximum of 10 consecutive firings of the peak pressure (in the same direction) for their analysis.

4.8.2 Plume Pressures for Off-Nominal Abort Case

The LDT worked with the JSC Applied Aerosciences team plume specialists to develop an off-nominal plume pressure case. The off-nominal case would assume a firing of a dual jet pair pointed directly normal to the Orbiter PLBD, with an interaction amplification factor applied to the plume pressure derived from the Soyuz jet plume flow field. The distance from the Orbiter would be the closest distance from an approved RV port, assuming a 15° abort corridor.

The Soyuz jet plume flow field data provided to the ISSP and the Applied Aerosciences team were used to develop the off-nominal abort case. The data were provided to the LDT in tabular format by the Applied Aerosciences team. To determine the correct region in the plume flow field, the closest distance from the edge of the 15° corridor approaching/departing from the DC-1 nadir port was determined. This distance was approximately 80 feet, yielding a plume pressure of 0.0043 psf per Soyuz jet firing. For the PLB, the distance was determined to be approximately 95 ft, yielding a plume pressure of 0.0027 psf per Soyuz jet firing.

The Applied Aerosciences team developed and recommended a bounding plume interaction amplification factor of 1.634. Therefore, to calculate the peak plume pressures for this case, refer to the following:

PLBD: 2 x 0.0043 psf x 1.634 = 0.014 psf

PLB: 2 x 0.0027 psf x 1.634 = 0.0088 psf

This peak pressure value for the off-nominal abort case was provided to the OPO for their Orbiter loads analyses. As for the nominal pressures, the LDT recommended that the OPO use a maximum of 10 consecutive pulses for the off-nominal case. However, for this abort case, it was recommended that only the first five pulses be at the peak abort plume pressure, with the next five at the peak nominal plume pressure.

4.8.3 Dual Jet Plume Interaction

This section documents the development of a bounding amplification factor to be applied to account for the firing of two jets simultaneously as opposed to the operation of a single jet.

The RV on occasion will simultaneously fire two jets in close proximity during maneuvers. It is known that under such circumstances a region of amplified dynamic pressure will develop in between the two thrusters. The magnitude of this amplification is above the value of just adding the two associated single jet environments together (i.e., superposition). To assess a bound for the magnitude of this amplification, high fidelity computational simulations were performed using a technique known as Direct Simulation Monte Carlo (DSMC). DSMC uses millions of representative molecules to simulate rarefied gas flows and is an appropriate method for simulating flows (e.g., a spacecraft reaction control system plume expanding into vacuum).

The single jet environment for the 13.3 kg (29.8 lb) RV thrusters has been developed by RSC-E and is of the source flow type. The algebraic form of this model is documented in SSP 50129, Annex 1.1.

Figure 4-40 shows the results of a DSMC simulation for the Soyuz dual jet firing with the most severe amplification (due to these thrusters having the minimum separation). The right-hand side of the figure shows the Soyuz vehicle and the "in flow" boundaries (colored by the flow density on these surfaces) for the two jets being simulated. The conditions on these "in flow" boundaries were obtained from a computational fluid dynamics simulation of the flow in 13.3 kg thruster nozzle and near plume flow. The results of the DSMC simulation are on the left-hand side of Figure 4-40. The region of amplified dynamic pressure between the two jets can be seen, especially in the region near the nozzle exit planes. This is the case because the magnitude of the amplification falls as the distance "downstream" in the plume increases. Note that the domain of simulation is finite and extends to about the length of the Soyuz solar array. This was necessary to ensure that there was sufficient resolution to adequately capture the relevant physics while keeping the simulation computationally tractable. A larger domain would have required significantly more simulated molecules than the 150 million employed in the simulation shown in Figure 4-40. However, since the purpose of this simulation was to determine a bound for the amplification and, as noted, this amplification factor falls as the distance downstream increases, it was decided that the maximum value of the furthest constant "y" plane in Figure 4-41 (i.e., y = 6 m (19 ft)) would bound the amplification factor at larger distances. Furthermore, this value would serve as a bounding value for all distances of interest since at distances less than 6 m, the Orbiter would have made contact with the Soyuz array.

To get a quantitative value for the amplification factor on this y = 6 m plane, additional DSMC simulations were performed for the two jets firing independently. The amplification factor could then be computed as the ratio of the simulation shown in Figure 4-40 to the sum of the simulations of the two jets firing independently. The results of such a computation are shown in Figure 4-41 where the peak amplification was found to be 1.634. This value will be conservative for this application since for distances greater than 6 m, the value of the amplification factor will be lower and since for application to the DDO scenario, the entire Orbiter will be more than 6 m from RV dual jets.

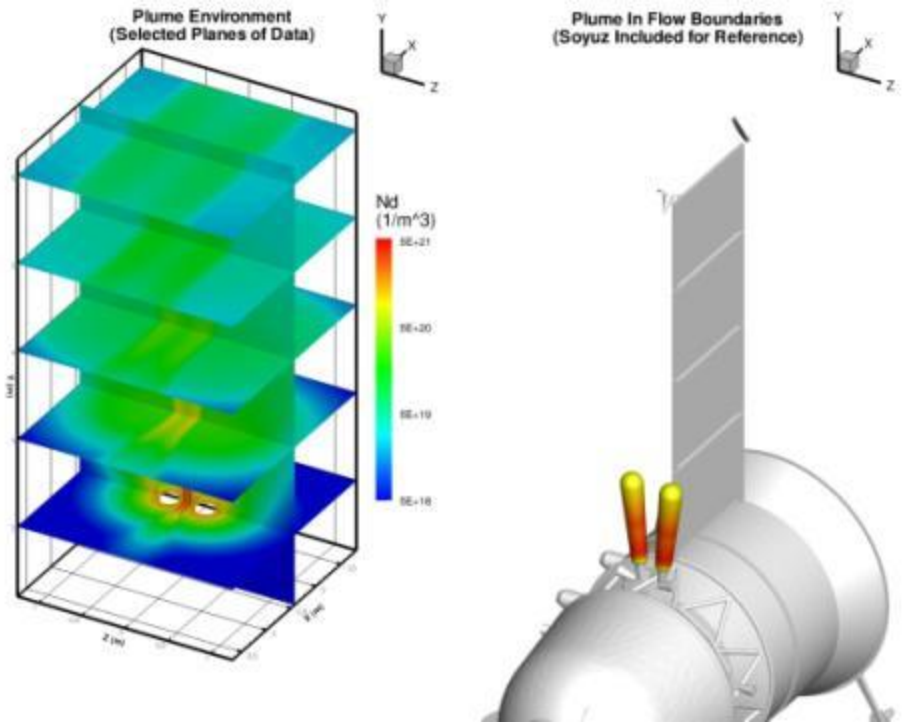

Figure 4-40. DSMC simulation of Soyuz dual jet firing.

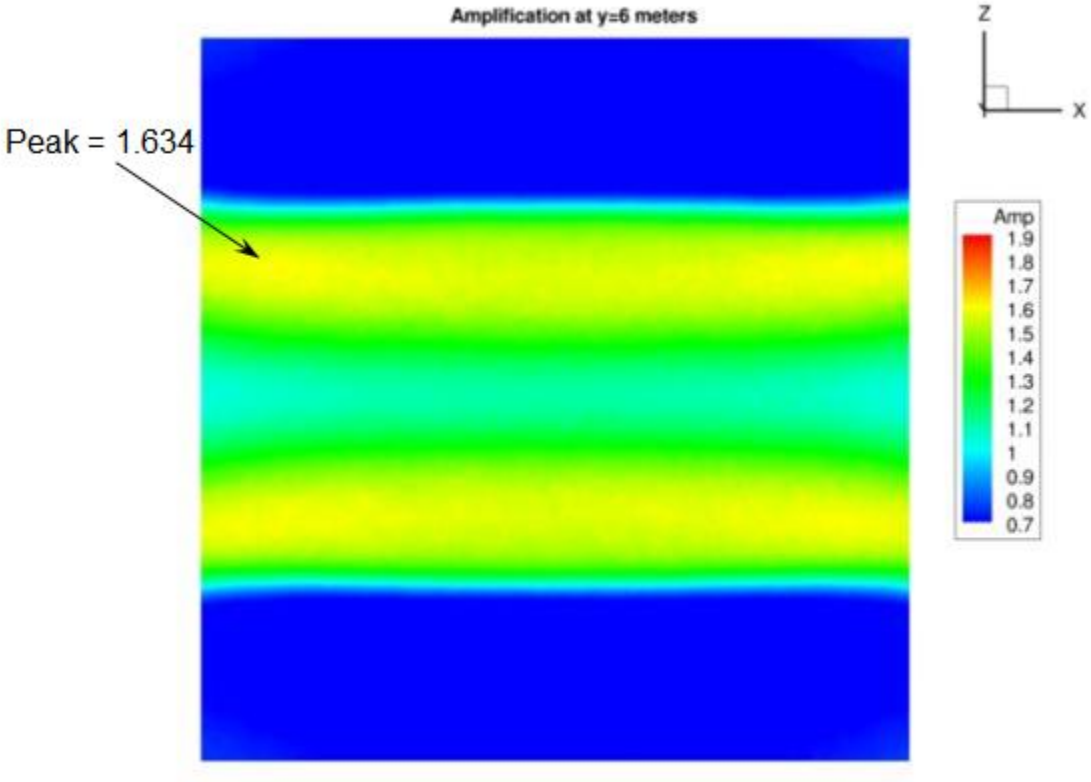

Figure 4-41. Dual jet amplification factor on y = 6 m plane.

In summary, conservative plume flow field environments have been developed and provided for single and dual jet firings of the RV 13.3 kg thrusters. These environments are suitable for assessing plume impingement loads during DDO.

5.0 Trajectory Clearance Assessments

DDO can be defined as the dynamic operations of the one or more RVs while the Orbiter is docked to the ISS. The purpose of this chapter is to describe trajectory analysis approach, discuss results, and provide recommendations for the Soyuz vehicle departure from all ISS ports. To ensure safe separation, the analysis has to be performed to demonstrate sufficient structure clearance between Soyuz vehicle, ISS structure, and any other docked vehicles, including the Orbiter. When docked at the PMA at Node 2 forward, the Orbiter body and tail extend below and under the ISS structure, thus adding constraints on the departing vehicle trajectory, which in turn may add constraints to the undock attitude.

This chapter details the analysis of Soyuz separations for a variety of initial conditions. Because the primary separation concerns involve nadir port docked Soyuz vehicles, the separations are focused on FGB nadir port separations only since it represents the most constraining case. However, as time and resources allow analysis can be extended to include the DC-1, MRM1, MRM2, Multipurpose Laboratory Module (MLM) and SM Aft port separations.

The described analysis is performed for the ISS at the STS-129/ULF3 flight configuration with a docked Orbiter at the PMA at Node 2 forward and the 19S Soyuz vehicle departing from FGB port. The atmospheric conditions chosen will be consistent with the ones predicted for the STS-129/ULF3 flight.

With the Orbiter present, the ISS has two preferred attitude control methods: the Orbiter VRCS control and the RS thruster control, each having their own defined attitude and attitude rate deadbands. The analysis will be performed for each of these attitude control methods and for a variety of initial ISS attitudes. These attitudes include the +X-axis Vertical Velocity (+XVV) +Z-axis Local Vertical (+ZLV) (Yaw-Pitch-Roll (YPR) 0,0,0 [0,0,0 Roll-Pitch-Yaw (RPY)]) attitude, the ISS 180 yaw or -XVV +ZLV (YPR 180,0,0 [0,0,180 RPY]) attitude, and the ISS 180 yaw attitude coupled with a 90° pitch or -XLV -ZVV (YPR 180,90,0 [0,-90,180 RPY]) attitude, and dispersions around these attitudes due to the individual attitude control options deadbands. The +XVV +ZLV attitude is used as the reference case for the analysis. The -XVV +ZLV attitude is the standard attitude for the Orbiter-ISS stack. Maneuvering to the undock attitude will be performed from this attitude. Orbiter VRCS vs. RS control method may be evaluated based on final undock attitude and amount of propellant required for specific maneuvers. The -XLV -ZVV attitude is an approved ISS attitude, and it was previously analyzed and approved for uncrewed Orbiter undockings in the Contingency Shuttle Crew Support (CSCS) scenario. Furthermore, -XLV -ZVV attitude meets the intent of Hazard Report RSCE-0021 for minimal pitch angle to provide for safe long-term clearance between the departing Soyuz and ISS in case of the Soyuz motion control system failure.

The performance of the Russian docking mechanism and the Soyuz vehicle motion control system determine the separation dynamics and relative motion. The docking mechanism nominal performance discrepancies and the potential failure of Soyuz motion control system drive are specific conditions that may lead to collision.

The relative motion analysis described further in this section addresses the mentioned conditions in a parametric fashion. Resulting relative motion trajectories represent the Soyuz vehicle center

of gravity (c.g.) motion, which in turn is used for the detailed structural clearance analysis by the Configuration Analysis Modeling and Mass Properties (CAMMP) team.

Even though this separation analysis focuses on the ISS/Orbiter stack and Soyuz vehicle relative motion, the resulting trajectories and initial conditions are applicable to the Progress vehicle.

Conclusions and recommendations based on the analysis results are presented.

5.1 Assumptions

This section discusses the assumptions that are made as a part of the analysis. Wherever possible, details and references are provided for the assumptions, and a detailed discussion follows. The assumptions include data assumptions, where choices of initial conditions are specified and referenced, and analysis assumptions, where analysis methods are discussed with particular concentration on the limitations of the methods chosen.

The ISS and RV parameters are primarily obtained from JSC-26557, Revision AD[1], On-Orbit Assembly, Modeling, and Mass Properties Data Book, with the exception of certain parameters provided by VIPER.

The RV separation follows a defined timeline, which begins when the ISS is commanded to free drift. One minute later the Soyuz crew or Mission Control Center-Moscow issues a command to the vehicle to open the RV docking mechanism hooks. At this point, hooks on the ISS side are already open. Once the "hook open" command is issued, the RV motion control system takes a "snapshot" of current ISS attitude and begins propagating it based on the attitude rate sensor data. This process allows the vehicle to maneuver to the proper attitude for the first separation burn that will follow physical separation. Note that the "starting" attitude in the motion control system is the undocking attitude, and it is set via an uplinked quaternion several orbits before undock. The hook opening process takes 180 (nominal, two hook drive motors operating) to 310 (off-nominal, one hook drive motor operating) seconds, at which time the physical separation occurs.

The separation analysis begins at physical disconnect. At this time, the vehicle receives an initial push-off velocity from springs in the docking port mechanism, allowing it to clear the structure. The RV motion control system is in the free drift mode in this timeframe, so the vehicle is subject to dispersions in the spring push-off velocity, and attitude and velocity dispersions due to separation dynamics. The springs generate a push-off velocity in the longitudinal direction (along the docking axis) that varies between 0.09 and 0.15 m/second as a function of the mass of the separating RV, docking mechanism spring pushers performance, docking mechanism operational dispersions, etc. Additionally, the effect of unequal spring contribution or unequal guide pin travel during separation may result in a 0.03 m/s velocity component in the transverse direction. This transverse velocity component is applied in the XY plane direction and is positive in the forward ISS direction and negative towards the aft.

[1] A later revision (AG) is available. Version referenced was used for most of the work in the report as it was the latest at the time [43].

Ten seconds after physical separation, the RV motion control system becomes active and commands the vehicle to return its attitude to the snapshot attitude obtained at the time of "hooks open" command. This attitude is held through the 15 second longitudinal body burn, which occurs 180 seconds after physical separation and increases separation velocity to approximately 0.6 m/s depending on RV mass properties. The attitude provides a general alignment with the docking port for purposes of monitoring the separation dynamics via the external camera view and sets the separation vector in the direction opposite from the ISS. This first burn sets up conditions for RV deorbit burn two orbits later and allows the vehicle to clear the ISS Keep-Out Sphere (KOS) within 22 minutes.

The vehicle may perform an optional retrograde burn to further distance itself from the ISS vicinity at 550 seconds after physical separation. This second burn is 30 seconds long bringing RV separation velocity to 1.4 to 2.0 m/s based on RV mass properties. This burn was developed for nadir port separations, but since ± ZVV -XLV attitudes had been approved for RV undockings, this burn is never applied.

The analysis employs relative motion calculations using the Clohessy-Wiltshire (CW) linearized relative motion equations coupled with rigid body rotation dynamics equations for attitude propagation and burn direction determination. The CW relative motion propagation is a three degrees-of-freedom (3-DOF) simulation and the ISS stack (ISS + Orbiter) and Soyuz are treated as point masses. Certain secondary effects, such as gravity gradient, solar flux, etc., have been ignored for this first-level analysis because they are negligible over the short duration during which the separating RV is in close proximity to the ISS. Additionally, the effect of the ISS stack mass change following the RV separation is also ignored as the mass change is negligible in comparison to the total ISS stack mass.

Each separation trajectory is simulated for 500 seconds. This duration is sufficient to cover the short-term clearance of ISS-stack structure as well as to capture the relative motion for nearly 5 minutes following the time of the expected first RV burn.

The ISS and RV relative motion and clearance assessment is not a part of this current analysis.

5.2 Scenario

The analysis was performed for 19S undock during STS-129/ULF3 flight; however, this approach can be used for a generic ISS-Orbiter and RV combination.

In this configuration, the RVs are docked at FGB, DC-1, and SM aft. The Orbiter is docked at the PMA at Node 2 Forward.

5.3 ISS Parameters

Mated configuration parameters selected per Configuration 268 - Step 020. Data for this stage was obtained from JSC-26557, Revision AD, On-Orbit Assembly, Modeling, and Mass Properties Data Book, Volume I, "ULF3 - Before Separation [MATED]" on page 7-143.

The ISS coefficient of drag (C_d) is not available in the aforementioned data book. A value of 2.07 was provided by the Trajectory Operations Officer (TOPO) group.

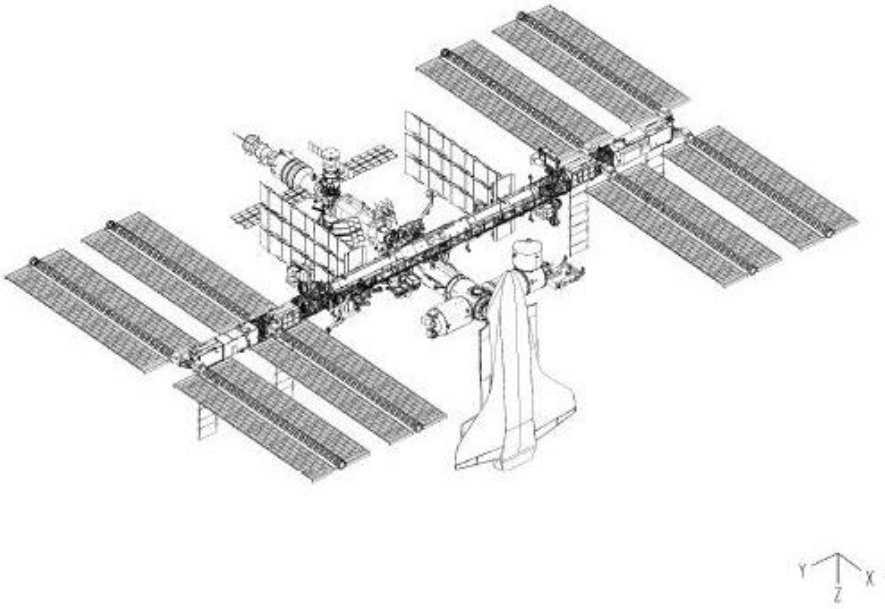

Figure 5-1. STS-129/ULF3 flight (before separation) [MATED], configuration 268 - Step 020.

Table 5-1. ULF3 Stage - ISS Parameters

Parameter	Value [Reference]
Mass	439941 kg [Ref: 1]
Center of Mass	0.88, -0.69, 6.18 m (Relative to ISS Analysis Coordinate System (ISSACS)) [Ref: 1]
Coefficient of Drag (C_d)	2.07 [Ref: 2]
Cross-Sectional Area	1080.32 m^2 (X projected area, used for the YPR 0,0,0, YPR 180,0,0 attitudes) 3214.46 m^2 (Z projected area, used for the YPR 180,+90,0 attitude) [Ref: 1]
Inertia Tensor	[138170844. 1369308. -20643473.] [. 1369308. 126205020. -244627.] [-20643473. -244627. 208345629.]$kg*m^2$ [Ref: 1]

Ref 1: JSC 26557 Revision AD "On-Orbit Assembly, Modeling, and Mass Properties Data Book," Volume I, "ULF3 - Before Separation [MATED]," Configuration 268, Step 020, on page 7-143

Ref 2: TOPO group

5.3.1 Soyuz Parameters

Mass Properties

The Soyuz parameters were obtained from JSC-26557, Revision AD, On-Orbit Assembly, Modeling, and Mass Properties Data Book, Volume I, for the specified docking ports detailed below. The coefficient of drag (C_d), 2.00, was provided by the TOPO group.

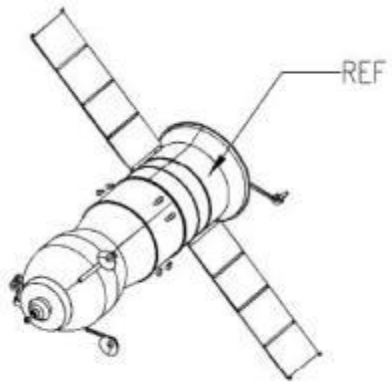

Figure 5-2. Soyuz vehicle.

Table 5-2. Soyuz Parameters

Parameter	Value [Reference]
Mass	6745 kg [Ref: 1]
Center of Mass (Relative to ISSACS)	FGB:. . -11.140, 0.000, 9.420 m [Ref: 1, Page 7-56] DC-1: . -23.700, 0.000, 13.450 m [Ref: 1, Page 7-56] SM Aft: . -39.820, -0.040, 4.160 m [Ref: 1, Page 7-103] MRM1 (mass at this port is 6700 kg): . -11.140, 0.000, 15.420 m [Ref: 1, Page 7-263] MRM2 (mass at this port is 6700 kg):. . -23.700, 0.000, -5.160 m [Ref: 1, Page 7-160] MLM: . No current data are available.
Coefficient of Drag (C_d)	2.00 [Ref: 3]
Cross-Sectional Area	24.2 m^2 for the YPR 0,0,0 and YPR 180,0,0 attitudes 6.0 m^2 for the YPR 180,90,0 attitude [See details below]
Inertia Tensor	[4639.. -161.. -589.] [-161. 24412.. 418.] [-589.. 418. 24454.]kg*m2 [Ref: 1, based on Soyuz at SM aft port orientation.]

Ref 1: JSC 26557 Revision AD "On-Orbit Assembly, Modeling, and Mass Properties Data Book," Volume I
Ref 2: TOPO group
Ref 3: VIPER/Evgeny Menkin

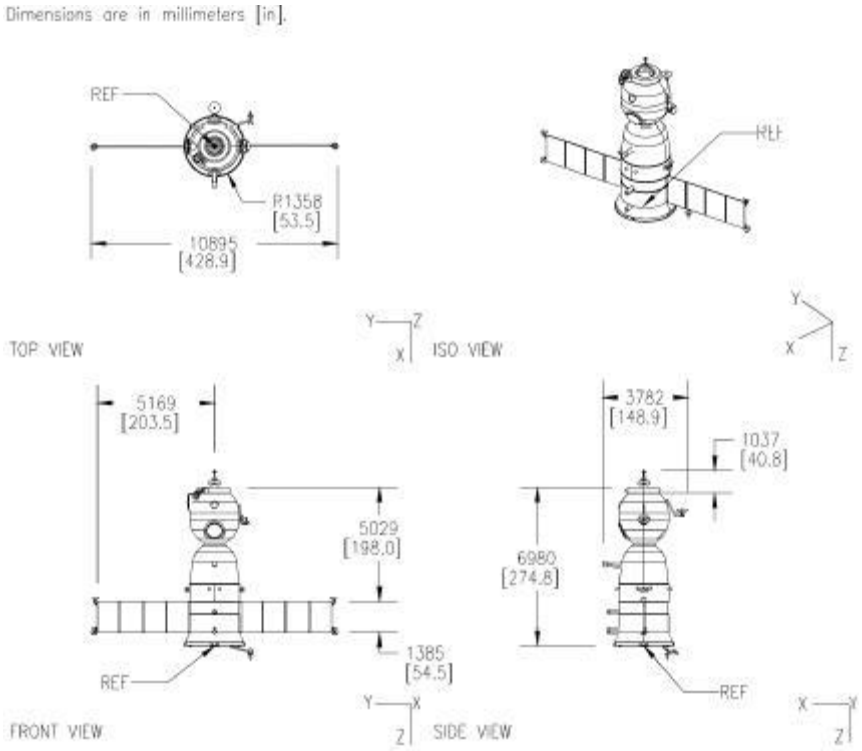

Source: JSC 26557 Revision AC "On-Orbit Assembly, Modeling, and Mass Properties Data Book," Volume I, page 7-89 (not available in Revision AD)

Figure 5-3. Soyuz vehicle structural reference data.

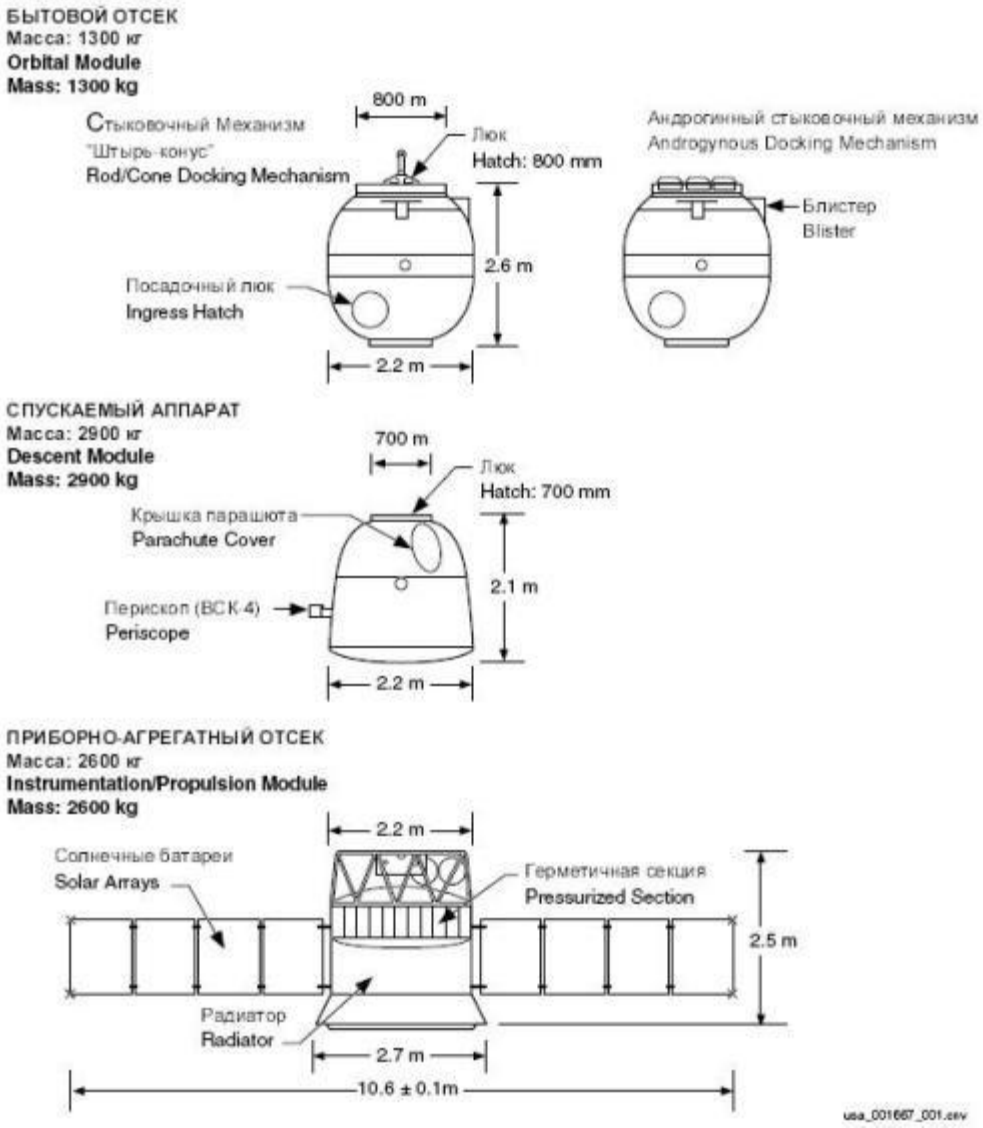

Source: USA001667 "Data Book: Soyuz/Progress," November 15, 2000, page 2-5

Figure 5-4. Soyuz modules sizing data.

5.3.1.1 Cross-Sectional Areas

The cross-sectional area of the Soyuz is a function of ISS stack attitude, docking port location, and the relative attitude of the vehicle at the port. Figures 5-2 to 5-4 serve as the source of data used to calculate the approximate planar cross-sectional areas:

X: ~ 6.0 m^2

Defined as the Soyuz YZ plane area or along the longitudinal direction and calculated using the largest radius component of 1.35 m (half of 2.7 m). The final result is rounded to 6.0 m^2 to account for area contributed to by the edges of the Soyuz solar arrays.

Y: ~ 28.0 m^2

Defined as the Soyuz XZ plane area or the top view, including the full solar array span. This area is calculated by summing up the rectangular areas of each module plus the area of the solar arrays:

- Orbital module area = 5.72 m^2 (2.2 m x 2.6 m)
- Descent module area = 4.62 m^2 (2.2 m x 2.1 m)
- Instrumentation/Propulsion module area = 5.5 m^2 (2.2 m x 2.5 m)
- Solar Array area = 11.6 m^2 (10.6 m wingspan minus the 2.2 m middle section multiplied by the 1.385 m height)

Z: ~16.0 m^2

Defined as the Soyuz XY plane area or the side view, looking edge on to the solar arrays. This area is calculated like the Y planar area, excluding the solar array contribution.

45° area (e.g., Roll at FGB nadir port): ~24.2 m^2

While docked at the FGB nadir port, the Soyuz vehicle is rotated approximately 45° around its X axis. This results in a reduced cross-sectional area facing along the velocity vector. This area is calculated using the Soyuz Z side area plus the projected area of its solar arrays when rotated by 45° (16.0 m + 11.6 m * cosine [45]).

5.3.1.2 Contact Sphere

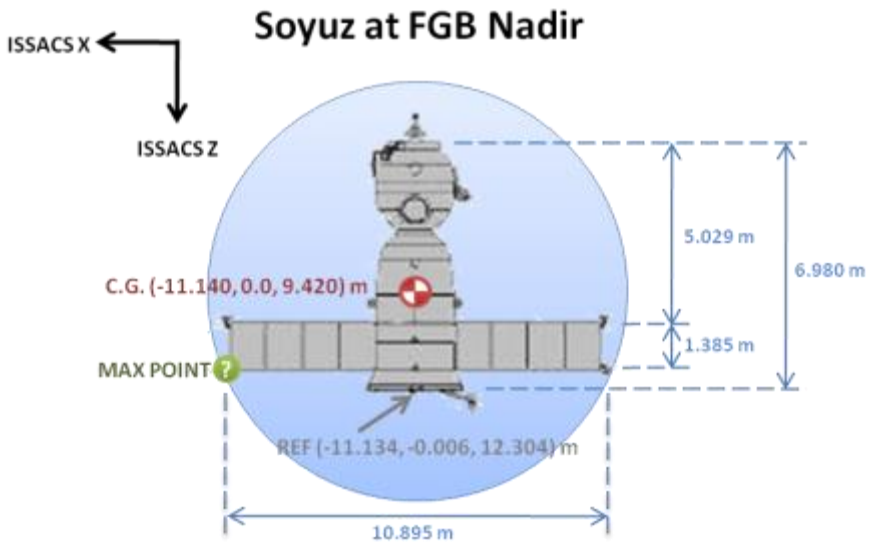

Data/Coordinate Source: JSC 26557 Revision AC "On-Orbit Assembly, Modeling, and Mass Properties Data Book," Volume I, page 7-89 (not available in Revision AD)

Figure 5-5. Soyuz at FGB Nadir ISSACS coordinates.

The contact sphere serves as first order analysis object to determine if potential contact exists between the RV and any other structure. It is defined as a 6.0 m radius sphere originating at the

RV center of mass, as seen in Figure 5-5, and large enough to account for any attitude of the vehicle enclosed within it.

The "MAX POINT" has been identified as the furthest point from the RV c.g. and was calculated to be (-5.687, 0.0, 11.738) m in the ISS Analysis Coordinate System (ISSACS) reference frame, based on a Soyuz vehicle docked at the FGB nadir port. The distance from this point to the Soyuz vehicle center of mass at FGB nadir was calculated to be 5.926 m within the bounds of the 6.0 m radius contact sphere defined for analysis purposes. Because of the physical similarity of the RVs, the 6.0 m radius analysis limit is valid for both vehicles.

If any interference is determined through the first order analysis, the contact sphere would be excluded, and direct structure to structure clearance would be analyzed. This analysis is performed by the CAMMP team.

5.4 Simulation Tools

The analysis was performed using the Proximity Analysis for Dynamic Motion Effects (PADME) tool and verified using the Flight Design and Dynamics (FDD) CW Spreadsheet tool.

PADME is a Java-based program developed within the Automated Rendezvous and Docking (AR&D) group specifically for RV separation analyses. The tool employs 3-DOF relative motion propagation algorithms, coupled with rigid body rotation dynamics for attitude propagation. The tool has shown good agreement with past analysis results provided by RSC-E, and has been in good agreement in 3-DOF relative motion with the NASA/FDD CW Spreadsheet tool.

Independent verification of the PADME results is achieved by using the FDD CW Spreadsheet tool, a certified analysis tool used by the ISS Visiting Vehicle Officer (VVO). This tool is limited to only providing 3-DOF relative motion analysis and verification.

5.4.1 3-DOF Relative Motion

A 3-DOF relative motion analysis was performed using the CW linearized relative motion equations (i.e., Hill's equations).

5.4.2 Rigid Body Rotation Dynamics

To increase the fidelity of the analysis, ISS stack attitude propagation was performed using a rigid body rotation dynamics algorithm available in the PADME analysis tool. This method employs vehicle inertia parameters to propagate the vehicle rotational parameters and more accurately account for the attitude rates at the time of physical separation.

The damping of the ISS stack attitude rates due to environmental, inertial, or forced effects is not accounted for as a part of this analysis because this model is not currently available within the PADME tool. Instead, it is assumed that a rotational effect will continue to propagate unimpeded for the duration of the simulation.

The source for the rigid body rotation dynamics implementation is the algorithm developed by William Lear [44].

5.5 Rotation Sequence

The SSP rotation sequence basis is the Roll-Pitch-Yaw (RPY) or the 1-2-3 sequence, while the ISSP rotation sequence basis is Yaw-Pitch-Roll (YPR) or the 3-2-1 sequence. For this analysis, the YPR sequence is primary, and any alternative sequences are explicitly noted in brackets "[ ]".

5.6 Altitude

The altitude chosen for this analysis is 370 km and is based on previous similar analyses. The choice of altitude only affects the period of an orbit because the atmospheric density is assumed constant for this analysis.

5.7 Atmospheric Density

The atmospheric density for STS-129/ULF3 flight timeframe provided by VIPER is 2.46e-12 kg/m^3.

5.8 Gravity Gradient Effects

Gravity gradient is a slow acting force and is assumed to have a negligible effect over the short duration during which the separating RV is in close proximity to the ISS. The effect on the RV is even less once the vehicle regains active attitude control 10 seconds following separation. Once attitude control is active, the gravity gradient effects are counterbalanced and therefore have no direct effect on the vehicle.

5.9 Aerodynamic Torques

The effect of aerodynamic torques is ignored for this analysis. This effect is assumed to be equally applied on the ISS stack and the separating RV, and, much like the gravity gradient effect discussed, its effect is minimal over the short duration during which the separating RV remains in close proximity to the ISS.

5.10 RV Separation Timeline

Every RV separation follows the same predefined timeline. A graphical representation of this timeline was provided by RSC-E during AR&D Mini-TIM no. 10 (October 2 to 13, 2006) in the presentation, "Gravitational Moment Effect on Initial Conditions of Vehicles Separation" and updated by VIPER, as shown in Figure 5-6.

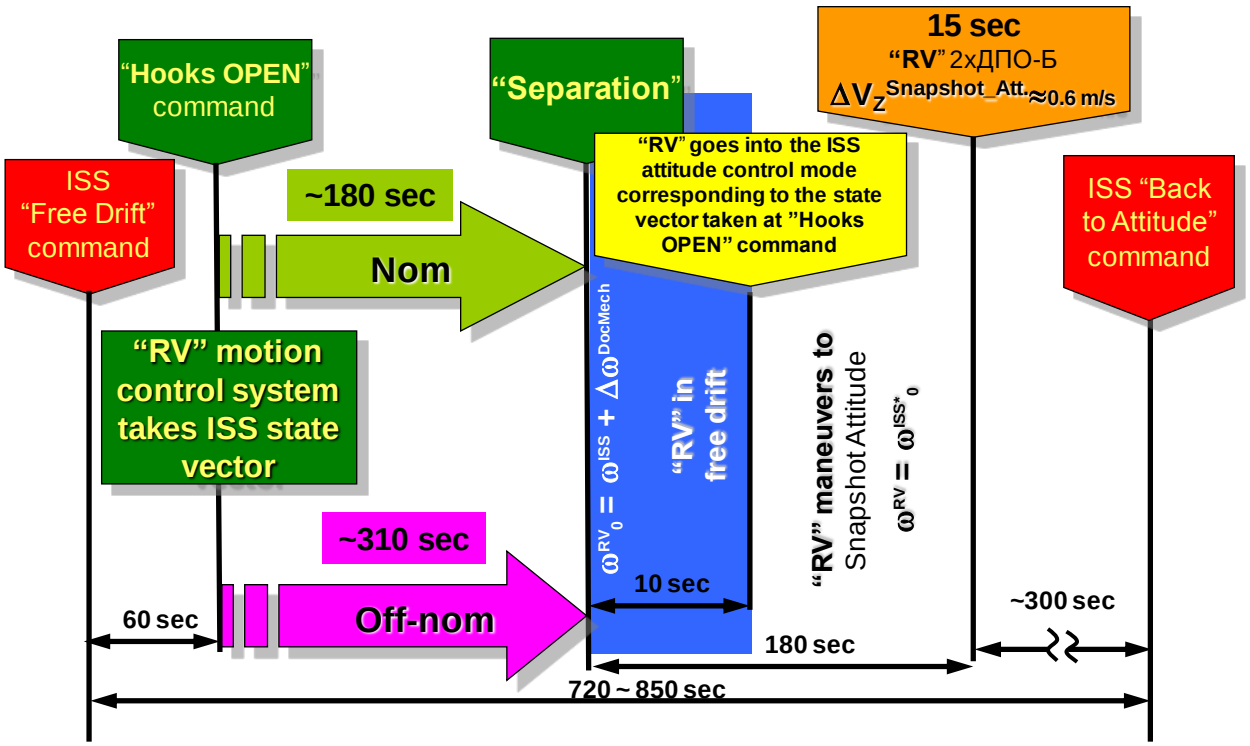

Source: Presentation, "*Gravitational Moment Effect on Initial Conditions of Vehicles Separation*," RSC-E, AR&D Mini-TIM #10 (October 2-13, 2006) with VIPER updates

Figure 5-6. RV separation timeline.

The nominal separation sequence initiates with a "Hooks OPEN" command, at which time the RV motion control system obtains a "snapshot" of the current attitude. For approximately the next 180 seconds, the RV docking mechanism active hooks are driven open, and the vehicle separates with an initial velocity imparted to it by the compressed docking springs in the ISS docking mechanism. At the time of physical separation, the RV is in a free drift mode, so any initial attitude rates and velocities imparted on the vehicle due to imperfect separation dynamics (e.g., failed spring, caught hook, etc.) cause it to move away from the ISS and changes attitude. Ten seconds after separation, the RV motion control system begins to maneuver back into the "snapshot" attitude it had at the time of the "Hooks OPEN" command. At 180 seconds after physical separation, the RV performs the separation burn. This 15 second longitudinal body burn increases separation velocity to approximately 0.6 m/s, depending on RV mass properties.

In the off-nominal separation sequence, the time between "Hooks OPEN" command initiation and physical separation can increase to 310 seconds. This off-nominal sequence would most likely be the result of a hook drive motor failure, resulting in extended hook opening duration and hence a delay in physical separation. The events that follow physical separation are the same as for the described nominal separation sequence.

5.10.1 ISS Attitude Profile during RV Separations

During the standard RV separations under RS control, the ISS stack is in free drift from 1 minute prior to the initiation of the separation sequence to 5 minutes after the vehicle has separated. For the duration of the free drift period, the ISS stack is not actively controlled, and hence its attitude

is based on the attitude rates determined by the initial rate plus any additions or subtractions due to external forces.

The magnitude of the initial rates, and the magnitude of the initial attitude, is primarily based on the attitude control scheme that maintains the stack attitude. The available attitude control schemes and their properties are covered in Section 5.12.

Figure 5-7 through Figure 5-12 describe the time ordered sequence of attitudes that the ISS could be at following the initiation of the separation sequence at a positive pitch attitude deadband and a positive pitch attitude rate deadband. The deadband attitude and attitude rate, and the final attitude and attitude rates, presented in the images are nonspecific and are dependent on the selected attitude control scheme.

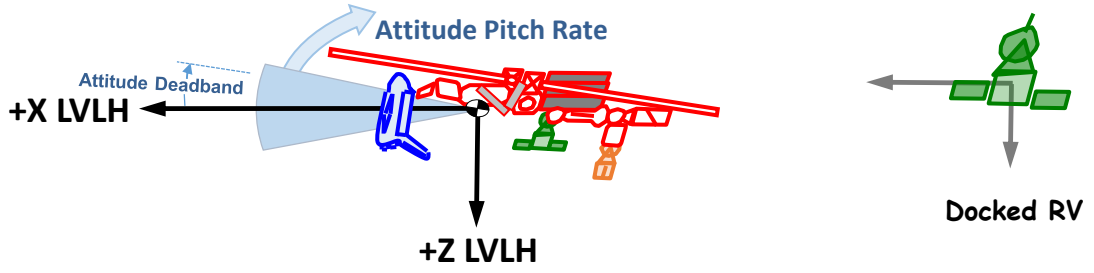

time = $t_{sep} - \Delta t_{HooksOpen} - 60$ sec

Figure 5-7. ISS attitude at maximum of deadband range, ISS commanded to “Free Drift”.

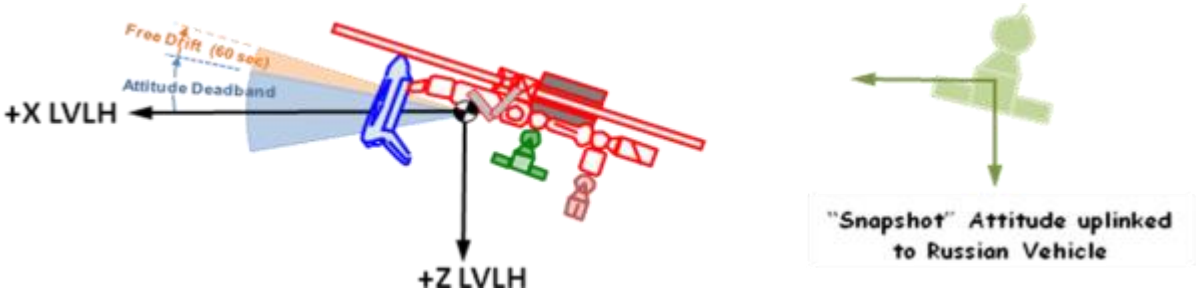

time = $t_{sep} - \Delta t_{HooksOpen}$

Figure 5-8. ISS in “Free Drift” for 60 seconds, RV commanded to “Hooks Open” and “Snapshot” attitude taken.

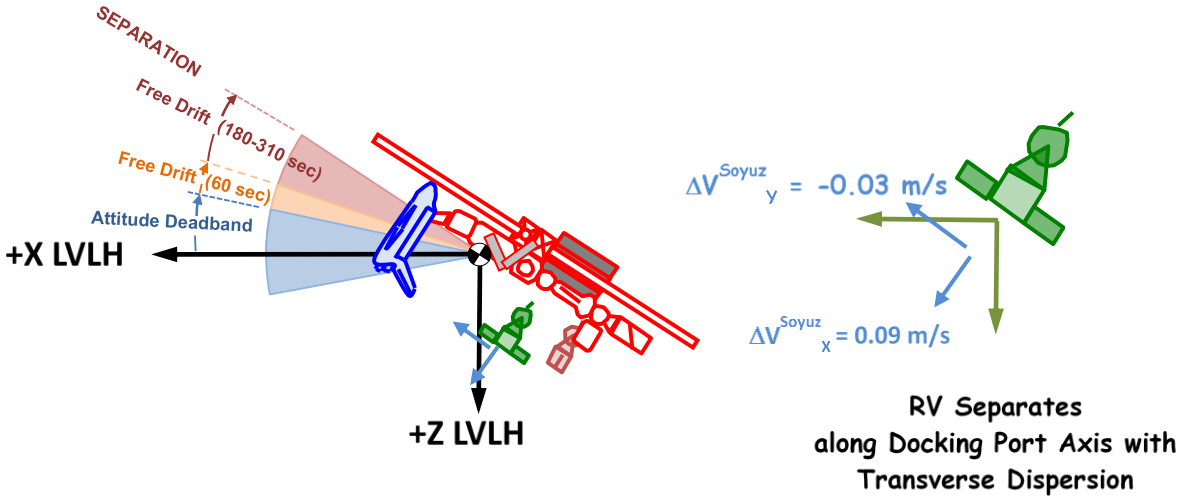

time = t_{sep}

Figure 5-9. ISS hooks drive for 180 (nominal) to 310 (off-nominal) seconds, vehicle separates.

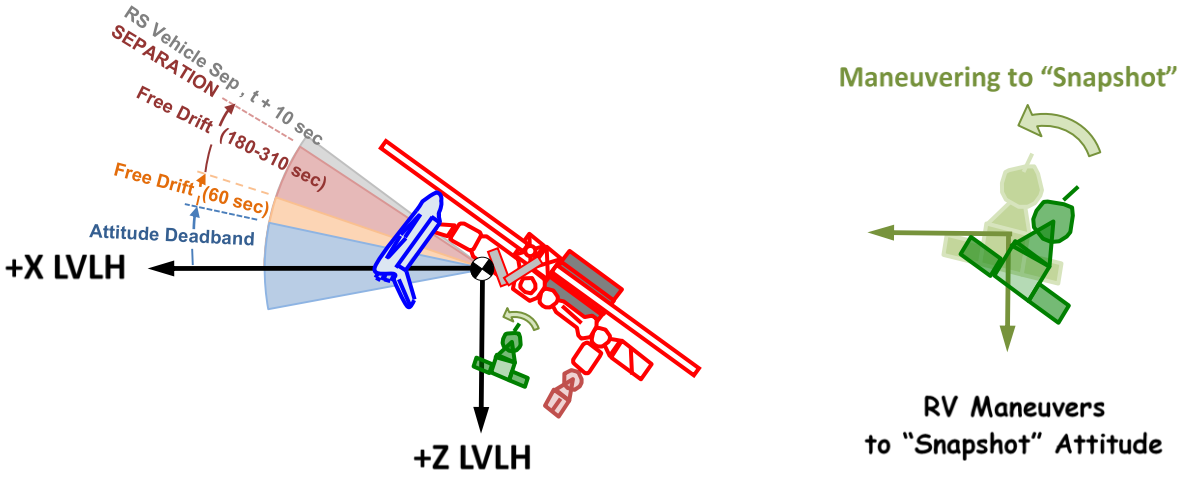

time = t_{sep} + 10 sec

Figure 5-10. RV has separated and is maneuvering back to "Snapshot" attitude.

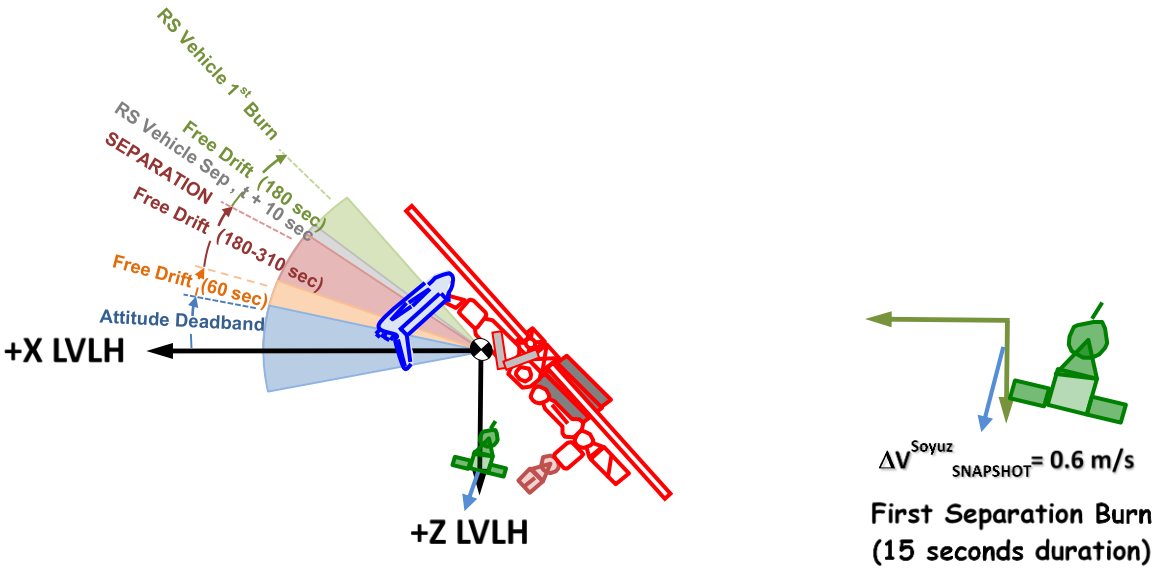

time = t_{sep} + 180 sec

Figure 5-11. RV - first separation burn with 0.6 m/s magnitude, 15 seconds duration.

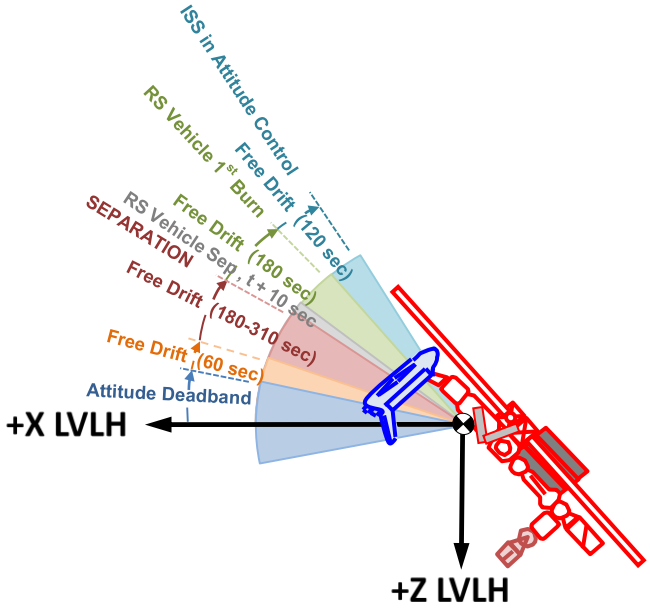

time = t_{sep} + 300 sec

Figure 5-12. ISS returns to attitude control.

5.10.2 Pertinent Flight Rules

The following Flight Rule is relevant to RV separations from the ISS and this analysis [45].

D4-101 SOYUZ/progress automated UNDOCKING AND SEPARation sequence [rC]

A. UNDOCKING (PHYSICAL SEPARATION) WILL OCCUR 3-6 MINUTES AFTER THE UNDOCKING COMMAND. SEPARATION WILL BE PROVIDED BY THE SPRING PUSHERS AND THE INITIAL RELATIVE VELOCITY WILL BE 0.09 TO 0.15 METERS/SECOND. ®[CR 7186] ®[072706-7094B]

B. TEN SECONDS AFTER UNDOCKING, THE SOYUZ/PROGRESS WILL MODE AUTOMATICALLY TO ACTIVE CONTROL TO KEEP THE SOYUZ/PROGRESS ALIGNED WITH THE DOCKING PORT.

1. WHILE IN ACTIVE CONTROL, SOYUZ WILL HOLD THE ATTITUDE IDENTICAL TO THE ISS ATTITUDE AT THE INSTANT OF PHYSICAL SEPARATION. ®[ED]

   THE UNDOCK ATTITUDE QUATERNION IS PUT ONBOARD IN THE UNDOCK SETPOINTS. THE SOYUZ WILL PROPAGATE THE ATTITUDE BASED ON ATTITUDE RATE DATA STARTING AT THE TIME THE UNDOCK COMMAND IS ISSUED, AND THE SOYUZ WILL RETURN TO THIS ATTITUDE WHEN IT MODES TO ACTIVE CONTROL.

2. WHILE IN ACTIVE CONTROL, PROGRESS WILL HOLD THE ATTITUDE IDENTICAL TO THE ISS ATTITUDE AT THE INSTANT OF PHYSICAL SEPARATION. ®[ED]

   THE UNDOCK ATTITUDE QUATERNION IS PUT ONBOARD IN THE UNDOCK SETPOINTS. THE PROGRESS WILL PROPAGATE THE ATTITUDE BASED ON ATTITUDE RATE DATA STARTING AT PHYSICAL SEPARATION, AND THE PROGRESS WILL RETURN TO THIS ATTITUDE WHEN IT MODES TO ACTIVE CONTROL.

C. 180 SECONDS AFTER UNDOCKING, THE SOYUZ/PROGRESS WILL AUTOMATICALLY PERFORM A 15-SECOND BURN AWAY FROM THE DOCKING PORT WITH THE ДПО +X THRUSTERS (APPROXIMATE delta V 0.6 M/S).

D. AFTER COMPLETION OF THE BURN, AN AUTOMATED TEST OF THE ДПО +X THRUSTERS WILL BE PERFORMED. IF ONE OR MORE OF THE THRUSTERS ARE FOUND TO BE FAILED, THE THRUSTERS WILL BE RECONFIGURED AND THE BURN WILL BE REPEATED WITHIN 45 SECONDS. ®[072706-7094B]

E. A SETPOINT FOR COMPLETING THE REMAINING STEPS (F, G) FOR UNDOCKING IN AUTOMATIC MODE WILL BE SET REGARDLESS OF ISS ATTITUDE, EXCEPT IN CASES OF TRANSVERSAL (± VELOCITY VECTOR) SEPARATION AND THEN ONLY BY DECISION OF MCC-M. ®[072706-7094B]

F. 420 SECONDS AFTER UNDOCKING, THE SOYUZ/PROGRESS WILL AUTOMATICALLY MANEUVER TO AN ATTITUDE THAT POINTS THE BODY +X AXIS ALONG THE NADIR AND THE BODY +Y AND -Z AXES BISECTING THE VELOCITY VECTOR.

G. 550 SECONDS AFTER UNDOCKING, THE SOYUZ/PROGRESS WILL AUTOMATICALLY PERFORM A 30-SECOND BURN WITH THE ДПО -Y AND +Z THRUSTERS. THIS IS A RETROGRADE BURN WITH APPROXIMATE DELTA V 1.4 to 2.0 M/S. ®[CR 7186]

DOCUMENTATION: HAZARD REPORT RSTV-0026; REPORT: SOYUZ-TM AND PROGRESS-M SOFTWARE VERIFICATION FOR ISS (VERSION [MO-17]); AND AUGUST 25, 2005 AR&D TELECON MINUTES, ATTACHMENT 2. *®[072706-7094B]*

FLIGHT/STAGE EFFECTIVITY: ALL FLIGHTS

5.11 Docking Port Separation Dynamics

Due to the design of the Russian docking mechanism, separation cannot always be assumed to be perfect. Potential snags of docking mechanisms can impart additional dynamics on the separating

vehicles. These dynamic dispersions have been identified by RSC-E and can be grouped into three distinct dispersion categories: longitudinal velocity, transverse velocity, and rotational. These categories are discussed in the following sections.

5.11.1 Longitudinal Velocity Dispersions

Nominally, the velocity imparted on the separating vehicle by the compressed docking port springs can vary from 0.09 to 0.15 m/s, depending on the mass of the departing vehicle. In the case of a single failed spring and heaviest departing vehicle, the smallest possible imparted velocity would be 0.09 m/s. For this analysis, only the minimum longitudinal velocity of 0.09 m/s is used since it provides the most conservative results and cannot be ruled out via experience or vehicle mass planning.

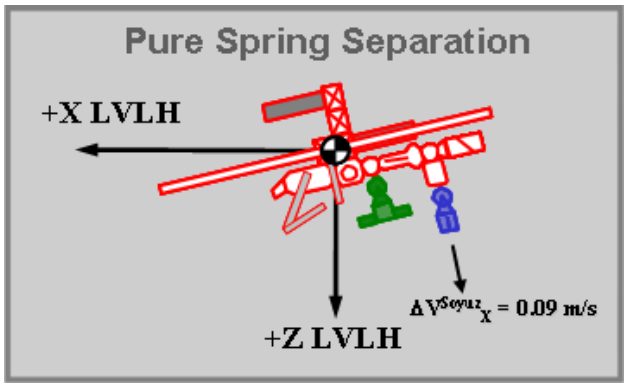

Figure 5-13. Longitudinal velocity component.

5.11.2 Transverse Velocity Dispersions

Due to possible misalignments in the Russian docking mechanism, an additional velocity component can be imparted on the separating vehicles. The transverse component has been calculated to be approximately 0.03 m/s and can be in any direction of the ISS XY plane perpendicular to the vehicle longitudinal axis. In the case of relative motion analysis, the in-plane positive and negative transverse components are of most interest because they have the most potential to negatively impact short- and long-term clearance. These transverse components are displayed in Figure 5-14. For this analysis, the positive and negative transverse components were used in separation calculations to determine the overall separation profile.

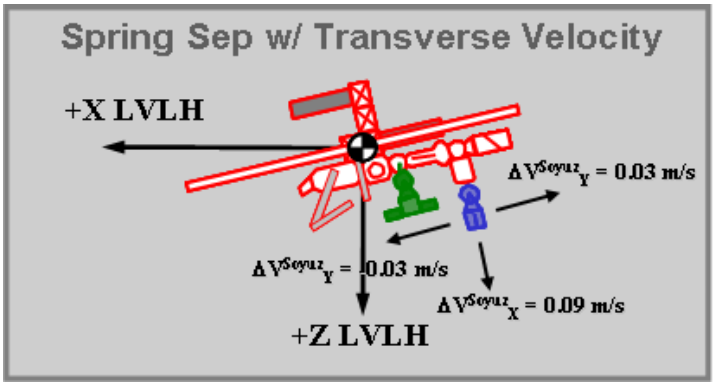

Figure 5-14. Transverse velocity components

5.11.3 Rotational Rate Dispersions

In addition to the velocity dispersions, it is possible that rotational rate is imparted into the separating RV resulting from the same imperfections in the ISS and RV docking mechanisms. These dispersions can be projected in both the lateral and longitudinal axes with the following values:

a. 0.2 degrees/s (longitudinal axis) - A roll attitude rate
b. 0.5 degrees/s (lateral axis) - A pitch/yaw attitude rate

To reduce the number of analysis cases, the rotational rate dispersion can be characterized by using a 6.0 m radius sphere encompassing all possible RV attitudes, thereby eliminating the need to vary this dispersion. From the "Contact Sphere" section 5.3.1.2, the 6.0 m radius sphere envelopes all the possible attitudes and attitude rates the RV could have at any point in its trajectory.

Use of the 6.0 m sphere, in lieu of rotational rate dispersions, has been agreed upon by the NASA AR&D team and RSC-E per the November 20, 2003, AR&D telecon.

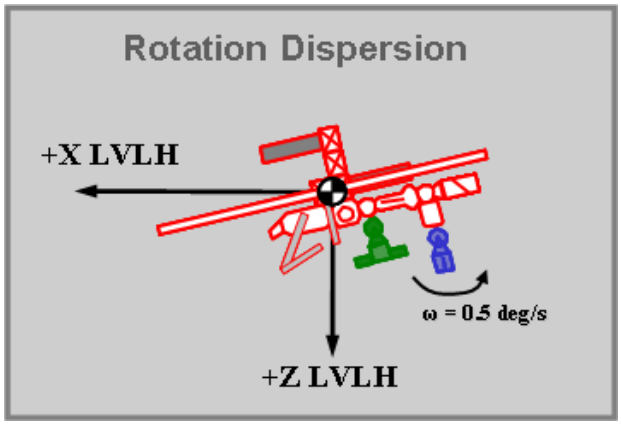

Figure 5-15. Rotational dispersions.

5.12 Attitude Control

The ISS attitude can be controlled through Russian or US attitude control methods. These include:

a. Control moment gyroscope (CMG) Momentum Management (MM) - Nonpropulsive
b. CMG Attitude Hold (AH) - Automatic thruster assist
c. RS Thruster Control - SM plus Progress and/or ATV
d. Orbiter VRCS

Source:

https://viperweb.jsc.nasa.gov/team_mai/web/VAC_MAPS.shtml

Below link no longer valid.

http://viperweb.jsc.nasa.gov/team_ei/MAPSData2004ISSOrbiterAttitudeControlModes.php

The RS thruster control and Orbiter VRCS attitude control schemes are discussed in the following sections.

5.12.1 RS Thruster Control

The RS implements a propulsive attitude control scheme using thrusters on the SM and attached Progress and ATV vehicles.

Per SSP 41163H, RS Specification, Section 4.3.7.2.3.57, Control Attitude - Propulsive, paragraph 14, there is a requirement for the SM Motion Control System (MCS) to have the capability to control the ISS stack attitude to within ±3.0° per axis when controlling to a Local Vertical/Local Horizontal (LVLH) or inertial attitude. In effect, these are the attitude deadband limits unless alternative operational limits are implemented.

> *The SM MCS shall maintain attitude within +/− 3.0 degrees per axis in the SM reference frame when controlling to a LVLH or inertial attitude with propulsive effectors or with nonpropulsive effectors assisted by propulsion effectors.*

The attitude rate requirement is ±0.03° per second for the X-axis and ±0.015° per second for the Y and Z axes, as defined in paragraph 17. In effect, these are the attitude rate deadband limits unless alternative operational limits are implemented.

> *The SM shall control attitude rates to within +/− 0.03 degrees per second for the X−axis and +/− 0.015 degrees per second for the Y− and Z−axes with respect to the commanded attitude when not performing translational or rotational maneuvers. …*

The operational limits, as defined in Flight Rule D2-303, ISS Attitude for Soyuz/Progress Undocking, Volume D, state that the total attitude error (root sum squared (RSS)) should be no greater than 3.0°, and the total attitude rate error (RSS) should be no greater than 0.02° per second [45].

5.12.2 Orbiter VRCS

The Orbiter digital auto pilot (DAP) has multiple attitude control schemes that can be selected, one of which is the VRCS. For attitude hold of the mated Orbiter-ISS stack, VRCS control is certified to 0.02° per second per axis rate deadband with a 1.0° attitude deadband, as provided by EG/Kenneth Lindsay for STS-128/17A. These values will be used to represent the VRCS attitude control capabilities for this analysis.

D2-303 ISS ATTITUDE FOR SOYUZ/PROGRESS UNDOCKING [HC] [RC] ®[052401-7519]

A. FOR SOYUZ/PROGRESS UNDOCKING FROM AN ISS NADIR PORT, THE ISS WILL MANEUVER TO AN APPROVED PITCH DOWN ATTITUDE PER RULE {B2-204}, PERMISSIBLE ISS STAGE ATTITUDES AND ATTITUDE DEVIATIONS [RC]. FOR NOMINAL UNDOCKING, ISS RS СУДН WILL MAINTAIN ISS ATTITUDE WITH A TOTAL ATTITUDE ERROR MAGNITUDE NO GREATER THAN 3 DEGREES AND TOTAL ATTITUDE RATE ERROR MAGNITUDE NO LARGER THAN +0.02 DEG/SEC. THE MANEUVER TO THIS ATTITUDE MUST BE COMPLETE NO LATER THAN 5 MINUTES PRIOR TO THE PLANNED UNDOCKING COMMAND TIME. ®[072706-5609B]

Analysis has shown that this attitude provides safe short term and long term clearance between an unmanned Progress and ISS for the unlikely case that the Progress MCS fails after undocking and no separation burns are performed. In this unlikely scenario, sufficient time would not be available for the ISS crew to set up the ТОРУ equipment and perform a burn manually.

Reference: Hazard Report RSCE-0021, Collision of a Spacecraft with the Station After Separating, Cause 2.

B. FOR SOYUZ/PROGRESS UNDOCKING FROM THE SERVICE MODULE AFT PORT, THE ISS WILL MANEUVER TO THE XVV ATTITUDE. FOR NOMINAL UNDOCKING, ISS RS СУДН WILL MAINTAIN ISS ATTITUDE WITH TOTAL ATTITUDE ERROR MAGNITUDE AND TOTAL ATTITUDE RATE ERROR NO GREATER THAN 3 DEGREES AND +0.02 DEG/SEC, RESPECTIVELY. THE MANEUVER TO THIS ATTITUDE MUST BE COMPLETE NO LATER THAN 5 MINUTES PRIOR TO THE PLANNED UNDOCKING COMMAND TIME.

C. THE ISS WILL BE MODED TO FREE DRIFT 1 MINUTE PRIOR TO THE TIME SEPARATION IS COMMANDED.

D. THE ISS WILL REMAIN IN FREE DRIFT UNTIL UNDOCKING +5 MINUTES. AFTER THAT, THE ISS WILL INITIATE MANEUVER TO THE PLANNED ATTITUDE. ®[072706-5609B]

FLIGHT/STAGE EFFECTIVITY: 12A THROUGH 12A.1 ®[072706-5609B] minutes, Attachment 2. *®[072706-7094B]*

FLIGHT/STAGE EFFECTIVITY: ALL FLIGHTS

5.13 Initial Conditions

The initial conditions, which determine the number of simulation runs that will be required, are made up of the ISS-Orbiter stack attitude and attitude rates prior to separation (defined by the selected attitude control scheme), the separation velocities and separation dispersions, and varying inclusion of the two RV separation burns.

5.13.1 Attitude Control

For the purpose of this analysis, only the RS thruster control and Orbiter VRCS attitude control schemes will be analyzed. The RS thruster control is analyzed because it is the primary attitude control scheme employed for RV separations. Orbiter VRCS was chosen as an alternative attitude control scheme because its use would allow for ISS propellant conservation with the Orbiter expending its own resources for all necessary maneuvers and attitude control.

5.13.2 Attitude and Attitude Rate Data

Separation analyses are to be performed for three primary ISS attitudes and a series of dispersed attitudes resulting from variations in starting attitude, attitude rates, and hook opening time. The three primary attitudes are as follows: +XVV +ZLV, -XVV +ZLV, and -XLV -ZVV.

The +XVV +ZLV attitude was chosen because it is the primary attitude flown by the ISS (without Orbiter present). Unfortunately, this attitude is not a valid attitude for RV separations. As a result, it serves as a mathematical exercise only.

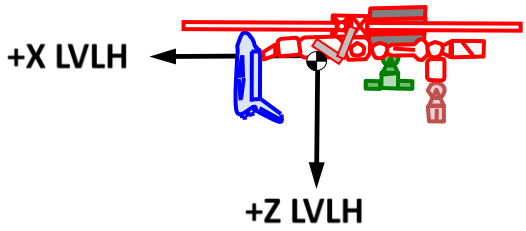

Figure 5-16. +XVV +ZLV (YPR 0,0,0 [RPY 0,0,0]) attitude.

The -XVV +ZLV attitude was chosen because it represents the primary attitude flown when the Orbiter is docked with the ISS. This attitude is not a valid attitude for RV separations.

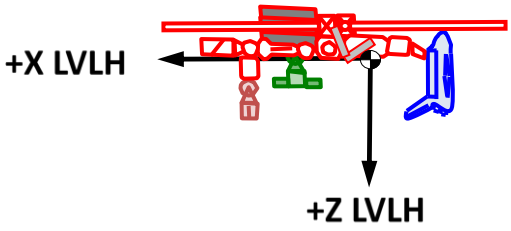

Figure 5-17. -XVV +ZLV (YPR 180,0,0 [RPY 0,0,180]) attitude.

The -XLV -ZVV attitude is the primary attitude of interest for DDO requiring RV separations. RV separations at this attitude are known to meet the requirement of Hazard Report RSCE-0021 to provide for safe long-term clearance between the departing Soyuz and ISS in case of a failure of the its thrusters. The primary concern for this attitude is the short-term clearance with the Orbiter and other ISS structure.

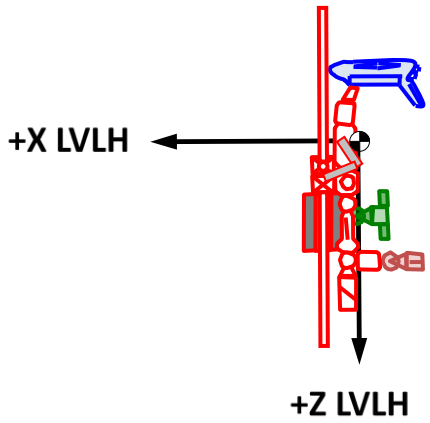

Figure 5-18. -XLV -ZVV (YPR 180,90,0 [RPY 0,-90,180]) attitude.

The dispersed attitudes, originating from the primary attitudes, account for the following variations:

a. Maximum and minimum attitude deadband limits, using in-plane Pitch deadband. The deadband limits represent the starting ISS attitude prior to any forthcoming attitude propagations.
b. Maximum attitude rate deadband in the positive and negative pitch directions. The direction of the attitude rate will drive the final attitude position at separation and the amount of rotation the ISS experiences.
c. Hook opening times of 180 or 310 seconds, for nominal and off-nominal operations, respectively. The hook opening time drives the amount of rotation the ISS experiences during the free drift period prior to separation when experiencing any attitude rates.

The following section provides an example of the separation attitude dispersions for the +XVV +ZLV primary attitude. Similar dispersions must be applied to the other analysis attitudes.

5.13.2.1 +XVV +ZLV (YPR 0,0,0) Attitude and Dispersions

The +XVV +ZLV attitude is depicted in Figure 4-16.

Dispersions around this attitude include an upper pitch dispersion and a lower pitch dispersion, the magnitudes of which depend on the attitude control scheme being used. For VRCS control, the attitude deadband is 1.0°, resulting in maximum pitch dispersions of ±1.0° from the X LVLH axis.

Per the RV separation timeline, the ISS stack modes to free drift from 240 (60 seconds + 180 seconds) to 370 (60 seconds + 310 seconds) seconds prior to physical separation, for the nominal and off-nominal hooks opening events, respectively. With a maximum potential pitch attitude rate of 0.02° per second, the attitude at separation can be dispersed an additional 4.8° (for 240 seconds of free drift) to 7.4° (for 370 seconds of free drift) from the starting deadband attitude and in the direction of the attitude rate (either positive or negative pitch direction). Figure 5-19 and Table 5-3 show the range of possible separation attitudes for nominal (180 seconds) hook opening times. Figure 5-20 and Table 5-4 show the range of possible separation attitudes for off-nominal (360 seconds) hook opening times.

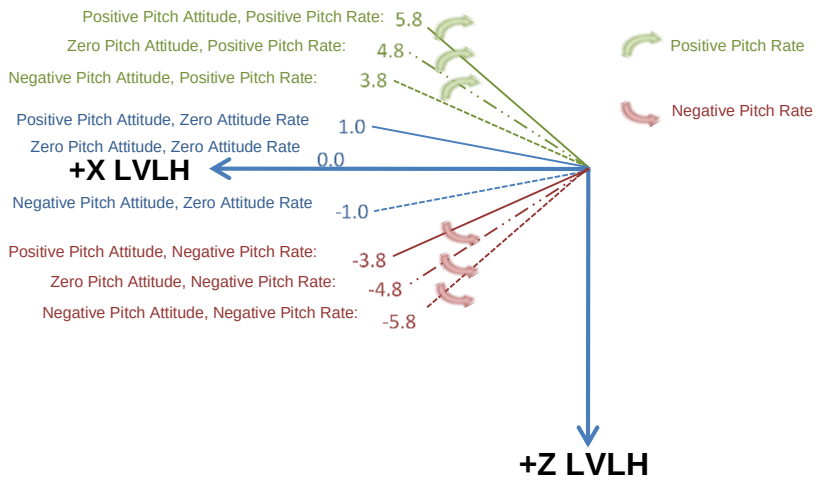

Figure 5-19. Graphical representation of dispersed separation attitudes for the +XVV +ZLV (YPR 0,0,0) attitude, with nominal (180 seconds) hook opening time.

Table 5-3. Tabular Representation of Dispersed Separation Attitudes for the +XVV +ZLV (YPR 0,0,0) Attitude, with Nominal (180 seconds) Hook Opening Time.

Description	Starting Free-Drift Pitch Attitude [deg]	Attitude Rate in Pitch Direction [deg/s]	Final Separation Pitch Attitude [deg]
Positive Pitch Attitude			
Positive Pitch Rate	0.0	0.02	5.8
Zero Attitude Rate	0.0	0.00	1.0
Negative Pitch Rate	0.0	-0.02	-3.8
Zero Pitch Attitude			
Positive Pitch Rate	1.0	0.02	4.8
Zero Attitude Rate	1.0	0.00	0.0
Negative Pitch Rate	1.0	-0.02	-4.8
Negative Pitch Attitude			
Positive Pitch Rate	-1.0	0.02	3.8
Zero Attitude Rate	-1.0	0.00	-1.0
Negative Pitch Rate	-1.0	-0.02	-5.8

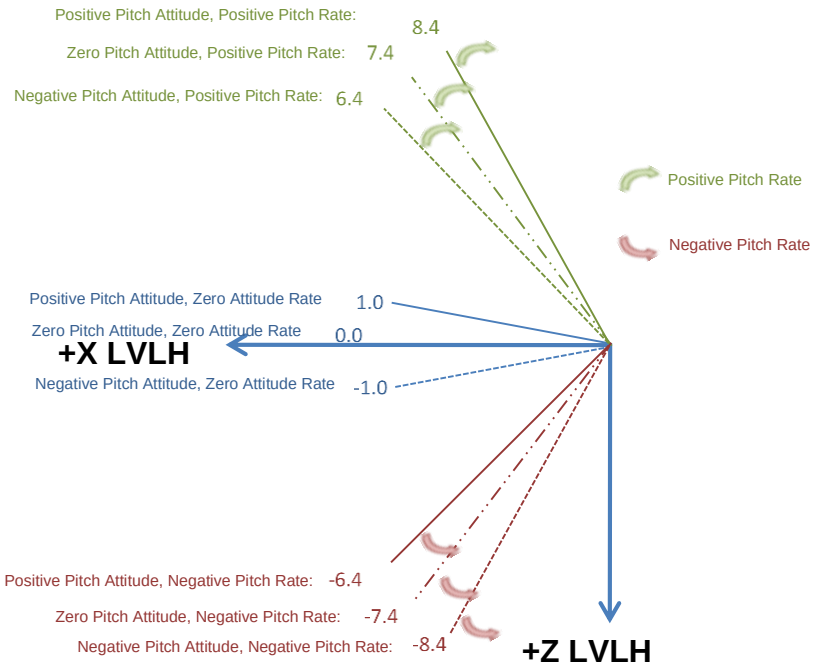

Figure 5-20. Graphical representation of dispersed separation attitudes for the +XVV +ZLV (YPR 0,0,0) attitude, with off-nominal (310 seconds) hook opening time.

Table 5-4. Tabular Representation of Dispersed Separation Attitudes for the +XVV +ZLV (YPR 0,0,0) Attitude, with Off-Nominal (310 seconds) Hook Opening Time

Description	Starting Free-Drift Pitch Attitude [deg]	Attitude Rate in Pitch Direction [deg/s]	Final Separation Pitch Attitude [deg]
Positive Pitch Attitude			
Positive Pitch Rate	0.0	0.02	8.4
Zero Attitude Rate	0.0	0.00	1.0
Negative Pitch Rate	0.0	-0.02	-6.4
Zero Pitch Attitude			
Positive Pitch Rate	1.0	0.02	7.4
Zero Attitude Rate	1.0	0.00	0.0
Negative Pitch Rate	1.0	-0.02	-7.4
Negative Pitch Attitude			
Positive Pitch Rate	-1.0	0.02	6.4
Zero Attitude Rate	-1.0	0.00	-1.0
Negative Pitch Rate	-1.0	-0.02	-8.4

5.13.3 Velocities and Dispersions

As discussed in Section 5.1, the velocities obtained at physical separation are the combination of the spring push-off imparted velocities and velocity dispersions due to possible imperfect docking mechanism dynamics.

The spring push-off separation velocity is the longitudinal velocity component, and for this analysis only the velocity component of 0.09 m/s (i.e., single spring failure and highest mass Soyuz vehicle) was used.

The velocity dispersions are 0.03 m/s positive transverse velocity, and 0.03 m/s negative transverse velocity.

5.13.4 Burn Profiles

There are no known failures that will cause a shortened burn, so no dispersions on the magnitude or duration of the burns were included. However, the failure of the RV motion control system to initiate the burn is a credible scenario. Therefore, for this analysis, both the no burn (spring-only) and the one burn trajectory profiles have been analyzed.

5.14 Analysis Planning

The separation analysis is performed by the RV Automated Vehicles team and Orbit Analysis Group in the MOD Flight Design and Dynamics Division.

This analysis was requested by the ISSP because of a potential overlap between the planned 19S undocking from the FGB nadir port and the planned STS-129/ULF3 flight, and because it provides an example "Soyuz undock from FGB Nadir" case for the generic analysis of DDO.

The analysis will be performed for the three primary attitudes discussed in Section 3.2: +XVV +ZLV, -XVV +ZLV, and -XLV -ZVV. For each of these primary attitudes, an additional set of separation attitudes have been chosen that account for the variation in attitude control mode, hook opening time duration, and deadband pitch attitude and deadband attitude rate and rate direction. An example of the varied number of separating attitudes was discussed in Section 5.13.2.1 for the +XVV +ZLV primary attitude, and similar dispersed attitudes will be used for the remaining two primary attitude cases.

In addition to the initial separating attitudes, the remaining dispersion that must be accounted for includes the burn profile and the transverse velocity components. The burn profile consists of a "no burn" separation using only springs, and a "one burn" separation that employs both springs and the first separation burn at 180 seconds. For the transverse velocity component, the analysis concentrates on dispersions within the LVLH X-Z plane, hence both a forward (positive) and aft (negative) transverse component is used, relative to the ISS body and perpendicular to the separation direction of the RVs.

Based on the number of variables that affect the analysis, there will be 144 individual separating trajectories per primary attitude for a total of 432 for all three attitudes.

Once the entire set of analyses runs is complete, comprehensive documentation of the data and results will follow. As there are multiple parameters that are being varied in this analysis, the resulting output will try to explain the effect each has on the separating trajectories.

A run matrix example is presented in Table 5-5 to illustrate the analysis runs. This run matrix will be used to present the run results in the Preliminary Results in the next section. Each run matrix is for a specific primary attitude and for the selected attitude control method. The results for each primary attitude will include two run matrices: the VRCS attitude control run matrix, and the RS attitude control run matrix. For each contact case, a reference to the plot is provided

by the use of a superscript text for the corresponding figure number (e.g., DC-1[90] signifies DC-1 vehicle contact shown in Figure 5-90).

Following each run matrix are two pages of result plots. The first page represents the results for the "no burn" and "one burn" profiles for the 180 second hook opening duration. The second page represents the same results, but for the 310 second hook opening duration.

Table 5-5. Sample Run Matrix

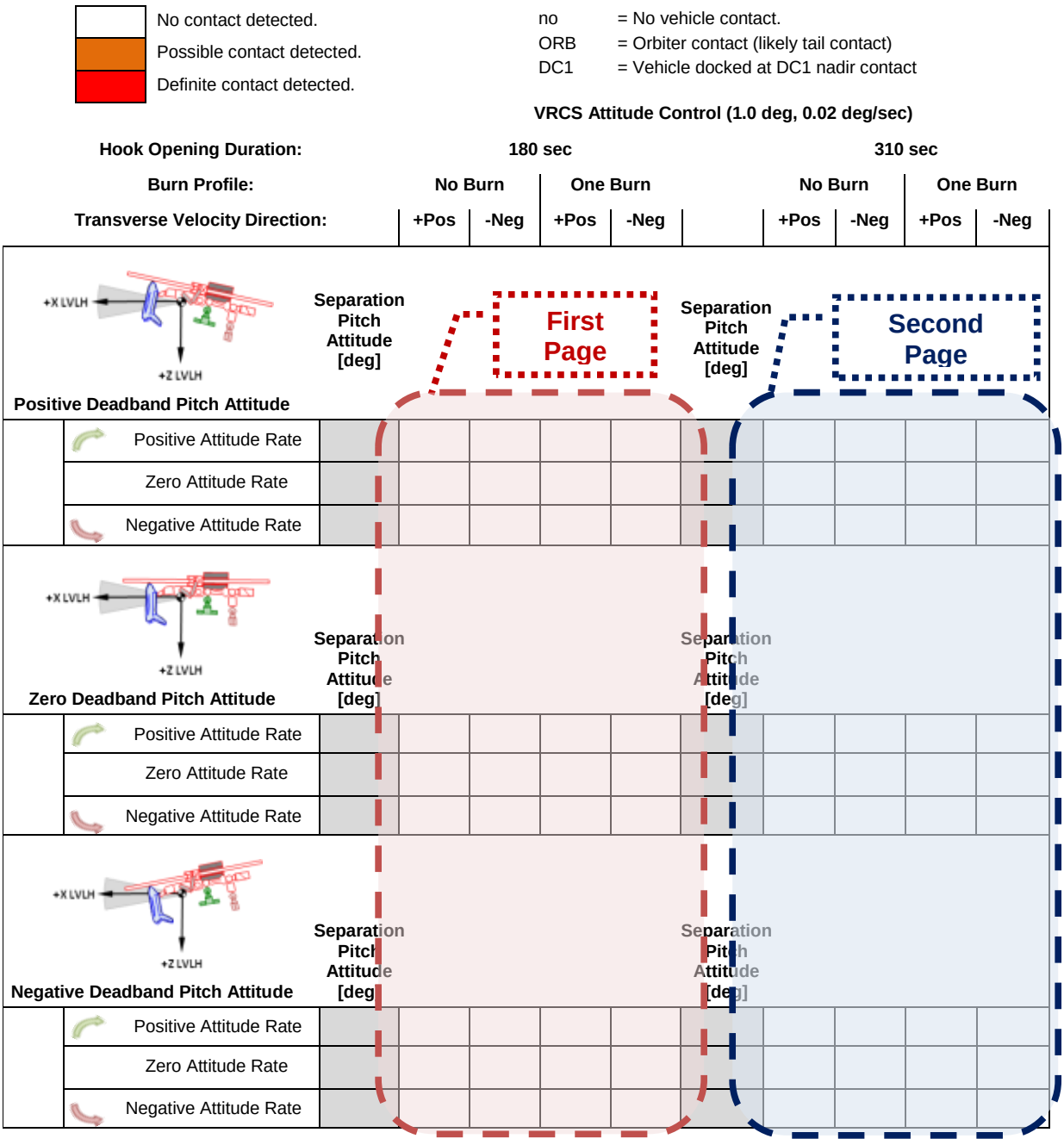

5.15 Preliminary Results

5.15.1 Results Introduction

The following analysis results are preliminary and require the concurrence of the Russian and International Partners before they can be used to make operational decisions.

Following this short introduction is a section describing the plots, which is followed by the results sections. Section 5.15.3 displays the composite plots for all the separating trajectories and Sections 5.15.4 through 5.15.6 detail the results for each of the three primary attitudes: +XVV +ZLV, -XVV +ZLV, and -XLV -ZVV.

Each primary attitude result section includes a short description of the results followed by a composite plot of the trajectories for the current analysis attitude. These are followed by two subsections that present the run matrix and the plots for each of the two attitude control schemes: RS and VRCS.

5.15.2 Plot and Key Information

Note that each plot shows the separation trajectories in the ISSACS coordinate system. The lines represent the center of mass location of the separating vehicle over time. An additional 6.0 m radius circle around each trajectory point should be used to represent the boundaries of the separating vehicle and consequently contact when that circle encroaches onto any ISS stack structure.

The ISS/Orbiter image is not a true representation. It is to be used for informational purposes only or for identification of possible cases for further evaluation.

The following line style and color key applies to all trajectory plots that follow.

Negative Attitude Rate at Separation - Positive Transverse Velocity

Negative Attitude Rate at Separation - Negative Transverse Velocity

Zero Attitude Rate at Separation - Positive Transverse Velocity

Zero Attitude Rate at Separation - Negative Transverse Velocity

Positive Attitude Rate at Separation - Positive Transverse Velocity

Positive Attitude Rate at Separation - Negative Transverse Velocity

5.15.3 Composite Plots for All Attitudes

The following show the composite trajectories for all the three primary attitudes. Figure 5-21 shows a composite of the “no burn” trajectories corresponding to the spring-only separations. Figure 5-22 shows a composite of the “One Burn” trajectories. Spring separation is followed by the first separation burn at 180 seconds.

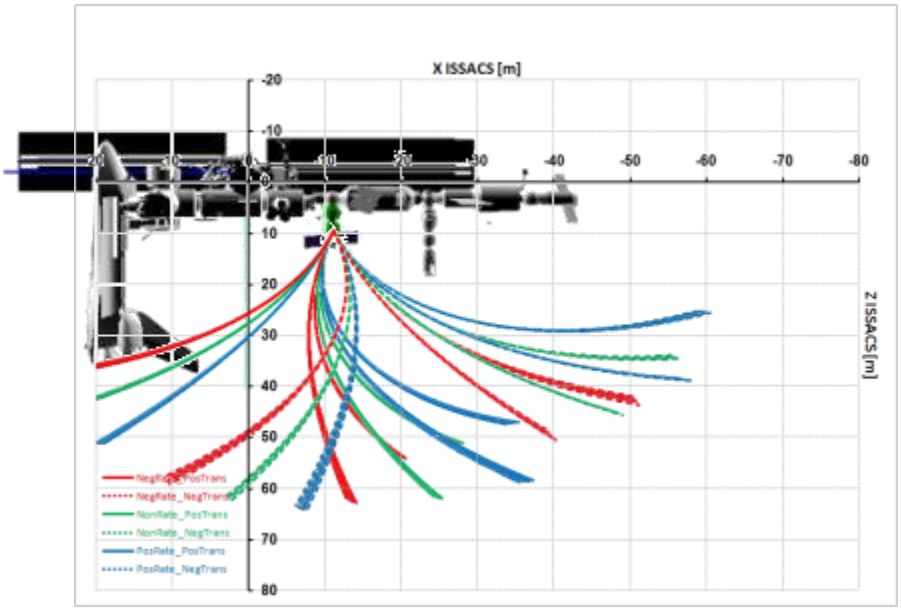

Figure 5-21. Composite plot of "no burn" trajectories for all attitudes.

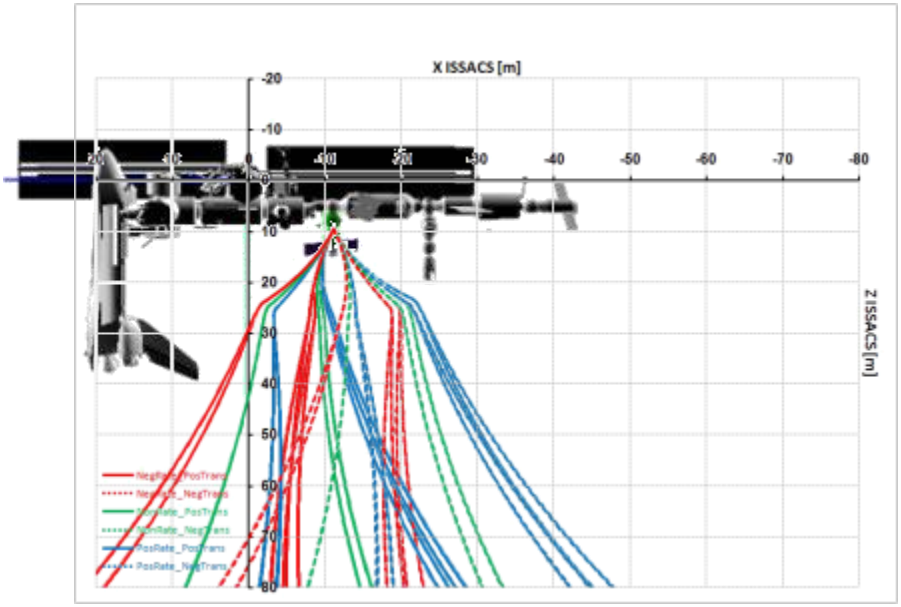

Figure 5-22. Composite plot of "one burn" trajectories for all attitudes.

Composite plots show the range of the trajectories that are displayed and the effect that the transverse component direction has. The positive transverse velocity component, or the velocity component towards the +X ISSACS direction, pushes the separation trajectories closer to the Orbiter tail, while the negative transverse velocity component, or the velocity component towards the -X ISSACS directions, pushes the separation trajectories away from the Orbiter tail and closer to vehicles docked at the DC-1 nadir port.

Based on the result plots, the effect of hook opening duration is not as significant as the effect of transverse velocity component direction, as can be observed by the nearly identical trajectory paths for these results.

Additionally, the selection of attitude control scheme results in a minor difference in the final separation trajectories. The effect is primarily observed in the numerical results and partially by the flared trajectory lines shown in the composite plots.

The "no burn" composite plot (Figure 5-21) shows definite structural contact due to the trajectories directly crossing the Orbiter tail. These trajectories are in the +XVV +XLV (YPR 0,0,0) attitude, which is not a primary concern and can be ignored. Likewise, though not directly apparent from the plots, the "one burn" composite plot (Figure 5-22) contains Orbiter tail contact for trajectories in the +XVV +XLV (YPR 0,0,0) attitude. Again, these results are of no concern.

Though this analysis was primarily concerned with RV to Orbiter contact, the results show that contact may exist with a vehicle docked at the DC-1 nadir port. These contact cases were found for the -XLV -ZVV (YPR 180, 90, 0) attitude and are of concern as this attitude is the primary attitude proposed for DDO operations that may require Soyuz vehicle separations. More detailed results for this attitude are presented in Section 5.15.6.

5.15.4 Results for the +XVV +ZLV (YPR 0, 0, 0) Attitude

5.15.4.1 Results Discussion

As previously mentioned, the +XVV +ZLV attitude case has been analyzed as a mathematical problem to provide a base reference for separation trajectories. Therefore, it can be excluded from any operational DDO decisions.

From the composite plots represented in Figure 5-23 and Figure 5-24, contact has been shown to occur primarily for the positive transverse velocity component. For the "no burn" (spring only) trajectories, the transverse component curves the trajectory directly over the Orbiter tail, clearly resulting in structural contact with high potential for damage. The composite plots are shown in Figure 5-23 with individual analysis results shown in Figure 5-25, Figure 5-27, Figure 5-29 for the 180 seconds hook opening and Figure 5-31, Figure 5-33, Figure 5-35 for the 310 seconds hook opening. When the first separation burn is activated, contact was shown for the positive transverse velocity component when coupled with a negative attitude rate of the ISS stack. The composite plots are shown in Figure 5-24 with individual analysis results in Figure 5-26, Figure 5-28, Figure 5-30 for the 180 seconds hook opening, and Figure 5-32, Figure 5-34, Figure 5-36 for the 310 seconds hook opening.

The effect of hook opening duration or attitude control method used does not have as significant of an impact as the effect of transverse velocity component direction.

5.15.4.2 Composite Plots

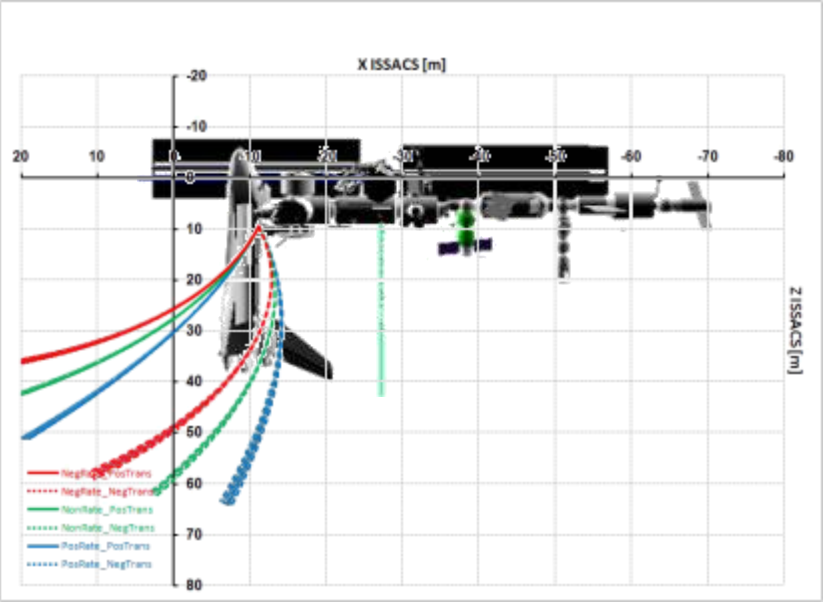

Figure 5-23. Composite plot of "no burn" trajectories for +XVV +ZLV attitude.

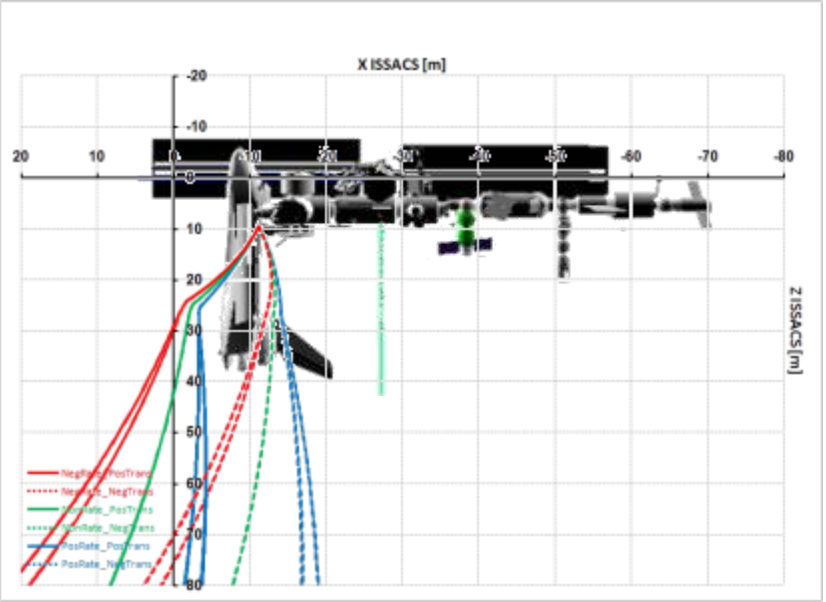

Figure 5-24. Composite plot of "one burn" trajectories for +XVV +ZLV attitude.

5.15.4.3 VRCS Attitude Control Results

VRCS Attitude Control (1.0 deg, 0.02 deg/sec)

Hook Opening Duration:	180 sec					310 sec				
Burn Profile:	No Burn		One Burn			No Burn		One Burn		
Transverse Velocity Direction:	+Pos	-Neg	+Pos	-Neg		+Pos	-Neg	+Pos	-Neg	
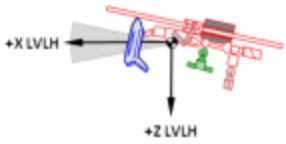 **Positive Deadband Pitch Attitude**	**Separation Pitch Attitude [deg]**					**Separation Pitch Attitude [deg]**				
Positive Attitude Rate	5.8	ORB[25]	no	no	no	8.4	ORB[31]	no	no	no
Zero Attitude Rate	1.0	ORB[25]	no	no	no	1.0	ORB[31]	no	no	no
Negative Attitude Rate	-3.8	ORB[25]	no	ORB[26]	no	-6.4	ORB[31]	no	ORB[32]	no
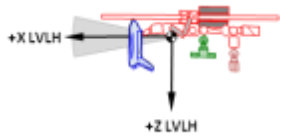 **Zero Deadband Pitch Attitude**	**Separation Pitch Attitude [deg]**					**Separation Pitch Attitude [deg]**				
Positive Attitude Rate	4.8	ORB[27]	no	no	no	7.4	ORB[33]	no	no	no
Zero Attitude Rate	0.0	ORB[27]	no	no	no	0.0	ORB[33]	no	no	no
Negative Attitude Rate	-4.8	ORB[27]	no	ORB[28]	no	-7.4	ORB[33]	no	ORB[34]	no
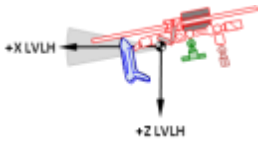 **Negative Deadband Pitch Attitude**	**Separation Pitch Attitude [deg]**					**Separation Pitch Attitude [deg]**				
Positive Attitude Rate	3.8	ORB[29]	no	no	no	6.4	ORB[35]	no	no	no
Zero Attitude Rate	-1.0	ORB[29]	no	no	no	-1.0	ORB[35]	no	no	no
Negative Attitude Rate	-5.8	ORB[29]	no	ORB[30]	no	-8.4	ORB[35]	no	ORB[36]	no

+XVV +ZLV (YPR 0,0,0), VRCS, 180 seconds Hook Opening Duration

No Burn (springs only)

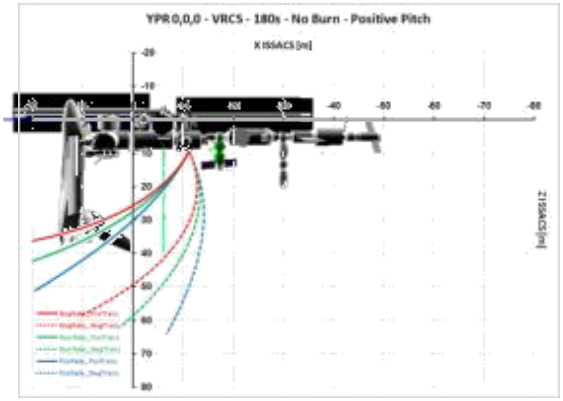

One Burn

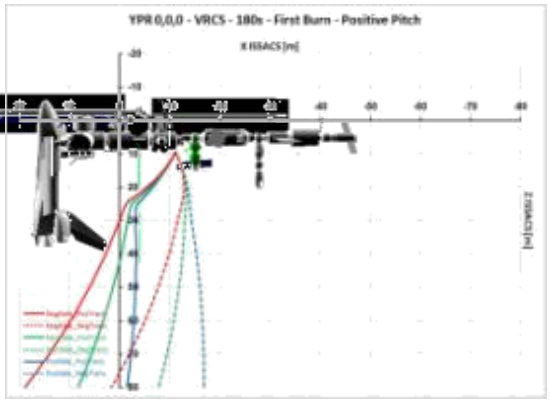

Figure 5-25 - 5-26. Positive deadband pitch attitude.

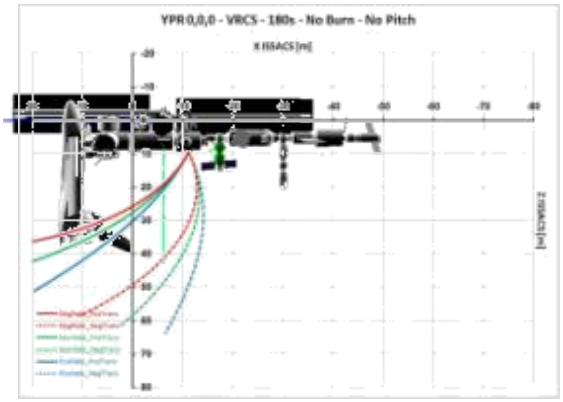

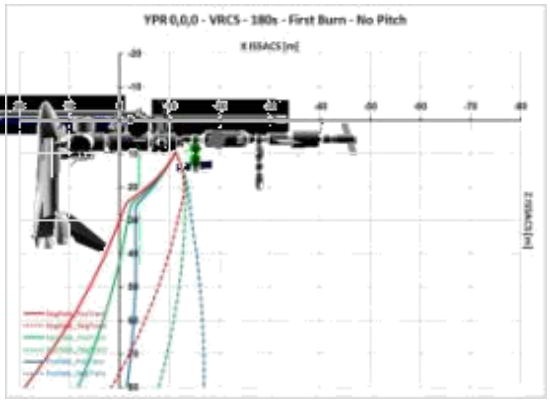

Figure 5-27 - 5-28. Zero deadband pitch attitude.

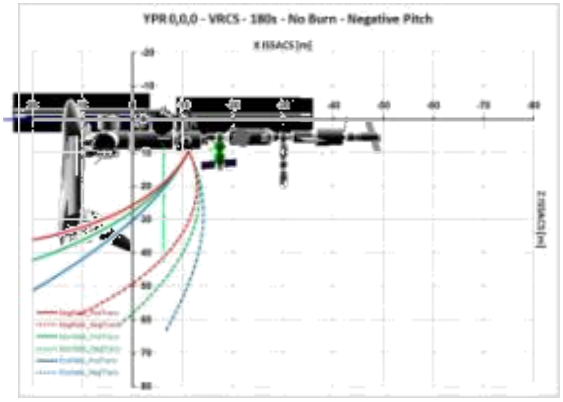

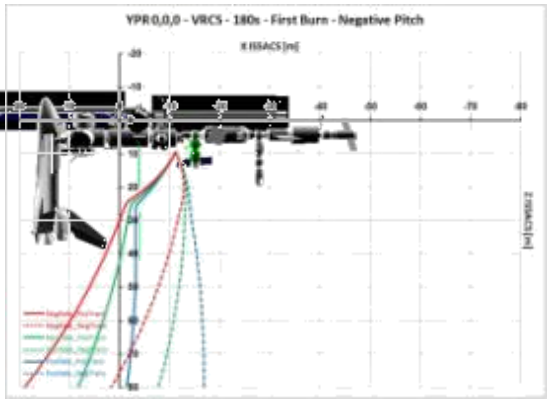

Figure 5-29 - 5-30. Negative deadband pitch attitude.

+XVV +ZLV (YPR 0,0,0), VRCS, 310 seconds Hook Opening Duration

No Burn (springs only) | One Burn

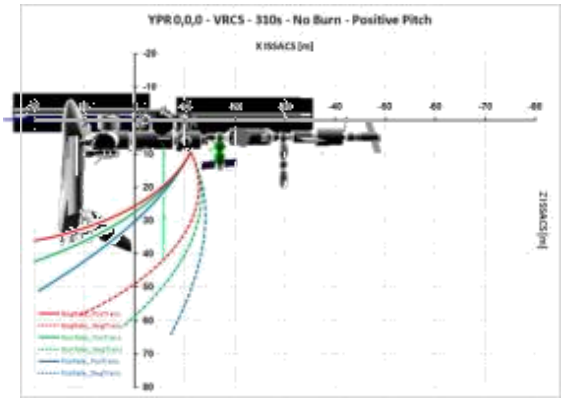

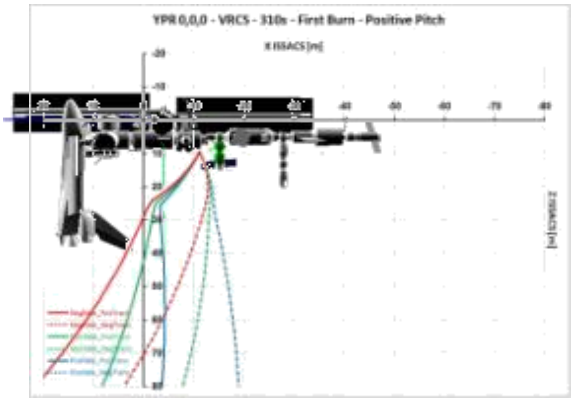

Figure 5-31 - 5-32. Positive deadband pitch attitude.

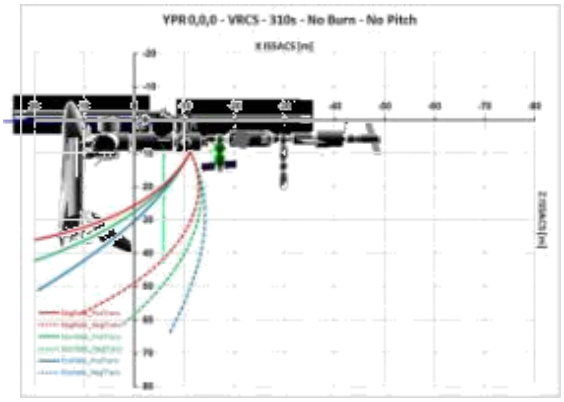

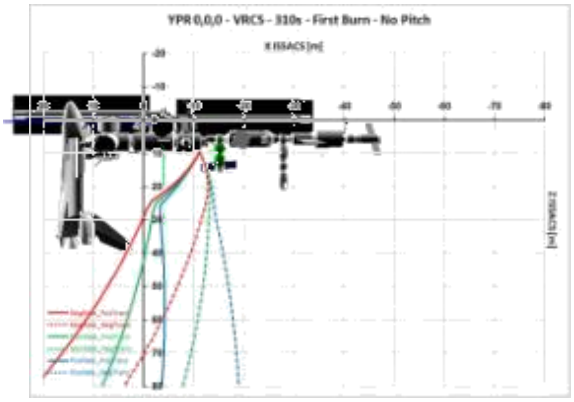

Figure 5-33 - 5-34. Zero deadband pitch attitude.

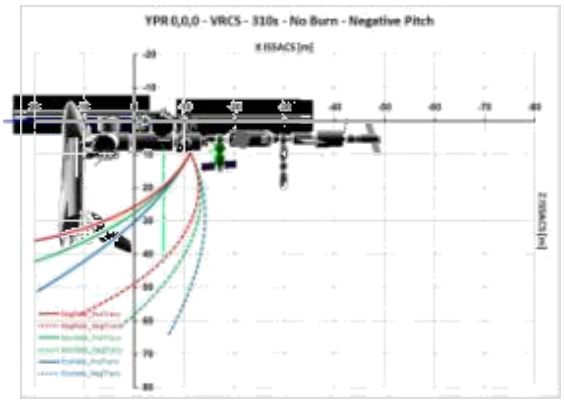

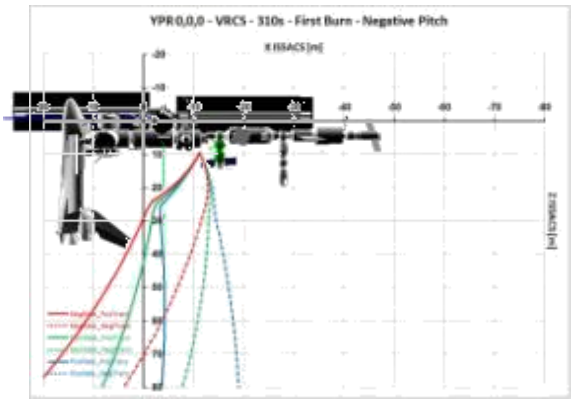

Figure 5-35 - 5-36. Negative deadband pitch attitude.

5.15.4.4 RS Attitude Control Results

RS Attitude Control (3.0 deg, 0.02 deg/sec)

		Hook Opening Duration:	180 sec					310 sec				
		Burn Profile:	No Burn		One Burn			No Burn		One Burn		
		Transverse Velocity Direction:	+Pos	-Neg	+Pos	-Neg		+Pos	-Neg	+Pos	-Neg
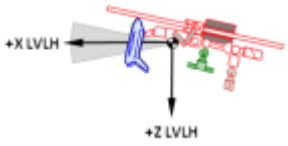 **Positive Deadband Pitch Attitude**			**Separation Pitch Attitude [deg]**					**Separation Pitch Attitude [deg]**				
		Positive Attitude Rate	7.8	ORB[37]	no	no	no	10.4	ORB[43]	no	no	no
		Zero Attitude Rate	3.0	ORB[37]	no	no	no	3.0	ORB[43]	no	no	no
		Negative Attitude Rate	-1.8	ORB[37]	no	ORB[38]	no	-4.4	ORB[43]	no	ORB[44]	no
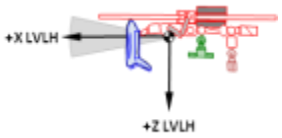 **Zero Deadband Pitch Attitude**			**Separation Pitch Attitude [deg]**					**Separation Pitch Attitude [deg]**				
		Positive Attitude Rate	4.8	ORB[39]	no	no	no	7.4	ORB[45]	no	no	no
		Zero Attitude Rate	0.0	ORB[39]	no	no	no	0.0	ORB[45]	no	no	no
		Negative Attitude Rate	-4.8	ORB[39]	no	ORB[40]	no	-7.4	ORB[45]	no	ORB[46]	no
 **Negative Deadband Pitch Attitude**			**Separation Pitch Attitude [deg]**					**Separation Pitch Attitude [deg]**				
		Positive Attitude Rate	7.8	ORB[41]	no	no	no	4.4	ORB[47]	no	no	no
		Zero Attitude Rate	-3.0	ORB[41]	no	no	no	-3.0	ORB[47]	no	no	no
		Negative Attitude Rate	-1.8	ORB[41]	no	ORB[42]	no	-10.4	ORB[47]	no	ORB[48]	no

+XVV +ZLV (YPR 0,0,0), RS, 180 seconds Hook Opening Duration

No Burn (springs only)

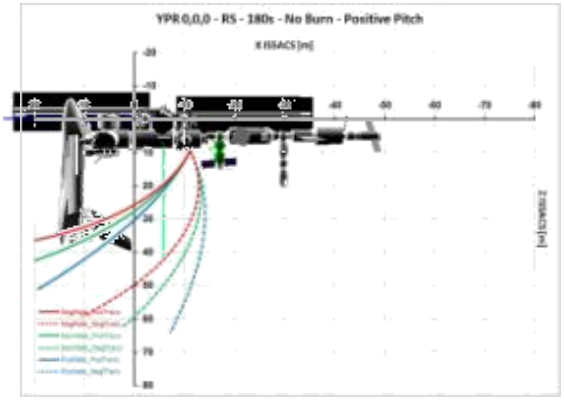

One Burn

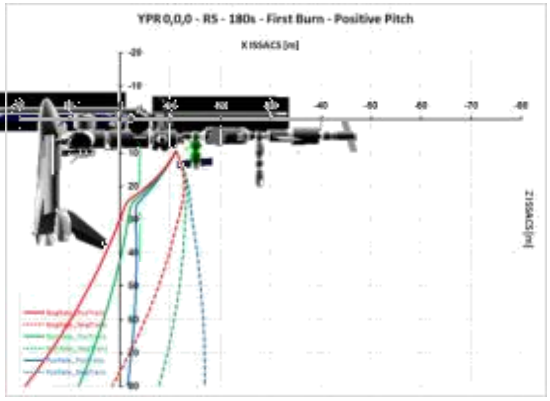

Figure 5-37 - 5-38. Positive deadband pitch attitude.

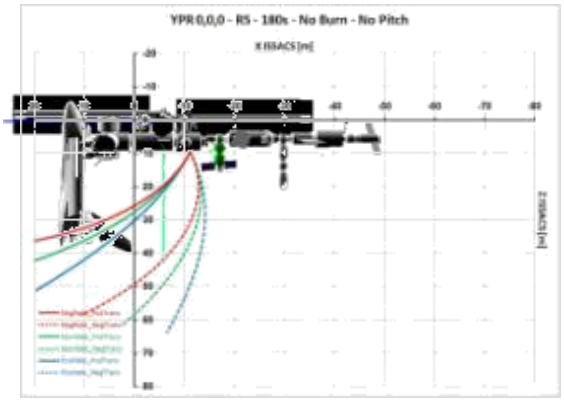

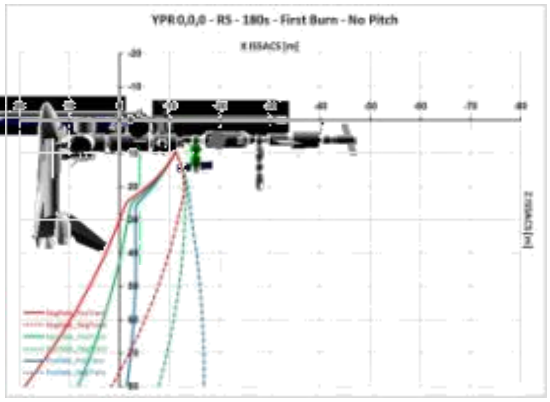

Figure 5-39 - 5-40. Zero deadband pitch attitude.

+XVV +ZLV (YPR 0,0,0), RS, 310 seconds Hook Opening Duration

No Burn (springs only)

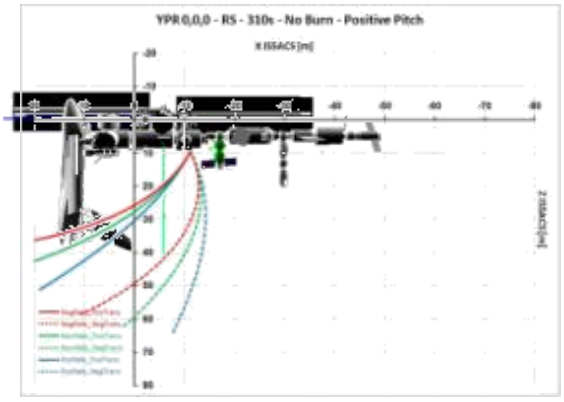

One Burn

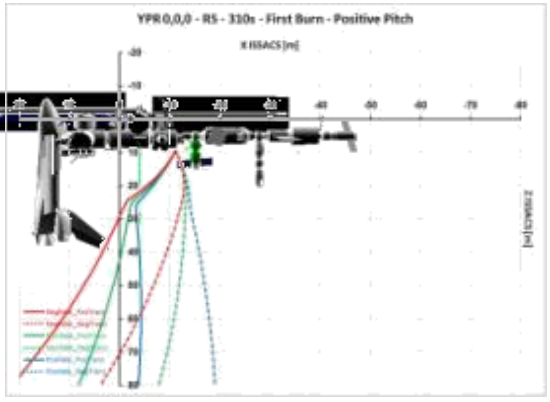

Figure 5-41 - 5-42. Positive deadband pitch attitude.

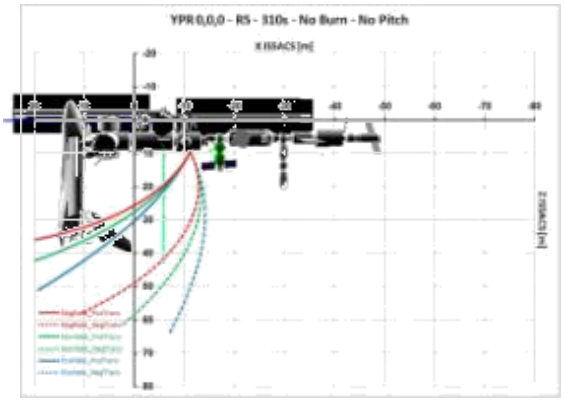

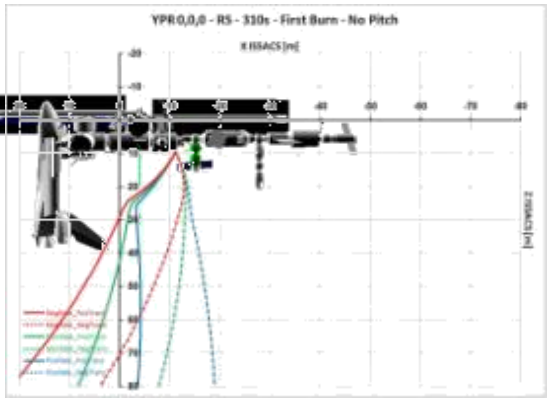

Figure 5-43 - 5-44. Zero deadband pitch attitude.

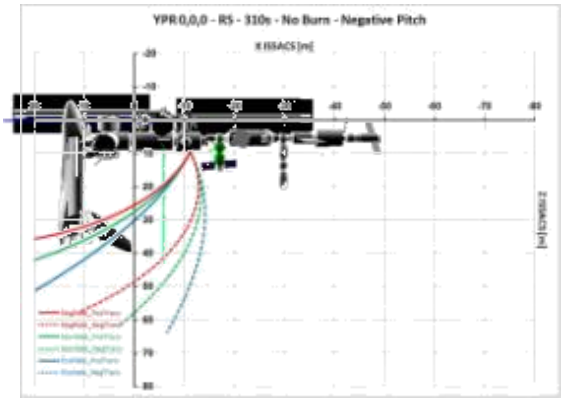

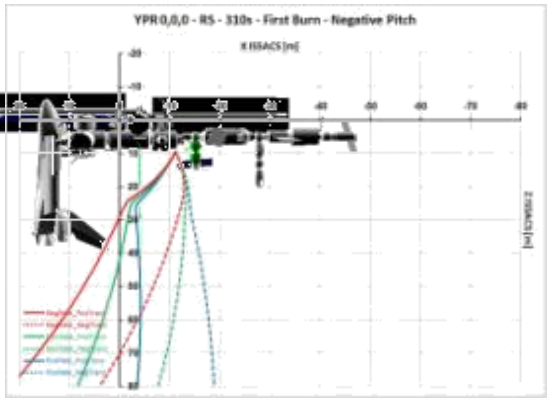

Figure 5-45 - 5-46. Negative deadband pitch attitude.

5.15.5 Results for the -XVV +ZLV (YPR 180, 0, 0) Attitude

5.15.5.1 Results Discussion

Though the -XVV +ZLV attitude is the standard DDO attitude, it is not a valid Soyuz separation attitude, and hence any possible contact during this case is of no concern.

No contact has been found for any of the separating trajectories in this attitude. With the ISS stack yawed by 180°, the Orbiter is aft facing (-XVV LVLH frame) while the separating trajectories are similar to the +XVV +ZLV attitude and hence no Orbiter contact was found. The only close approach observed was with the RV docked at the DC-1 nadir port. This approach was outside the 6.0 m radius sphere, so it has not been logged as a contact. Further investigation of this close approach would be required if this separation attitude is approved.

As for the previous attitude case, the direction of the transverse velocity component has the largest effect on the separating trajectories, and the effect of hook opening duration or selection of attitude control scheme are not significant, in comparison.

5.15.5.2 Composite Plots

1.1.1.1

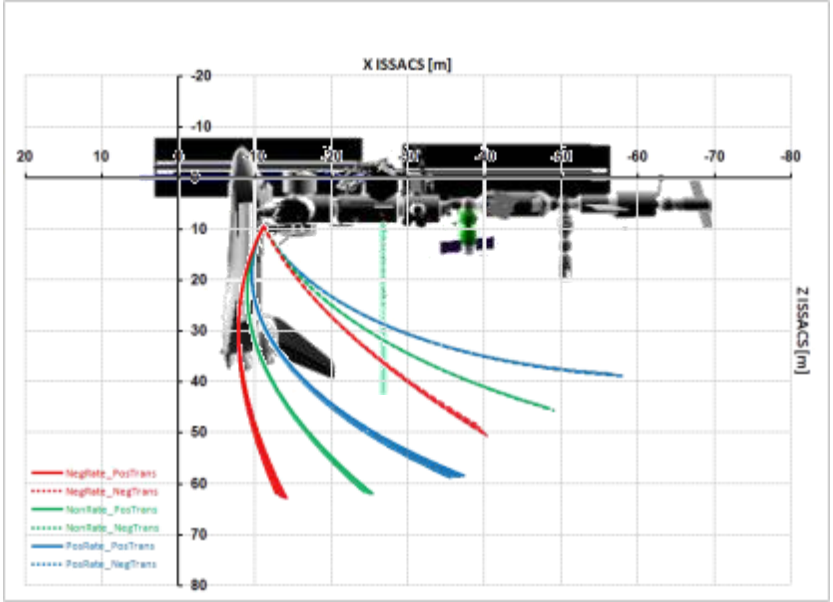

Figure 5-47. Composite plot of "no burn" trajectories for -XVV +ZLV attitude.

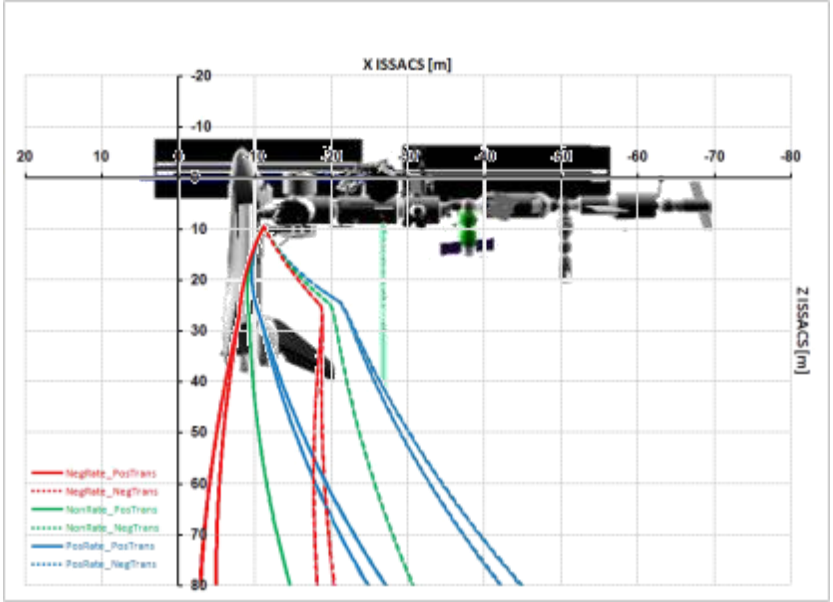

Figure 5-48. Composite plot of "one burn" trajectories for -XVV +ZLV attitude.

5.15.5.3 VRCS Attitude Control Results

VRCS Attitude Control (1.0 deg, 0.02 deg/sec)

Hook Opening Duration:	180 sec					310 sec				
Burn Profile:	No Burn		One Burn			No Burn		One Burn		
Transverse Velocity Direction:	+Pos	-Neg	+Pos	-Neg		+Pos	-Neg	+Pos	-Neg	
 **Positive Deadband Pitch Attitude**	**Separation Pitch Attitude [deg]**					**Separation Pitch Attitude [deg]**				
Positive Attitude Rate	5.8	no	no	no	no	8.4	no	no	no	no
Zero Attitude Rate	1.0	no	no	no	no	1.0	no	no	no	no
Negative Attitude Rate	-3.8	no	no	no	no	-6.4	no	no	no	no
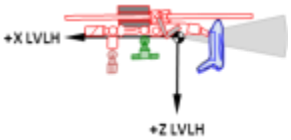 **Zero Deadband Pitch Attitude**	**Separation Pitch Attitude [deg]**					**Separation Pitch Attitude [deg]**				
Positive Attitude Rate	4.8	no	no	no	no	7.4	no	no	no	no
Zero Attitude Rate	0.0	no	no	no	no	0.0	no	no	no	no
Negative Attitude Rate	-4.8	no	no	no	no	-7.4	no	no	no	no
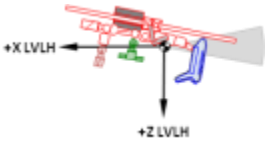 **Negative Deadband Pitch Attitude**	**Separation Pitch Attitude [deg]**					**Separation Pitch Attitude [deg]**				
Positive Attitude Rate	3.8	no	no	no	no	6.4	no	no	no	no
Zero Attitude Rate	-1.0	no	no	no	no	-1.0	no	no	no	no
Negative Attitude Rate	-5.8	no	no	no	no	-8.4	no	no	no	no

-XVV +ZLV (YPR 180,0,0), VRCS, 180 seconds Hook Opening Duration

No Burn (springs only) One Burn

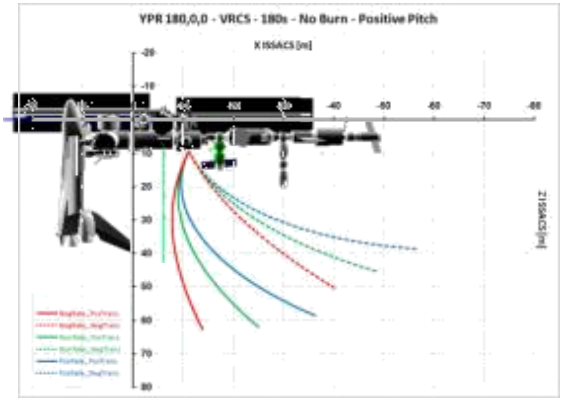

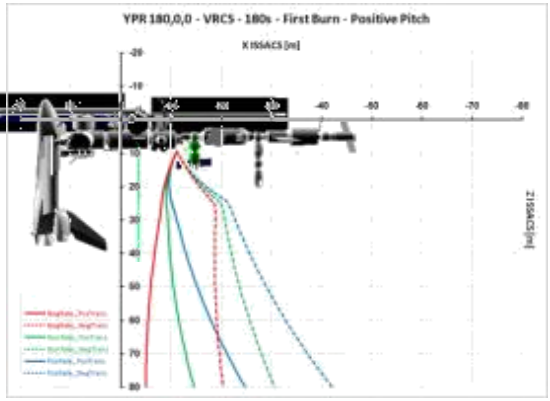

Figure 5-49 - 5-50. Positive deadband pitch attitude.

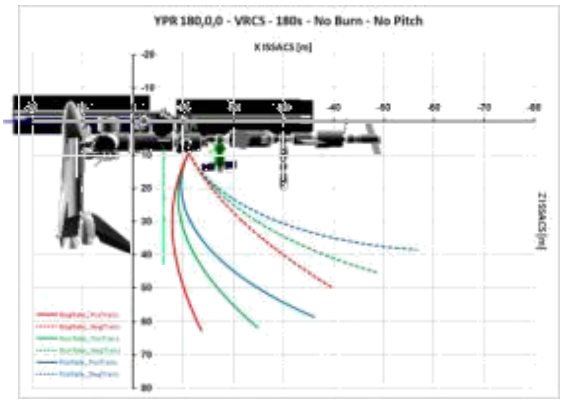

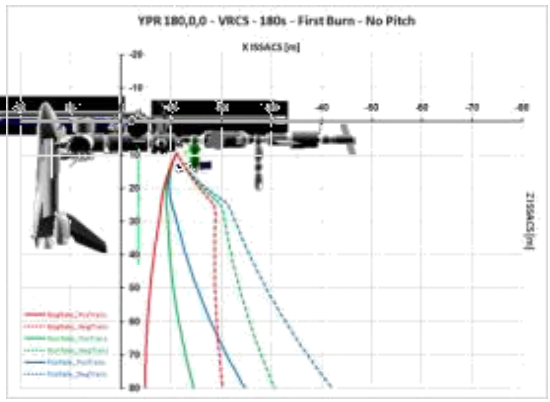

Figure 5-51 - 5-52. Zero deadband pitch attitude.

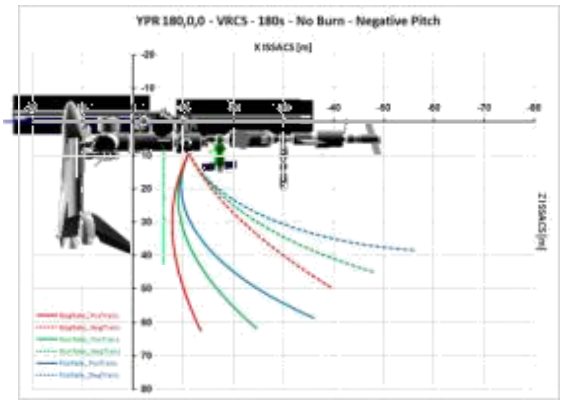

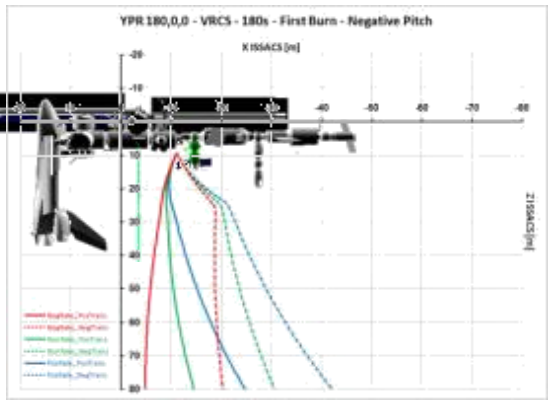

Figure 5-53 - 5-54. Negative deadband pitch attitude

-XVV +ZLV (YPR 180,0,0), VRCS, 310 seconds Hook Opening Duration

No Burn (springs only)

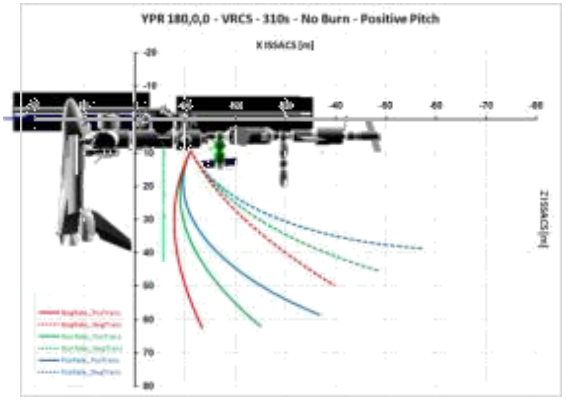

One Burn

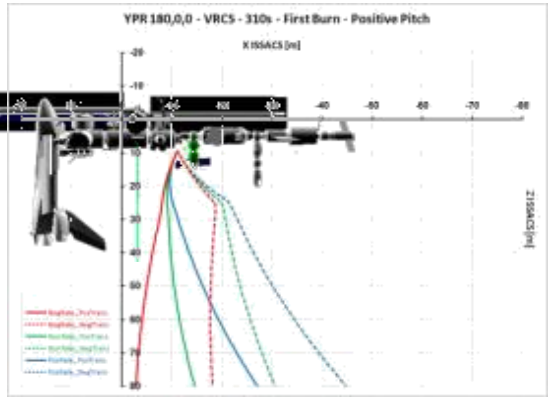

Figure 5-55 - 5-56. Positive deadband pitch attitude.

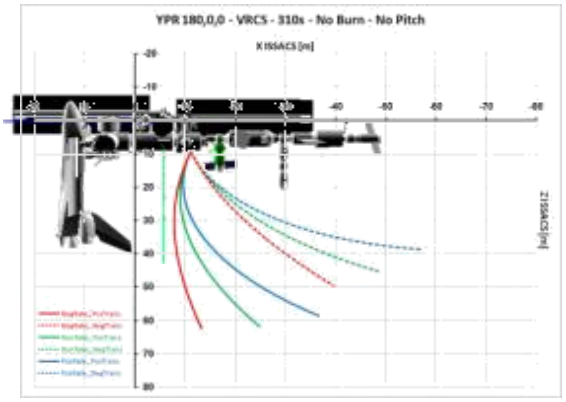

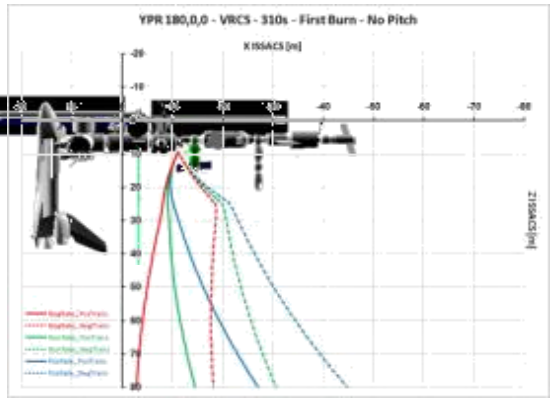

Figure 5-57 - 5-58. Zero deadband pitch attitude.

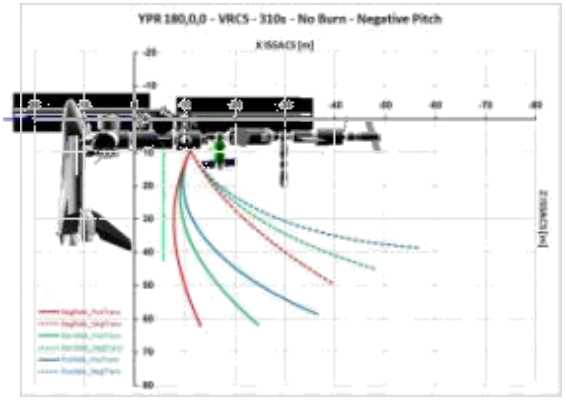

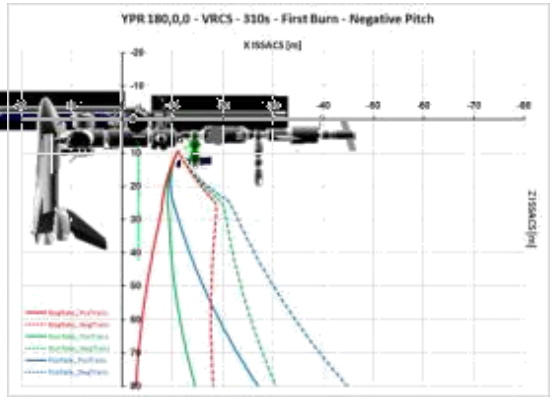

Figure 5-59 - 5-60. Negative deadband pitch attitude.

5.15.5.4 RS Attitude Control Results

RS Attitude Control (3.0 deg, 0.02 deg/sec)										
Hook Opening Duration:		**180 sec**					**310 sec**			
Burn Profile:		**No Burn**		**One Burn**			**No Burn**		**One Burn**	
Transverse Velocity Direction:		**+Pos**	**-Neg**	**+Pos**	**-Neg**		**+Pos**	**-Neg**	**+Pos**	**-Neg**
 **Positive Deadband Pitch Attitude**		**Separation Pitch Attitude [deg]**					**Separation Pitch Attitude [deg]**			
	Positive Attitude Rate	7.8	no	no	no	no	10.4	no	no	no	no
	Zero Attitude Rate	3.0	no	no	no	no	3.0	no	no	no	no
	Negative Attitude Rate	-1.8	no	no	no	no	-4.4	no	no	no	no
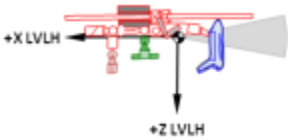 **Zero Deadband Pitch Attitude**		**Separation Pitch Attitude [deg]**					**Separation Pitch Attitude [deg]**			
	Positive Attitude Rate	4.8	no	no	no	no	7.4	no	no	no	no
	Zero Attitude Rate	0.0	no	no	no	no	0.0	no	no	no	no
	Negative Attitude Rate	-4.8	no	no	no	no	-7.4	no	no	no	no
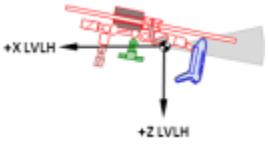 **Negative Deadband Pitch Attitude**		**Separation Pitch Attitude [deg]**					**Separation Pitch Attitude [deg]**			
	Positive Attitude Rate	1.8	no	no	no	no	4.4	no	no	no	no
	Zero Attitude Rate	-3.0	no	no	no	no	-3.0	no	no	no	no
	Negative Attitude Rate	-7.8	no	no	no	no	-10.4	no	no	no	no

-XVV +ZLV (YPR 180,0,0), RS, 180 seconds Hook Opening Duration

No Burn (springs only) One Burn

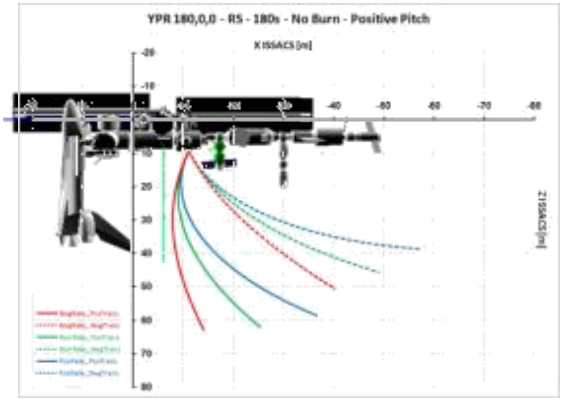

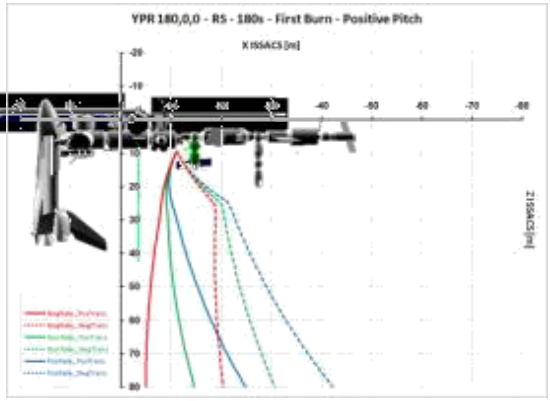

Figure 5-61 - 5-62. Positive deadband pitch attitude.

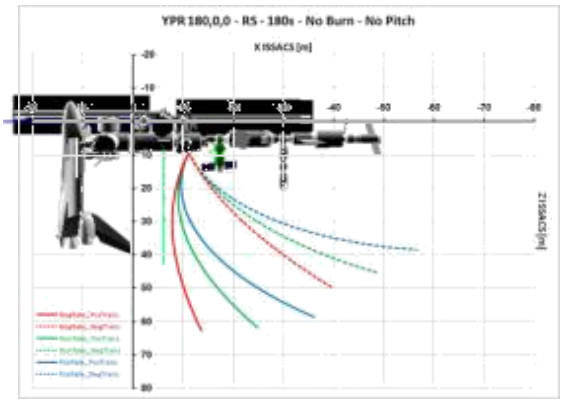

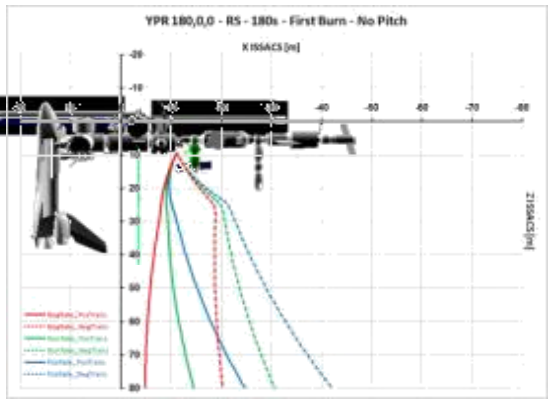

Figure 5-63 - 5-64. Zero deadband pitch attitude.

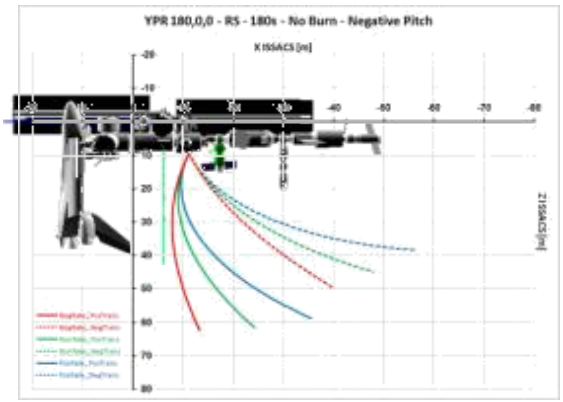

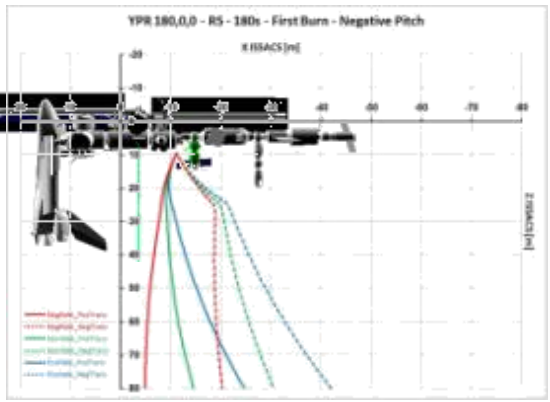

Figure 5-65 - 5-66. Negative deadband pitch attitude.

-XVV +ZLV (YPR 180,0,0), RS, 310 seconds Hook Opening Duration

No Burn (springs only) | One Burn

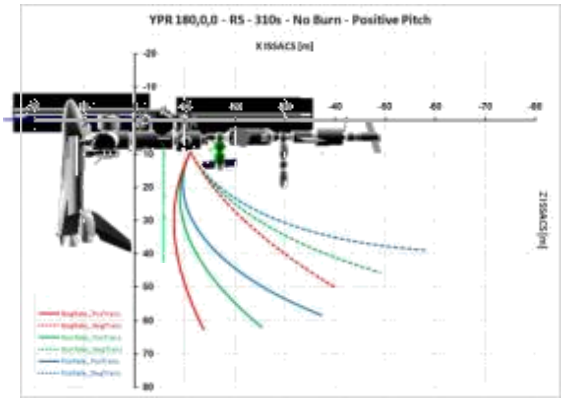

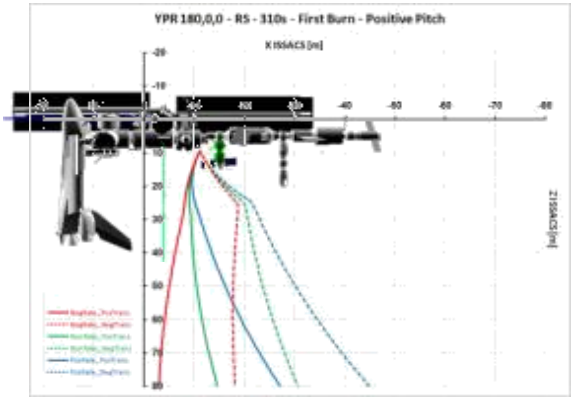

Figure 5-67 - 5-68. Positive deadband pitch attitude.

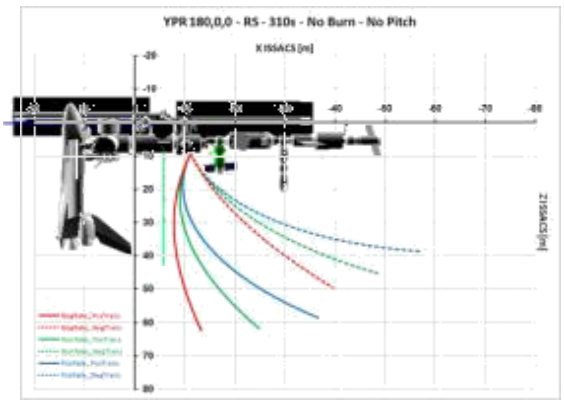

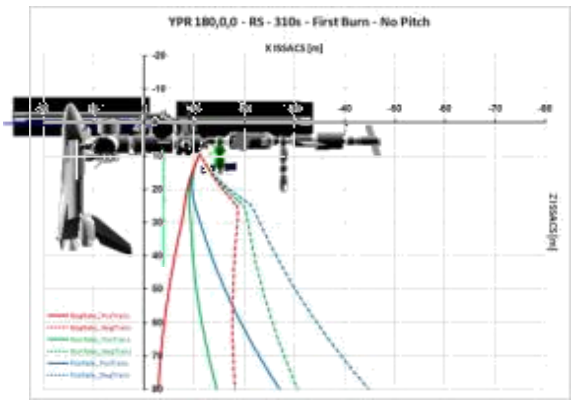

Figure 5-69 - 5-70. Zero deadband pitch attitude.

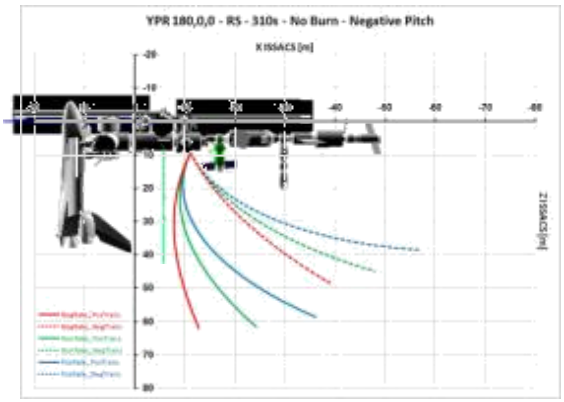

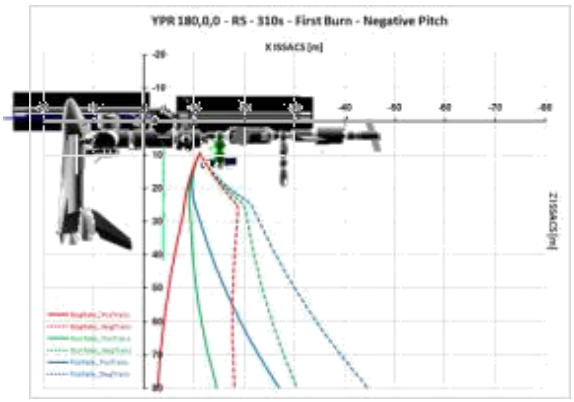

Figure 5-71 - 5-72. Negative deadband pitch attitude.

5.15.6 Results for the -XLV -ZVV (YPR 180, 90, 0) Attitude

5.15.6.1 Results Discussion

The -XLV -ZVV attitude is the primary DDO attitude of concern. This attitude meets the RV separation attitude requirement and meets all the safe trajectory requirements.

No Orbiter contact has been found for any of the separating trajectories in this attitude, but potential contact was found between the separating vehicle and the vehicle docked at the DC-1 nadir port. This contact was the result of the encroachment of the 6.0 m contact sphere with the bottom of the DC-1 docked vehicle.

The DC-1 Nadir vehicle contact was primarily found for the negative transverse velocity component (component directed aft towards the -X ISSACS direction), coupled with a positive attitude rate of the ISS stack at separation. With the ISS stack pitching up, the aft end of the ISS (including the DC-1 nadir port) begins to curve closer to the separating trajectory resulting in these contacts.

This contact, with VRCS attitude control, is shown in Figure 5-75 through Figure 5-82 for the 180 seconds hook opening, and Figure 5-81 through Figure 5-88 for the 310 seconds hook opening. With the RS attitude control method, contact is shown in Figure 5-87 through Figure 5-94 for the 180 seconds hook opening, and Figure 5-93 through Figure 5-100 for the 310 seconds hook opening.

5.15.6.2 Composite Plots

1.1.1.1

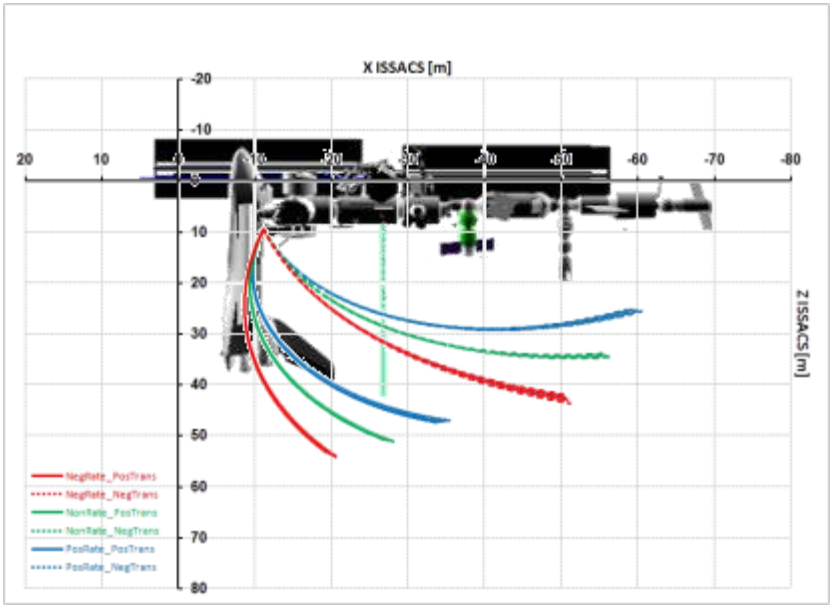

Figure 5-73. Composite plot of "no burn" trajectories for -XLV -ZVV attitude.

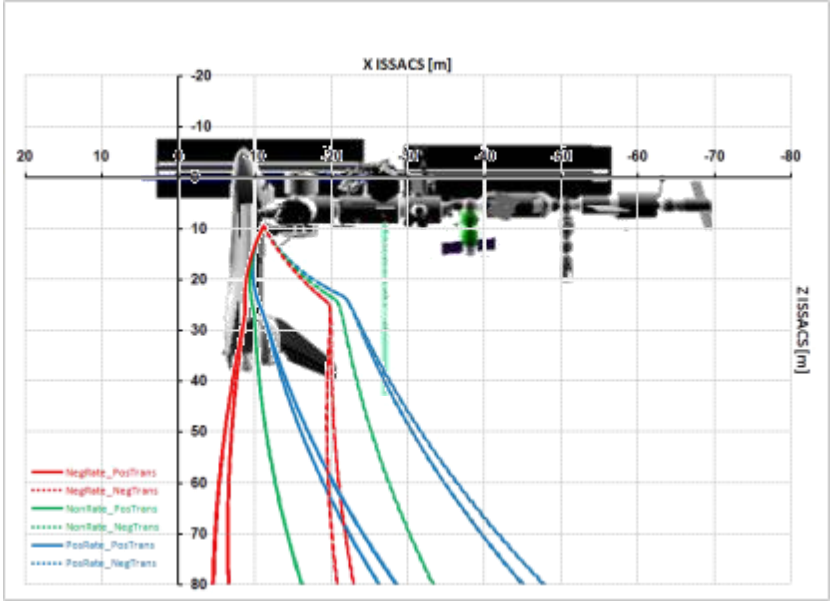

Figure 5-74. Composite plot of "one burn" trajectories for -XLV -ZVV attitude.

5.15.6.3 VRCS Attitude Control Results

VRCS Attitude Control (1.0 deg, 0.02 deg/sec)											
Hook Opening Duration:		**180 sec**							**310 sec**		
Burn Profile:		**No Burn**		**One Burn**			**No Burn**		**One Burn**		
Transverse Velocity Direction:		**+Pos**	**-Neg**	**+Pos**	**-Neg**		**+Pos**	**-Neg**	**+Pos**	**-Neg**
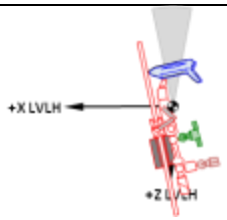 **Positive Deadband Pitch Attitude**	**Separation Pitch Attitude [deg]**					**Separation Pitch Attitude [deg]**				
Positive Attitude Rate	95.8	no	DC1[77]	no	DC1[78]	98.4	no	DC1[83]	no	DC1[84]
Zero Attitude Rate	91.0	no	no	no	no	91.0	no	no	no	no
Negative Attitude Rate	86.2	no	no	no	no	83.6	no	no	no	no
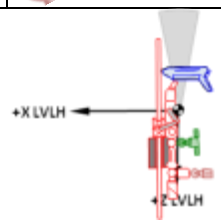 **Zero Deadband Pitch Attitude**	**Separation Pitch Attitude [deg]**					**Separation Pitch Attitude [deg]**				
Positive Attitude Rate	94.8	no	DC1[79]	no	DC1[80]	97.4	no	DC1[85]	no	DC1[86]
Zero Attitude Rate	90.0	no	no	no	no	90.0	no	no	no	no
Negative Attitude Rate	85.2	no	no	no	no	82.6	no	no	no	no
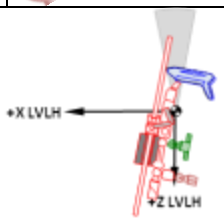 **Negative Deadband Pitch Attitude**	**Separation Pitch Attitude [deg]**					**Separation Pitch Attitude [deg]**				
Positive Attitude Rate	93.8	no	DC1[81]	no	DC1[82]	96.4	no	DC1[87]	no	DC1[88]
Zero Attitude Rate	89.0	no	no	no	no	89.0	no	no	no	no
Negative Attitude Rate	84.2	no	no	no	no	81.6	no	no	no	no

-XLV -ZVV (YPR 180,90,0), VRCS, 180 seconds Hook Opening Duration

No Burn (springs only) | One Burn

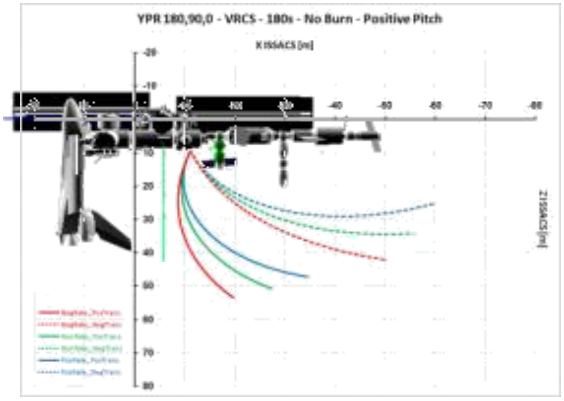

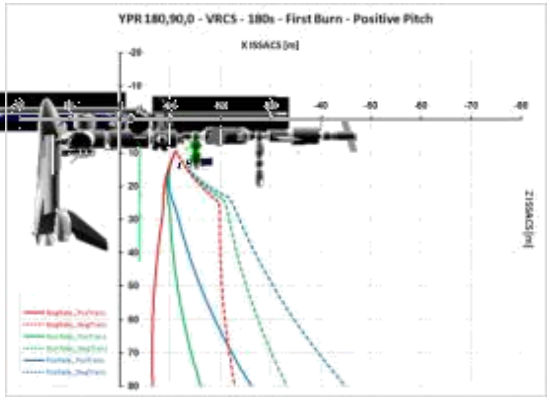

Figure 5-75 - 5-76. Positive deadband pitch attitude.

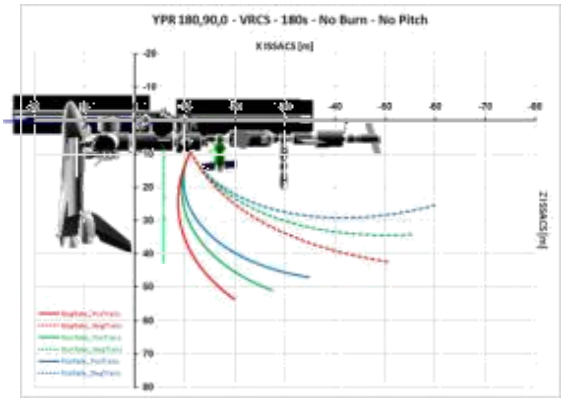

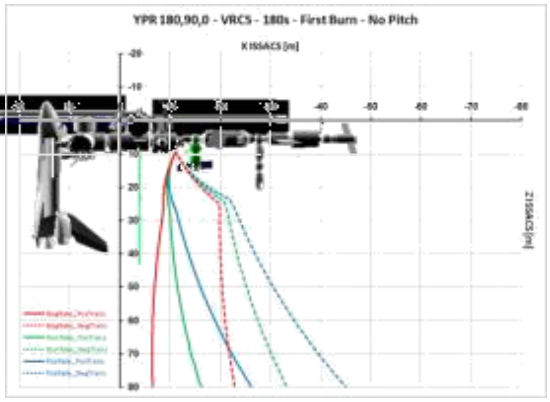

Figure 5-77 - 5-78. Zero deadband pitch attitude.

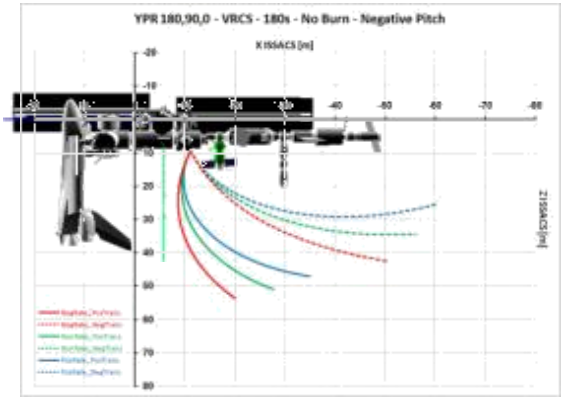

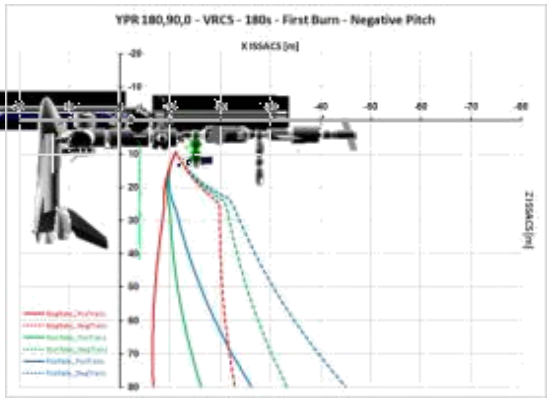

Figure 5-79 - 5-80. Negative deadband pitch attitude.

-XLV -ZVV (YPR 180, 90, 0), VRCS, 310 seconds Hook Opening Duration

No Burn (springs only) | One Burn

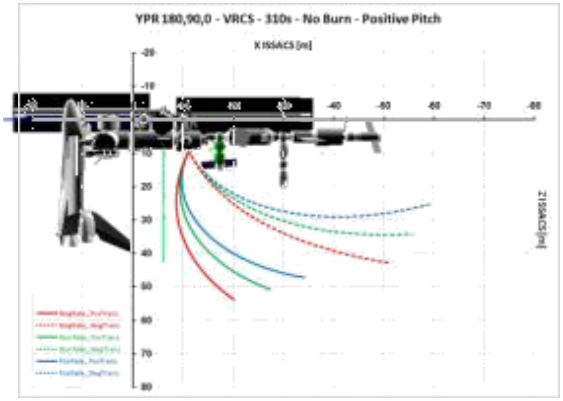

Figure 5-81 - 5-82. Positive deadband pitch attitude.

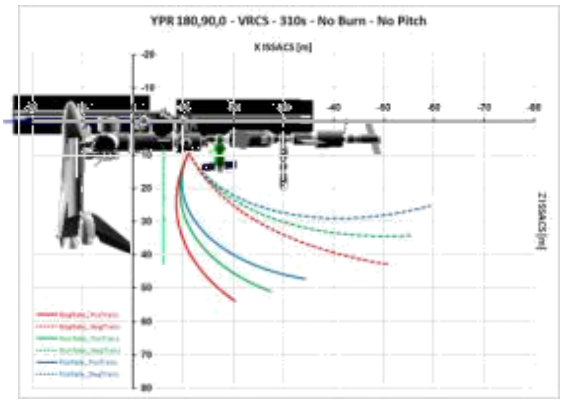

Figure 5-83 - 5-84. Zero deadband pitch attitude.

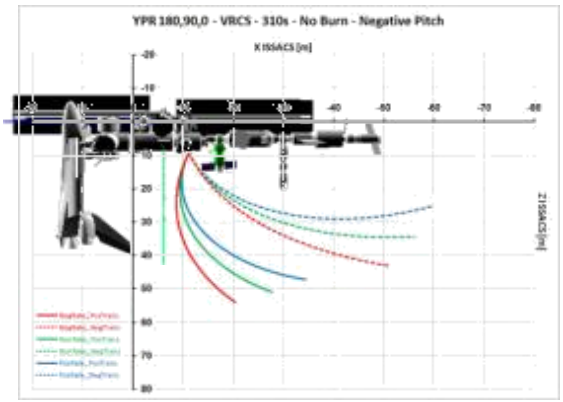

Figure 5-85 - 5-86. Negative deadband pitch attitude.

5.15.6.4 RS Attitude Control Results

RS Attitude Control (3.0 deg, 0.02 deg/sec)

Hook Opening Duration:	180 sec					310 sec				
Burn Profile:	No Burn		One Burn			No Burn		One Burn		
Transverse Velocity Direction:	+Pos	-Neg	+Pos	-Neg		+Pos	-Neg	+Pos	-Neg	
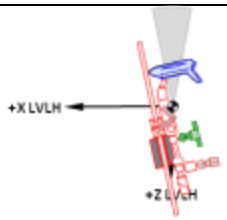 **Positive Deadband Pitch Attitude**	**Separation Pitch Attitude [deg]**					**Separation Pitch Attitude [deg]**				
Positive Attitude Rate	97.8	no	DC1[89]	no	DC1[90]	100.4	no	DC1[95]	no	DC1[96]
Zero Attitude Rate	93.0	no	no	no	no	93.0	no	no	no	no
Negative Attitude Rate	88.2	no	no	no	no	85.6	no	no	no	no
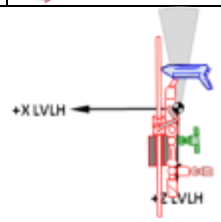 **Zero Deadband Pitch Attitude**	**Separation Pitch Attitude [deg]**					**Separation Pitch Attitude [deg]**				
Positive Attitude Rate	94.8	no	DC1[91]	no	DC1[92]	97.4	no	DC1[97]	no	DC1[98]
Zero Attitude Rate	90.0	no	no	no	no	90.0	no	no	no	no
Negative Attitude Rate	85.2	no	no	no	no	82.6	no	no	no	no
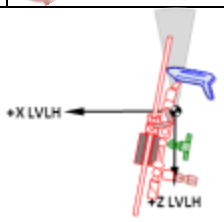 **Negative Deadband Pitch Attitude**	**Separation Pitch Attitude [deg]**					**Separation Pitch Attitude [deg]**				
Positive Attitude Rate	91.8	no	DC1[93]	no	DC1[94]	94.4	no	DC1[99]	no	DC1[100]
Zero Attitude Rate	87.0	no	no	no	no	87.0	no	no	no	no
Negative Attitude Rate	82.2	no	no	no	no	79.6	no	no	no	no

-XLV -ZVV (YPR 180, 90, 0), RS, 180 seconds Hook Opening Duration

No Burn (springs only) | One Burn

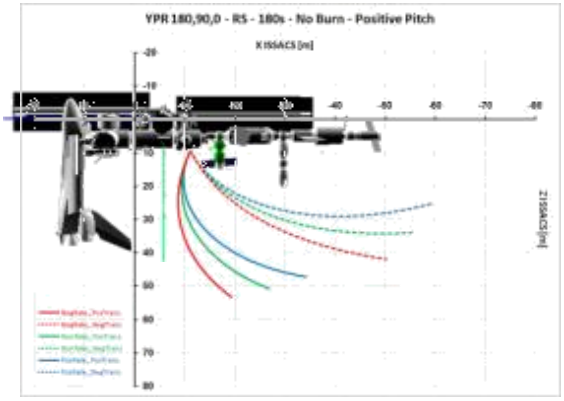

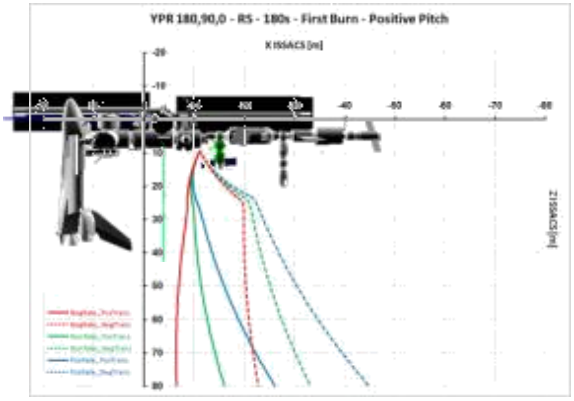

Figure 5-87 - 5-88. Positive deadband pitch attitude.

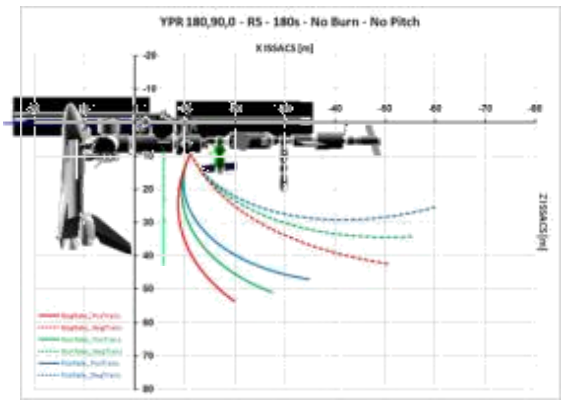

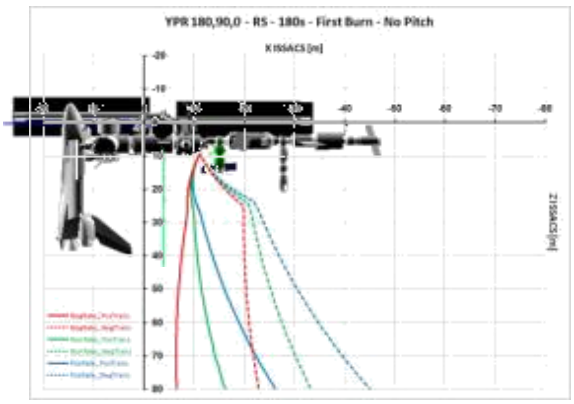

Figure 5-89 - 5-90. Zero deadband pitch attitude.

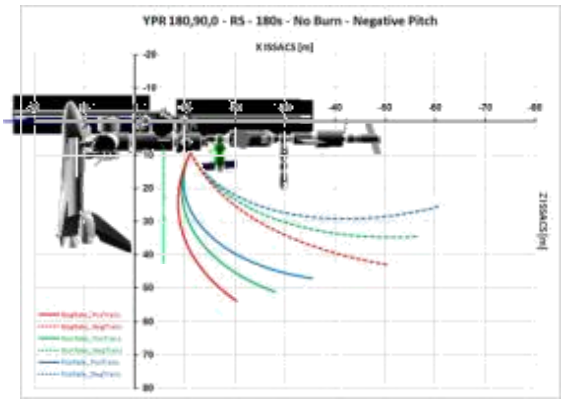

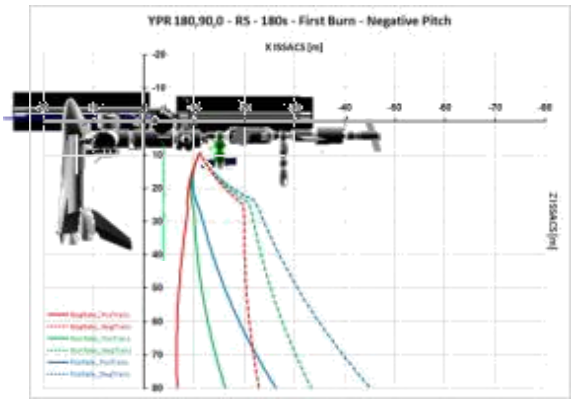

Figure 5-91 - 5-92. Negative deadband pitch attitude.

-XLV -ZVV (YPR 180, 90, 0), RS, 310 seconds Hook Opening Duration

No Burn (springs only)

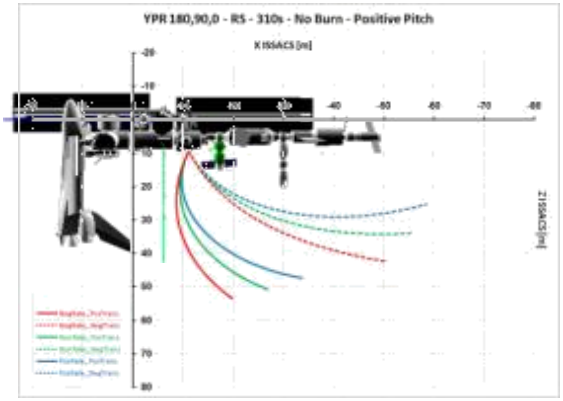

One Burn

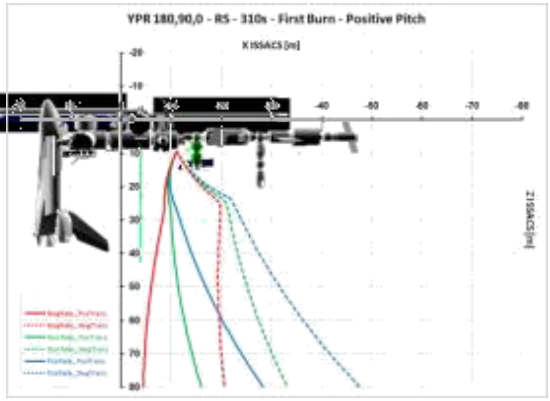

Figure 5-93 - 5-94. Positive deadband pitch attitude.

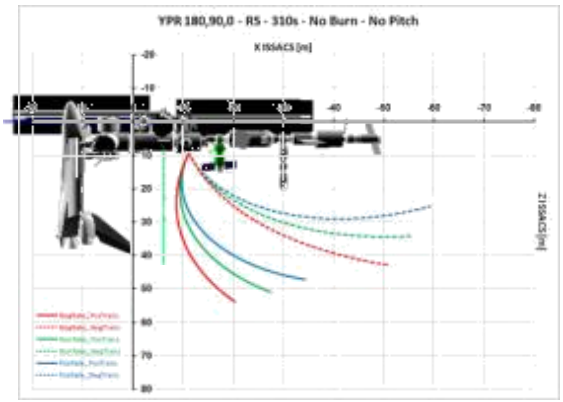

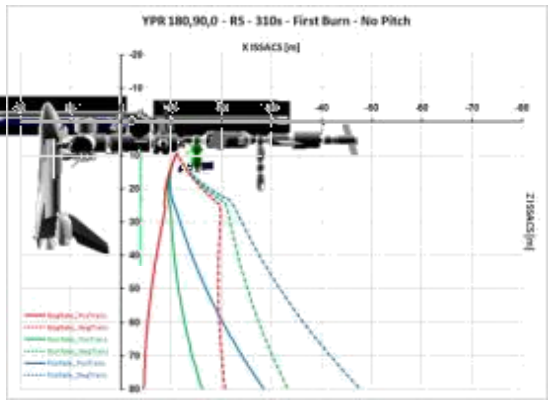

Figure 5-95 - 5-96. Zero deadband pitch attitude.

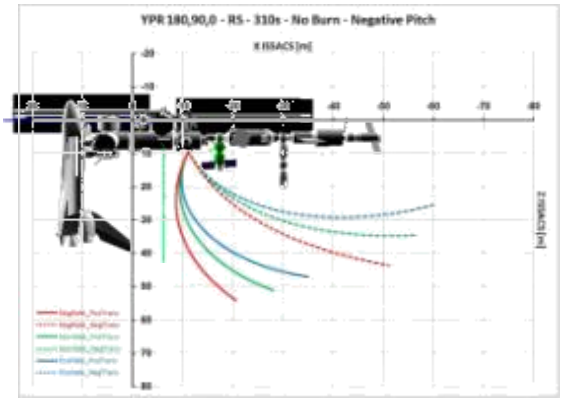

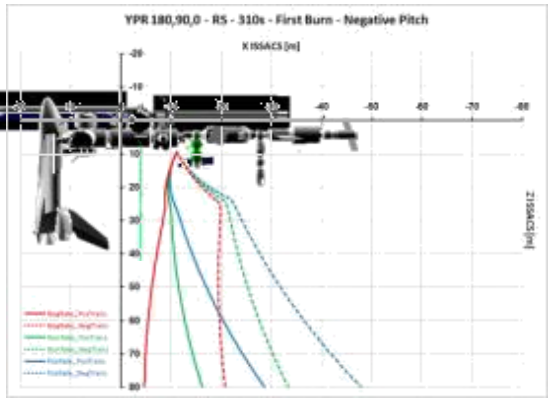

Figure 5-97 - 5-98. Negative deadband pitch attitude.

5.16 Close Clearance Analysis

The data acquired from the VVO analysis was provided to CAMMP specialists to perform RV and ISS clearance assessment for -ZVV -XLV (YPR 180, 90, 0) attitude. This attitude was chosen to meet RV separation requirements and to provide clearance with the Orbiter. It was agreed the +ZVV -XLV attitude was unacceptable since departing vehicle trajectory could cross the Orbiter tail.

From over 500 cases performed by the VVO, only 12 worst-cases were selected for detailed vehicle clearance analysis. Cases include RV failed MCS and nominal separation scenarios. The close clearance trajectories were selected from composite plots provided by the VVO.

CAMMP specialists used the ProEngineering® tool to build trajectories and the STS-129/ULF3 flight simplified ISS model to determine relative position of the RV and ISS. Relative position of c.g. points were populated into the model and provided relative trajectory of the RV that encompasses initial ISS attitude determination error, ISS initial drift rates, docking mechanism operation dispersions (e.g., longitudinal, transverse, and rotational components). To account for the rotational component, a 6 m sphere around the RV c.g. was used.

The analysis results have shown interference between the sphere around the departing RV and RV docked to DC-1 nadir port for -ZVV -XLV YPR (180°, 90°, 0°), with hook opening time at 180 and 310 seconds. Interference occurs when the RV fails to execute the post separation burn at 180 seconds and when ISS had max positive pitch and max positive pitch rate with a negative transverse component from the RV.

A close proximity of 0.3 m was determined between the sphere around the departing RV and RV docked to DC-1 nadir port for -ZVV -XLV YPR (180°, 0°, 0°), with hook opening time at 180 and 310 seconds. Interference occurs when the RV fails to execute the post separation burn at 180 seconds and when ISS had max negative pitch and max positive pitch rate with a negative transverse component from the RV.

Closest distance between the sphere around the RV and Orbiter was determined to be ~8.0 m. Such clearance was determined for -ZVV -XLV YPR (180°, 0°, 0°), with hook opening time at 180 and 310 seconds. The closest distance occurs when the RV fails to execute the post separation burn at 180 seconds and when ISS had max negative pitch and max negative pitch rate with positive transverse component from the RV. The same close proximity was determined for two cases in -ZVV -XLV YPR (180°, 90°, 0°) attitude, with hook opening time at 180 and 310 seconds, when the RV executes the post separation burn at 180 seconds and when ISS had maximum positive pitch, maximum negative pitch rate with positive transverse component from the RV.

Graphical representation of analysis results is shown on Figure 5-99 through Figure 5-105.

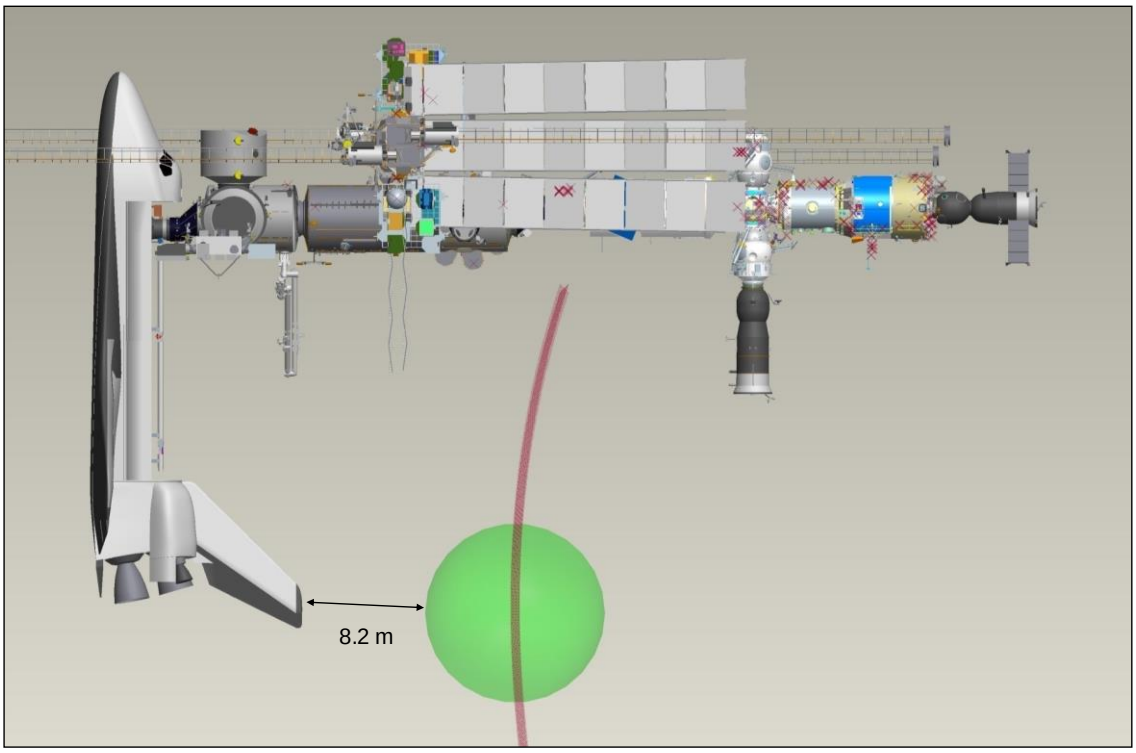

Figure 5-99. -XVV +ZLV, hook time 180s, RV no Burn, ISS NegPitch, NegRate, RV PosTrans.

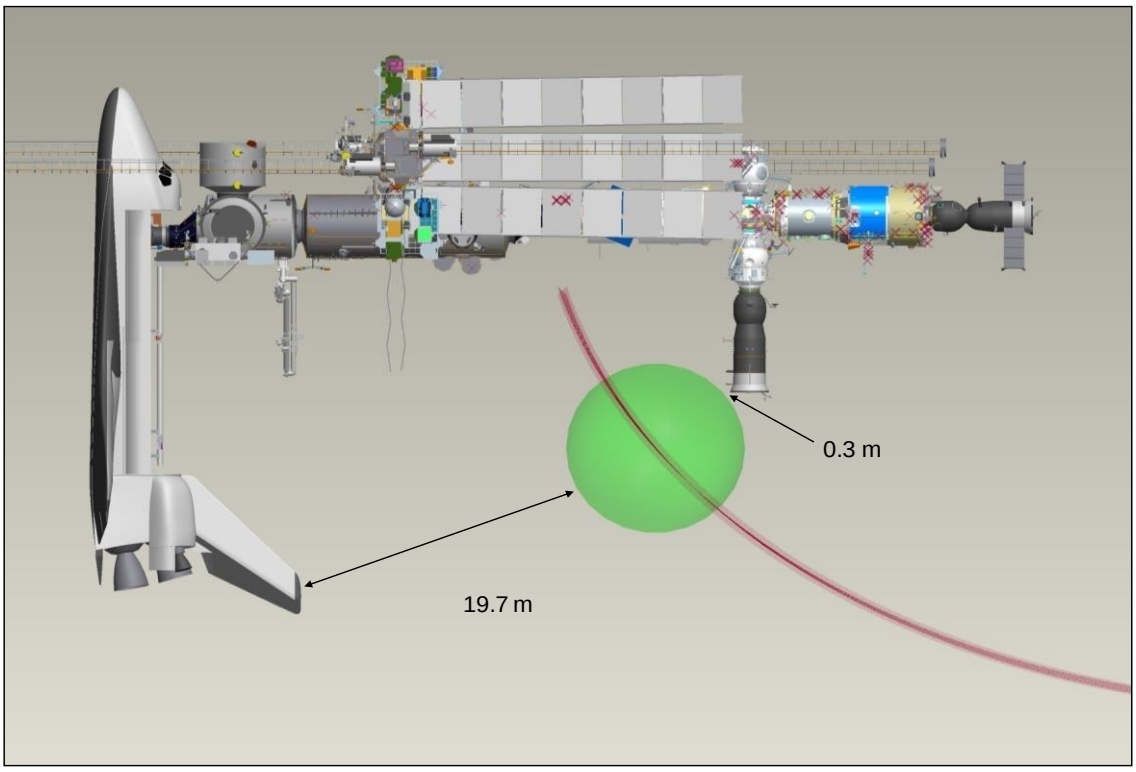

Figure 5-100. -XVV +ZLV, hook time 180s, RV no Burn, ISS NegPitch, PosRate, RV NegTrans.

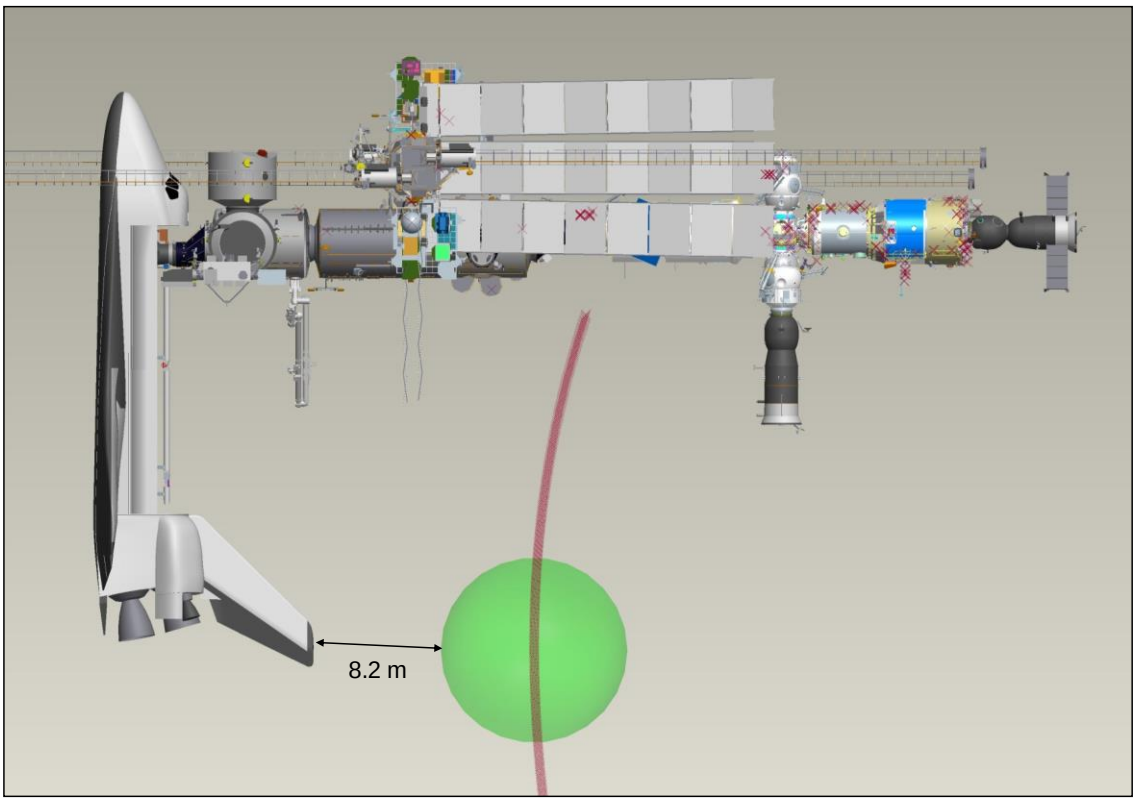

Figure 5-101. -XVV +ZLV, hook time 310s, RV no Burn, ISS NegPitch, NegRate, RV PosTrans.

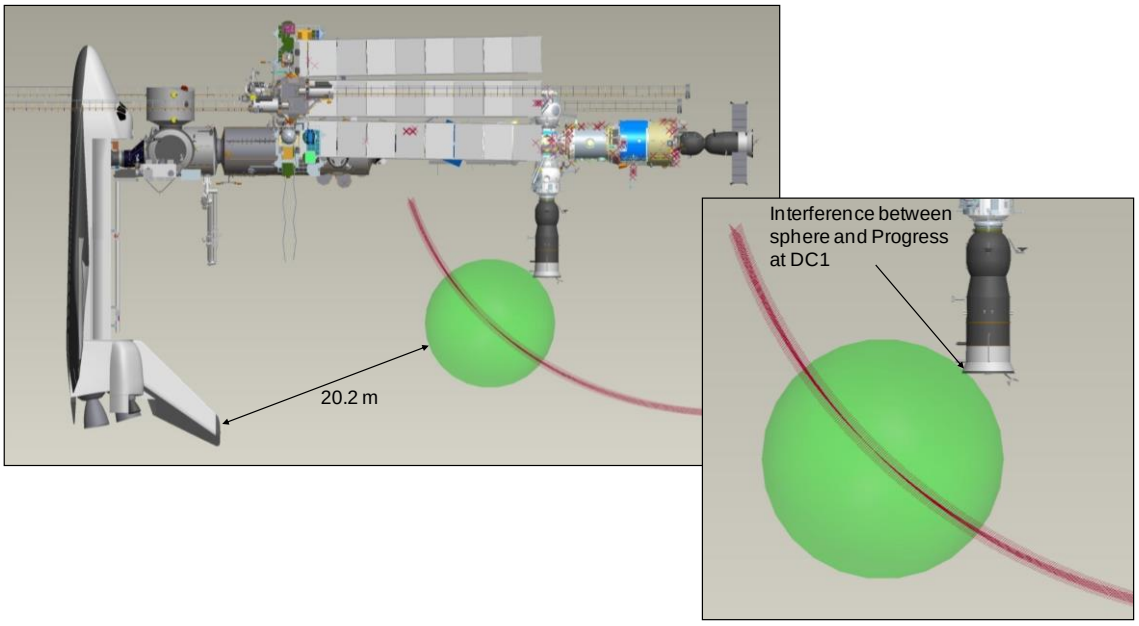

Figure 5-102. -ZVV -XLV, hook time 180s, RV No Burn, ISS PosPitch, PosRate, RV NegTrans.

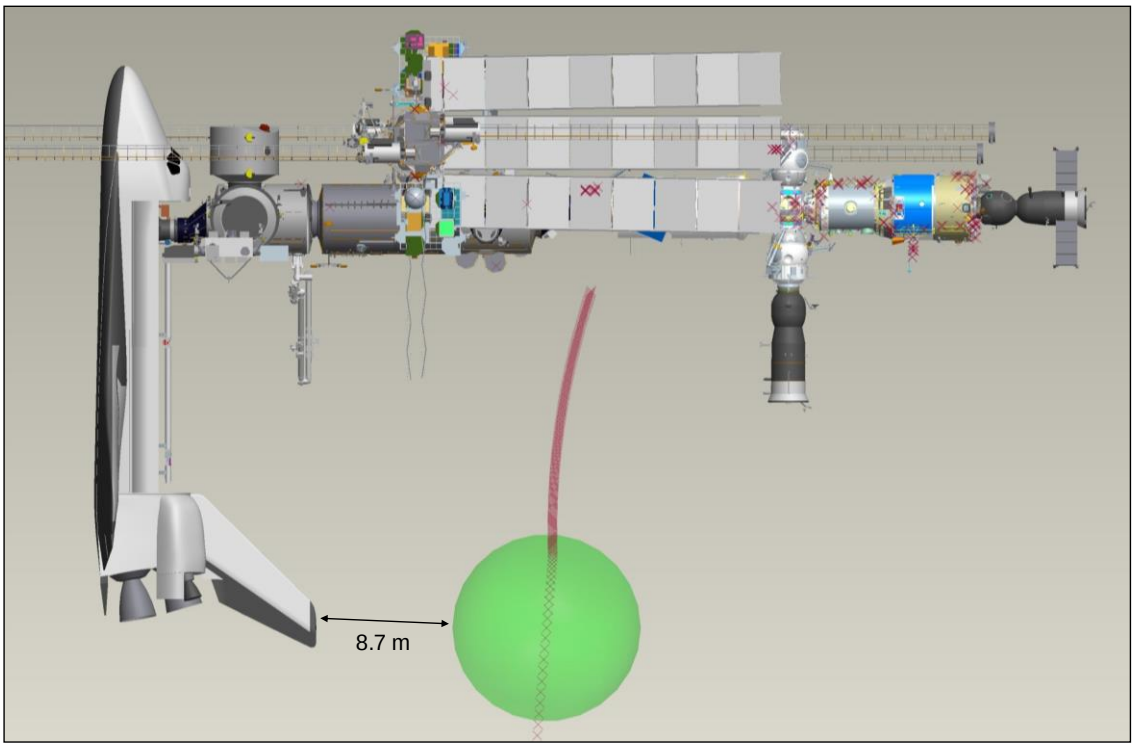

Figure 5-103. -ZVV -XLV, hooks time 180s, RV one Burn, ISS PosPitch, NegRate, RV PosTrans.

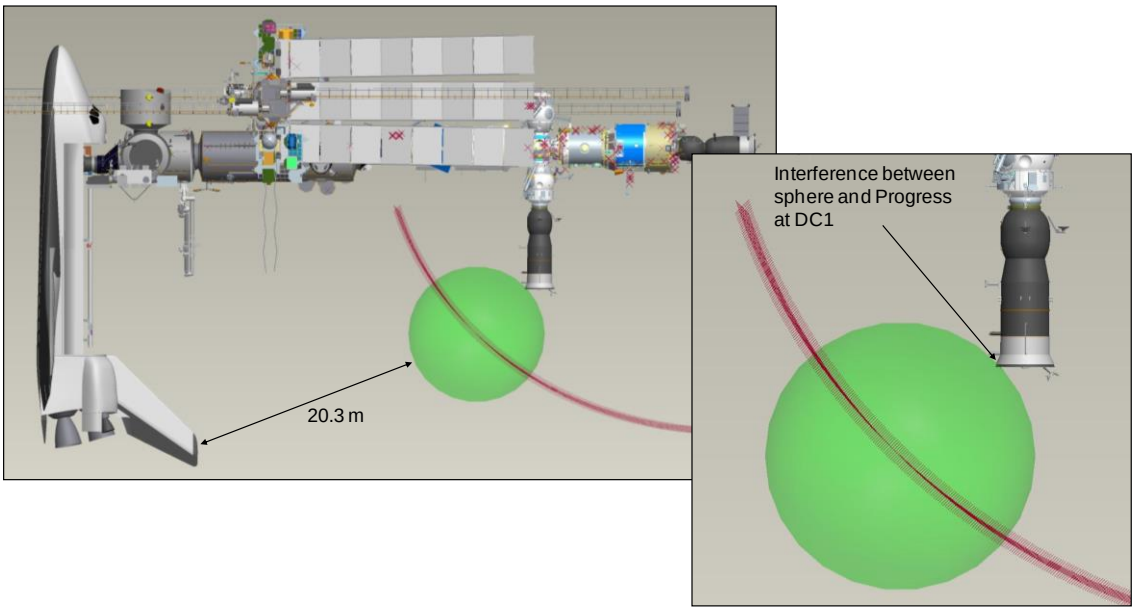

Figure 5-104. -ZVV -XLV, hooks time 310s, RV one Burn, ISS PosPitch, PosRate, RV NegTrans.

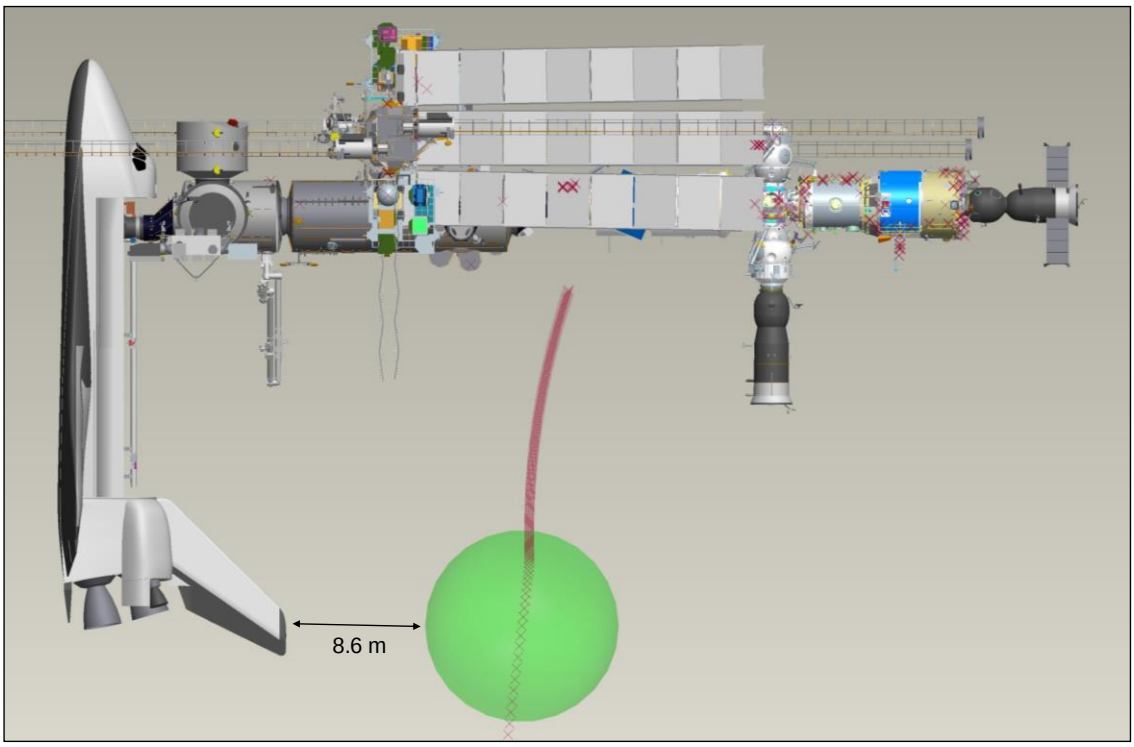

Figure 5-105. -ZVV -XLV, hooks time 310s, RV one Burn, ISS PosPitch, NegRate, RV PosTrans.

Additional analysis was performed for the two cases that have shown interference between the sphere around the departing RV and RV docked to DC-1 nadir port. CAMMP team used worst-case RV rotation rates to determine the closest proximity.

Detailed analysis has demonstrated that departing RV clears the vehicle docked to DC-1 nadir port with close clearance. Figure 5-106 through Figure 5-109 show the results of detailed analysis.

The closest proximity of 0.51 m (Figure 5-109) was determined between the departing RV and the RV docked to DC-1 nadir port for -ZVV -XLV YPR (180°, 90°, 0°), with hook opening time at 180 seconds. This occurs when the RV fails to execute the separation burn at 180 seconds post separation and when ISS had maximum positive pitch and max positive pitch rate with a negative transverse component from the RV with 0.5°/s pitch/yaw and 0.2°/s roll rates.

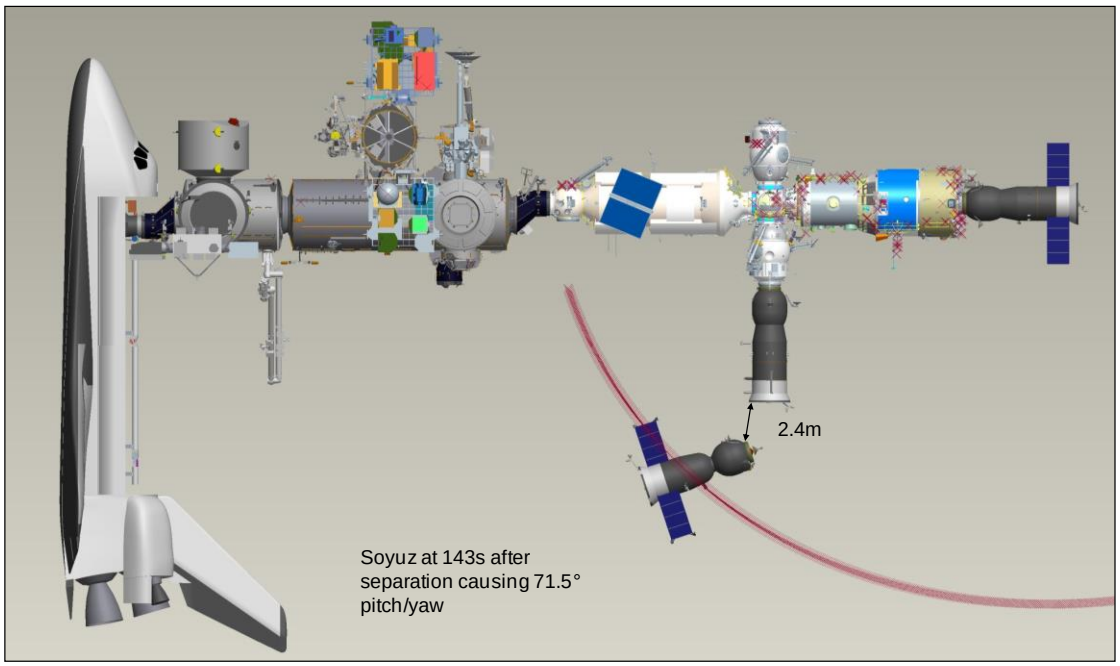

Figure 5-106. -ZVV -XLV, hooks time 180s, RV no Burn, ISS PosPitch, PosRate, RV NegTrans with 0.5°/s pitch/yaw rate

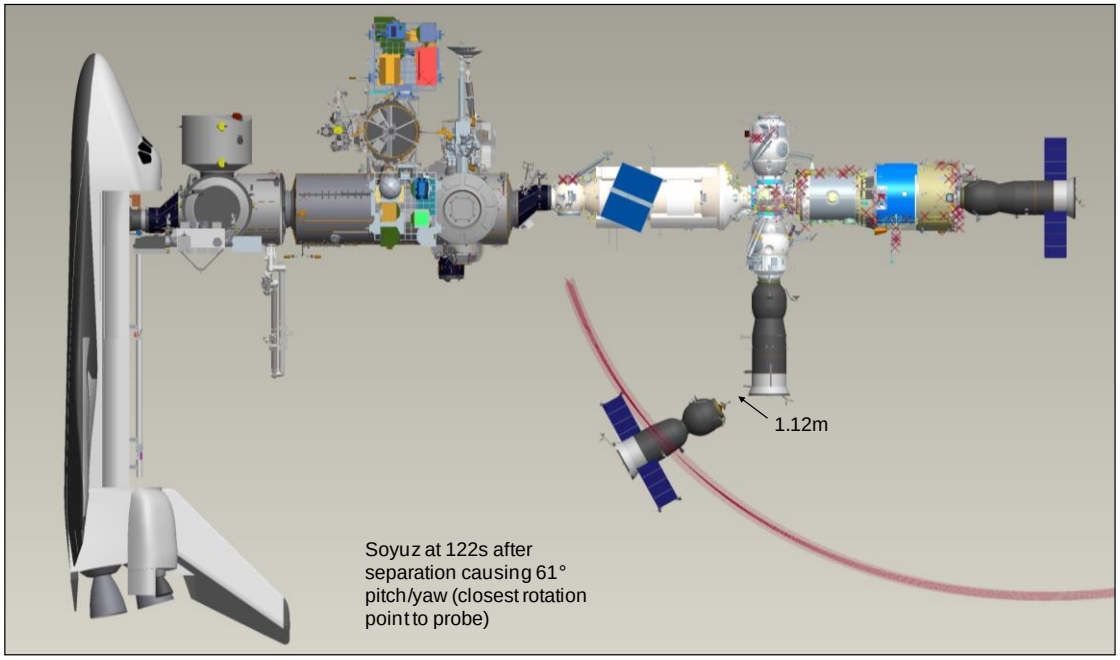

Figure 5-107. -ZVV -XLV, hooks time 180s, RV no Burn, ISS PosPitch, PosRate, RV NegTrans with 0.5°/s pitch/yaw rate

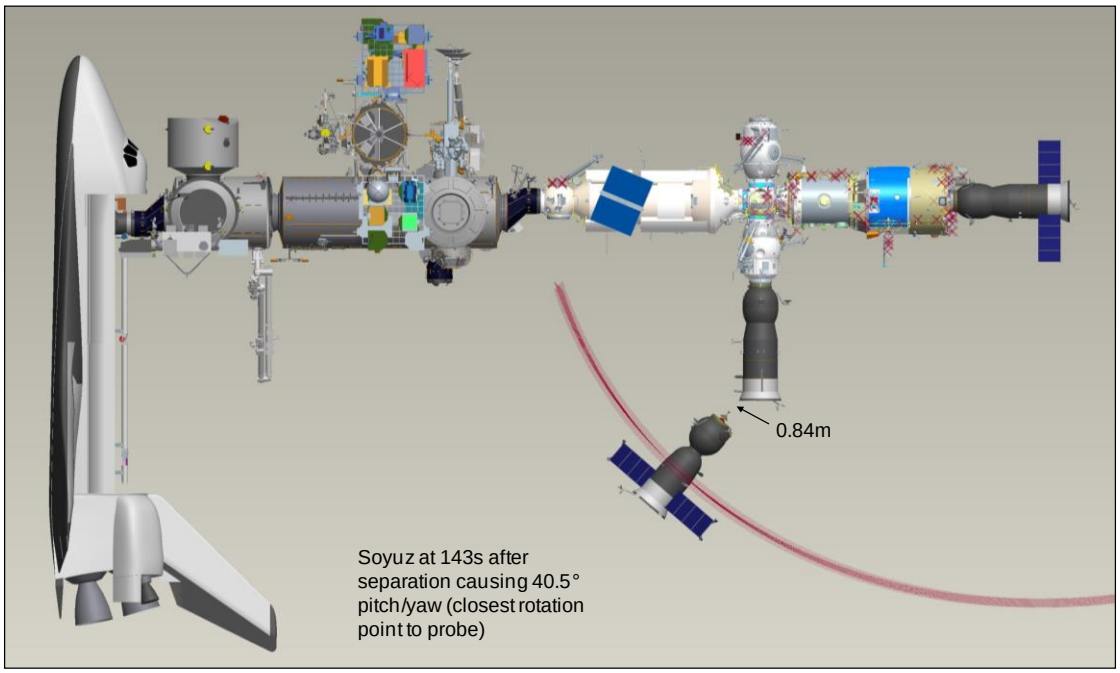

Figure 5-108. -ZVV -XLV, hooks time 180s, RV no Burn, ISS PosPitch, PosRate, RV NegTrans with 0.28°/s pitch/yaw rate

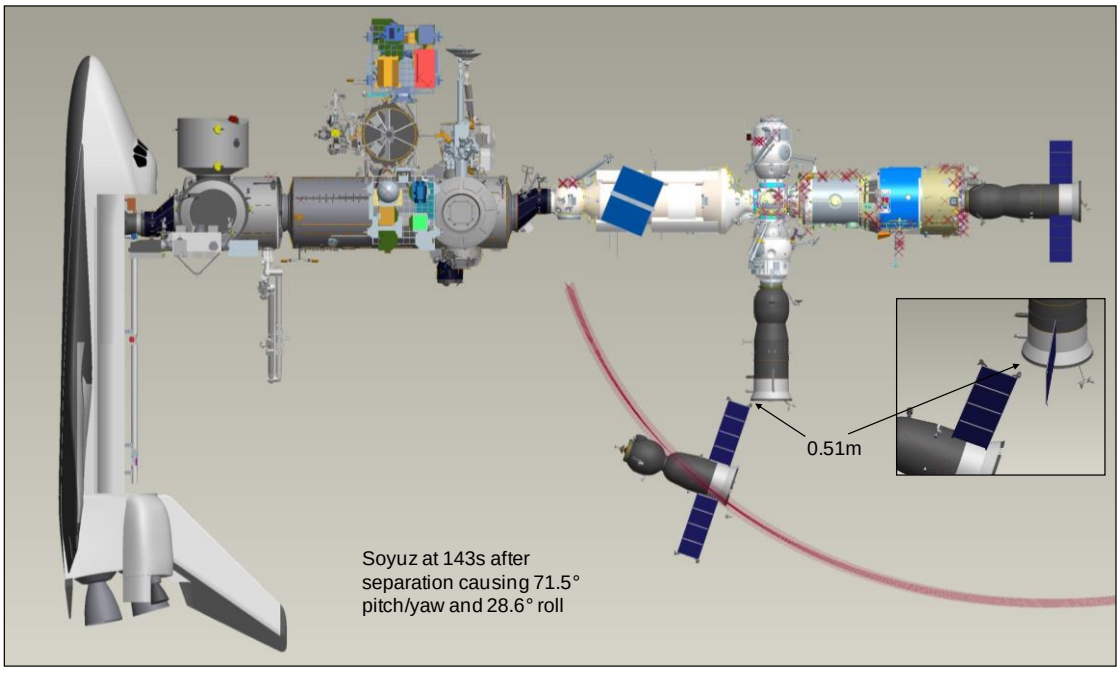

Figure 5-109. -ZVV -XLV, hooks time 180s, RV no Burn, ISS PosPitch, PosRate, RV NegTrans with 0.5°/s pitch/yaw and 0.2°/s roll rate

5.17 Conclusions and Recommendations

This section will provide a summary of clearance analysis results, discuss uncertainties and caveats, and provide recommendations for future DDO and required analysis.

5.17.1 Conclusions

DDO scenario for 19 Soyuz departure during STS-129/ULF3 flight has shown that the RV when undocked from FGB port with ISS in -ZVV -XLV (YPR 180, 90, 0) attitude can clear ISS and Orbiter structure. However, close clearances were predicted between RV undocking from FGB port for the worst-case docking mechanism disturbances and failed RV MCS. Figure 5-110 shows minimum vehicle approach to the Orbiter and docked RV structures.

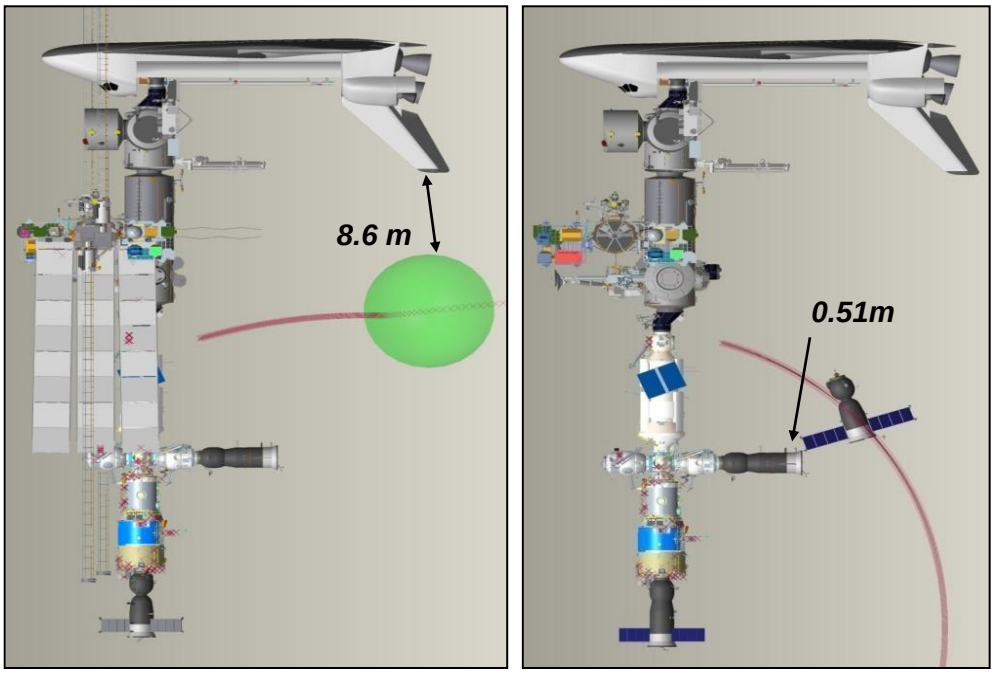

Figure 5-110. -ZVV -XLV, RV worst-case trajectories.

The review of RS Specifications document has shown that there is no requirement for minimal clearance between ISS structure and ISS-docked vehicles. Even though the analysis has shown that there is no collision between the departing vehicle and the ISS structure, there were several factors (e.g., gravity gradient effects and Aero Torques) that were not accounted for in analysis that may lead to increased ISS rates and lead to potential collision.

The later studies have shown that delta rates imparted into the ISS by spring pushers cause significant increase in ISS pitch rates to 0.015°/s post departure, which provides additional uncertainty to the position of the ISS elements. The ISS LVLH body rates increase post RV separation as shown in Figure 5-111.

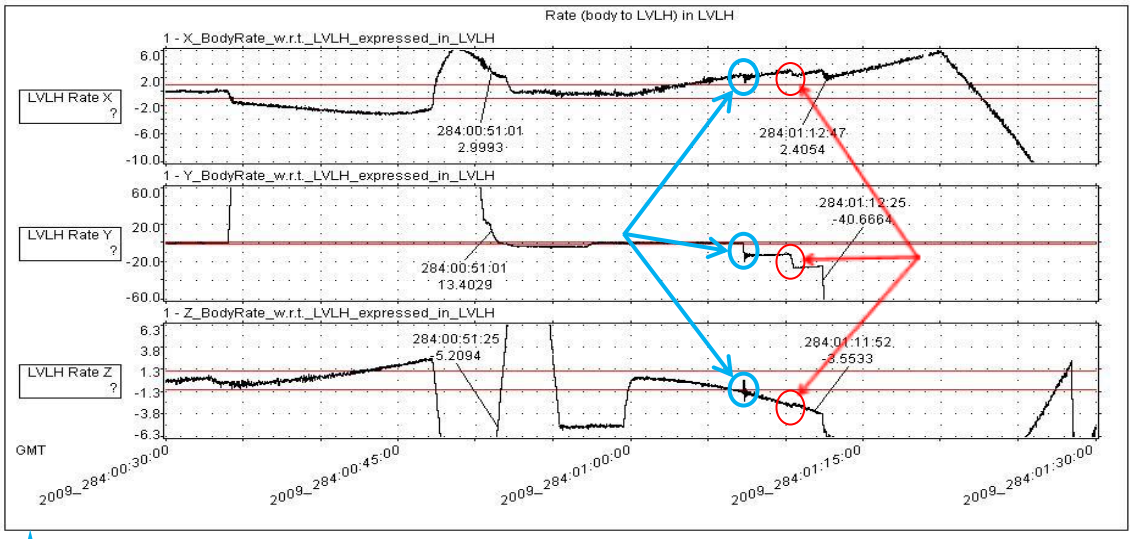

Courtesy of Rita Schrock

Figure 5-111. Additional rates imparted into ISS by RV pushoff.

Given all the analysis uncertainties, the 0.51 m between the RV docked to DC-1 nadir port and departing RV represent a close clearance.

5.17.2 Other ISS Ports Assessment

VIPER, VVO, and CAMMP teams agreed that RV undocking from FGB port for DDO represents the worst-case scenario. All other scenarios will significantly improve the clearance, and some may not require additional analysis. The teams have agreed that RV departure trajectories from FGB port may be applied to determine generic relative motion trajectories for MRM1, MRM2, DC-1, and SM aft ports since, due to orbital mechanics, relative motion trajectories will be similar, but not exact.

The RV departure from MRM1 and DC-1 ports in -ZVV -XLV attitude will be safer than from FGB since MRM1 extends FGB port by 6 m (19.7 feet), reducing the time of the RV in close proximity of the Orbiter or the RV on DC-1 nadir port. DC-1 is located 14 m (45.9 feet) below the FGB port, does not have the ISS structure or elements close to departure trajectory, and moves departing vehicle trajectory further from the Orbiter tail. Relative trajectories for MRM1 and DC-1 ports are shown on Figure 5-112.

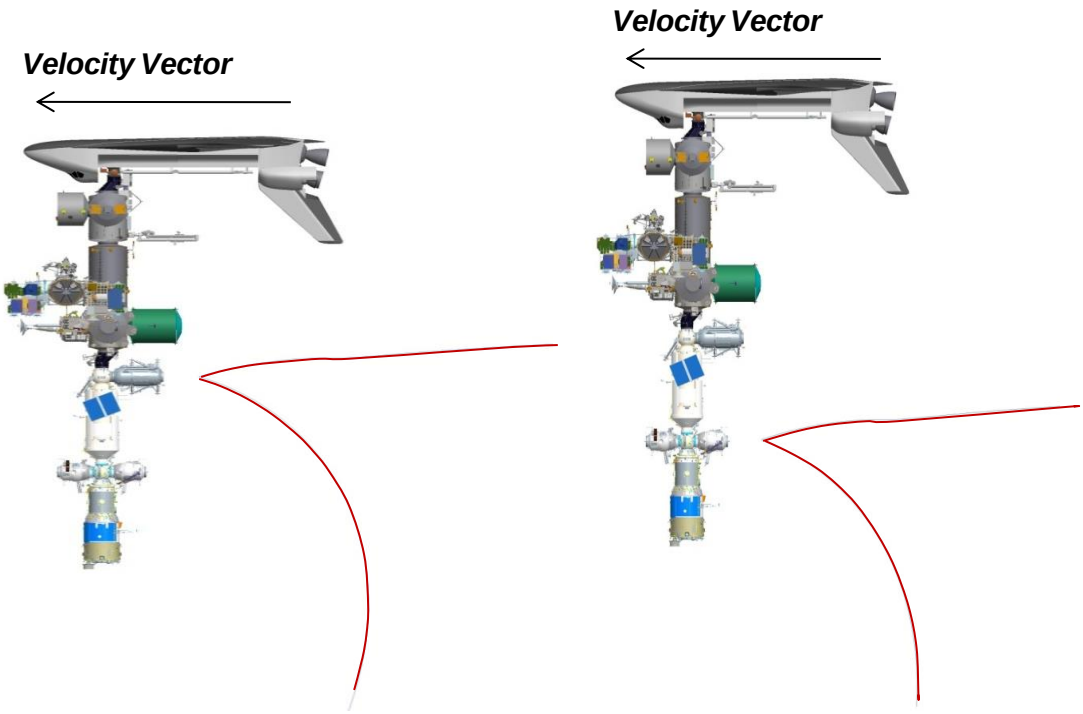

Figure 5-112. RV departure trajectories from MRM1 and DC-1 ports in -ZVV -XLV.

RV undocking from MRM2 port in the ISS -ZVV -XLV (YPR 180°, 90°, 0°) attitude may potentially lead to the departing RV passing in close proximity to the Orbiter. This would be possible only in the case of RV MCS failure. If the decision is made to undock in -ZVV -XLV (YPR 180°, 90°, 0°), attitude-specific analysis will be required. However, the ISS +ZVV -XLV (YPR 0°, 90°, 0°) attitude provides safest separation trajectory from MRM2 and will not require additional analysis. Generic separation trajectories of the RV from MRM2 port in ISS ±ZVV -XLV attitude are shown on Figure 5-113.

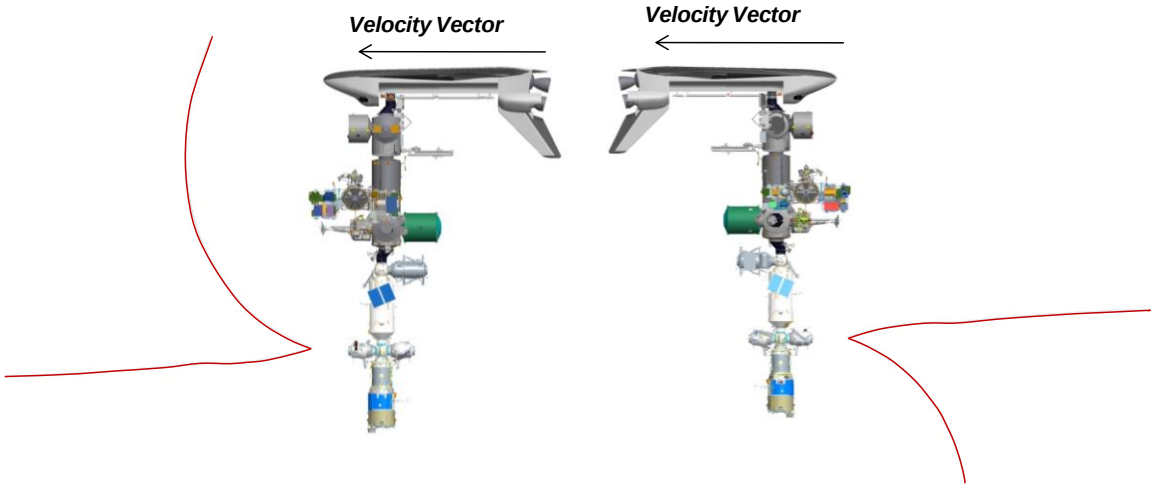

Figure 5-113. RV departure trajectories from MRM2 in -ZVV -XLV and +ZVV -XLV attitudes.

RV undocking from SM aft port represents the most safe separation trajectory from all DDO scenarios. SM aft docking port is the furthest from the Orbiter, and the departing vehicle trajectory had been analyzed for the ISS structural clearance many times and was proven to be the safest. The other benefit of undocking from SM aft port is that no maneuver will be required, and undocking can be performed in mated Torque equilibrium attitude (TEA). This attitude satisfies maximum pitch angle required for safe separation and second orbit clearance for the departing RV.

Potentially, undocking can be performed under CMG momentum management (no free drift), which provides the attitude with the best known parameters and reduces separation corridor. However, mission-specific GN&C analysis may be required. The departure trajectory from SM aft port is shown on Figure 5-114.

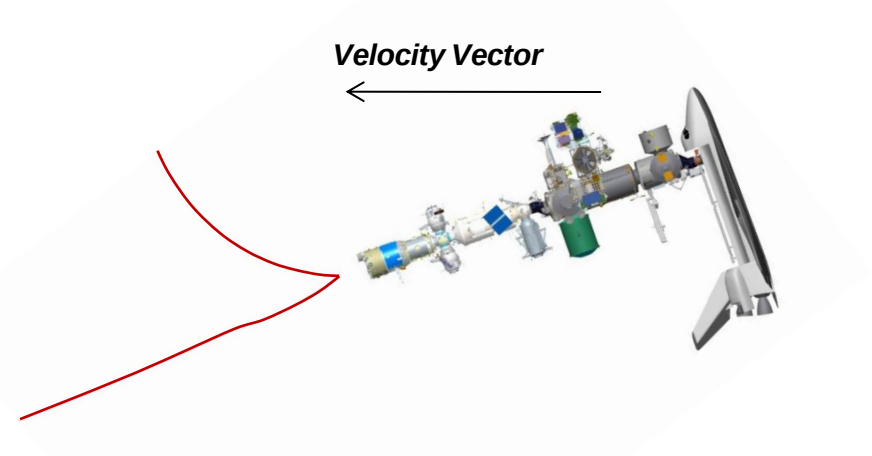

Figure 5-114. RV departure trajectory from SM aft port in mated TEA (-XVV +ZLV).

5.17.3 Recommendation

The analysis has shown that the RV undock from FGB port represents the worst-case DDO scenario and brings the RV closest to the ISS elements and the Orbiter. Detailed analysis limiting uncertainties is required if DDO is performed for FGB port.

SM aft undockings do not pose a threat to the Orbiter or the ISS structure, and specific separation analysis is not required.

If RV undocking is performed from MRM2 port with the Orbiter present, the ISS +ZVV -XLV (YPR 0, 90, 0) attitude must be used to avoid additional analysis. If the decision is made to use ISS -ZVV -XLV (YPR 180°, 90°, 0°), specific analysis is required.

The only analysis that was determined to be mandatory for DDO is the RV undocking from MRM1 port.

6.0 SSP Assessments

This section provides analysis and study results based on the environments discussed in Section 4.0, and the visiting vehicle trajectories described in Section 5.0. Included in these sections are results from the FO&I JTWGs, FO&I functional areas, and the OPO.

The goal of each of these assessments was to evaluate the viability and readiness of the SSP to protect for DDO on any given mission. Where possible generic assessments were performed and for those subsystems and/or functions where mission specific analysis is required, operational impacts and future work have been defined.

6.1 Flight Operations and Integration JTWGs

All JTWGs have assessed the ISSP-provided environments for viability to perform DDO. Power/Avionics, ECLSS, Power/Avionics, and C&T, and electromagnetic effects panels have completed generic assessments with no issues identified. The TCS, VC, Loads and Dynamics, and Flight Control and Structures panels require mission-specific analyses and documentation updates.

6.1.1 Power/Avionics

Mated ISS/Orbiter avionics interfaces and operations do not change for DDO flights. DDO flights could result in mission duration changes, which require consumables adjustments and will be addressed on a mission-specific basis. Engineering products are not impacted since the Orbiter configuration is not expected to change for DDO flights.

6.1.2 Vehicle Configuration

The VC JTWG is responsible for defining the on-orbit mission physical interface configurations of the mated stack from prelaunch through post undocking activities. These mission configurations are documented in Section S.3.0 of the mission specific on-orbit ICDs.

Section S.3.0 is developed with ISS configuration data from several sources, including the Increment Definition and Requirements Document (IDRD), End-to-End Berthing Integration Team (EBIT), Assembly Matrix, and Blue Book 3-Dimensional Computer Aided Drawing (CAD) models. The tactical plan for the flight is reviewed, and CAD models are updated to produce figures documenting the configuration pre, during, and post Orbiter/ISS mated stack. The models are used to generate ISS dimensions. For DDO, each on-orbit ICD's Section S.3.0.1.10.5 entitled "ISS Visiting Vehicle Docking Ports" provides a list of available docking ports for all ISS visiting vehicles. Figures shown within Section S.3.0 are a representative case of the visiting vehicle port utilization. Any combination of nominal or contingency docking ports may be used for a given flight.

All on-orbit ICDs for the remaining SSP manifests have been approved and contain the current combination of nominal or contingency docking ports utilization plan for that specific flight.

6.1.3 Proximity Operations, Plumes, Structures, and Flight Control JTWG

6.1.3.1 Loads and Dynamics Team

The LDT is a joint ISS/SSP team responsible for defining the on-orbit loads that include proximity operations plume effects from various vehicles, and docking and undocking loads. Analyses are performed on a mission-specific basis with environments and constraints documented in mission-specific on-orbit ICDs. For DDO, the LDT's work and results are discussed in Section 4.8.

6.1.3.2 Flight Control and Structures JTWG

The Flight Control and Structures JTWG prepares a mission-specific Digital Auto Pilot (DAP) Modes and Constraints memo for each flight. This memo addresses Orbiter control of the mated stack during the mission. To protect for potential SSP launch slips, this memo typically certifies Orbiter mated control for multiple ISS visiting vehicle configurations. However, propellant usage estimates are typically provided only for the nominal configuration and sometimes a contingency configuration.

As long as both ISS configurations (before and after DDO) have been certified, then from a flight control perspective, Orbiter control is acceptable outside of close range proximity operations. This is based on the assumption that the Orbiter attitude hold DAP settings (currently 1°, 0.02°/s) will be acceptable if Orbiter attitude control is to be used immediately prior to undocking. The Flight Control team will need to be informed if this assumption changes. Orbiter control during close range proximity operations is not expected because the RS is expected to have attitude control during a docking approach, and the Orbiter/ISS mated stack is expected to be in free drift for undocking until a sufficient separation distance has been achieved.

However, to support a planned DDO event, the operations team will need propellant estimates to determine if Orbiter propellant is available to support the attitude maneuvers to and/or from the docking (or undocking) attitude. The Flight Control team will need to include these operations in the propellant usage estimates in the DAP Modes and Constraints memo. To produce these estimates, the Flight Control team will need to know the docking (or undocking) attitude. If the Orbiter will be used to recover attitude control after undocking, then the Flight Control team will need to know the planned timeline, including free drift time before and after physical separation and the plume time history in terms of force and torque on the mated Orbiter/ISS stack.

The DAP Modes and Constraints memos (portions pertaining to DDO) for STS-130/20A, STS-131/19A, and STS-132/ULF4 are found in references [33,34,35].

6.1.4 Thermal Control System - Active/Passive JTWG

The TCS JTWG is chartered to verify that shading effects from a docked RV do not negatively impact thermal environments. They verify the Orbiter and payloads are thermally compatible during DDO predocking, docking, mated, undocking and post-undock attitudes. Since thermal attitudes are highly dependent on mission timelines and seasonal parameters, it was consciously decided that these analyses would be performed on a mission-specific basis and folded into the standard thermal verification analysis process for each mission.

6.1.5 Environmental Control and Life Support System JTWG

The ECLSS JTWG assessment of DDO was discussed in September 2009. Results of these discussions found that no special life support system analyses are required since consideration of joint crew sizes greater than 13 were ground ruled out. Operations associated with DDO are not expected to interrupt nominal functioning of Orbiter or ISS life support systems, and brief interruptions in power to ISS systems can be tolerated. Joint vehicle ECLSS systems are mission specific and generically compatible with all currently defined DDO scenarios. For each mission, the ECLSS JTWG will take into account approaching/departing vehicles when planning pre-docked and post-undocked water dumps.

6.1.6 Communications and Tracking

The C&T panel assessed the DDO impacts on the communications systems of the Orbiter, ISS and RVs. An assessment of Soyuz transmitters on Orbiter receivers was performed with no issue found [22]. An assessment of Orbiter transmitters on Soyuz receivers was completed with no issue found [23]. An assessment of Orbiter transmitters on the Russian ground station receivers supporting Soyuz operation identified two potential system conflicts. They are the Orbiter WLE Impact Detection System to Russian command link and the Space to Space Communication System (SSCS) to Russian TV link. Additional information has been requested from the Russians to ensure there are no DDO impacts. That data request is pending. A short turnaround assessment is anticipated when that information is received.

6.1.7 Electromagnetic Environmental Effects

The Payload Electromagnetic Effects Working group assessed the DDO impacts on the payloads manifested for the last two flights of the Orbiter to the ISS. No payload impacts were identified.

6.2 Flight Operations and Integration Payload Cargo Engineering

The following assessment summarizes the DDO impacts to SSP cargo integration flight products and hardware for which Payload Cargo Engineering provides support. Payload Integration Hardware is exposed during DDO to emissions, fuels, and loads generated during the final RV approach through docking.

General assumptions used in the assessment are:

a. The Orbiter is docked to the PMA2 of Node 2.

b. A RV is approaching or has docked to any port identified in the STS-130/ISS-20A mission-specific ICD, ICD-A-21549-OOR, Table S.3.0.1.10.5-1 (ISS Visiting Vehicle Docking Ports).

    1. A Soyuz spacecraft docks to the FGB nadir port.

    2. A Progress spacecraft docks to the SM aft port.

c. Thermal operational profile is similar to STS-131/19A with a March 2010 launch.

d. Structural on-orbit loads were assessed with a Orbiter configuration to generate worst-case responses for STS-132/ULF4 and subs.

e. STS-134/ULF6 Orbiter mass properties and payload configuration.

f. Contamination is limited to varying states of expended propellants and nitrite salts (present in the propellant mixture).

Refer to the following detailed assessments for specific assumptions.

6.2.1 Cargo Avionics

Cargo avionics interfaces are not affected during DDO. The performance of avionic interfaces to cargo elements will meet all requirements documented in the payload unique ICD and SSP Mission Integration Plan (MIP) for any flight environment including DDO.

6.2.2 Payload Integration Hardware (PIH) and Contamination

During DDO, PIH will be exposed to combustion effluents. The products of combustion will include unconsumed and partially combusted UDMH and noncombustible impurities. The DC-1 nadir docking location was assessed for impacts to PIH operation, life, and ground handling [36]. The docking port orientation imparted the greatest contamination on the Orbiter. The DDO environment will not impact PIH operation or ground personnel. PLB surface temperatures during the ISS docked and post undock planned attitudes are expected to exceed the surface temperature above which UDMH evaporates (-71°F). The presence of UDMH will be insignificant because the temperatures in the PLB are expected to volatize any unconsumed or partially combusted UDMH.

Though residual UDMH is not anticipated, precautionary PLB surface sampling should be planned to ensure ground personnel are not exposed to residual contaminants.

6.2.3 Cargo Thermal and Environmental Control and Life Support System

DDO is expected to have a minimal effect on cargo thermal compatibility [37,38]. ECLSS parameters for Orbiter supply water production and Lithium Hydroxide canister consumption may be impacted as a result of DDO operations. Generalized impacts cannot be captured because of the number of influencing variables. A specific mission analysis is required to define the magnitude of consumable impacts

6.2.4 Cargo Structures

All cargo structural on-orbit loads resulting from DDO events are within the Interface Definition Document (IDD) ISS parameters for the Orbiter Docking system (ODS) interface and were enveloped by the Verification Loads Analysis (VLA) for launch and landing for the cargo elements [39]. Significantly lower undocking loads are enveloped by the DDO docking loads and are considered within IDD ISS parameters.

6.2.5 Reconfiguration Engineering

Cargo reconfiguration engineering is not impacted by DDO. Cargo will be configured to meet all IDD ISS requirements as documented in the payload unique Interface ICD and the SSP MIP for any flight environment to include DDO.

6.2.6 Cargo Safety

Cargo safety is not impacted by DDO. Cargo elements and payloads are screened by appropriate Safety Review Panels (SRPs) to ensure and verify compliance with IDD ISS requirements as

documented in the payload unique ICD, and the MIP for any flight environment to include DDO. PIH will not be impacted by DDO nor will PIH cause an impact to Cargo Elements or payloads.

6.2.7 Operations and Maintenance Requirements and Specifications (OMRS) Document

DDO will not impact OMRS for the handling and testing of PIH. Cargo Elements and PIH post-flight processing assessments suggest that precautionary PLB surface sampling should be performed to ensure ground personnel will not be exposed to any unexpected residual contamination of DDO. Documentation of a non-repetitive sampling requirement is appropriately documented in a chit to provide optimal implementation flexibility.

6.2.8 Cargo Electro Magnetic Emission (EME)

There are no credible EME threats to PIH or payload hardware that could occur during DDO. The worst-case proximity of RV transmitter antennas (21 m) is outside the minimum allowable calculated distance (6.2 m) to the PLB that could cause RF interference [40].

6.3 OPO Assessments

The OPO was originally tasked to assess DDO for a November 2008 Soyuz 31P dock to DC-1 Nadir during STS-126/ULF2, but a manifest change alleviated the dual dock scenario. The concern was raised for the May 2009 Soyuz 19S dock to FGB Nadir during STS-127/2J/A, but a slip in the SSP launch alleviated that dual dock condition. SSP management directed that specific flight assessment efforts be expanded to a generic study for a Soyuz docking operation while the Orbiter was docked to ISS in February 2009. The scope was expanded further in July 2009 to include RVs as potential docking/undocking vehicles.

For the February 2010 Program Verification Review (PVR), the only RV environment available for assessment was the nominal trajectory. OPO's assessment of DDO at the February PVR was that the SRMS cameras and the OBSS sensors should be parked in a protected position, the PLB cameras should be pointed away from the plume field, and that the star tracker doors should be closed. It was recommended that post-flight testing of the thermal control blankets and cleaning of the trajectory control sensor be performed. For the February PVR, the windows testing had not yet been completed.

During the February PVR, board members pushed back on the lack of a dispersed nominal trajectory and an abort case. Consequently, a request was made to ISSP to provide such cases with updated analysis results be presented at a delta PVR. For the August 2010 PVR, OPO personnel provided results for the bounded nominal and abort cases. No new constraints were added based on this data. The Windows PRT reported that for the nominal and bounded nominal cases the pane strength test of lab created specimens showed no adverse degradation to the thermal pane strength as a result of the nominal and bounded nominal DDO environments. The assessment enveloped the ascent loads environment for future flights. Visibility for these environments was assessed by the JSC Crew Office, and no concerns were expressed. However, the testing that had been performed did not encompass the abort scenario. The PRT does know from previous analysis and experience that the cumulative effects of the solid rocket booster plume demonstrate that there is a threshold at which the fluence degrades the pane strength. It is unknown whether the prescribed abort scenario crosses that threshold. The PRT concluded for the abort scenario that the pane would perform its function as thermal protection, but the pane

could crack in atmospheric conditions. Therefore, the worst-case consequences could be glass debris impacting the Orbiter Orbital Maneuvering System (OMS) pod or rudder speed brake and reduced commander/pilot visibility through the windows. OPO's recommendation was to perform additional windows testing using the abort environment so that the risk could be quantified.

6.3.1 Windows

Impact testing was conducted at the JSC White Sands Test Facility (WSTF) to investigate the performance of Orbiter thermal panes when impacted by 5 and 10 µm glass beads, simulating the thruster plume debris environment from RV docking operations on ISS. Impact density, projectile sizes, and impact speeds were provided by the ISS Space Environments team [9, 10]. Glass test specimens were created based on the prescribed environments. Figure 6-1 and Figure 6-2 represent the WSTF specimens created to simulate the 5 and 10 µm particle impacts.

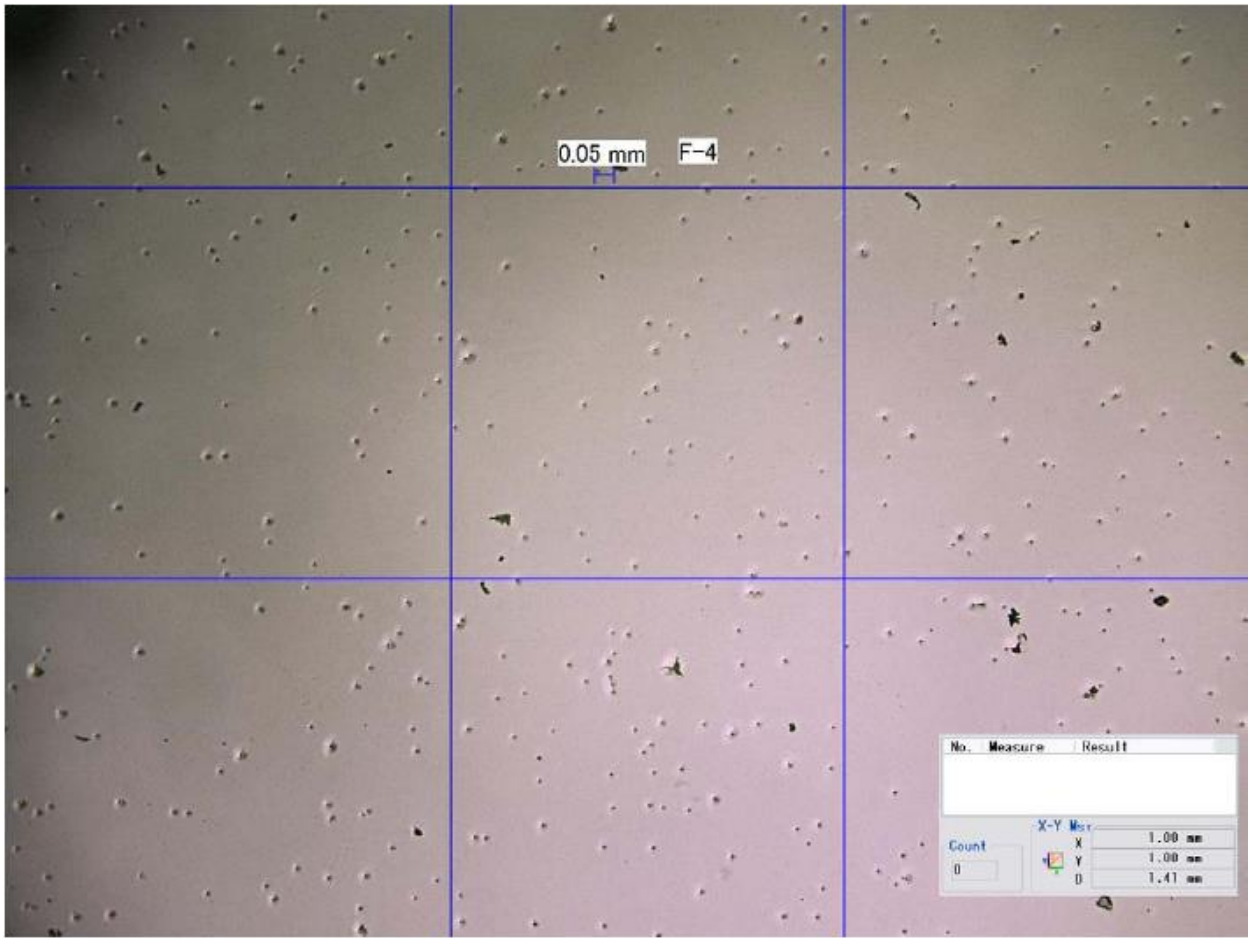

Figure 6-1. Typical distributed 5 µm impact test specimens.

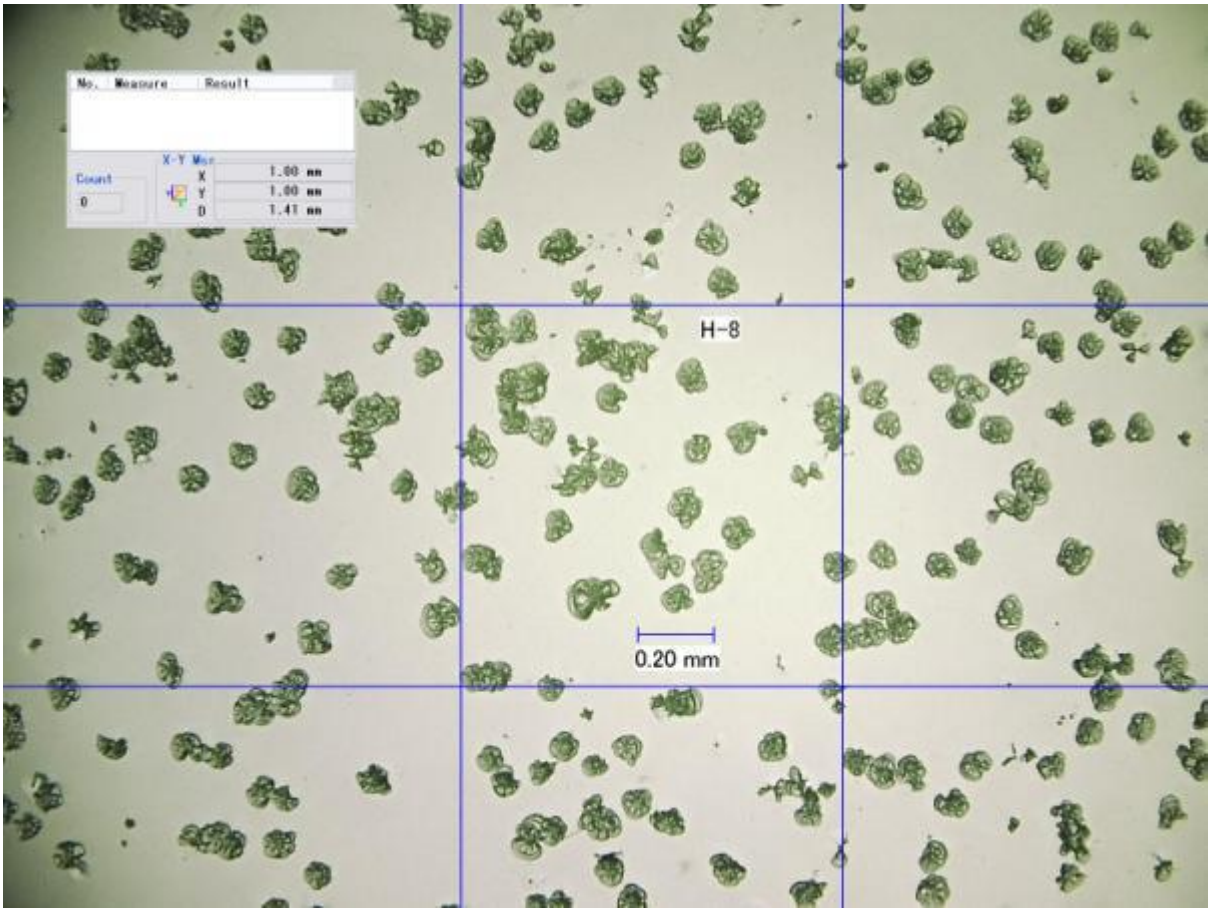

Figure 6-2. Typical distributed 10 µm impact test specimens.

Retired Orbiter thermal panes were used as targets. Testing revealed the possibility of minimal damage to the Orbiter thermal panes from such impacts. However, all damage was below the 0.0006 in (15.24 µm) allowable depth per MT0501-514, and below the allowable thermal pane damage limits for impact assessment of 0.0025 in (63.5 µm) for descent, indicating that single-flaw strength reduction is within the acceptable limits of thermal panes.

Additionally, subsequent strength testing of the cored out glass specimens was conducted at Southwest Research Institute to evaluate erosion-related strength reduction [46]. The residual strength test consisted of a ring-on-ring test setup as shown in Figure 6-3. Glass specimens' residual strength was recorded and evaluated, and a Weibull statistical assessment was performed by the Window Problem Resolution Team (WPRT) to quantify the effects and potential risks associated with the exposure of orbiter windows to the DDO environments.

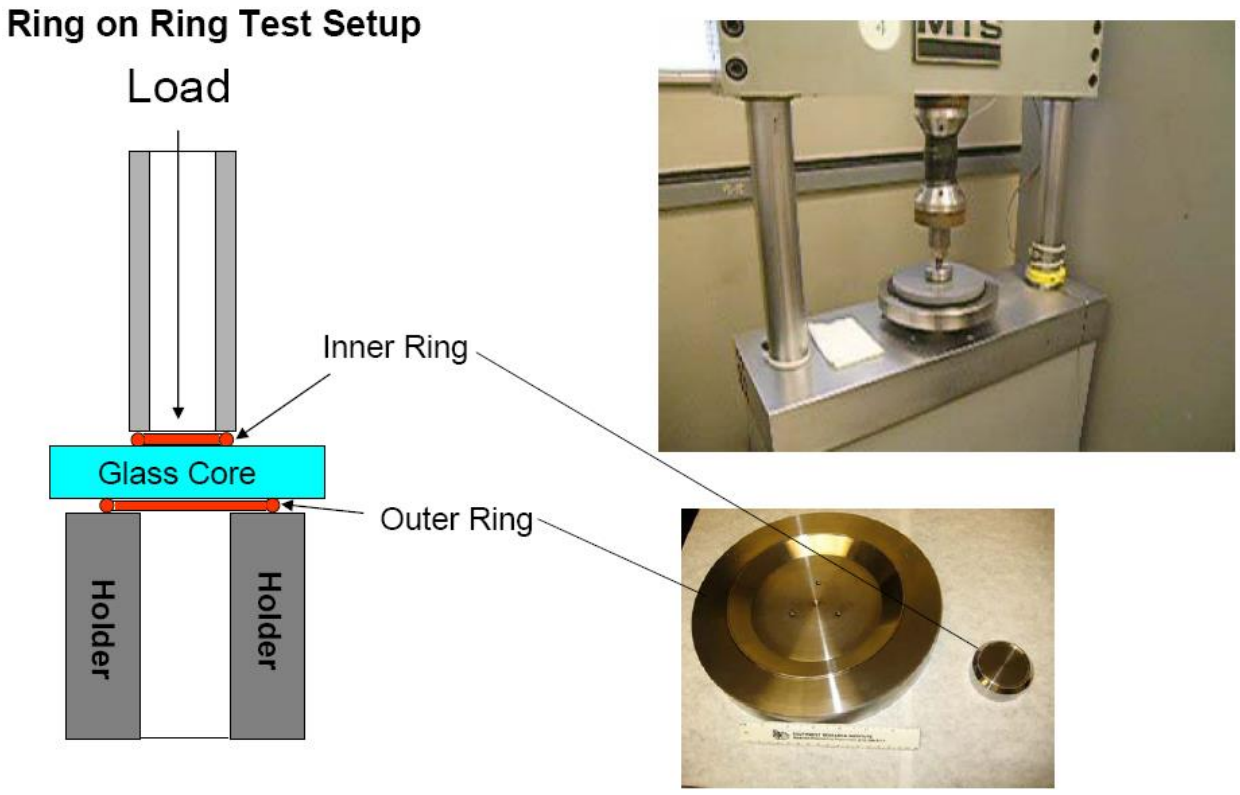

Figure 6-3. Residual strength ring on ring test setup.

The collected residual strength testing data were evaluated relative to the use of the glass ultimate strength values employed for Orbiter certification method. The data were converted to equivalent static fatigue strength values that match the static fatigue assumptions used for certification and then plotted in a probabilistic manner to determine minimum ultimate strength values for comparison to certification standards. For minimum probabilistic strength determination, a best fit Weibull distribution is used as a tool for determining 99.865 percent or "3-σ" Ftu strength values (see Figure 6-4). Using the combined 5 and 10 µm samples and the resulting 3-parameter Weibull curve fit allows for minimum strength predictions at the 3-σ level for comparison to certification values for descent (DES) (t = 10 seconds) and ascent (ASC) (t = 2 seconds) Ftu parameters. The minimum strength prediction at the 3-sigma level of the combined 5 and 10 µm samples (Ftu_{DDO}) was 6,233 psi. The current thermal fused silica glass Ftu_g values, which are based on a proof test derived maximum surface flaw depth of 0.0006 in (15.24 µm), are Ftu_g = 5,234 psi (ASC) and Ftu_g = 5,010 psi (DES).

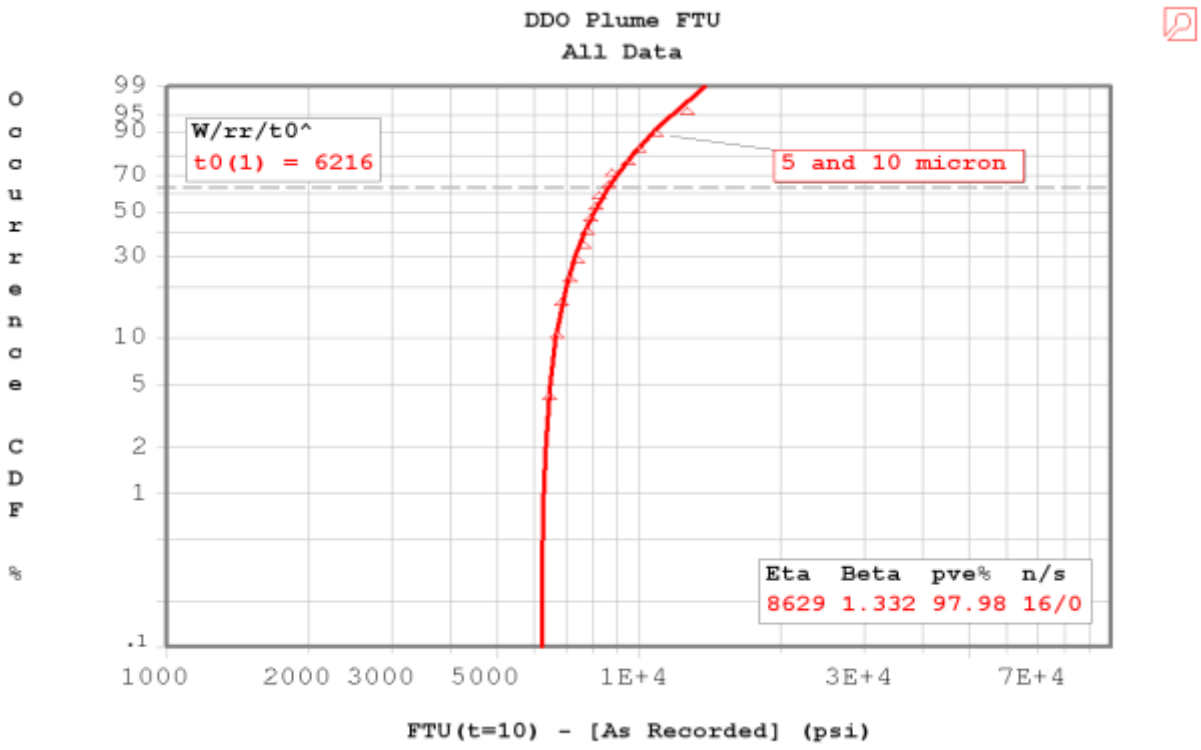

Figure 6-4. Three parameter Weibull distribution - combined 5 and 10 µm data.

Therefore, the assessment concluded that for the environments provided by ISS Space Environments team on November 24, 2009, and March 5, 2010 (nominal and bounded nominal docking/undocking operations), particle impingement does not adversely affect the ascent and descent certification thermal pane strength ($Ftu_{DDO} > Ftu_g$). The test specimens enveloped the environments using particle fluences ranging from 100 particles/cm^2 to approximately 7,400 particles/cm^2.

However, after testing was completed, the WPRT was requested to assess an additional plume environment simulating an MRM2 contingency abort. The total estimated particle fluence associated with this case, including approach and backout environments, is approximately 37,000 particles/cm^2. This particle fluence is outside the limitations of the test data, and the conclusions from the test cannot be extrapolated to these higher fluences. Therefore, the WPRT concluded the degree of window degradation (visual and strength) is unknown, and acceptance rationale cannot be generated. A subsequent WPRT request to disclose abort cases for other docking ports to determine/verify environments were within the bounds of the previously tested specimens, was dismissed. Testing or analysis has not been performed for any off-nominal docking events. Therefore, the extent of the hazing or degradation of the windows for these cases is unknown. Exposing the Orbiter windows to any off-nominal event may constitute an increase in risk.

6.3.2 ECLSS (Life Support and Active Thermal)

6.3.2.1 Radiators - Particle Impingement

For the analytical evaluation, the ISSP-provided environments were used and compared to requirements. The results showed that worst-case impingement affects 0.5 percent of radiator surface area. The vendor specifications allows for a loss of up to 10 percent of radiator surface area. The loss of the 0.5 percent would cause the Orbiter active thermal water usage to increase by 12 pound-force (lbm) for a 10-day mission, and the flash evaporator system would use more water to offset radiator system reduced thermal performance.

This assumes total loss of emissive properties in the affected area. However, this would not be considered a constraint to DDO, and mission and flow impacts would be negligible, producing an increased possibility of having to perform a standard repair.

6.3.3 Fuel Cell/Power Reactant Storage and Distribution (PRSD) Systems

The fuel cells and the PRSD subsystem were determined to not be affected by DDO.

6.3.4 Auxiliary Power Unit (APU)/Hydraulics/Water Spray Boiler Systems

The APU/hydraulics/water spray boiler subsystems were determined to not be affected by DDO.

6.3.5 Structures and Mechanisms/ODS

6.3.5.1 Payload Bay - Particle Impingement

The concern of the PLB exposure to RV particle impingement environment was degradation to line-of-sight surfaces, in particular surface coatings. The PLB structures and mechanisms/orbital docking systems surfaces were assessed based on impact tests on window and RCC targets. The conclusion is that the particle impingement will likely result in a superficial hazing of exposed coatings surfaces, with possible minor erosion, leaving surface pits on the same order of magnitude as the impactor size. There are no expected issues for metal or soft goods. Any coating degradation due to RV particle impingement environment in the midbody is not a constraint to DDO. If the environment results in degradation, then standard OMRS inspections will detect and appropriately disposition.

6.3.5.2 PLBD - Plume Force

The Orbiter PLBDs and radiators were assessed for plume pressure loads imparted by a Soyuz vehicle during approach to and separation from the various docking ports of the ISS ULF4 configuration. The maximum nominal and off-nominal plume pressures assessed were 0.0112 and 0.014 psf, respectively. For the doors, a bounding assessment case was constructed by assuming a maximum of 10 consecutive firings, 5 nominal and 5 off-nominal. The plume force was conservatively applied uniformly over the entire door. The resulting hinge moment of this case was determined to be 8,687 in-lb. The PLBDs and drive mechanism have been certified to 10,000 in-lb, so structural capability is maintained in the identified plume force environment. The capability of the radiators was originally demonstrated by acoustic testing at 148 decibels (dB) (31.5 psf peak) [20]. The test level of 31.5 psf is greater than the worst-case off-nominal plume force of 0.014 psf, so the radiators can be cleared by inspection.

The assessment results of the plume pressure forces on the Orbiter PLBDs and radiators imparted by the approach and separation of a Soyuz vehicle suggest that there are no related constraints to DDO. Further assessment would be required if the docking of a RV was considered at the MRM1 port.

6.3.5.3 ODS - Dock/Undock Loads

The data used for analysis were forcing functions originally provided by RSC-E to the LDT; reference Section 4.2. The peak loads and accelerations were determined at the Orbiter to PMA-2 interface. Results of the flight-specific analysis, which was performed for STS-130/20A, indicated no load exceedances at the interface. Therefore, there are no constraints to DDO.

6.3.6 Avionics, Communication, Tracking, and Instrumentation Systems

6.3.6.1 Ku-Band Deployed Assembly - Particle Impingement

The worst-case window test results were reviewed and applied to the Ku-band Deployed Assembly. The window testing showed micropits on the window glass. Likewise, micropitting could occur on the Ku-band Deployed Assembly surfaces, but the impact should be insignificant. Visual inspections are nominally done during OMRS evaluation. Any visual damage can be addressed by existing Fair Wear and Tear or material report-repair activities. Therefore, there are no constraints to using the Ku-band antenna systems if exposed to DDO particle impingement.

6.3.6.2 Ku-band Deployed Assembly - Plume Force

The Orbiter Ku-band antenna assembly was assessed for plume pressure loads imparted by a Soyuz vehicle during approach and separation to the various docking ports of the ISS ULF4 (STS-132), configuration. The maximum nominal and off-nominal plume pressures assessed were 0.0019 and 0.0088 psf, respectively. The capability of the Ku-band antenna was originally demonstrated by acoustic testing designed to represent the acoustic environment for the ascent flight phase [21]. The tests were conducted at 141 dB, which is approximately equivalent to 4.68 psf root mean square (rms). The test level of 4.68 psf is greater than the worst-case off-nominal plume force of 0.0088 psf, so the Ku-band antenna can be cleared by inspection.

The assessment results of the plume pressure forces on the Orbiter Ku-band antenna imparted by the approach and separation of a Soyuz vehicle suggest that there are no related constraints to DDO. Further assessment would be required if the docking of a RV was considered at the MRM1 port.

6.3.6.3 RF Interference Assessments

The impact of the RV transmitters on communication links was examined during proximity operations while the Orbiter is docked to the ISS and the RV is in the final approach for docking or already docked with the ISS. The Orbiter is docked to the PMA-2 of Node 2, and the RVs are docked to any of the following docking ports: DC-1, FGB Nadir, MRM2, or SM Aft. The closer a RV is to the Orbiter the greater the interference. Therefore, DC-1 Nadir envelopes all other docking ports: FGB Nadir, MRM2 and SM Aft.

The degradation of the Orbiter communication systems by the RV transmitters is determined by a three-step process, each with a different level of accuracy depending on the potential for link susceptibility.

First-order Analysis

In this analysis, several simplifying assumptions are made, where the goal is to determine whether the Orbiter receiver noise floor has been degraded by more than 0.5 dB due to interference. The simplifying assumptions include: (a) no structural blockage exists between transmitter and receiver, which implies that line-of-sight conditions are applicable; (b) the transmitter antenna and the receiver antenna are aligned boresight-to-boresight such that maximum antenna gain can be used in the analysis; and (c) the transmit spectrum roll-off versus frequency is conservative, which implies a steep decay with frequency that may not hold true in practice. If this first-order analysis does not result in an interference condition, then the Orbiter link in question is considered free of interference, and step 2 analysis (i.e., more precision) is not required.

Second-order Analysis

If the first-order analysis leads to the result that an inference condition exists, then a second-order analysis is employed where structure blockage is taken under consideration. The analysis is repeated with the addition that a nominal structural blockage exists, and its impact consists of reducing the potential interference by 20 dB. If the second-order analysis does not result in an interference condition (i.e., noise floor degradation greater than 0.5 dB), then the Orbiter link in question is considered free of interference, and step 3 analysis is not required.

Third-order Analysis

This analysis is rigorous in several respects: the separation distance between transmitter and receiver is more realistic, the antenna gains take into consideration any off-boresight roll-off, and structural blockage is included at the 20 dB rate. An interference condition is considered to exist whenever the Orbiter link margin reduced by the calculated noise floor degradation drops below a value of 10 dB.

Based on the most rigorous analysis, the potential for interference exists in the following two cases:

> RV tracking transmitter operating at 2860 megahertz (MHz) may cause interference with the Orbiter wireless video system (WVS) video receiver operating at 2410/2470 MHz if the crewman on EVA strays a distance greater than 28 m from the nearest S-band WVS antenna.
>
> RV tracking transmitter operating at 2860 MHz may cause interference with the Orbiter WVS telemetry receiver operating at 2410/2470 MHz if the crewman on EVA strays a distance greater than 65 m from the nearest S-band WVS antenna.

EVA activities should not take place during DDO. Otherwise, a constraint on EVA crewman movement would be necessary (i.e., EVA crewman must remain within a distance of 28 m of the Orbiter PLB, Starboard or Port sides to prevent the RV S-band Tracking Radar (2860 MHz) from interfering with either of the Orbiter S-band video or telemetry link). These links relay video and telemetry data from the EVA helmet-mounted camera back to an Orbiter-based S-band receiver.

This assessment concluded that with the exception of EVA activities, RF interference environment from RV to Orbiter is not a DDO constraint. Further details on analyses used to support these conclusions can be found in references [22] and [23].

6.3.6.4 Electromagnetic Interference (EMI)

The impact of the RV transmitters on the Orbiter subsystems was examined during proximity operations while the Orbiter is docked to the ISS and the RV is in the final approach for docking, or already docked with the ISS. The Orbiter is docked to the Node 2 PMA-2, and the RVs are docked or preparing to dock to any of the following docking ports: DC-1, FGB Nadir, MRM2, or SM Aft. The closer a RV is to the Orbiter, the greater the interference; thus, DC-1 Nadir envelopes all other docking ports: FGB Nadir, MRM2 and SM Aft.

The incident electromagnetic field (E-field) on the Orbiter that is produced by each RV transmitter radiation is compared to an allowable incident E-field limit for the Orbiter equipment as specified in NSTS 21000-IDD-ISS, ISS Interface Definition Document, or SSP-30237, Space Station Electromagnetic Emission and Susceptibility Requirements. NSTS 21000-IDD-ISS defines applicable E-field limits for pyros, avionics, windows, and crewmen. SSP-30237 defines applicable E-field limits for the OBSS components. The separation distance between a RV transmitter and an Orbiter equipment or subsystem below which the allowable limit is exceeded is then recorded as the boundary below which the Orbiter equipment or subsystem may become susceptible.

The following Orbiter equipment or subsystems have potential susceptibilities as indicated in Table 6-1, due to radiation from RV transmitters.

Table 6-1. Orbiter Systems Susceptible to Transmitters

Soyuz/Progress Vehicle Transmitters								
Potential SSO Victims	Voice	Telemetry	TV	Command	Tracking	KURS-A	Exceedances will occur at a separation distance less than or equal to R (meters)	Plausibility Statement
	Frequency [MHz]							
	121.75	166	463	922.76	2860	3294.2		
	E-field [V/m]	E-field [V/m]	E-field [V/m]	E-field [V/m]	E-field [V/m]	E-field [V/m]		
EMU	5.0	5.0					2.9 (voice) 3.5 (telemetry)	EVA events are unlikely when Soyuz or Progress Transmitters are still active.
RMS Avionics	7.1	7.1	8.0				2.0 (voice) 2.5 (telemetry) 3.0 (TV)	The Shuttle arm end effector electronics need to come within 3 meters of Soyuz/Progress antennas; Not likely to occur.
ORBITER Avionics and Windows	4	4	4	8.8		45.8	3.6 (voice) 4.4 (telemetry) 6.1 (television) 2.0 (command) 1.4 (KURS-A)	The Soyuz/Progress Antennas need to come within 6.2 meters of the Cargo Bay, or ODS pyros, during docking or undocking; this scenario is not likely to occur.
ODS Pyros					29.9	29.9	1.2 (tracking) 2.2 (KURS-A)	
Orbiter Payloads	4.0	4.0	4.0	8.1	20.0	20.0	3.6 (voice) 4.5 (telemetry) 6.2 (television) 2.2 (command) 1.7 (tracking) 3.3 (KURS-A)	
OBSS: LDRI, IDC Camera, and LCS Sensor						60.0	1.1 (KURS-A)	The Soyuz/Progress Antennas need to come within 1.1 meters of the OBSS, while the OBSS is performing its scan maneuvers. This scenario is not likely to occur.

Under all approach and departure scenarios that can be prescribed, the separation distance between the RV and the Orbiter should be at least 10 m. When this taken into consideration, all Orbiter potential susceptibilities drop off except for the extravehicular mobility unit (EMU) hardware that is carried by an EVA astronaut. To guarantee that the Orbiter equipment will not be impacted by the RV radiation, EVA activities should not take place during DDO. Otherwise, a constraint on EVA crewman would be necessary (i.e., EVA crewman must keep a distance of at least 3.5 m from RV very high frequency (VHF) transmitter antennas that are used for voice and telemetry services.)

EVA activities should not be scheduled while DDO are in progress. EMU hardware may malfunction due to RV radiation, causing interruption of audio, video, and telemetry between the EVA crewman and the Orbiter vehicle and by extension mission control personnel. This assessment concluded that with the exception of EVA activities, EMI environment from RV to Orbiter is not a DDO constraint.

6.3.7 Integrated GN&C

6.3.7.1 Star Trackers

Due to the optical properties of the star tracker there is a concern for contaminants entering the star tracker cavity and degrading the performance. The degraded performance, worst case, may make it difficult to track dim stars. Therefore, the recommendation is to close star tracker doors during DDO. If the constraint cannot be met, beside the mission impact, the star tracker may require removal for cleaning.

6.3.8 Passive Thermal

6.3.8.1 TCS Blankets/Liners - Payload Bay - Particle Impingement

The potential effects to the TCS blankets/liners were assessed based on results from window and RCC impact tests. The conclusion is the energy imparted by the 10 µm particles at 3 km/s would be absorbed by the soft goods resulting in no impact damage. Thus, particle impingement on the TCS blanket/liners from RV firings is not a constraint to DDO.

6.3.8.2 Thermal Control Blankets - Payload Bay - Contamination

The evaluation used a predicted worst-case DC-1 Nadir approach with available predicted impingement and contamination data. A worst-case particle fluence of ~10,000 particles/cm^2 would be expected in the PLB aft portion, for DC-1 Nadir approach, with expected particles sizes of 1 to 5 µm. Predicted worst-case initial contamination deposition for DC-1 Nadir is ~$2.93x10^{-7}$ g/cm^2. Predicted worst-case permanent contamination deposition for DC-1 Nadir is ~$2.51x10^{-8}$ g/cm^2. Estimate of deposition of nonvolatile salts for midbody area is ~0.046 grams. Based on predicted contamination data for DDO [9], and data from PIC experiments [1] significant contamination deposition are unlikely. However, optical properties of blanket covers may deteriorate.

The UDMH/nitrogen tetroxide (N_2O_4) propulsion systems on the RVs generate non-combustion product residues that contain toxic chemical species. The product residue is referred to as UDMH Fuel Oxidizer Reaction Products (UFORP). Of the multitude of chemical compounds in UFORP, NDMA is a major concern. One method of NDMA formation is by the partial oxidation of UDMH. A second method of formation is by the reaction of non-combustion products (UFORP) with water. Specifically, dimethylamine and nitrite can react with water to form NDMA. The dimethylamine and nitrite are bound in a nonvolatile salt and do not liberate in a vacuum. This was noted as a concern with deposition on space suits during EVA, resulting in possible ISS contamination. Upon entering the airlock, water could cause the NDMA formation. There is a possibility that these nonvolatile compounds/salts could contaminate TCS blankets, but not in the course of a single event. No Orbiter Hazard Reports exist to address this concern for hardware or processing personnel, although it appears this hazard has been evaluated for astronaut safety [30].

The potential contamination on TCS blankets/liner from a single DDO is not sufficient to constrain the operation. The TCS Hardware PRT recommends sampling after the first DDO to gather empirical data on contaminant quantity and chemical composition. All current data are based on test plates and model predictions. Sampling would provide valuable information for extrapolation of cumulative deposition of all nonvolatile contaminants should DDO become

commonplace. Sampling would consist of destructive testing of TCS blanket beta cloth cover, in area of highest particle fluence, to determine worst-case contaminant quantity and contaminant chemical composition. Possible Orbiter processing changes may be invoked if personnel hazards exist. Nondestructive testing of a TCS blanket is recommended, in area of highest particle fluence, to determine if optical properties are affected. There is no impact to processing unless optical properties are significantly degraded.

6.3.8.3 Thermal Control Blankets - Payload Bay - Plume Force

The evaluation was performed using predicted pressure data from worst-case DC-1 Nadir approach and available Orbiter delta pressure data from purge, vent, drain analysis. The predicted pressure for DC-1 Nadir for the PLB is 0.00474 psf. The plume pressure is below the delta pressure of approximately 8.064 psf, across the blankets from normal venting during ascent. Plume pressure was eliminated as a concern for TCS blankets and hardware. Blankets are inspected for damage per OMRS requirements during subsequent vehicle processing. RV plume forces on the TCS in the PLB are not a constraint to DDO.

6.3.9 GFE and Flight Crew Equipment

6.3.9.1 Cameras - Particle Impingement and Contamination

For evaluation purposes, the forward and aft bulkhead cameras and the SRMS elbow and wrist camera in the SRMS stowed position were used. One of the initial concerns was possible degradation of the thermal blankets, the outer surface of which is Teflon™ coated aluminized Mylar®. The SPIFEX report [2] indicates that a Teflon™ ring involved in the test was pristine after exposure. Therefore, the PRT concluded that the concern of degradation of the thermal blankets is a non-problem. The illuminator electronics box and the light emitting diode (LED) box housings plus the Orbiter RMS sideview camera (RSC) housing all are aluminum painted with white paint (Aeroglaze A276). The PRT concluded that the plume contamination and residue will not cause any damage to these painted surfaces other than possibly to require cleaning post mission. The top surface of the camera is a reflective, silver tape with a Teflon™ outer surface without any thermal blanket. Using the same rationale as for the thermal blanket surfaces, the PRT concluded that the concern of degradation of the reflective surfaces is a non-problem. The exposed front element of the lens of the color television camera (CTVC) and intensified (black and white) television camera (ITVC) cameras (located on the forward and aft bulkheads, the SRMS elbow and wrist locations, and OBSS sensor package (SP)-1) is a high-quality optical glass with a magnesium fluoride antireflective coating. The PRT concluded that this is the part of the CCTV hardware that is most sensitive to damage. It can be pitted by the plume particles and degraded by the contaminant residue. The PRT concluded that the damage cannot be accurately quantified and therefore the camera lenses must be protected to the extent possible. They concluded that the forward and aft bulkhead cameras (A, B, C, and D) and the SRMS elbow camera must be pointed away from the plume flow to avoid direct particle contact. The PRT further concluded that the SRMS wrist camera and the RSC should be protected from direct contact by the plume particles. The protective cover over the illuminator LEDs is Lexan. The PRT concluded that the plume material will not damage the Lexan. The effect of the contamination on the illuminator front face will be limited to a possible coating of plume residue, which can be cleaned post mission. This residue would result in a reduced illumination capability for the rest of the mission. The front cover of the RSC pressurized housing is Pyrex®. The PRT

concluded that the plume material will not damage the Pyrex®. The effect of the contamination on the RSC front face will be limited to a possible coating of plume residue, which can be cleaned post mission. This residue would result in degraded, blurred video for the rest of the mission. The front cover of the keel camera pressurized housing is Pyrex®. The PRT concluded that the plume material will not damage the Pyrex®. It concluded that the keel camera (if manifested) cannot be protected if the multi-purpose logistics module (MPLM) has been removed from the PLB and, therefore, may sustain damage to the front lens surface. The damage will be limited to a possible coating of plume residue, which can be cleaned post mission. This residue would result in degraded, blurred video for the rest of the mission. The PRT concluded that the pan tilt unit (PTU) pan and tilt moveable rotating surfaces will not be degraded due to the protective covering provided by the thermal blankets. The bearings of both the pan and tilt mechanisms are contained within a protective housing where the plume material cannot penetrate. Minimal contaminant will be able to be deposited on the moving surfaces and is not expected to result in hampering the PTU motion.

Given the results, the PRT consider the following constraints to DDO activities:

1. The forward and aft bulkhead cameras, and the SRMS elbow camera must be pointed away from the plume flow.
2. The SRMS wrist and sideview cameras should be protected from direct contact by the plume particles.

If these constraints are not met, then the mission impacts would be degraded video caused by unwanted glints from pits on the wrist camera lens, and/or blurring from the residue. The flow impacts would be that all lenses would have to be examined and inspected to determine if cleaning or replacement will be required.

6.3.9.2 OBSS Sensors - Contamination

The OBSS sensors were evaluated, assuming the stowed position in the Orbiter PLB with the manipulator pedestal mounts (MPMs) rolled out. For the SP-1 ITVC/laser dynamic range imager (LDRI) sensors, it has been determined that they are not hermetically sealed. The biggest risk is getting internal contamination onto the LDRI laser diode. Any condensation/contamination on this surface will result in the diode failing upon laser activation and failing the LDRI. In all proximity operations, some level of contamination was noted with the DC-1 Nadir being the worst. The subsequent off-gassing of contaminated sensor surfaces and the surrounding PLB surfaces may be the principal damage mechanism. The concern of secondary emission from nearby surfaces was raised. The ISS Space Environments team discounted this potential, but the OBSS team still felt that there is potential for contamination and is requesting to position SP1 so that any nearby objects in the LDRI field of view should be out of plume line of sight. Keeping the LDRI in Mode 2 will keep the internal components warm and will aide in protecting from internal contamination/condensation. Mode 1 will not activate the camera components and will not protect from condensation. The LDRI has heater power (equivalent to Mode 1) when in the OBSS stowed position, and the sensor is typically in Mode 2 when the OBSS is in a MPLM or Node viewing position.

For SP-2, laser camera head (LCH), the predicted worst-case contamination rate at the DC-1 location will be 1/3 of the rate experienced during the PIC experiment (6.4×10^{-8} gm/cm^2 vs

$19.3x10^{-8}$ gm/cm^2). This level of contamination had no apparent performance impact on the SRMS wrist camera. Given the levels of contamination predicted, impact on performance due to contamination is unlikely. However, the effect of this contamination at 1500 nanometers (nm) (wavelength of the laser camera system (LCS) laser) on the coherence and/or geometry of the laser beam is unclear and cannot be assessed without testing. To address the risk contamination on the LCH window during a flight, the LCS developer has developed and validated an analytical assessment procedure to identify the presence of contamination that might impact its performance. This procedure is executed each flight during the analysis of the LCS checkout scans captured on flight day (FD) 2 and during the late inspection checkout. Should contamination be identified during the analysis of the scans, there exists a special "Contamination Risk Mitigation" database included as part of the flight load, which can provide a certain degree of compensation to offset the laser attenuation effects of contamination.

Due to the results of the evaluation, it was recommended that the OBSS be placed out of the line of sight of plume. If the constraint is not met, then the mission impacts would include requiring cooling off phases during inspection and potential failure of LDRI. Placing the sensor in Modes 3-6 may mitigate risk. The post-mission impacts to the hardware and to the ground operations would be to repair the silver tape and replace the laser diode.

6.3.9.3 OBSS Sensors - Particle Impingement

The OBSS sensors were evaluated, assuming the stowed position in the Orbiter PLB with the MPMs rolled out. In all port locations, SP-1 does receive particle impacts to some degree. The most impacted surface of SP-1 is the Orbiter zenith/ISS aft during DC-1 Nadir and SM Aft operations. This will result in damage to the thermal silver tape on the outside of the sensor requiring repair to maintain thermal properties. In the OBSS stowed position, the ITVC/LDRI lenses are pointing in the Orbiter aft/ISS nadir direction. This is the surface of the greatest concern to protect the optics. The ITVC/LDRI optics are not to be in the line of sight of the source of particle fluence. For the DC-1 Nadir and FGB Nadir operations, this sensor receives particle impacts on the lens, so moving the OBSS to a more protected location or not allowing RV operations at these ports is recommended.

For SP-2, the lens surface of the LCH and Integrated sensor inspection system (ISIS) digital camera (IDC) is the Orbiter zenith/ISS aft surface, which in all vehicle operations is the most impacted surface. DC-1 Nadir and SM Aft operations are drastically worse than FGB Nadir and MRM2. Based on the DTO-829 test results of a fused silica lens, which LCH has, similar results are expected. The LCS performance may be impacted for the duration of the mission by window contamination or pitting. Assuming the LCS experiences a similar 2 percent pitting effect as the SRMS camera during the PIC test, the effect of pitting on performance of the LCS should be negligible (i.e., resulting in a ~2 percent drop in intensity due to scattering effects).

Due to the results of the evaluation, it was recommended that the OBSS be placed out of the line of sight of plume. If the constraint is not met, then the mission impact would include requiring cooling off phases during inspection, and potential failure of LDRI. The post-mission impacts to the hardware and to the ground operations would be to repair the silver tape.

6.3.9.4 Trajectory Control Sensor - Particle Impingement and Contamination

The trajectory control sensor shutter is constructed of an aluminum alloy (6061-T651) with a clear anodized coating. The shutter operates on a sliding track with a screw type mechanism and a gap of 0.41 mm during movement. The rest of the sensor area is protected by a thermal blanket. In the worst case, the projected contamination levels are not expected to cause concern for the shutter operations or the thermal blanket. The shutter is closed during times when the Orbiter is docked, thus preventing the buildup of contaminants on internal sensor optics or mechanical interfaces. Thermal degradation to the thermal blanket would have a minor impact to the thermal properties of the trajectory control sensor unit.

Based on the evaluation, trajectory control sensor does not have any constraints to DDO. Therefore, there are no mission impacts. However, there would be a flow impact in that a cleaning of the trajectory control sensor unit after the mission is recommended. This would eliminate the possibility of cumulative contamination buildup. The cleaning of the sensor surfaces could be performed still mounted in the vehicle.

6.3.10 SRMS/OBSS

Both the SRMS and OBSS were assessed for contamination issues, and there were no issues identified. The thermal effect due to the thruster firings was negligible, and the concern for the multi-layer insulation (MLI) blanket was not an issue. Therefore, no constraints were placed on DDO with any mission or flow impacts identified.

The SRMS was evaluated at pre-cradle, SRMS/OBSS at undock, and SRMS/OBSS contingency DDO positions. The data used was the forcing functions provided by RSC-E, and only docked loads were evaluated since undock loads are bounded by the docked loads. No issues were found, so no constraints were levied upon DDO. No mission or flow impacts were identified.

The pressure summary provided by the LDT, reference Section 4.2, was used for the evaluation. Due to the low forces from the data, it was deemed that the plume forces would have no effect on RMS loads.

6.3.11 WLE Subsystem/TPS

6.3.11.1 WLE Subsystem - Particle Impingement

Particle impingement generated from any of the various RVs approaching the ISS has the potential of ejecting droplets of uncombusted or partially combusted fuels along with noncombustible impurities in the form of particles in the discharge of thruster firings. Given the velocity imparted to these uncombusted particles, an assessment for potential effects to exposed Orbiter components is required. The WLE RCC is one such external structural component that would be exposed to potential impact from thruster firings.

The areas of the Orbiter WLE RCC exposed to the thruster firings presented concern over what type of damage to the SiC coating would occur, if any, due to a single particle impingement, and the type of erosion that would occur to the SiC coating due to multiple particle impacts.

Analytical work was performed to determine the effects of particle impingement [19, 9] on the RCC. The location of the docked Orbiter and its view factor to thruster particle impingement from RVs is centered on four docking locations of the ISS. These locations are

a. FGB Nadir

b. DC-1 Nadir

c. MRM2

d. SM Aft

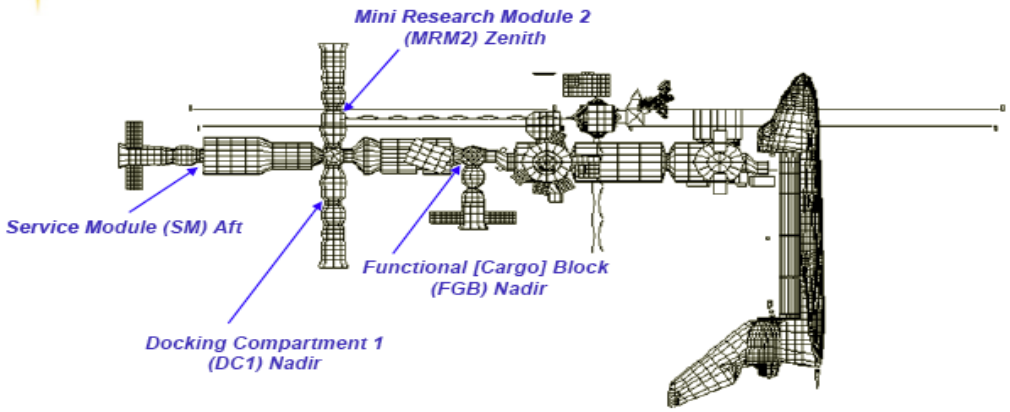

Figure 6-5. ISS and docked Orbiter with visiting RVs.

The ISS Space Environments team's analytical assessment developed a plot of the particle impingement for space operations of the different docking port locations with the expected particle fluence to the Orbiter docked position. Results show up to "4.64 million particles per cm^2 are possible on some parts of the Orbiter RCC per event" [19]. The expected particle distribution and diameter for three of the docking ports are shown graphically in Figure 6-6 [19].

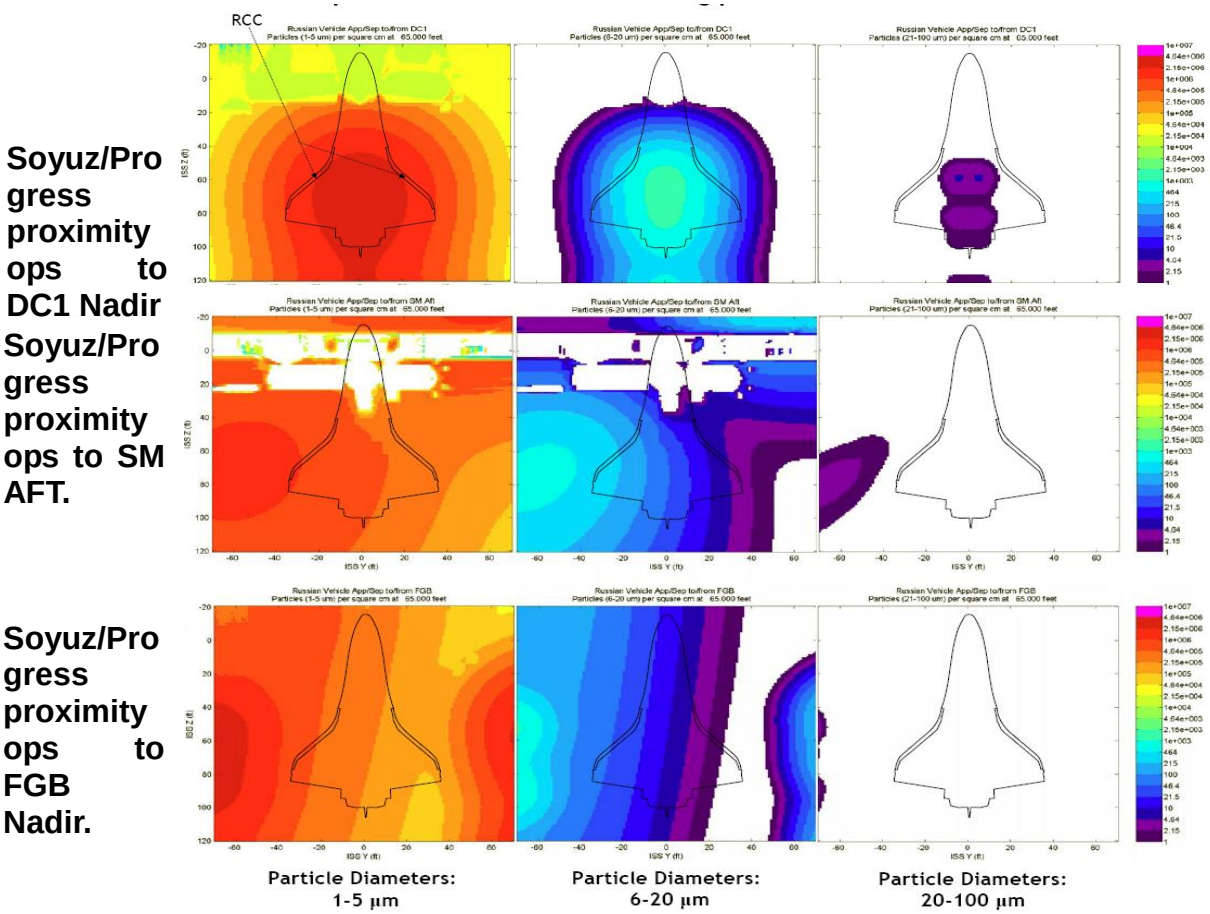

Figure 6-6. Particle fluence scatter on the Orbiter for three docking locations and particle diameters.

Figure 6-7 through Figure 6-10 show the Orbiter only with examples of particle fluence results for all four docking ports [9].

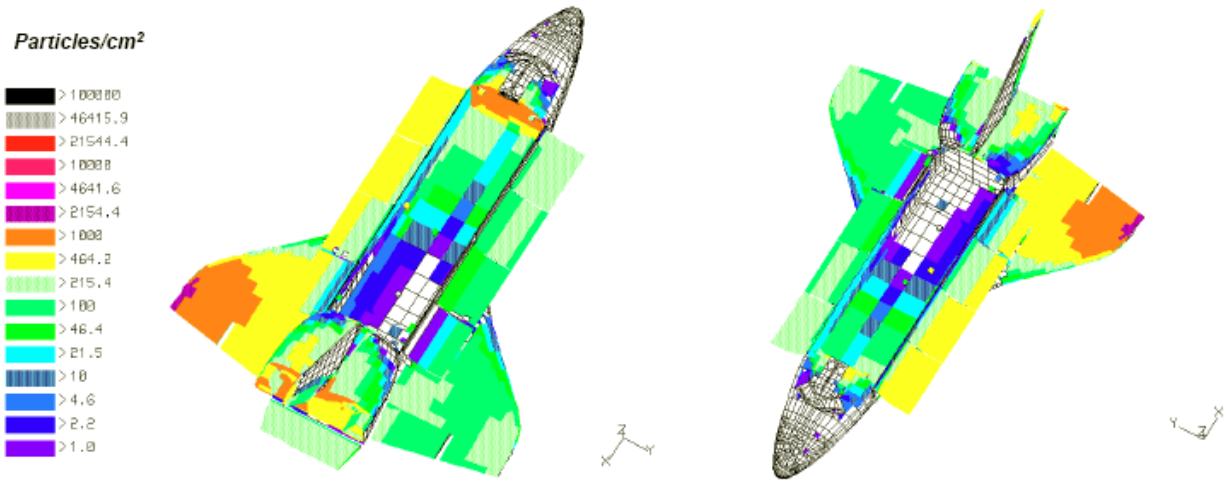

Figure 6-7. Orbiter only shown with example of particle fluence for FGB Nadir approach.

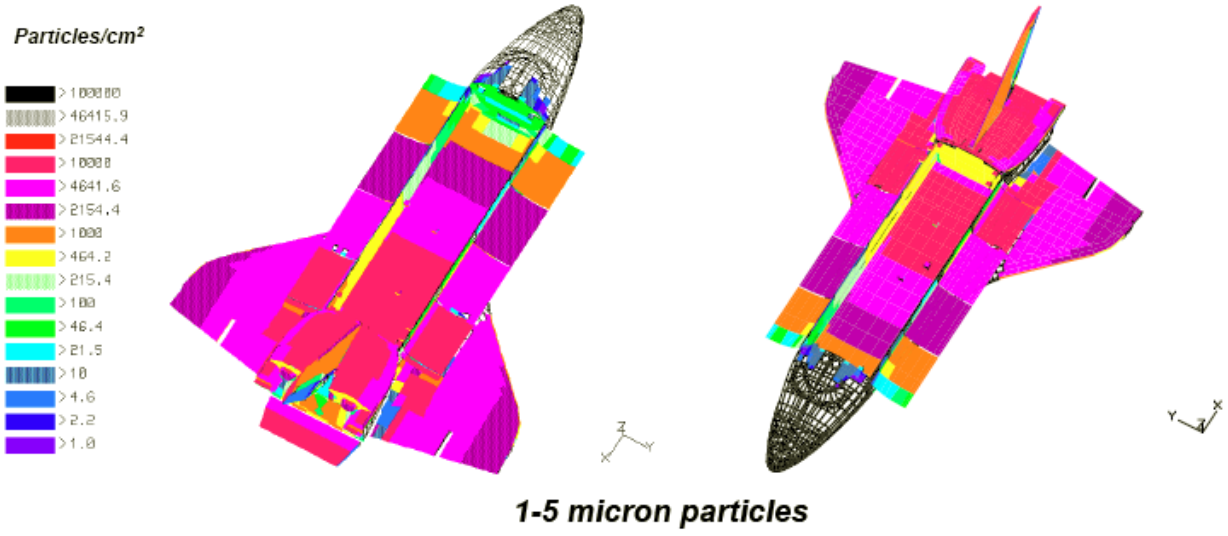

Figure 6-8. Orbiter only shown with example of particle fluence for DC-1 Nadir approach.

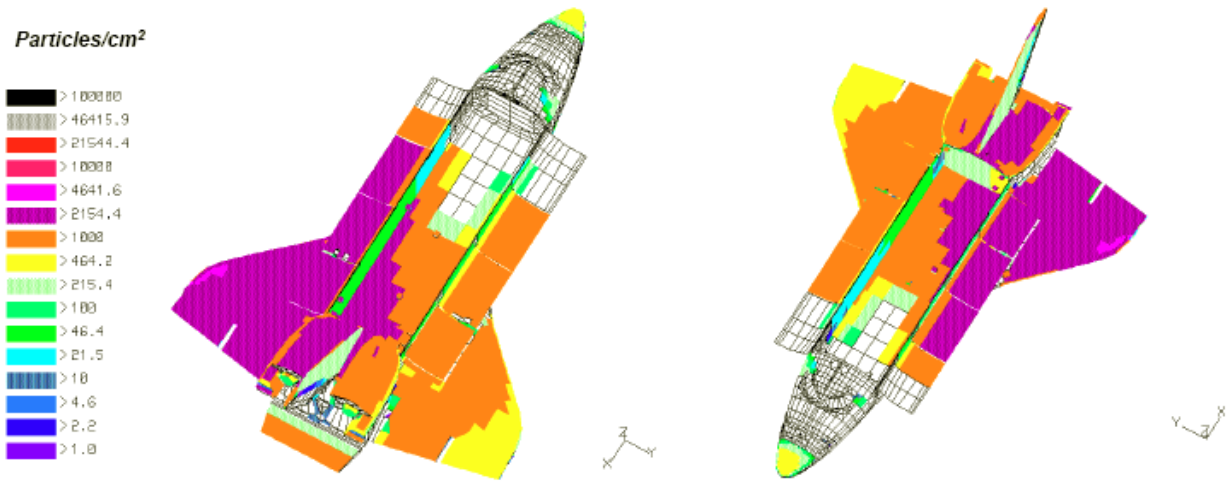

Figure 6-9. Orbiter only shown with example of particle fluence for SM Aft approach.

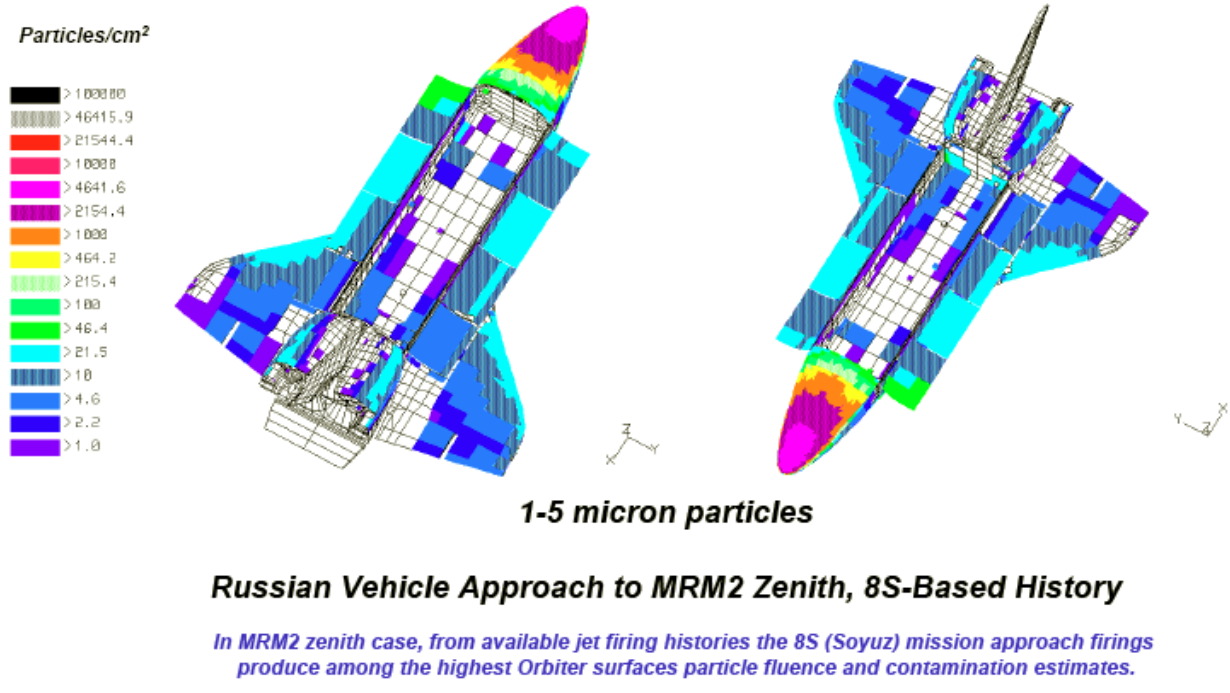

Figure 6-10. Orbiter only shown with example of particle fluence for MRM2 Zenith approach.

Various other analytical studies and testing contributed to an understanding and bounding of the DDO study. Numerous RCC impact testing conditions and scenarios were accomplished as a

post STS-107 Columbia accident effort to further understand material characteristics and capabilities under adverse conditions. While two primary tests conducted were SSP external tank ice and foam impacts, additional tests focused more on smaller MMOD type impact damages. The MMOD type of impacts are more in-line with the type of impingement that thruster particles would impose on exposed components of the Orbiter. The data obtained from MMOD type impact studies set a basis for comparison for the thruster particle impingement concerns.

SSP management directed resources to study the level of MMOD impact damage tolerated for reentry environments. Different sizes of hypervelocity impact damages generated by a range of spherical projectiles, ranging from 0.4 to 1.0 mm in diameter, on numerous RCC specimens have been characterized [25]. The hypervelocity impact damage and corresponding projectile sizes are given in Table 6-1. A photo of one test specimen to convey the type of coating damage incurred prior to Arc Jet Testing is shown in Figure 6-11 [25].

Table 6-2. Hypervelocity impact results to WLE RCC specimens prior to Arc jet testing [25].

Facility ID#	Customer ID #	Projectile Diameter (mm)	Projectile Velocity (km/s)	OML Damage (Exposed Substrate)	IML Damage (Exposed Substrate)	Crater Depth from (OML/IML)
2233	A307-1	0.4	7.05	0.028 x 0.019 in.	None	0.027 in. / NA
2234	A307-4	0.6	4.54	0.089 x 0.099 in.	None	0.036 in. / NA
2235	A307-5	0.6	5.64	0.100 in. diameter	Small crack but no exposed coating	0.040 in. / NA
2236	A307-6	0.6	6.8	0.084 x 0.091 in.	None	0.041 in. / NA
2237	A307-7	0.6	6.67	0.140 x 0.130 in.	0.17 in. diameter	0.046 in. / 0.030 in.
2238	A308-9	0.8	7.07	0.250 x 0.255 in.	0.280 x 0.256 in.	0.070 in. / 0.034 in.
2239	A308-11	1.0	6.43	0.335 x 0.268 in.	0.426 x 0.440 in.	0.090 in. / 0.073 in.

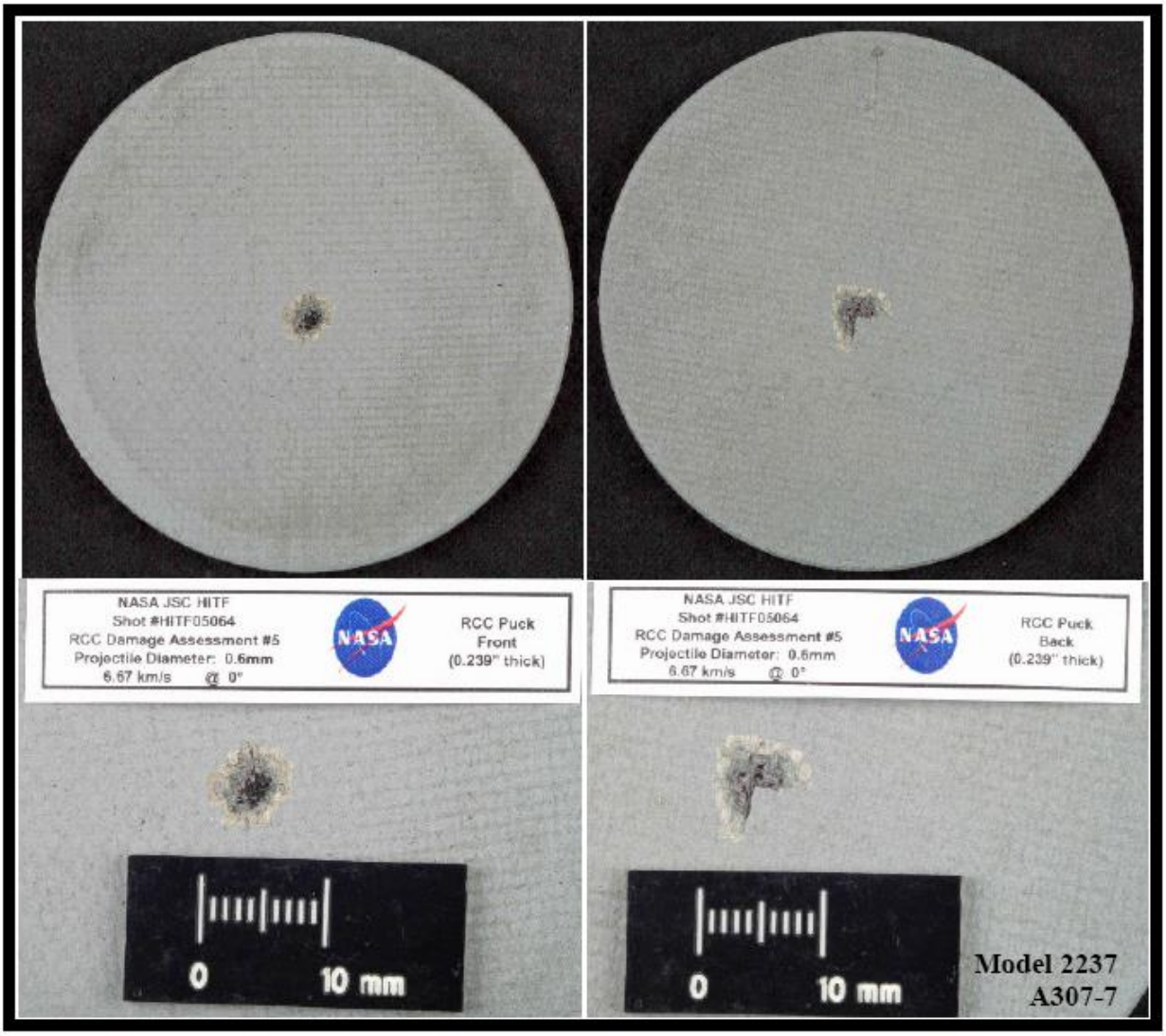

Front side (left photo)-projectile impact
Backside (right photo) – resultant damage to back surface from projectile impact

Figure 6-11. Representative WLE RCC surface damage from hypervelocity impact [25].

The various specimens were then subjected to conditions that represent the temperature and pressure of the WLE RCC during reentry. The duration of the test was designed to extend through the peak heating cycle critical for a successful reentry. The results of the Arc Jet test for each of the impact damaged specimens exposed to flight environment testing are listed in Table 6-3 [25].

Table 6-3. Arc jet test results summary of hypervelocity impacted WLE RCC specimens [25].

Model #	Run #	Damage Configuration	Test Conditions	Result
2233	2-2880-5	OML: 0.028 x 0.019 in. IML: None	**2960°F/141 psf**	Survived with no visible breach. **Test Duration: 1000 sec.**
2234	2-2880-5	OML: 0.089 x 0.099 in. IML: None	**2800°F/104 psf**	Survived with no visible breach. **Test Duration: 900 sec.**
2235	2-2881-5	OML: 0.100 in. diameter IML: Small crack but no exposed coating	**2800°F/104 psf**	Survived with no visible breach. **Test Duration: 900 sec.**
2237	2-2881-5	OML: 0.140 x 0.130 in. IML: 0.17 in. diameter	**2800°F/104 psf**	Survived with no visible breach. **Test Duration: 900 sec.**
2238	2-2882-5	OML: 0.250 x 0.255 in. IML: 0.280 x 0.256 in.	**2700°F/98 psf**	No surface activity until 811 sec., when hot spot develops. Hole develops at 830 sec., but hole growth arrested shortly by glass flow. **Test Duration: 900 sec.** **IML Damage: 0.134 in. dia. hole**
2239	2-2882-5	OML: 0.335 x 0.268 in. IML: 0.426 x 0.440 in.	**2500°F/104 psf**	No surface activity until 374 sec., when hot spot develops. Hole develops at 422 sec. Hole grows slowly for remaining of test duration **Test Duration: 900 sec.** **IML Damage: 0.343 in. dia. hole**
2236	2-2883-5	OML: 0.084 x 0.091 in. IML: None	**2960°F/141 psf**	Survived with no visible breach. **Test Duration: 900 sec.**

The resultant Arc Jet testing defined various levels of survivability with respect to the hypervelocity impact damage. Table 6-4 provides a summary of the Arc Jet test results for the MMOD impact test. With respect to the data in Table 6-3 and Table 6-4, specimen no. 2236 was identified as the test that defined the largest damage size for the "worse case" heating zone/location for all the WLE panels that did not result in a visible breach through the inner mold line (IML) (i.e., no through hole). This "worse case" heating location aligns with RCC panel 9 zone 3. The pre-Arc Jet test damage size for that test case, 0.084 x 0.091 x 0.041 in depth, was adopted as the largest acceptable RCC damage from a single particle impact [19, 25].

Table 6-4. WLE RCC Arc jet test summary for MMOD impacts.

TEST #	Facility #	Customer #	Projectile Dia. (mm)	OML Damage (in.)	Crater Depth (OML/IML)*	Test Condition	Results
1	2233	A307-1	0.4	0.028 x 0.019	0.027 in./NA	2960F/141psf	Pass
2	2234	A307-4	0.6	0.089 x 0.099	0.036 in./NA	2800F/104psf	Pass
3	2235	A307-5	0.6	0.100	0.040 in./NA	2800F/104psf	Pass
4	2236	A307-6	0.6	0.084 x 0.091	0.041 in./NA	2960F/141psf	Pass
5	2237	A307-7	0.6	0.140 x	0.046in./0.030 in.	2800F/104psf	Pass

				0.130			
6	2238	A308-9	0.8	0.250 x 0.255	0.070 in./0.034 in.	2700F/98psf	Fail @ 830 sec.
7	2239	A308-11	1.0	0.335 x 0.268	0.090 in./0.073 in.	2500F/104psf	Fail @ 420 sec.
8	2305	A306-1	0.7	0.185 x 0.161	0.061 in./0.040 in.	2800F/100psf	Fail
9	2306	A306-4	0.9	0.295 x 0.335	0.092 in./0.062 in.	2700F/100psf	Fail
10	2307	A306-3	0.8	0.217 x 0.228	0.068 in./0.038 in.	2200F/81psf	Pass
11	2308	A306-2	0.7	0.185 x 0.161	0.056 in./0.021 in.	2700F/100psf	Pass
12	2314	A307-10	0.8	0.236 x 0.220	0.072 in./0.030 in.	2600F/100psf	Fail @ 759 sec.
13	2315	A307-11	0.8	0.197x 0.307	0.068 in./0.027 in.	2500F/100psf	Fail @ 717 sec.
14	2316	A307-13	0.9	0.362 x 0.362	0.069 in./0.050 in.	2200F/88psf	Fail @ 600 sec.

*Crater depth measured from outer silicon carbide surface

The Arc Jet test results were correlated with the temperature zones of the WLE RCC panels (reference Figure 6-8) to establish a maximum allowable surface damage/defect size acceptable for each zone. Table 6-5, generated based on the Arc Jet testing results, is the basis for acceptability criteria that is used for on-orbit imagery inspections for ascent (e.g., external tank ice and foam, solid rocket booster TPS, and Orbiter tile gap fillers) and MMOD impact damage [25, 26].

The follow-on work related to the DDO study identified the potential thruster plume particle sizes to be in the range of 1 to 100 μm. Testing of particle impacts using projectiles that would mimic the expected thruster plume particle of 1 to 100 μm range was conducted at Rice University on RCC samples. The velocities for those particle impact tests were determined to be between 1 to 3 km/s [19].

Comparison of projectile sizes and velocities used for the MMOD tests versus the Thruster Particle test indicate a difference in the amount of impact energy that the two types present. The largest thruster particle projectile size of 100 μm (0.0001 m) [19] with velocities 1 to 3 km/s tested at Rice University, versus the smallest size projectile size tested for MMOD 400 mm (0.4 m) at 4.54 to 7.07 km/s [25], indicates that potential damage from thruster plume impingement is significantly less than representative test for MMOD.

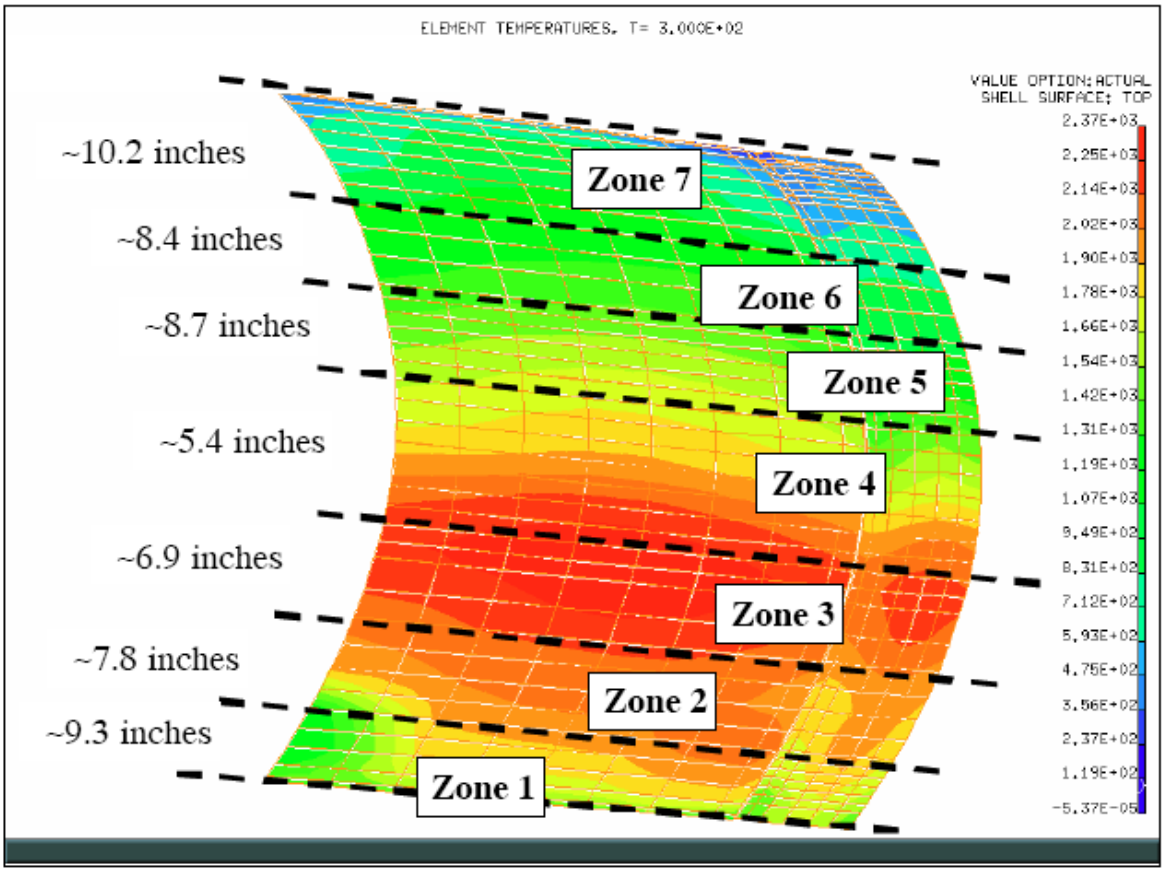

Figure 6-12. WLE surface inspection zones (reference April 6, 2006 PRCB S063202BR2, RCC Damage Criteria for Inspection and MMOD Risk Assessment [16]) (Don Curry and Alvaro Rodriguez), (RCC Critical Impact Damage Map [26]) (Don Curry) [16] and [26].

Table 6-5. WLE coating loss criteria [16] and [26].

ISS Hvy Wt Fwd CG EOM Entry Trajectory

Panel(s)	1-4	5	6	7	8	9	10	11	12	13	14	15	16	17	18	19-22
Zone 7	1.0	1.0	1.0	1.0	1.0	1.0	1.0	1.0	1.0	1.0	1.0	1.0	1.0	1.0	1.0	1.0
Zone 6	1.0	1.0	1.0	1.0	1.0	1.0	1.0	1.0	1.0	1.0	1.0	1.0	1.0	1.0	1.0	1.0
Zone 5	0.21	0.21	0.21	0.21	0.16	0.16	0.21	0.21	0.21	0.21	0.21	0.21	0.21	0.21	0.21	0.21
Zone 4	0.21	0.21	0.21	0.16	0.13	0.08	0.16	0.16	0.16	0.16	0.16	0.16	0.16	0.16	0.16	0.16
Zone 3	0.21	0.21	0.21	0.16	0.08	0.08	0.13	0.16	0.16	0.16	0.16	0.16	0.16	0.16	0.16	0.16
Zone 2	0.21	0.21	0.21	0.16	0.08	0.08	0.16	0.16	0.16	0.21	0.21	0.21	0.21	0.21	0.21	0.21
Zone 1	0.21	0.21	0.21	0.16	0.16	0.16	0.16	0.16	0.21	0.21	0.21	0.21	0.21	0.21	0.21	0.21

Exposed Substrate Diameter (in.)

- **1.0" hole is acceptable in Zones 6-7**

Hypervelocity Impact Test and SPHINX analysis were conducted to characterize thruster plume particle impact damage to WLE RCC. The objective of the hypervelocity test was to characterize RCC SiC coating damage due to a single particle impact. SPHINX analysis was performed using data from the hypervelocity test to characterize surface erosion of SiC due to multiple particle impacts [19].

The hypervelocity impact test for single particle impact involved the use of 5 to 100 μm diameter glass beads accelerated to 1 to 3 km/s then impacting WLE RCC samples at normal impingement angles. The glass beads, 2.44 g/cm^3, were chosen because of the similarity in density with thruster plume conditions, 2.33 g/cm^3, (MMH density of 0.88 g/cm^{3}and NTO density of 1.45 g/cm^3). Five 1.5 x 1.0 in RCC sample plates, labeled 1-A through 1-E, were subjected to glass beads varying in size from 5 to 100 μm accelerated to varying speeds of 1 to 3 km/s.

The SPHINX analysis was performed using results from the hypervelocity impact test. SPHINX analysis' success in the duplication of measurements from the impact test allowed for the characterization of other damages resulting from thruster plume particle impacts. The following identifies the range of particle characterizations:

a. 5 μm diameter particle, normal impact of NTO to SiC at 2.9 km/s

b. 20 μm diameter particle, normal impact of NTO to SiC at 2.2 km/s

c. 100 μm diameter particle, normal impact of NTO to SiC at 1.0 km/s

The particle fluence of the RV docking was calculated for proximity to Orbiter WLE RCC. A conservative representation of available RV thruster firing data were used to simulate only proximity operations. This conservatism was due to the limited number of post-flight thruster firing histories available, and the available data does not account for attitude variations or lateral transitions.

The SPHINX characterizations with the calculated particle fluence of thruster plumes during RV proximity operations were used to linearly scale RCC impact damage. To correlate SPHINX results with ground test measurements, a SiC yield strength of 90,000 psi was used. These results were then assessed using the following two methods [19]:

a. Method 1: ***Average*** erosion depth estimate based on crater damage volume for single particles scaled linearly by particle fluence for a single event.

b. Method 2: ***Maximum*** erosion depth estimate based on total damage surface area and individual crater depths.

Damage characterization for impact testing was conservative. All impacts were assumed to have normal impingement due to the fact that normal impingement would lead to greater impact damage results. All thruster plume particles were assumed to be traveling at the limiting velocity for RV RCS thrusters. Damage modeled was taken for the largest particle in each size class and damage estimate was taken for the highest fluence point on the RCC for worst docking port.

In addition to particle impact damage, unreacted propellant contamination of RCC due to Soyuz thruster plume impingement was identified. Material compatibility assessment for this effort was based on the similarity of the RV propellants to those used on the Orbiter. A RCC material compatibility test was performed by Vought Corporation during the development of the LESS RCC hardware [27]. The purpose of the test was to determine the effects of various contaminants

on the flexural strength and plasma performance of coated RCC material. SSP procurement specification MC621-0007 requires "the outer surface of the leading edge shall be unaffected by intermittent exposure or spillage of hydrazine, MMH, and NTO."

All specimens used for the RCC material compatibility test were prepared in accordance with Vought Specification 208-7-42. Nineteen ply thick material was used in the flexure and plasma specimens, and were exposed, via full immersion, to the fluids in question.

After contamination, flexure specimens were point loaded, at a speed of 0.05 in/minute until failure. Plasma specimens were tested in Vought's 180 kilowatt (KW) plasma arc in a stagnation holder. Two half-hour cycles at a 2500° F surface temperature were applied.

The results of the hypervelocity impact test for single particle impact revealed no through penetration of the SiC coating would occur. Sample 1-D (100 µm particle at 3.04 km/s) was the only test sample that produced distinguishable impact features. It is important to note that while impact features were present, Sample 1-D represents 15 times the maximum kinetic energy possible in thruster plume particles. Additionally, the deepest impact crater measured in Sample 1-D was 100 µm with a minimum depth for SiC penetration of 500 µm.

From the hypervelocity impact test, the average damage center diameter was calculated at 129.6 µm, average flake diameter 251.3 µm and crater depth 43.1 µm. The largest acceptable diameter from a single particle impact is 2100 x 2300 x 1000 µm.

The results of the SPHINX modeling indicate that a plume of up to 4.64×10^6 particles/cm² is possible. However, multiple impacts revealed less than a 5 percent SiC loss per thruster event.

Results of the flexural strength and plasma performance of RCC samples contaminated, via full immersion, in hydrazine, MMH, and NTO revealed no degradation to strength or difference in mass loss rates between contaminated and uncontaminated specimens.

a. The impact assessment results indicated that no through damage of the RCC SiC was anticipated.

b. Hypervelocity impact testing did not penetrate SiC for any single event.

c. SPHINX analytical modeling for multiple impacts showed less than 5 percent SiC loss per thruster event (5, 20, and 100 µm particles).

d. A significant margin exists between the kinetic energy allowables for RCC damage and that which is predicted from the RV RCS thrusters.

e. No issues with unreacted propellant contamination based on material compatibility testing during RCC development.

f. The threat posed to the RCC hardware is taken seriously, and inspections for surface damage will be included as appropriate with the "Late Mission" MMOD inspection performed in accordance with operational flight rules.

6.3.11.2 TPS (Tile/Reusable Surface Insulation) - Particle Impingement

The Orbiter TPS was assessed for a plume impingement environment for DDO at the docking ports (i.e., DC Nadir, FGB Nadir, SM Aft, and MRM2). The TPS assessment was performed

using the original impingement environment provided for the RCC panels [19] and the guidelines used for the RCC.

A comparison was made to previous tests/results and performance of TPS in the plume impingement area of the Orbiter upper body flap. The distance from RV to Orbiter is several times greater than Orbiter OMS to body flap distance. The down firing Orbiter OMS thruster impingement on the tiles results in minor coating/substrate erosion with negligible effect on overall effectiveness of the tiles and no discernable deposits. By similarity, any coating damage or deposits from RV thrusters would be expected to be less severe and not a flight issue. Any degradation would be addressed following post-flight inspections.

Post-flight MMOD inspections demonstrate that damage to tiles/blankets/FRSI from light fast particles is generally less severe than the damage of light fast particles to RCC. Since the detailed Soyuz docking evaluation has determined there is no issue for RCC, no issue would be expected for tiles/blankets/FRSI.

6.3.12 Contamination

The Orbiter as a whole was assessed for contamination, but the focus was on PLB as the most likely area of concern for exposure to the propellant contamination environment imparted from a RV. The DC-1 Nadir docking approach was assessed projecting the largest debris field on the Orbiter.

The RV maneuvering thrusters use UDMH and N_2O_4 for propulsion. Combustion products are mostly gasses, N_2, H_2, and NH_3. However, droplets of uncombusted or partially combusted UDMH can be ejected [28] with associated noncombustible impurities and reaction products, including dimethyl-ammonium nitrate and other nitrite salts [29].

The purpose of the PIC flight experiment [1] was to measure the initial and permanent plume induced molecular contamination produced by the Orbiter PRCS and Russian 130 N thrusters. The SPIFEX flight experiment provided relevant, although not continuous, data. The PIC data were taken throughout the thruster firing cycle while the SPIFEX was analyzed post flight, looking at only the results of being in the plume. Both the PIC and SPIFEX experiments were performed using a test package mounted on a boom at the end of the SRMS that was maneuvered into the plume of a thruster firing. Hence, plume effects are representative of the plume at that location. Plume modeling could be performed to represent plume effects at other locations [9].

To analyze the potential contamination concern, the referenced documents were reviewed. The thruster product species, form, and mass were identified. References [28] and [29] provide the product species, and reference [9] provides the mass and distribution. Reference [1] provides a verification of references [28] and [29] and serves as the basis for the development of reference [9].

Ignoring the gaseous combustion products, which are not a contamination concern, the remaining constituents are primarily the result of incomplete or partial combustion and preexisting noncombustible contaminants [1, 2]. These consist of uncombusted UDMH and various organic compounds produced through partial combustion and nonvolatile dimethylammonium nitrate and other metal nitrite salts.

The amount of contaminant can be determined [9] by limiting the analysis to the PLB. From a contamination standpoint, the PLB becomes the only area of interest as the species of contamination, if deposited on the Orbiter external surfaces, would be dispersed on reentry.

6.3.12.1 Nonvolatile Particulate Contamination

The dimethylammonium nitrate and nitrite salts are dispersed throughout the PLB in the form of a powder/particulate. Dimethylammonium nitrate and nitrite salts are, per their Material Safety Data Sheets, an irritant to eyes, respiratory system, and skin. Protective clothing is recommended for handling. However, the amount of material introduced into the PLB is very small. Estimates, per reference [9], place the total mass of these salts at less than 3 milligrams (mg) (worst case, one approach, test and separation operation combined) dispersed throughout the PLB and do not take into account material removal via post-landing purges.

6.3.12.2 Particulate Contamination Acceptance Rationale

From a material compatibility and corrosion aspect, these minor amounts of salts are not expected to be of concern over and above the normal atmospheric salt deposits experienced in the coastal environment. From a particulate contamination aspect, the SN-C-0005 [32] document places the cleanliness requirements on the PLB as "Visibly Clean," which does not measure or count the particulate, but places pass/fail based on the appearance of being free of all particulate or nonparticulate matter visible to the unaided eye.

6.3.12.3 Volatile Constituent Contamination

The volatile products, UDMH and other organics, are of concern (i.e., flammable, explosive, toxic, and carcinogenic). Analyses shows that concerns about residual UDMH in the PLB are absolved by the environment and material properties (i.e., none of the UDMH or other organics survive the environment because they are volatile).

6.3.12.4 Volatile Constituent Contamination Acceptance rationale

Reference [29] notes that the residual UDMH and organic compounds are volatile and are removed via exposure to a vacuum environment. This fits with the results of reference [1] wherein the PIC experiment noted roughly 94 percent of the initial thruster deposit evaporated within 1 minute of deposition, and the SPIFEX experiment, which did not detect any organic contamination in post-flight analysis.

However, it must be noted that these experiments were conducted at relatively warm temperatures, the PIC experiment from 53 to 94°F, and reference [29] at room temperature. Impacted areas of the Orbiter could be at temperatures significantly less, and volatility is a function of temperature and pressure. Materials and Processes Engineering assumes that UDMH deposited on a surface at a temperature greater than the triple point (i.e., -71°F and 0.01 psia) will volatilize, but if deposited on a surface lower than the triple point, sublimation becomes the mode of evaporation requiring energy from solar or other radiative inputs. Note that the low pressure environment depresses the sublimation temperature below the triple point. Using -71°F is conservative for this assessment.

The Orbiter Thermal Analysis group was requested to assess the on-orbit mission attitude timelines and provide typical docked attitude thermal data for the Orbiter PLB and MPLM [31].

Numerous locations were investigated, but the only location where the local surface temperature dipped below the triple point of UDMH was the MLI blankets on the aft bulkhead at low solar beta angles (±10°). Mitigating this is that in this location the temperature cycles from approximately -110 to +20°F (worst case) every 45 minutes. Higher beta angles have warmer minimum temperatures since the ISS shading of the PLB decreases. In addition, after undocking, the nominal PLB to Earth attitudes will result in temperatures above -20°F for all surfaces. This assessment did not include any payloads, except MPLM post undocking, but the payload temperatures would be no lower than the aft bulkhead minimum. So, while it is possible that uncombusted UDMH could survive initial deposition on the aft bulkhead, it would be exposed to an environment that would cause it to volatilize.

6.3.12.5 Addressing the Improbable Concern that the UDMH Deposits do not Volatilize

It is not expected that any uncombusted UDMH or FORP would survive the environmental conditions, but, even if it did, a simple calculation [9] yields 9 mg of total material on the aft bulkhead.

The concern is whether 9 mg of UDMH could produce an explosive atmosphere. The lower explosive limit for UDMH in air is 2 volume percent. This mass of UDMH converted to vapor produces approximately 3.6 cm^3 by volume at standard temperature and pressure. The volume of the PLB is roughly 432,000,000 cm^3 yielding $8x10^{-9}$ volume percent UDMH.

There was a concern [28] that partial combustion of UDMH and/or exposure of certain organic constituents of the partially combusted UDMH and water could form a toxic carcinogen NDMA. A toxicological assessment was performed [30], to address toxicity concerns. Toxicity concerns for ground processing primarily center on the NDMA residue from the UFORP. A secondary consideration is the nonvolatile salts that may accumulate in the PLB since these do no liberate in a vacuum environment. The UFORP components evaporate within 45 minutes from a surface at 25° C. The nonvolatile particulate salts are eye and skin irritants per the MSDS, but use of personal protective equipment (PPE) will mitigate these concerns. Therefore, there are no constraints pertaining to toxicity. Forward work will involve sampling after the first DDO to include destructive testing of the TCS blanket cover to determine worst-case contamination quantity and composition. The Kennedy Space Center (KSC) industrial hygiene group has been engaged in this study and no issues are foreseen. As an additional precaution, EVA is not allowed as per ground rules during a DDO, and the only exposure risk to the UFORP is in the area immediately around the SM engine bells.

6.3.12.6 Contamination Conclusion

Using data for one complete RV proximity operation, worst-case docking location and worst-case plume impingement, no concerns regarding thruster effluent contamination of the Orbiter remain. Potential residual contamination from DDO is considered minor with minimal degradation of any hardware due to RV plume propellant environment, thus not a constraint to DDO. Contamination sampling of the PLB should be conducted if more than two DDOs are performed on the same Orbiter visit to ISS due to potential buildup of particulate contamination.

6.3.13 Ground Operations

The TCS hardware PRT and United Space Alliance (USA) Safety and Industrial Hygiene recommended sampling after the first DDO to gather empirical data on contaminant quantity and chemical composition. All the current data are based on test plates and model predictions. Sampling would provide valuable information for extrapolation of cumulative deposition of all nonvolatile contaminants. The sampling protocol would be under the direction of KSC Safety and Industrial Hygiene, and PPE would be required until hazard is cleared. Samples using a solvent wipe would be taken on the Orbiter PLB frames and hard surfaces for contamination.

This could have a possible impact to beginning-of-flow Orbiter processing if personnel hazards are found to exist. Other possible Orbiter processing impact would be the offline sampling of the TCS blanket. This would consist of destructive testing of TCS blanket beta cloth cover, in area of highest particle fluence, to determine worst-case contaminant quantity and contaminant chemical composition and to determine if optical properties were affected. No impact to processing unless optical properties are significantly degraded.

7.0 S&MA Assessments

The integrated S&MA team members (i.e., ISSP, JSC, and SSP) met numerous times over the course of the DDO analysis period. Joint S&MA discussions and efforts included reviewing the affected integrated hazard and risk baseline for docked operations and detailed background of the content development and rationale for the hazard reports, exchange of corporate knowledge, and identification of potential areas where engineering analysis might be needed to obtain a thorough review of the risk baseline. Some areas of open work and additional risk were identified.

ISS Risk Management approach requires two-fault tolerance protection against catastrophic effect. Noncompliance situations require a NCR to be brought forward to the ISSP Manager to be considered as an acceptable risk. For such cases, risk has been accepted by the ISSP Manager but, per the process, was never presented to the SSP management for acceptance because DDO was ground ruled out. It is recommended that all NCRs be reviewed by the joint SSP and ISSP prior to a DDO mission.

Integrated Hazard Reports (HRs), which were identified to be affected by DDO, are listed as follows. The Safety Review Panel (SRP) will support any effort to ensure that DDO is analyzed and any additional controls are captured appropriately in mission-specific integrated HRs. These analyses will be completed no earlier than (NET) launch (L) minus 4 weeks for the applicable flight.

a. COL-1003 - This HR would potentially address the controls for preventing Orbiter pluming from a RV docking or undocking. Cause 1 addresses pluming effects caused by visiting vehicles. Cause 2 addresses clearances for approaching vehicles, while Cause 7 addresses clearances for departing vehicles. Although the arrival and departure corridors remain the same, there could be unique integrated controls required due to the nature of having an Orbiter present. Additionally, Cause 1 will require updates to account for arriving/departing RS vehicle pluming to the Orbiter while mated to the ISS.

b. C&T-1101 - This HR includes references to Russian HRs and analyses concerning the transmission of RF from RV sources onto the ISS, Orbiter, and EMU. Updates for RF onto the Orbiter while mated to ISS at 19A have been included in this HR.

c. GNC-0701 - This HR would address any impacts to the mated stack attitude control philosophy (i.e., how attitude control is normally maintained during RV dockings or undockings and during periods of Orbiter presence, and if these two existing plans mesh). No changes are required because operational controls, flight rules, and the real-time operational procedures exist to maintain attitude control for nominal and off-nominal operations.

d. STR-0108 - Cause 1 of this HR addresses dock/undock loads. If loads are within margin, based upon “On-Orbit Transient Loads Analysis,” then no HR updates are needed. If there is a loads violation, then HR controls, and verification updates will be required. There will be a possible NCR, and there is a pending Orbiter and ISS loads analysis.

7.1 SSP

The probability of an off-nominal scenario involving a RV dynamic operation remains high, although there is not a consensus in the Safety Community or an agreed-to methodology for computing the probability. However, because the joint ISS/Shuttle/US/Russian operational response to an off-nominal scenario is undeveloped, an off-nominal scenario may increase risk to the Orbiter. All integrated hazard analyses are described in the JSC S&MA section, Section 7.4. SSP Safety Panel chairs have reviewed the approach to DDO Safety assessment and have no additional concerns.

Recommendations from the SSP S&MA office include: (1) concurrence with the hazard analyses and risk characterization contained in the JSC S&MA analysis, (2) no show stoppers have been identified that preclude DDO, although there is a high level of uncertainty concerning the hazard analyses, (3) if the ISSP requirements mandate DDO, that these risks be considered against the requirements mandating DDO and, if possible, reconsider scheduling and other constraints to avoid DDO, (4) any risk mitigation such as development of operational responses. However, extensive or further engineering analysis, including Russian-generated engineering analysis, be pursued to reduce the potential risk that the current limited and high-level assessment presents.

7.2 ISS

The ISS S&MA Office working in collaboration with the SSP Office is in agreement that no show stoppers have been identified that preclude DDO and if the ISSP requirements mandate DDO, that these risks be carefully considered against the requirements mandating DDO. ISS S&MA has evaluated hazards associated with visiting vehicles and has incorporated their findings into their HRs and controls. For any risk mitigation on a specific mission where DDO is required, mission-specific development of operational responses. However, extensive, or further engineering analysis, including Russian-generated engineering analysis, will be pursued to further reduce the potential risks.

7.2.1 ISS Visiting Vehicle Probability Risk Assessment (PRA)

The ISS PRA team completed an assessment of the "demonstrated reliability" of RV dockings. Specifically, ISS PRA evaluated historical RV Aborts and Manual Dockings. A RV abort is a hazard for a docked Orbiter because of the unknown consequences that may arise from an increase in propulsive maneuvers. A RV manually controlled docking may increase their respective propulsive maneuvers, potentially increasing the hazard to a docked Orbiter.

The ISS PRA team completed probabilistic risk assessments on RV collision with the Orbiter docked to the ISS. Non-collision risks that can potentially affect the Orbiter were calculated, including RV probabilistic risk assessments to calculate the risk of hard mate failure, partially docked stuck vehicle, and docking failure, RV probabilistic risk assessment of their MCS digital system, and RV specific component failures rates for hook motors and springs.

7.2.1.1 Russian Demonstrated Reliability

As of August 10, 2010, the RVs have a combined 146 docking attempts (see Table 7-1), using the Kurs radar system. The MOD DM/AR&D team have documented records on previous docking attempts through November 5, 2006. ISS PRA updated DM/AR&D data through August

10, 2010, and did not include any planned manual dockings. The first Soyuz vehicle to use Kurs was TM-1 in 1986. The first Progress vehicle to use Kurs was M-1 in 1989.

Table 7-1. RV Docking Data.

	Docking Attempts	Successful Automated Dockings	Aborts	Manual Dockings
Progress	94	81	7	8
Soyuz	52	43	2	9
Total	**146**	**124**	**9**	**17**

Seven of the nine documented aborts are assumed to have had the potential to impact a docked Orbiter. Two RV aborts have occurred outside of station keeping (~200 m), and the PRA team assumed these do not impact a docked Orbiter. Two aborts occurred at an unknown distance and are assumed to have impact potential to a docked Orbiter. The seven distances where an abort was initiated are 8, 10, 12, 47, and 150 m, and two unknown distances. Progress 38P is the most recent aborted docking.

Eleven of the seventeen documented manual dockings are assumed to have had the potential to impact a docked Orbiter. The PRA team assumed that a manual takeover inside of 20 m would not be an increased hazard to a docked Orbiter. Three of the last eight Progress vehicles have docked manually (i.e., 37P, 34P, and 31P). Soyuz 18S is the most recent Soyuz to manually dock.

7.2.1.2 PRA of Docking and Undocking Scenarios

The PRA models are based on Soyuz PRA v1.2 and Progress PRA v1.2 baseline models. It is assumed that RV pyrotechnics will not be used while the Orbiter is docked to the ISS. Therefore, pyrotechnics are not included in the PRA models. All Russian component failure rates are based on similar US component failure rates because of insufficient Russian component reliability data.

The PRA model of Soyuz calculates a probability of a hard mate failure after a successful soft mate to a mean value of 5.08×10^{-5} (1 in 19,700) with uncertainty as shown in Figure 7-1. A successful soft mate is achieved when the Soyuz probe latches have successfully latched to the ISS. A failure of hard mate is when the Soyuz or ISS hooks cannot be closed due to hook system failure or failure of probe retraction. Failure to undock after the hard mate failure (without attempting to use pyrotechnics) is calculated to have a mean value of 1.10×10^{-8} (1 in 90,900,000) with uncertainty (see Figure 7-1). These two combined failures, mean probability of 1.10×10^{-8}, would result in a partially docked stuck Soyuz vehicle. The model of the Progress vehicle has similar failure modes and failure probabilities. A Progress hard mate failure has a mean probability value of 5.09×10^{-5} (1 in 19,600), and a Progress partially docked stuck vehicle has a mean probability of 1.10×10^{-8} (1 in 90,900,000), both with uncertainty; see Figure 7-2.

The PRA model of Soyuz calculates a probability of Soyuz docking failure after initial probe contact with the ISS cone to have a mean value of 1.10×10^{-4} (1 in 9,100) with uncertainty; see Figure 7-1. A Progress docking failure has a mean failure probability of 8.02×10^{-5} (1 in 12,500) with uncertainty; see Figure 7-2.

A Soyuz or Progress hook motor failure is calculated to have a mean probability of $3.40X10^{-5}$ (1 in 29,400) with uncertainty; see Figure 7-3.

A Soyuz MCS failure during undocking is calculated to have a mean probability of $3.61x10^{-5}$ (1 in 27,700) with uncertainty; see Figure 7-4. A Progress MCS failure during undocking is calculated to have a mean probability of $3.62x10^{-5}$ (1 in 27,600) with uncertainty; see Figure 7-4.

A single Soyuz or Progress spring failure is calculated to have a mean probability of $2.14x10^{-6}$ (1 in 467,000) with uncertainty; see Figure 7-5. A dual Soyuz or Progress spring failure is calculated to have a mean probability of $1.07x10^{-7}$ (1 in 9,350,000) with uncertainty; see Figure 7-5.

7.2.1.3 PRA of Russian Docking Collision

The PRA models are based on Soyuz PRA v1.2 and Progress PRA v1.2 baseline models. Only the final approach (~200 m) to contact is modeled. Earlier vehicle failure leading to collision is not considered credible due to the offset Targeting approach used by RVs. All RV component failure rates are based on similar US component failure rates because of insufficient Russian component reliability data. Ideally a demand failure rate would be used for the short duration mission of a RV final approach (i.e., final approach concludes in approximately eight minutes). However, a 24-hour mission time is used as a conservative approach to modeling component failure data that is based on an hourly failure rate. A combination of expert elicitation and Cognitive Reliability and Error Analysis Method (CREAM) based analyses determined the percentage of manual dockings and human error probabilities.

The RV PRA models calculate collision probabilities with mean values of $2.40x10^{-5}$ (1 in 41,700) and $2.71x10^{-5}$ (1 in 36,900) with uncertainty (see Figure 7-6). The collision probability does not differentiate between a collision with ISS or with Orbiter; either collision scenario is assumed to be catastrophic to the ISS and Orbiter.

7.2.1.4 PRA of Russian Undocking Collision

The PRA models are based on Soyuz PRA v1.2 and Progress PRA v1.2 baseline models. For a Russian collision during undocking to occur, a combination of failures must transpire, which include one hook motor failure, MCS digital loop failure, 100 percent worst-case ISS drift rate, and worst-case docking mechanism performance. Worst case docking mechanism performance is varied between 100 and 25 percent to observe the sensitivity. All Russian component failure rates are based on similar US component failure rates because of insufficient Russian component reliability data.

The PRA model of Soyuz calculates undocking collision probabilities assuming 100 percent worst-case docking mechanism performance to have a mean value of $1.23x10^{-9}$ (1 in 815 million) with uncertainty; see Figure 7-7. If the probability of worst-case docking mechanism performance is 25 percent, then a mean value of $1.99x10^{-10}$ (1 in 5 billion) with uncertainty is calculated for Soyuz; see Figure 7-7. The PRA model of Progress calculates undocking collision probabilities assuming 100 percent worst-case docking mechanism performance to have a mean value of $1.24x10^{-9}$ (1 in 808 million) with uncertainty; see Figure 7-8. If the probability of worst-case docking mechanism performance is 25 percent, then a mean value of $1.94x10^{-10}$ (1 in 5 billion) with uncertainty is calculated for Progress; see Figure 7-8.

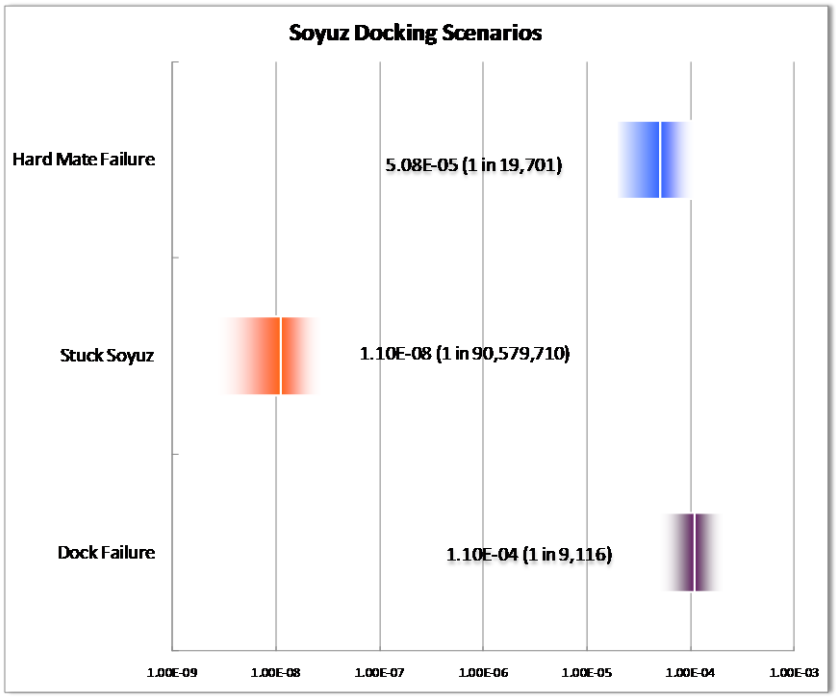

Figure 7-1. Soyuz docking scenarios PRA results.

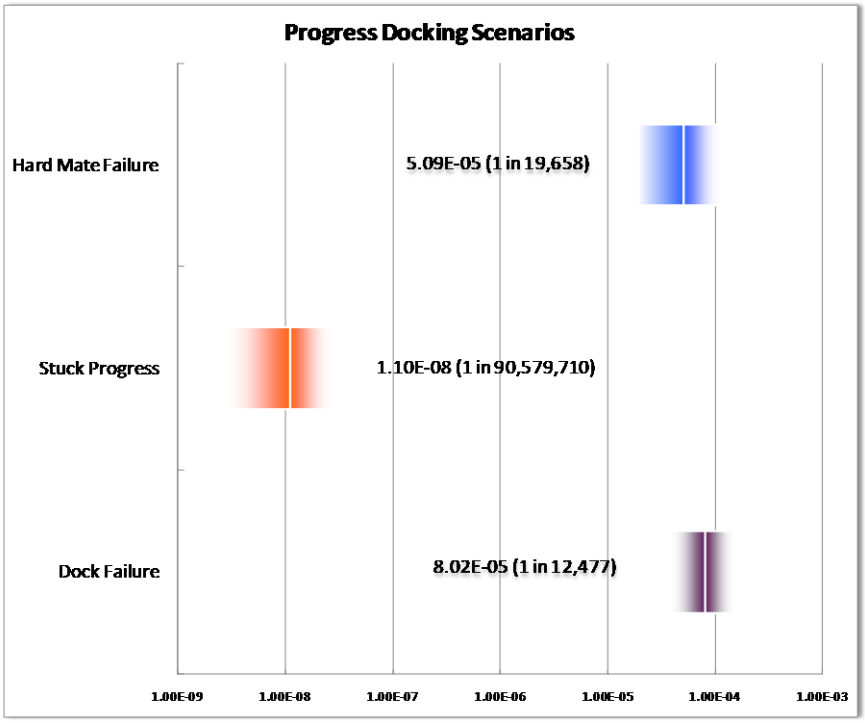

Figure 7-2. Progress docking scenarios PRA results.

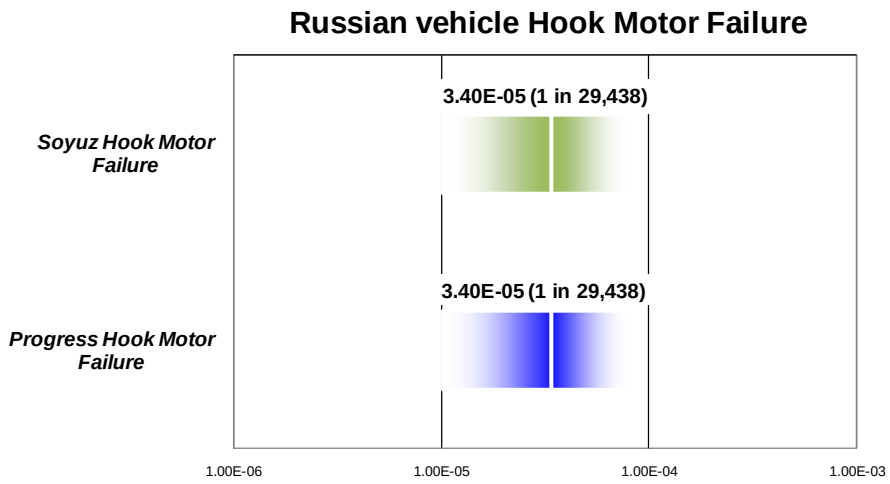

Figure 7-3. RV hook motor failure PRA results.

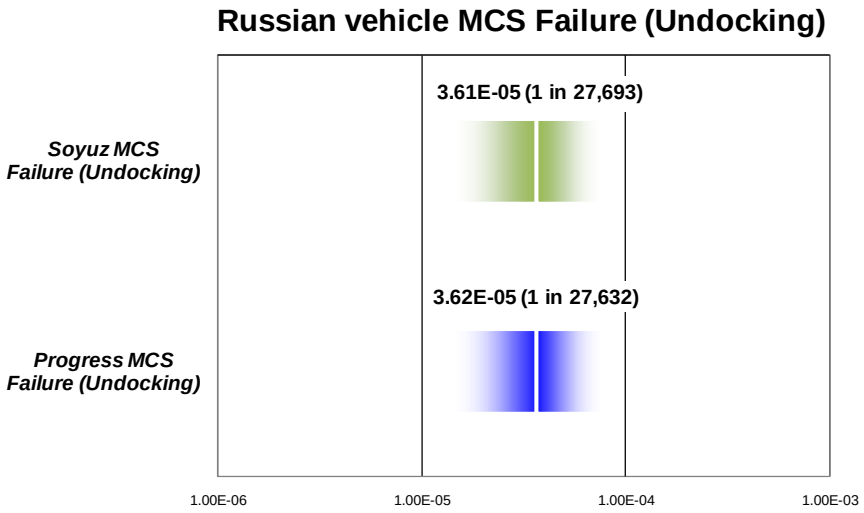

Figure 7-4. RV MCS failure (undocking) PRA results.

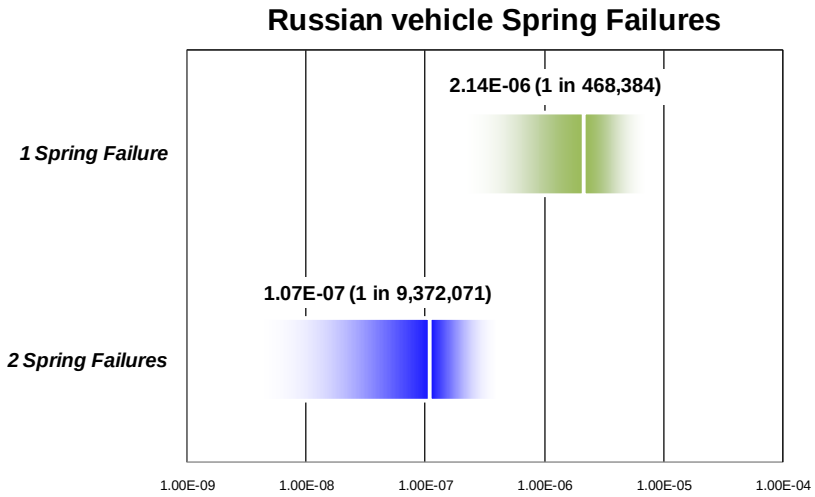

Figure 7-5. RV spring failures PRA results.

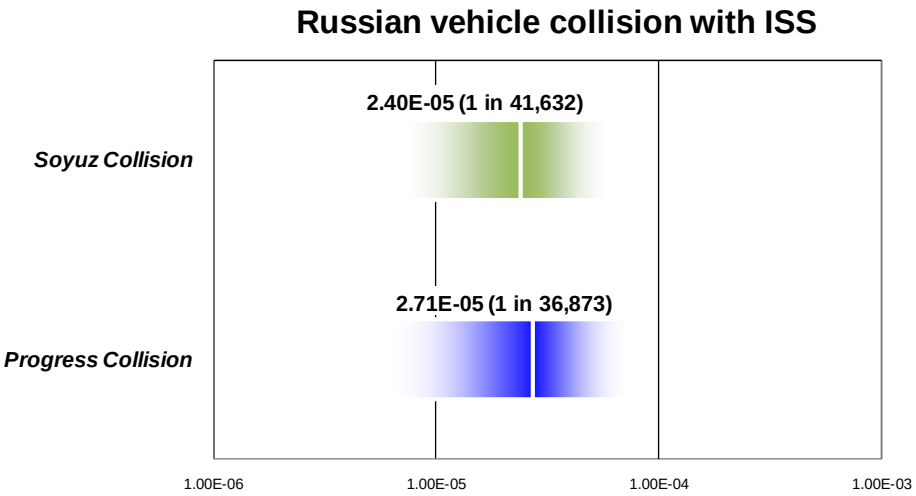

Figure 7-6. RV collision with ISS PRA results.

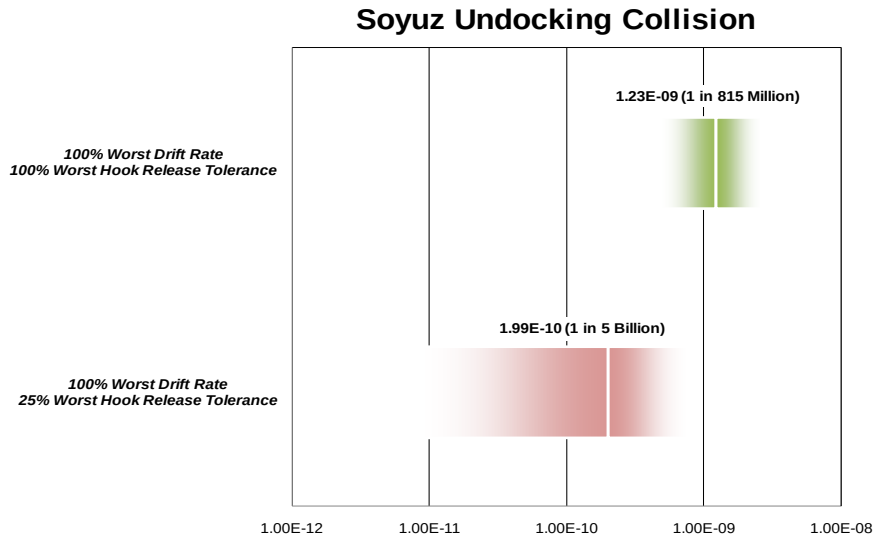

Figure 7-7. Soyuz undocking collision PRA results.

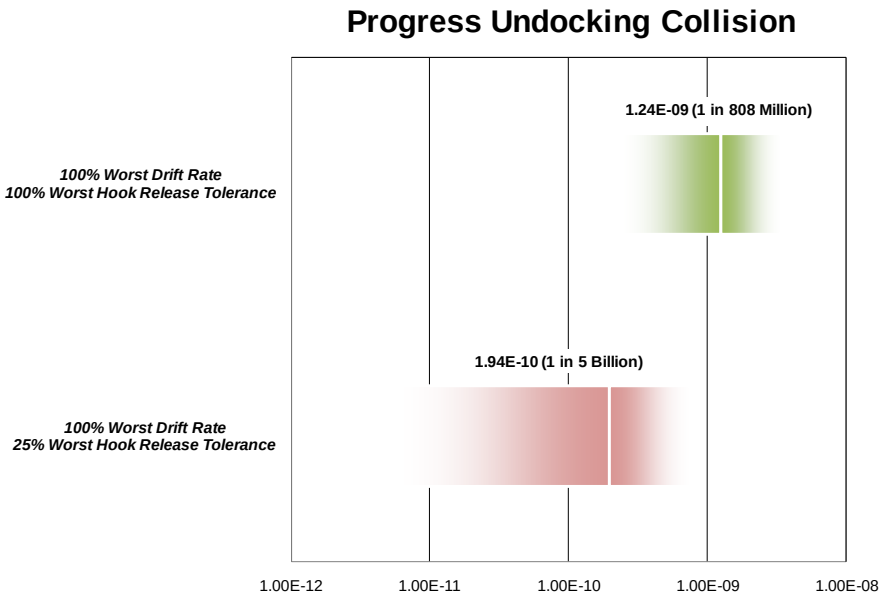

Figure 7-8. Progress undocking collision PRA results.

7.3 KSC S&MA Summary

In the event of DDO, there is a potential for the Orbiter PLB to become contaminated with NDMA, which is a by-product from firing the RV thrusters. The National Institute for Occupational Safety and Health (NIOSH) lists this material as an occupational carcinogen. It is expected that this by-product could remain on the PLB liner thermal blankets at the time the Orbiter PLBDs are opened in the Orbiter Processing Facility (OPF), potentially exposing workers at that time.

To be prepared to eliminate the exposure hazard and provide processes for cleaning up the contamination, if required, KSC S&MA, Ground Operations, and Occupational Hygiene specialists have completed assessments and have identified the following processing changes: (1) define the level for which the labs will be able to detect the NDMA by-products; (2) define the level for which the labs will be able to detect the NDMA by-products on the swabs and thermal blanket; (3) define the template for completing sample processing in the labs, considering schedule impacts to routine work; and (4) provide a draft plan, with a final plan to be completed in the event of a DDO flight, for how to clean the PLB should the sampling reveal a positive reading.

These swab sampling and analysis procedures were performed to baseline the NDMA levels on a non-DDO flight. The STS-131/19A PLB post-flight swab test were performed on March 23 and 26, 2010. These test samples were sent to the NASA labs at KSC where they were tested simultaneously for NDMA, MMH, N2H4, and UDMH. As expected, no hypergolic residues nor NDMA were found on the samples. As a result of executing these processes and analyses, future test samples can be processed in a timely manner.

7.4 JSC S&MA Summary

This section presents an integrated hazard and risk assessment performed by JSC S&MA. The objectives of this assessment for DDO are to characterize the increase in risk to the SSP; identify and characterize hazards, causes, uncertainties, and mitigations; define and frame the risk acceptance posture using past flight history and results of DDO analyses; and ensure that SSP management recognizes that there is significant effort required, nor any means, to analyze many hazard causes and develop risk mitigations.

7.4.1 Assessment Findings

It is the opinion of JSC S&MA that DDO represents an increase in risk to the SSP. From this organization's perspective, qualitatively, the risk level may be equivalent to the program top 10 infrequent risks, although as previously asserted, there exists no means to numerically quantify the increase in risk. Aborts present a higher level of risk than nominal. Quantifying the risk with an acceptable measure of uncertainty is difficult given lack of data, open causes, and undeveloped operational impacts.

Primary hazards for DDO are collision, ISS structural overload, and Orbiter structural overload. Secondary hazards are in-flight readiness assessment limitations and operations impacts. Given engineering assessments for nominal proximity operations (Prox Ops), collision and structural overload hazards have been defined to be improbable. However, limitations, uncertainties, and lack of formal certification engender some unknown level of risk for these hazards. Additionally, although limited analysis has cleared the loads, plume loads on the Orbiter PLBD may exceed the certification limit, given certain off-nominal, yet unanalyzed trajectories and resulting jet firings.

Figure 7-9 provides a risk scorecard for the DDO primary hazards. Figure 7-10, Figure 7-11, and Figure 7-12 elaborate on the 10 specific hazards and explain each risk cause, description, severity, likelihood, and classification, as ascertained in the risk assessment performed.

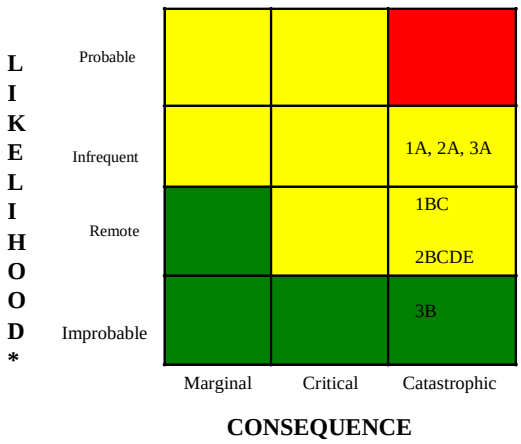

Hazard #	Title
1	**Collision (3 causes)**
2	**ISS Structural Overload (5 causes)**
3	**Orbiter Structural Overload (2 causes)**

Figure 7-9. Primary hazard risk scorecard.

ID	Cause	Description	Severity	Likelihood	Classification
1A	Approach Abort	RV collision with ISS or Orbiter during automated or manual abort after terminated approach	Catastrophic	Infrequent (abort likelihood ~5%)	ISS Accepted Risk
1B	Failed Capture Bounce	RV collision with ISS or Orbiter after approach (AUTO or MIL) ends with contact conditions outside of docking mechanism envelope or FOD present resulting in failure to capture RV "rebound" and initial recovery trajectory to prevent collision are unknown	Catastrophic	Remote ("low" probability per RS HRs)	ISS Accepted Risk – 2 FT and DFMR
1C	Failed Docking Release after mechanism retract failure	After successful capture, zero fault tolerant docking mechanism fails to or FOD prevents retraction & structural hooks from being driven FOD event examples include trash bags on Mir, Progress 8P seal and Progress 23 P antenna failed deployed RV collision with ISS or Orbiter after capture latch release and contingency separation during mated stack LOAC RV trajectory to prevent collision (with Orbiter or ISS) are unknown	Catastrophic	Remote ("low" probability per RS NCR)	ISS Accepted Risk – RS NCR

Figure 7-10. DDO hazard assessment - collision.

ID	Cause	Description	Severity	Likelihood	Classification
2A*	Abort ISS Plume Loads	Automated or manual abort after terminated approach Jet histories are unavailable to assess USPVA or TCS loads	Catastrophic	Infrequent (abort likelihood ~5%)	Unknown
2B*	Failed Capture Bounce ISS Plume Loads	Approach contact conditions outside of docking mechanism envelope or FOD present resulting in failure to capture RV "rebound" and subsequent recovery trajectory jet firings are unknown to assess USPVA or TCS loads	Catastrophic	Remote ("low" probability per RS HRs)	ISS Accepted Risk – 2 FT and DFMR
2C*	Failed Capture Docking Loads	Approach contact conditions outside of docking mechanism envelope or FOD present resulting in failure to capture Docking contact loads & IGN&C response are unknown	Catastrophic	Remote ("low" probability per RS HRs)	ISS Accepted Risk – 2 FT and DFMR
2D*	Failed Docking Mechanism Release ISS Plume Loads	After successful capture, 0 FT docking mechanism fails to or FOD prevents retraction & structural hooks from being driven RV collision with ISS or Orbiter after capture latch release and contingency separation during mated stack LOAC Subsequent recovery trajectory jet firings are unknown to assess USPVA or TCS loads Shuttle undock with ISS LOAC has not been assessed	Catastrophic	Remote ("low" probability per RS HR & NCR)	ISS Accepted Risk - DFMR
2E	Failed Docking Mechanism IGN&C Loads	After successful capture, 0 FT docking mechanism fails to or FOD prevents retraction & structural hooks from being driven Subsequent IGN&C recovery loads using Orbiter or ISS assets are unknown	Catastrophic	Remote ("low" probability per RS HR & NCR)	ISS Accepted Risk - DFMR

**Causes 2ABCD are routinely certified as part of Shuttle/ISS mission CoFR Verification Analysis Cycle (VAC); Cause 2A for ATV (BCDE are accepted risk) and HTV (BCDE are N/A) have equivalent certifications as hazard controls; ISS stage VAC does not include these potential RV contingencies*

Figure 7-11. DDO hazard assessment - ISS structure overload.

ID	Cause	Description	Severity	Likelihood	Classification
3A*	Abort Orbiter Window Erosion	Automated or manual abort after terminated approach Worst case relative position/attitude and duration assumed to estimate maximum thruster effluence Eroded thermal pane fails after entry peak heating during descent; failure effects may include loss of visibility and debris release Eroded thermal pane is etched/hazed resulting in degraded visibility	Catastrophic	Remote (abort likelihood ~5%)	Pending
3B*	Abort Orbiter PLB Door Plume Loads	Automated or manual abort after terminated approach Worst case relative position/attitude assumed to estimate maximum pressure Inability to close doors after hinge overload	Catastrophic	Remote (abort likelihood ~5%)	Pending

**RV plume impingement environments for failed capture bounce and failed docking release (see causes 2BCD) have not been defined for or assessed by Orbiter - these causes present additional unknown risk*

Figure 7-12. DDO hazard assessment - Orbiter structural overload.

7.4.2 Recommended Additional Characterization of Primary Hazard Risk Level

In an effort to better characterize the primary hazard risk level, data generation and analysis must first be performed. These efforts include forward work for the Russian engineering disciplines, which would provide data for analysis. Specific analyses requested include:

a. RSC-E conduct automated and man-in-the-loop RV trajectory and docking system simulations. As reported by the VIPER team's bilateral discussions with their Russian counterparts, a limited abort data development is in work, with completion expected on or around November 2010. For this analysis set space to be complete, it should consist of Monte Carlo run sets focusing on credible dispersions and concurrent failure/anomaly events. Simulators should have adequate capabilities and fidelity to model RS MCS, contact dynamics, etc. The Russians should develop ISS relative motion and RV firing histories, which include approach abort, failed capture, and docking mechanism release scenarios. Additionally, they should use simulation docking contact conditions to verify capture performance and synthesize failed capture docking forcing functions.

b. Several key ISS analyses should then be performed, using the Russian simulation products as inputs. As was conducted to certify Orbiter dockings to ISS, the ISS analysts could then verify adequate vehicle clearance for failed capture and the docking mechanism release scenarios. Also from the Russian data, the ISS engineers could develop updated fluence and plume pressure estimates, which could then be used to assess integrated vehicle loads for failed capture, docking mechanism retraction failure and release, including mechanism contact forces and applicable Integrated ISS GN&C system thruster firings, assess integrated ISS GN&C systems controllability and stability margins for Orbiter VRCS and ISS RS MCS for failed docking mechanism retraction. These data would be used by engineers to assess Orbiter contingency separation, assuming ISS loss of attitude control (which is a catastrophic hazard for ISS) after docking mechanism retraction failure. As stated, all of these analyses were performed during certification of Orbiter to ISS docking. Failure to perform these analyses results in increased analysis uncertainty.

c. Orbiter analyses to be performed, given ISS environments, include conducting additional window erosion testing and reassessing PLBD plume loads analysis with a more representative and comprehensive database than has been performed to date.

d. Pending simulation and analyses, Russian procedures and training (and perhaps United States On-orbit Segment (USOS) and SSP operations products and training) could then be updated, and additional operational mitigations could be developed to further reduce risk.

Figure 7-13 provides a more detailed and methodical depiction of this analysis process and provides background rationale and examples.

Risk	Description	Impacts	Classification	Examples
Certification Rigor	Non-certification and limited assessment of induced environments. Despite best efforts, program assessments completed to date have significant limitations	Collision, structural overload, mission success	ISS Accepted Risk given Stage VAC / SSP Accept assessment limitations for Orbiter (and ISS USPVA overload?)	Shuttle/ISS VAC uses 400+ Monte Carlo simulations (dispersed nominal & abort cases) for PROX OPS versus only 8 RV nominal flight cases
Operational Anomaly Potential	Potential for unanticipated anomalies, late changes to or unplanned OPS, and human errors – separate from failures	Collision, structural overload, mission success	ISS Accepted Risk / Constrained by agency directive & International Partner agreements	The last six RV events (dock/undock/relocate)
MIL Soyuz Inertial Approach & Docking	No analysis has been conducted for this contingency where failures or OPS anomalies result in transition from automated to MIL approach and mated stack is required to hold solar inertial attitude	Unknown thermal effects, collision, structural overload, mission success	ISS Accepted Risk given FT, crew training, FRs, Chits / SSP Accepted risk for no environment assessment given lack of trajectory histories and ATL	Soyuz 9S abort and subsequent inertial approach (after ISS solar inertial snap & hold)
Orbiter Out-of-Configuration	Failures leave Orbiter systems or payloads "unprotected" from RV-induced environments	Degraded TPS inspection/increased entry risk, mission success, ground T/A	Shuttle accepted risk given FT on critical systems, flight rules	SRMS (0 FT) failure leaves OBSS sensors exposed
Joint OPS Complexity	Concurrent visiting vehicle resource management challenges	Mission success	Joint Accepted Risk	Orbiter debris damage assessment may be delayed given RV contingencies

Figure 7-13. Secondary integrated risks.

7.4.3 DDO Integrated Safety Assessment Possible Mitigations for Secondary Integrated Risks

Additional mitigations, which would include extensive coordination effort between the SSP, ISSP, and RSC-E, would help mitigate secondary risk. These include, but are not limited to:

a. Using joint flight history (Space Shuttle, ISS, RS, and RV), catalog credible failures and contingencies, review them for DDO impacts, and trade contingency planning costs versus risk level.

b. Conduct VVO/AR&D team technical interchange meetings to review contingency procedures and plans for Orbiter situational awareness.

c. Verify RV on-orbit safety critical systems tests are tested or verified prior to vehicle final rendezvous or undock and separation.

d. Require the use of video assets to monitor the active RV, and have the ability to process and assess trajectory and jet firing performance.

e. Preplan and position engineering and operations personnel to react to RV contingencies, including the authority to stop an operation, should the need arise.

f. Consider conducting at least one bilateral multi-Program Mission Management Team simulation to establish effective lines of communication.

g. Conduct trades for Orbiter contingency undock and re-rendezvous in the event of RV contingencies.

h. Generate considerations to preclude DDO altogether or limit "overlap." Negotiate the RV launch schedule to mitigate mission impacts. After a SSP launch delay with RV launch dates

regarded as inflexible, evaluate a “slip” into DDO after scrubbing the mission objectives and timeline.

i. Consider mission-specific risk acceptance given dock or undock, RS port utilization, integrated timeline complexity, etc.

7.4.4 JSC S&MA Integrated Safety Assessment Summary and Conclusion

No safety concerns have been identified with DDO for nominal RV rendezvous, proximity operations, docking, and undocking scenarios. Identified risk for Orbiter PLBD limit load exceedances may be avoided with a more detailed analysis, which could be based on reduced conservatism of key input parameters, if the appropriate input dataset were generated and shared by the Russian engineers. DDO catastrophic hazards are collision and structural overload due to aborts and docking failures. However, some hazard controls have significant limitations due to lack of data and analysis. Operational recovery from off-nominal docking and undocking has an indeterminate increase in complexity and will not be fully developed, given the level of effort currently scoped to prepare for a DDO flight. Follow-on actions to potentially reduce the DDO risk have been identified in this section. It is noted that additional risk mitigation is not possible in some cases due to limited resources and time constraints.

It is the opinion of JSC S&MA that DDO Hazards can be eliminated with schedule management. Therefore, the JSC S&MA directorate does not support implementation of DDO unless required for mitigation of potentially catastrophic hazards to the ISS.

8.0 PVR Summary

Two PVRs were conducted to ensure that the DDO mission objectives and technical requirements for the development and implementation effort were fully understood. The purpose of both reviews was to evaluate program technical requirements and to evaluate the analysis, techniques, results, procedures, agreements, etc., used by all participants in determining the viability of DDO for all flights. Both reviews encompassed all major SSP participants and included the ISS VIPER and S&MA communities.

The following sections provide a synopsis from these reviews.

8.1 PVR

The DDO PVR was held February 23, 2010, and the main purpose of the review was to evaluate the analysis techniques and results against program technical requirements used by SSP technical areas in determining the viability of DDO for STS-132/ULF4 and subsequent missions.

There were four stated goals for the meeting: (1) evaluate the data against the requirements for generic DDO; (2) identify constraints; (3) identify forward work; and (4) identify risks and mitigation methods for the SSP. A thorough review of analysis completed to date was conducted. The Orbiter window analysis and discussion of test results were not discussed at this meeting as testing was in process. Discussion of this subject was deferred to the delta DDO PVR. From this review a formal action was assigned: ISSP is to develop jet-firing data for the worst-case scenario and provide the environments data to the SSP. Once received, the OPO and PRTs will evaluate the data against SSP requirements for the new environment. The ISSP and SSP are to continue working through the joint verification process. Results are to be presented at the delta DDO PVR.

The general consensus from the PVR was that significant work had been completed and that all the teams are waiting for the updated environments data. Any future DDO flights will be analyzed on a mission-specific basis. It was recognized that a delta PVR would be required to address the additional environments and the results of the Orbiter windows testing. Further details on the meeting results can be found in reference [41].

8.2 Delta PVR

The DDO Delta PVR was held August 13, 2010. The meeting's purpose was to follow up on the PVR held February 23, 2010, and review Orbiter window test results, additional environments, and FO&I and Orbiter assessments of those environments and to provide an integrated S&MA assessment of risk.

The intent of the review is to provide SSP managers with flexibility to schedule flights for times currently blocked out for DDO. This discussion concerns RV docking and undocking. It does not concern HTV, ATV, or any commercial vehicles. There is less "wiggle room" in the manifest as the end of the SSP approaches, and more flexibility is desired. This review included a response to actions assigned at the February 23, 2010, PVR. The generic case will be examined, and recommendations for DDO will be provided.

From the review, the following summarizes the recommendations and opinions from the functional disciplines and program offices involved in this multilateral effort. It is important to

note that the DDO decision process is in two parts: (1) determine whether DDO can be performed, and (2) determine whether DDO should be performed. The second part would be determined on a case-by-case basis, including operational, clearance and other considerations, and schedule.

All the PVR board members agreed with the exception of JSC S&MA that DDO could be performed, if necessary, but should be avoided if possible by pursuing slips to Space Shuttle manifest, RV docking/undocking, stage EVAs, or other scheduling adjustments.

a. Current DDO analysis lacks knowledge of RV abort or off-nominal trajectories and environments, which resulted in the inability to quantify SSP operational risks. Using Mir space station and ISS historical data, probability of close-in RV abort is 5 percent (i.e., 7 in 146 dockings); ISS-only abort probability is 3 percent (i.e., 2 aborts in 62 dockings).

b. JSC S&MA expressed the strongest opposition to DDO, stating, "JSC S&MA directorate does not support implementation of DDO unless required for mitigation of potentially catastrophic hazards to the ISS." However, all risks identified by JSC S&MA were Yellow (infrequent-catastrophic); none were in the Red (probable-catastrophic).

Operational impacts not considered, the PVR board agreed on the following:

a. RV undocking is feasible, because the thruster firings are believed to be enveloped by the "bounded nominal" cases assessed for docking aborts (10° approach cone, 4° max pitch angle). The trajectories should be safe since orbital mechanics will create a separation after undocking.

b. All ISSP ports are acceptable for undocking except the FGB/MRM 1 nadir port, which needs further analysis because of close proximity to the Orbiter tail. Previously, this port had been ground-ruled out. However:

    1. FGB/MRM1 nadir port is planned for Soyuz 23S undock for the November DDO cutout and 25S docking for the December DDO cutout. Both cutouts could be used by STS-133/ULF5 for launch attempts, but time is limited for necessary coordination and planning.

    2. FGB/MRM1 nadir port is planned for 25S undock for the May DDO cutout, which could be used by STS-134/ULF4 if STS-133 slips to February 2011.

    3. Nominally, Progress docks to SM aft and DC-1 nadir ports, and Soyuz docks to FGB/MRM1 nadir and MRM2 zenith ports.

c. For RV dockings, no issues were identified for nominal (down the centerline) or bounded nominal (10° approach cone, 4° pitch angle). The only unresolved issue was risk of Orbiter window damage from thruster particles for a docking abort to MRM2 Zenith. Worst-case consequences are window(s) shattering and subsequent debris during high-Q, after entry thermal phase, or hazing/cracking, which prevents crew from seeing through forward windows for landing.

    1. Since the ISSP has received no abort data from the Russians, data was synthesized based on nominal thruster firings and RV abort specifications. For worst-on-worst abort case assumptions for MRM2 zenith port (15° backout cone, 15° maximum pitch angle

with mid thrusters always pointed at windows), the thruster particle fluence (particles/cm2) exceeded the maximum fluence tested on windows by 7.5 times.

2. Although windows passed the nominal and bounded nominal cases, the Windows PRT was unable to extrapolate their test data to the fluence level for the worst-case abort because the fluence necessary to cause windows to fail is unknown. Board members recommended additional window testing to clear MRM2 port, estimated at $50,000 SSP funding and an approximate 3 to 4 month duration. MRM2 is worst docking port for windows and is planned for 26S docking in April 2011. This DDO cutout could potentially be used by STS-134/ULF6.

The overriding consensus is that DDO can be performed, but it should not be done unless absolutely required because of Program or Agency priorities. In addition, mission-specific risks and operational complexities will need to be assessed as part of the risk trade if a decision is made to protect DDO for a particular flight.

Further details on the meeting results can be found in reference [42].

9.0 References

1. Soares, C.E. and Mikatarian, R.R. "Thruster Plume Induced Contamination Measurements from the PIC and SPIFEX Flight Experiments," *SPIE 4774-20 International Symposium on Optical Science and Technology*, Seattle, July 2002.
2. Koontz, S., Melendez, O., Zolensky, M., and Soares, C. "SPIFEX Contamination Studies," *JSC-27399*, May 1996.
3. Soares C. E., Mikatarian, R. R., and Barsamian, H., "International Space Station Bipropellant Plume Contamination Model," *Proceedings of the 8th AIAA/ASMT Joint Thermophysics and Heat Transfer Conference*, AIAA 2002-3016, St. Louis, Missouri, 24-27, June 2002.
4. Larin, M., Lumpkin, F., and Stuart, P. "Modeling Unburned Propellant Droplet Distribution and Velocities in Plumes of Small Bipropellant Thrusters," *AIAA 2001-2816, 35th AIAA Thermophysics Conference*, 11-14 June 2001.
5. Mikatarian, R. R., et al. "Space Environments Plume Erosion Model Update," *Presentation to VIPeR Working Group*, 21 August 2008.
6. Pankop, C., Alred, J., and Boeder, P. "Mitigation of Thruster Plume-Induced Erosion of ISS Solar Array Coatings," *AIAA Journal of Spacecraft and Rockets*, Vol. 43, No. 3, May-June 2006.
7. "Space Station Reference Coordinate Systems," *SSP 30219, Rev. J*, 1 May 2008.
8. "Тест СУД No. 2 (MCS Test No.2)," Procedure in Орбитальный Полет (Orbital Flight), Soyuz Flight Data File.
9. Olsen, R. "Dual Docked Operations: Predicted Thruster Plume Particle Fluence and Contaminant Deposition on Orbiter Surfaces from Soyuz/Progress Proximity Operations," *Boeing Engineering Information Document EID684-13765*, 24 Nov. 2009.
10. Olsen, R. "Dual Docked Operations: Predicted Thruster Plume Particle Fluence and Contaminant Deposition on Orbiter Surfaces from Soyuz/Progress Proximity Operations," *Boeing Engineering Information Document EID684-13765, Rev. A*, 9 Mar. 2010.
11. Steagall, C. "Dual Docked Operations: Thruster Plume Particle Fluence to Orbiter Windows for Soyuz/Progress Abort Scenario," *Boeing Engineering Information Document EID684-13936*, 26 Mar. 2010.
12. "Russian Segment Specification," *SSP 41163, Rev. J*, 28 Nov. 2008.
13. Green, A. B. "Russian Vehicle Docking While Shuttle Mated," *Presentation to VIPeR Working Group*, 2 May 2006.
14. NASA Kennedy Space Center. "Space Shuttle Orbiter Systems (Website)," http://science.ksc.nasa.gov/shuttle/technology/sts-newsref/sts_sys.html#sts-rcc, 28 Aug 2006.

15. NASA Glenn Research Center. "As-Fabricated Reinforced Carbon-Carbon Characterized (Website)," http://www.grc.nasa.gov/WWW/RT/2004/RM/RM01D-jacobson1.html, 28 Aug 2006.
16. Curry, D. and Rodriguez, A. "RCC Damage Criteria for Inspection and MMOD Risk Assessment," *Presentation to the PRCB,* 6 April 2006.
17. Mems and Nanotechnology Clearinghouse. "Material Silicon Carbide, bulk (Website)," http://www.memsnet.org/material/siliconcarbidesicbulk/ , 23 Jan. 2007.
18. NASA Human Space Flight. "Shuttle Operational Data Book (Website)," http://spaceflight.nasa.gov/shuttle/reference/sodb/, 28 Aug. 2006.
19. Steagall, C., et al. "Thruster Plume Particle Impacts to Orbiter RCC, Integrated Damage Assessment," *Presentation to the Orbiter Leading Edge Structural System Problem Resolution Team*, 28 February 2008.
20. "Radiator Flight Verification Report," *Vought Report 224RP0094*, January 20 1978.
21. "Space Shuttle System Acoustics and Shock Data Book," *SD74-SH-0082B*, Table 1.3-3.
22. Abebe, T. Z. "SSO-Soyuz Vehicles Radio Frequency Compatibility (RFC) Analysis," *EV7-06-4154*, August 3, 2006.
23. Abebe, T. Z. "RFC between the SSO and Soyuz Vehicles," EV7-09-4452, May 19, 2009.
24. Olsen, R., "Dual Docked Operations: Predicted Thruster Plume Particle Fluence and Contaminant Deposition on Orbiter Surfaces from Soyuz/Progress Proximity Operations," *EID684-13765, ISS-HOU-ENV-RLO-090103*, November 2009.
25. Rodriguez, A., "Micrometeoroid Orbital Debris (MMOD) Damage Tolerance Arc Jet Test for Reinforced Carbon-Carbon (RCC)," JSC-62998, May 2005.
26. Curry, D., "RCC Critical Damage Map," *Internal Letter No.: ATA-TPS-TM-2007-018*, April 13, 2007.
27. "RCC Material Compatibility Tests," Vought Test Information Release No. 221TIR00541, May 1977.
28. Greene, B. and Buchanan, V., "Contamination Detection and Mitigation Strategies for Unsymmetrical Dimethylhydrazine/Nitrogen Tetroxide Non-Combustion product Residues," WSTF, 2003.
29. Dee L.A., Davidson V.D., Johnson H.T., "Laboratory Preparation and Characterization of UDMH/NO_2 Reaction Products," *JANNAF Propulsion and Subcommittee Meeting*; 2002.
30. Meyers, V., "Toxicological Assessment of Thruster Deposits prior to Docking," *TOX-VM-2009-11*, Wyle Laboratories, June 2, 2009.
31. Garcia, F., "Thermal Analysis Data for Assessment of Dual Dock Operations (TAD 30254)," *TM-SJ00-SJC0D-2010-003*, January 29, 2010.
32. "Contamination Control Requirements, Space Shuttle," S*N-C-0005, Revision D*, Lyndon B. Johnson Space Center, July 20, 1998.

33. Bhatt, S. et. al., "STS-130/20A Mated Shuttle/ISS Operations DAP Modes and Constraints, Revision A," *Charles Stark Draper Laboratory, Inc. Memorandum GCD-09-694-A, SSA-09-080-A*, January 15, 2010.

34. Bhatt, S. et. al., "STS-131/19A Mated Shuttle/ISS Operations DAP Modes and Constraints, Revision A," *Charles Stark Draper Laboratory, Inc. Memorandum GCD-10-433A, SSA-10-099A*, March 26, 2010.

35. Bhatt, S. et. al., "STS-132/19A Mated Shuttle/ISS Operations DAP Modes and Constraints," *Charles Stark Draper Laboratory, Inc. Memorandum GCD-10-478, SSA-10-023*, April 30, 2010.

36. Alvarez, R., "Dual Docked Impacts on Cargo Integration Hardware," *Boeing Memorandum 10MA003*, February 8, 2010.

37. Chapman, K., "STS-131 Dual Docked Operations (DDO) Impacts to Orbiter Environmental Control Life Support Subsystem (ECLSS)," *Boeing Memorandum TS-TM-2010-003*, February 19, 2010.

38. Marshall, S., "STS-131 Passive Thermal Verification Analysis L-1 Addendum to SE10HOU126," *Boeing Memorandum TS-TM-2010-10*, March 9, 2010.

39. Dean, J., "Dual Docked Operations (DDO) Study Results," *Boeing Memorandum CINS-TM-10-023*, May 19, 2010.

40. Stump, D., "STS-130(20A) Assessment of Soyuz and Progress Vehicles Transmitter Radiation on the Orbiter during Dual Docked Operations with the ISS," *Boeing Memorandum EME-0110-001*, February 5, 2010.

41. Sills, J., "Dual Docked Operations Verification Review," *NASA Memorandum MO2-10-0xx*, March 12, 2010.

42. Sills, J., "Dual Docked Operations (DDO) Delta Program Verification review (PVR)," *NASA Memorandum MO2-10-032*, August 27, 2010.

43. NASA JSC, "On-Orbit Assembly, Modeling, and Mass Properties Data Book, Volume 1," JSC-26557, Rev. AD, at: https://iss-www.jsc.nasa.gov/nwo/seio/vcer/cammp/web/ec_BlueBookArchive.shtml

44. NASA JSC, "A New Look at Rigid Body Rotation Dynamics", JSC-20637, Rev 1, February 1986.

45. Space Shuttle Program, "Soyuz/Progress ISS Joint Flight Rules Final", NSTS-12820, Volume D, PCN-6, May 4, 2009.

46. Lankford, James, Jr. "Effect of Damage Due to Particulate Debris from ISS Progress and Soyuz Thruster Plumes on Residual Strength of Shuttle Orbiter Thermal Panes," Southwest Research Institute, May 2010.

REPORT DOCUMENTATION PAGE

Form Approved
OMB No. 0704-0188

1. REPORT DATE *(DD-MM-YYYY)*	2. REPORT TYPE	3. DATES COVERED *(From - To)*
01- 11 - 2016	Technical Memorandum	

4. TITLE AND SUBTITLE
Space Shuttle Program (SSP) Dual Docked Operations (DDO)

5a. CONTRACT NUMBER

5b. GRANT NUMBER

5c. PROGRAM ELEMENT NUMBER

6. AUTHOR(S)
Sills, Joel W., Jr.; Bruno, Erica E.

5d. PROJECT NUMBER

5e. TASK NUMBER

5f. WORK UNIT NUMBER
869021.03.05.01.05

7. PERFORMING ORGANIZATION NAME(S) AND ADDRESS(ES)
NASA Langley Research Center
Hampton, VA 23681-2199

8. PERFORMING ORGANIZATION REPORT NUMBER
L-20769

9. SPONSORING/MONITORING AGENCY NAME(S) AND ADDRESS(ES)
National Aeronautics and Space Administration
Washington, DC 20546-0001

10. SPONSOR/MONITOR'S ACRONYM(S)
NASA

11. SPONSOR/MONITOR'S REPORT NUMBER(S)
NASA/TM-2016-219350

12. DISTRIBUTION/AVAILABILITY STATEMENT
Unclassified - Unlimited
Subject Category 16 Space Transportation and Safety
Availability: NASA STI Program (757) 864-9658

13. SUPPLEMENTARY NOTES

14. ABSTRACT

This document describes the concept definition, studies, and analysis results generated by the Space Shuttle Program (SSP), International Space Station (ISS) Program (ISSP), and Mission Operations Directorate for implementing Dual Docked Operations (DDO) during mated Orbiter/ISS missions. This work was performed over a number of years. Due to the ever increasing visiting vehicle traffic to and from the ISS, it became apparent to both the ISSP and the SSP that there would arise occasions where conflicts between a visiting vehicle docking and/or undocking could overlap with a planned Space Shuttle launch and/or during docked operations. This potential conflict provided the genesis for evaluating risk mitigations to gain maximum flexibility for managing potential visiting vehicle traffic to and from the ISS and to maximize launch and landing opportunities for all visiting vehicles.

15. SUBJECT TERMS
Automated Transfer Vehicle; Dual Docked Operations; H-II Transfer Vehicle; Space Shuttle Program

16. SECURITY CLASSIFICATION OF:			17. LIMITATION OF ABSTRACT	18. NUMBER OF PAGES	19a. NAME OF RESPONSIBLE PERSON
a. REPORT	b. ABSTRACT	c. THIS PAGE			STI Help Desk (email: help@sti.nasa.gov)
					19b. TELEPHONE NUMBER *(Include area code)*
U	U	U	UU	204	(443) 757-5802